universität wien

DISSERTATION

Titel der Dissertation

„Synthesis and Bioevaluation of Novel PET Tracers for the Imaging of P-glycoprotein“

Verfasser

DI (FH) Florian Bauer

angestrebter akademischer Grad

Doktor der Naturwissenschaften (Dr.rer.nat.)

Wien, 2014

Studienkennzahl lt. Studienblatt:	A 091 490
Dissertationsgebiet lt. Studienblatt:	Dr.-Studium der Naturwissenschaften Molekulare Biologie
Betreuer:	Ao. Univ.-Prof. Mag. Dr. Thomas Erker

Acknowledgements

The experiments for this thesis were conducted within a multidisciplinary project which has recieved funding from the Austrian Science Fund (FWF) project 'Transmembrane Transporters in Health and Disease' (SFB 35) and from the European Community's Seventh Framework Programme (FP7/2007-2013) under grant agreement number 201380 ('Euripides').

I would like to thank all the people who made this project possible and who contributed to the research described in this thesis.

In particular I would like to thank my supervisor Ao. Univ.-Prof. Dr. Thomas Erker for his support and the possibility to do research in a fascinating field with an excellent interdisciplinary project team.

Further thanks go to Priv.-Doz. Dr. Oliver Langer, our partner in this project, who also acted as a supervisor during the radiochemical experiments, for his great help, especially when drafting scientific publications.

I also want to thank PD Dr. Claudia Kuntner and the rest of the team at the AIT Seiberdorf, Thomas Wanek, Johann Stanek and Michael Sauberer for providing a friendly working environment as well as for conducting the bioevaluation and for technical assistance during radiosynthesis.

I would like to thank Dr. Jens Bankstahl and Dr. Marion Bankstahl from the University of Veterinary Medicine Hannover for their help during the *in vivo* experiments in rats.

Of course I want to thank my colleagues at the University of Vienna for the great working environment. Special thanks go to Severin Mairinger and Bernd Dörner for interesting and constructive discussions at the topic of this project and beyond. Also, I thank my laboratory colleague Mario Gabriel for the great cooperation.

I would like to thank the FWF (SFB35) for financial support during this project.

Finally, I want to express my deep gratitude to my family and friends, who were always a priceless support for me.

Contents

I Abstract (English/German)

The blood-brain barrier (BBB) maintains homeostasis in the brain by regulating the supply of nutrients and by protecting the brain from potential harmful influences. This protective function is, amongst other factors, maintained by the expression of adenosine triphosphate binding cassette (ABC) transporters, such as P-glycoprotein (P-gp), multidrug resistance-related proteins (MRPs) and breast cancer resistance protein (BCRP). These transporters are capable of transporting a broad variety of substances including drugs out of the brain. There is evidence that changes in the expression of ABC transporters play an important role in the pathophysiology and in the development of drug resistance in different neurological disorders including epilepsy, Alzheimer's and Parkinson's disease. The non-invasive imaging method positron emission tomography (PET) can be used to examine ABC transporters at the BBB in patients *in vivo*. PET tracers such as (*R*)-[^{11}C]verapamil and [^{11}C]*N*-desmethyl loperamide were developed which allow for measuring the functional activity of P-gp at the BBB. However, these radiotracers possess low brain uptake and are therefore not suitable for mapping the expression of P-gp.

In this thesis it was attempted to develop novel PET tracers for the visualization of P-gp expression, which, unlike earlier developed probes, are not based on high-affinity substrates like verapamil and *N*-desmethyl loperamide, but on third generation P-gp inhibitors.

O-Desmethyl derivatives of the tracer candidates tariquidar and HM30181 were synthesized in six-step syntheses, with overall yields of 26 % and 16 %, respectively, as precursors for radiolabelling. These precursors were subsequently reacted with [^{11}C]methyl triflate to obtain [^{11}C]tariquidar and [^{11}C]HM30181. The newly developed PET tracers were evaluated in rats and in transporter-deficient mice. Contrary to initial expectations both radiotracers possessed low brain uptake, which was due to efflux transport by P-gp and BCRP. Therefore, both radiotracers are not suited to measure the regional distribution of P-gp at the BBB.

Nevertheless, [^{11}C]tariquidar merits further investigation, as additional experiments suggested that this tracer might be suited for imaging the expression of P-gp in solid tumours and for measuring the functional activity of P-gp and BCRP at the BBB.

Die Blut-Hirn-Schranke (BHS) trägt wesentlich zur Erhaltung der Homöostase im Gehirn bei, indem sie die Zufuhr von Nährstoffen reguliert und als Schutz vor potenziell schädlichen Einflüssen fungiert. Diese Schutzfunktion wird unter anderem durch die Expression von Adenosintriphosphat-Binding-Cassette (ABC) Transportern wie P-Glycoprotein (P-gp), Multidrug resistance-related-Proteinen (MRP) und Breast cancer-resistance-Protein (BCRP) erfüllt. Diese Transporter sind in der Lage eine breite Auswahl an Substanzen, wie z.B. Arzneistoffe, aus dem Gehirn zu transportieren. Es gibt Hinweise, dass Änderungen in der Expression der ABC Transporter eine bedeutende Rolle bei der Ätiologie und Resistenzentwicklung diverser neurologischer Erkrankungen wie Epilepsie, Alzheimer und Parkinson spielen. Die Methode der Positronen-Emissions-Tomographie (PET) könnte dazu verwendet werden um *in vivo* im Patienten ABC Transporter an der BHS zu untersuchen. Daher wurden PET-Tracer wie beispielsweise (*R*)-[^{11}C]Verapamil oder [^{11}C]*N*-Desmethyl-loperamid entwickelt, die es erlauben die funktionelle Aktivität von P-gp an der BHS zu messen. Diese PET-Tracer zeigten jedoch nur sehr geringe Gehirnaufnahme und sind für ein Mapping der P-gp-Expression ungeeignet.

Aus diesem Grund wurde in dieser Arbeit der Versuch gestartet neuartige PET-Tracer zur Visualisierung der P-gp Expression an der BHS zu entwickeln, die, anders als vormals vorhandene Tracer, nicht auf hochaffinen Substraten wie Verapamil oder *N*-Desmethylloperamid, sondern auf P-gp-Inhibitoren der dritten Generation beruhen.

O-Desmethylderivate der beiden Tracerkandidaten Tariquidar und HM30181 wurden in sechsstufigen Synthesen, in Gesamtausbeuten von 26 % beziehungsweise 16 %, als Vorläufermoleküle zur Radiomarkierung synthetisiert. Diese wurden im Anschluss mit [^{11}C]Methyltriflat zu [^{11}C]Tariquidar und [^{11}C]HM30181 umgesetzt. Die so gewonnenen PET Tracer wurden in einer Bioevaluierung in Ratten und Transporter-defizienten Mäusen getestet. Es zeigte sich, dass beide Tracer nur eine geringe Aufnahme ins Gehirn aufweisen und sich *in vivo* wie duale P-gp/BCRP Substrate verhalten. Für eine Anwendung als Tracer zur Messung der regionalen Verteilung von P-gp an der BHS sind beide Verbindungen daher ungeeignet.

Dennoch ist vor allem [^{11}C]Tariquidar ein PET-Tracer der näher untersucht werden sollte, da weiterführende Experimente eine Eignung als Marker für die Darstellung der P-gp Expression in soliden Tumoren beziehungsweise zur Messung der funktionellen Aktivität von P-gp und BCRP an der BHS nahelegten.

II Introduction

II.A Blood Brain Barrier

Disorders of the central nervous system (CNS) are generally difficult to treat, as the blood-brain barrier (BBB) restricts the entry of systemically administered drugs into brain tissue. The primary physiological role of the BBB is to maintain the homoeostasis of the brain, in order to ensure smooth operation of this highly complex organ [de Vries, 1997]. A crucial part of this task is the protection of the brain against outside influences, such as toxic metabolites, xenobiotic compounds and, to a certain extent, the body's own chemical messengers [Wolf, 1996, Ohtsuki, 2004]. Furthermore the BBB acts as an obstacle to prevent pathogenic germs and antibodies from entering the brain and it restricts the entry of leucocytes into the brain. Part of this defense system is mediated by active efflux transporters belonging to the adenosine triphosphate-binding cassette (ABC) family. Moreover active uptake transporters at the BBB also regulate the uptake of essential nutrients, including glucose and amino acids [Ohtsuki, 2004]. By these characteristics the BBB ensures, that the CNS can exist as highly regulated body compartment, possessing well-defined physiological conditions, which differ from the neighbouring compartments like the blood circuit.

The Structure of the BBB

The BBB is a combined diffusion and metabolic barrier, which is principally built up by the endothelial cells of the brain capillary system that are supported by astrocytes and pericytes (Fig. 1) [Bradbury, 1985]. The endothelial cells of the BBB are connected by tight junctions and, unlike endothelial cells of peripheral capillaries, they do not possess fenestrations (Fig. 1). This restrains the passive diffusion of predominantly polar compounds as well as migration processes of cells (e.g. leucocytes) between the endothelial cells [Engelhardt, 2006]. Lipophilic substances may still enter the brain parenchyma by passive diffusion across the cell membranes [Oldendorf, 1974; Bradbury, 1985].

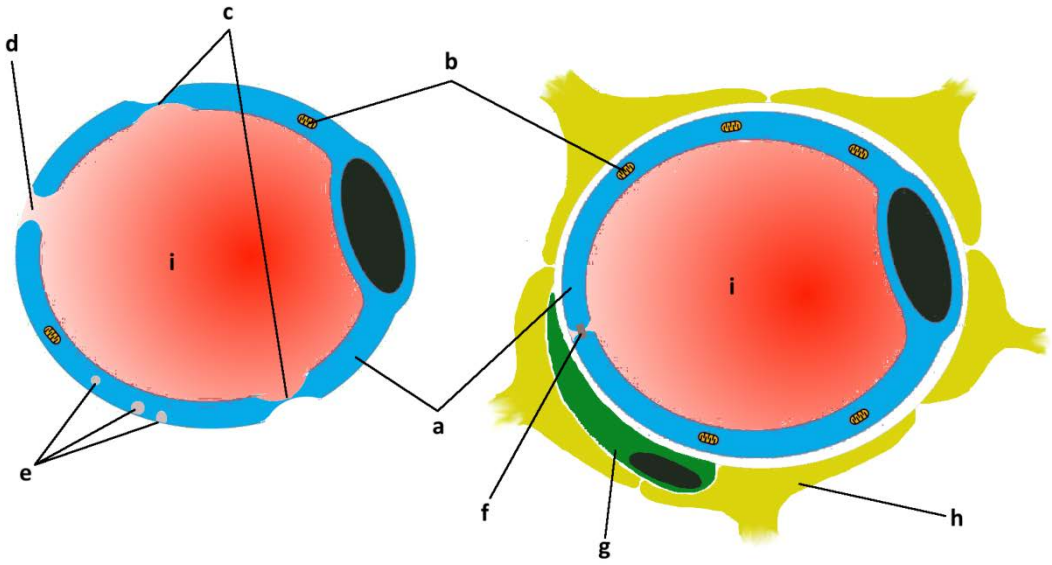

Fig. 1| Comparison of capillaries in CNS and non CNS environment (a) endothelial cell, (b) mitochondria, (c) fenestrations, (d) intercellular gap, (e) transport vesicles, (f) tight junction, (g) pericytes, (h) astrocyte end-foot and (i) lumen [adapted from Wolf, 1996, de Vries, 1997 and Löscher, 2005a]

In order to, at the one hand, limit passive diffusion and, on the other hand, to ensure the supply of the brain with essential nutrients, the endothelial cells of the BBB express a multitude of various transporter proteins (e.g.: glucose transporter (GLUT1), organic anion transporter (OAT3), amino acid transporter (LAT1) and other different influx and efflux transporters) [Löscher, 2005b]. In order to provide enough energy for these transporters, endothelial cells of the BBB also possess an about five- to tenfold higher amount of mitochondria, than peripheral endothelial cells [de Vries, 1997].

The focus of this thesis lies on ABC efflux transporters at the BBB. The most important transporters at the BBB are P-glycoprotein (P-gp), multidrug resistance-associated proteins (MRPs) and breast cancer resistance protein (BCRP). Recent studies showed, that especially BCRP and P-gp are highly expressed in mammalian brain capillary endothelial cells (mice: P-gp 14.1 fmol/µg protein, BCRP 4.41 fmol/µg protein; human: P-gp 6.06 fmol/µg protein, BCRP 8.14 fmol/µg protein) [Uchida, 2011; Kamiie, 2008] and thus these two transporters are considered to be the most important ABC transporters at the BBB.

II.B ABC transporters

ABC transporters are transmembrane proteins, which can actively relocate their substrates against a concentration gradient. The energy for this purpose is generated by hydrolysis of ATP at the transporters' nucleotide binding domains (NBD). In humans this transporter family

consists of 48 known members, which are subdivided into seven subfamilies, encoded by the *ABCA* to *ABCG* genes [Dean, 2001a; Dean 2001b]. Apart from their important role in protecting the brain as a pharmacological sanctuary, ABC transporters also limit oral absorption of drugs in the intestine and mediate excretion of drugs or drug metabolites into urine or into bile. Moreover, ABC transporters have been implicated in multidrug resistance (MDR) of tumours. Several different inhibitors of ABC transporters have been tested in clinical oncology trials, but this concept has so far largely remained unsuccessful.

ABC transporters play an important role in the development of new drugs. For instance affinity of CNS-targeted drugs to P-gp or BCRP is undesired as this may prevent these drugs from reaching their target sites in the brain. On the other hand, affinity to ABC transporters may be voluntarily designed into peripherally acting drugs in order to avoid CNS side effects (e.g. antihistaminics like cetirizine and fexofenadine).

II.B.1 P-glycoprotein

P-gp, also known as multidrug resistance protein 1 (MDR1), an ABC efflux transporter encoded by the *ABCB1* gene, was among the first MDR related transporters to be identified and has been investigated extensively. P-gp was first described in 1976, after the analysis of colchicine resistant Chinese hamster ovary cells revealed the existence of a, by that time unknown, membrane protein [Juliano, 1976]. Although several models on the structure and the functionality of this transporter have been developed so far [Ambudkar, 2003; Stockner, 2009; Jin, 2012], some questions regarding its function and its structure still remain unanswered.

Under regular physiological conditions, the transporter is highly expressed in the intestine, the kidney, the liver [Thiebaut, 1987] and in blood-tissue barrier forming endothelial cells (e.g. BBB or blood-testis barrier) [Cordon-Cardo, 1990], but it has also been observed in drug resistant tumour tissue [Juliano, 1976; Cordon-Cardo, 1990]. P-gp is capable of recognising and transporting a large variety of different substances. It is assumed that general recognition patterns for P-gp substrates are hydrophobic and cationic moieties, while anionic structures seem to be a criterion for exclusion, regarding P-gp mediated transport [Ambudkar, 1999; Ambudkar, 2003]. Based on detailed analyses of known P-gp substrates, specific distribution patterns of electron donors have been identified, which may act as an identification mark for P-gp substrates, if encountered in hydrophobic molecules [Seelig, 1998]. It also has been shown that the interactions between P-gp and its substrates are governed by the formation of

hydrogen bridges [Seelig, 1998]. Among the most prominent substrates of this transporter are drugs for diverse applications including antiepileptic drugs (AEDs), antiviral agents, chemotherapeutics and analgesics (e.g. phenytoin, indinavir, paclitaxel, morphine and nifedipine) [Löscher, 2005b].

Besides its role as multidrug transporter and thus its involvement in drug resistance, changes of P-gp expression have also been associated with several neurological disorders including epilepsy, Alzheimer`s and Parkinson's disease, depression and schizophrenia [Löscher, 2005a].

Structurally, P-gp is a transmembrane protein consisting of 12 transmembrane domains (TMD) and two NBDs, located in the cytosol. These TMDs form two transmembrane regions, which contain the substrate recognition sites and are responsible for the transport of compounds [Ambudkar, 2003].

II.B.2 Multidrug resistance-associated proteins

The MRPs are the translation products of the genes from the *ABCC* family, which also includes cystic fibrosis transmembrane regulator (CFTR, ABCC7) and sulfonylurea receptors (SUR). MRP1 was first discovered in 1992 in a lung cancer cell line, which had been treated with doxorubicin [Cole, 1992]. MRPs are expressed at the BBB, in the intestine, the kidney and the liver [Ambudkar, 2003]. Similarly to P-gp and BCRP, the MRPs have been implicated into MDR. In general, the MRP family seems to prefer negatively charged substrates, such as glutathione conjugates of drug metabolites, glucuronates and bile acids, as well as nucleoside analogues and several other chemotherapeutic drugs (e.g. vincristine) [Ambudkar, 2003].

II.B.3 Breast cancer resistance protein

The most recently described mammalian ABC transporter related to MDR is BCRP, which has been first detected in 1998 in anthracycline-resistant breast cancer cells [Doyle, 1998]. This transporter is encoded by the *ABCG2* gene and fulfils, apart from its role as multidrug transporter, a variety of important physiological functions. It is expressed in high levels in mammary glands, the liver, the kidney, in hematopoietic stem cells and endothelial cells of the different blood-tissue barriers [Vlaming, 2009]. Indeed, recent data show that, at the human BBB, BCRP is expressed in higher levels than P-gp [Uchida, 2011]. BCRP is considered to form the most important protective mechanism against harmful compounds for hematopoietic and

other stem cells [Ni, 2010]. Furthermore studies show a correlation between the occurrence of single nucleotide polymorphisms, which lead to reduced activity of BCRP, and an increased risk of developing gout [Woodward, 2009; Woodward, 2013]. In the mammary glands BCRP has been shown to contribute to the secretion of vitamins and xenobiotics into the milk [Vlaming, 2009]. Recent data indicate that BCRP and P-gp form a cooperative efflux system at the BBB and that dual substrates of both transporters (e.g. tyrosine kinase inhibitors) only gain brain access when both transporters are inhibited [Agarwal, 2011].

Unlike P-gp and MRP1, BCRP consists only of six TMD and one NBD and is therefore regarded as a half transporter. It has been proposed, that BCRP has to form a homodimer in order to create a functional transporter [Ni, 2010].

II.C Diseases in which P-gp has been implicated

II.C.1 Epilepsy

Estimations of the WHO state that up to 10 % of all humans suffer from a seizure in their life time. By definition, epilepsy is determined by the occurrence of at least two causeless seizures. According to the WHO the prevalence of epilepsy lies between 0.4 and 1 % of the whole human population[1].

The first-line approach to treat epilepsy is the use of anticonvulsant drugs. In about two thirds of the cases, the seizures can be suppressed by pharmacotherapy. Unfortunately the remaining patients display pharmacoresistance, rendering standard medication protocols useless and leaving chirurgical therapy, e.g. dissection of the epileptic focus, as sole feasible treatment.

The two main theories [Remy, 2006], which try to explain the occurrence of therapy resistant epilepsy, are the target and the transporter hypothesis (Fig. 2):

Target Hypothesis

This hypothesis states that alterations at the targets of AEDs lead to diminished responsiveness to pharmacological therapy (Fig. 2). There have been several findings strengthening this explanation. It has been shown that functional changes of voltage-

[1] WHO fact sheet 999, October 2012

dependent sodium channels can occur in the epileptic focus [Remy, 2006]. These changes may lead to resistance against AEDs targeting this ion channel. Similar variations have been shown for potassium and calcium channels [Remy, 2006]. Another important target for AEDs is the GABA-A receptor. Again, in several cases of pharmacoresistant epilepsy, alterations of the receptor have been observed that lead to reduced effectiveness of common anticonvulsants [Remy, 2006].

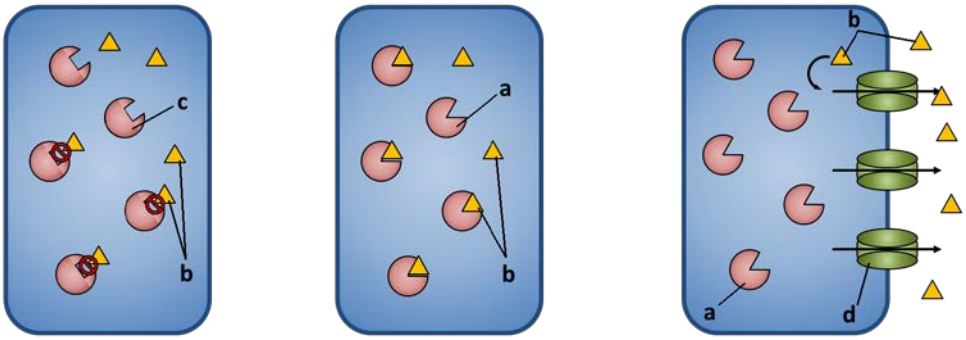

Fig. 2| Comparison between target- and transporter hypothesis Responsive patient (center): an active compound (a) accumulates in the cell and interacts with the drug target (b). Target hypothesis (left side): although the active compound (b) is able to accumulate in the cell, alterations of the target (c) lead to no or diminished responsiveness. Transporter hypothesis (right side): Due to the presence of ABC transporters (d) the active compound (b) cannot reach pharmacologically effective concentrations.

Transporter hypothesis

In this hypothesis the phenomenon of pharamocoresistance is explained by the active transport of AEDs by different ABC transporters, thus rendering the concentration of these drugs in the epileptic focus pharmacologically ineffective (Fig. 2). Several studies were able to show increased expression levels of some ABC transporters, especially P-gp and members of the MRP family, in tissue samples of patients displaying therapy refractory epilepsy [Tishler, 1995; Aronica, 2004; Löscher, 2005a, Löscher, 2011; Liu, 2012]. Furthermore, there are known genetic polymorphisms, which may increase transporter expression levels, and may correlate with the occurrence of therapy resistant epilepsy [Qu, 2012].

II.C.2 Alzheimer's disease

Alzheimer's disease is a neurodegenerative disorder, causing progressive dementia and ultimately death. In the affected brain, a loss of neurons and synaptic crosslinks plus the

formation of amyloid plaques (insoluble deposits of amyloid-β peptide) and neurofibrillary tangles can be observed.

It has been proposed that dysfunctions of the BBB, especially of P-gp, contribute to the pathogenesis of Alzheimer's disease [Zlokovic, 2005; van Assema, 2012]. This theory was strengthened, as amyloid-β peptide has been described as a substrate for P-gp [Lam, 2001; van Assema, 2012].

II.C.3 Cancer

ABC transporter-mediated chemoresistance poses a major obstacle in the chemotherapeutic treatment of cancer. The potential impact of efflux transporters on the success of chemotherapy is underlined by the fact that P-gp, as well as BCRP have first been described in the context of therapy resistant cancer [Juliano, 1976; Cole, 1992; Doyle, 1998].

Since the crosslink between ABC transporters and drug resistance has been found, many commonly used chemotherapeutic drugs have been identified as substrates for different ABC transporters [Ambudkar, 1999; Ambudkar, 2003; Löscher, 2005b]. Due to their ability to transport chemotherapeutic drugs, ABC transporters have been regarded as a viable target for preventing chemoresistance by inhibiting the transporters. Up to now, no inhibitor for ABC transporters has successfully passed clinical trials due to lack of efficacy and toxic side effects caused by transporter inhibition at other sites than the tumour. It is therefore highly questionable whether the inhibition of ABC transporters really is a feasible approach to counteract transporter-related MDR in tumors [Tamaki, 2011]. An upcoming strategy is to utilize the phenomenon of collateral sensitivity to eliminate chemoresistant tumor cells [Hall, 2009]. Despite the fact that inhibition of efflux transporters has remained unsuccessful in cancer therapy, diagnostic tools which allow for assessing the functional transporter status of tumors may be of interest to determine the probability of therapeutic success in a personalized medicine approach.

II.D Measuring P-gp

Several methods can be used to gain information about ABC transporters in biological specimens. DNA sequencing may provide information on the occurrence of single nucleotide polymorphisms (SNPs), which can be related to diminished, as well as to increased function of

the affected ABC transporter. Still, this information does not allow any statements concerning expression levels and transporter function *in vivo*. Other methods to gain information about ABC transporters are immunohistochemical staining or Western blotting, which can reveal expression levels and, in the case of immunohistochemical staining, exact localization of ABC transporters, but do not provide data on their functionality. In addition these methods necessitate a biopsy of the tissue of interest. Nuclear medical imaging techniques potentially represent a powerful *in vivo* tool to examine ABC transporters. These imaging methods are strongly dependent on suitable radiotracers, which are molecules that are labelled with radionuclides. An important imaging method in nuclear medicine is positron emission tomography (PET). This imaging method allows, provided the availability of suitable radiotracers, the measurement of biochemical processes *in vivo*.

Up to now, several potential tracers for P-gp have been identified including [^{11}C]colchicine, [^{99m}Tc]sestamibi, (*R*)-[^{11}C]verapamil, [^{11}C]loperamide and [^{11}C]*N*-desmethyl loperamide [Luurtsema, 2003; Lazarova, 2008; Kannan, 2009; Mairinger, 2011].

III Scope of Thesis

III.A Problem

When this project started, all known P-gp PET tracers were based on substrates of P-gp [Luurtsema, 2003; Bankstahl, 2008; Lazarova, 2008]. These compounds made it possible to provide functional information about P-gp. Using these substrate-based radiotracers rendered it possible to determine the effectiveness of putative P-gp inhibitors *in vivo*. Unfortunately, due to their substrate properties, these tracers show low brain uptake and are not suited for regional mapping of P-gp function, especially in diseases in which an up-regulation of P-gp might occur (e.g. epilepsy).

As P-gp is known to play an important role in the development of MDR in tumours and as it is believed that alterations in P-gp expression contribute to pharmacoresistance and pathogenesis in several neurological disorders, such as refractory epilepsy [Lee, 2004; Löscher, 2005b], Alzheimer's disease [Lee, 2004] or depression [Löscher, 2005b], visualisation of the regional distribution of P-gp in tissue may offer an interesting complimentary approach to the imaging of P-gp function. For this purpose radiotracers are needed, which bind to P-gp without being transported. Such radiotracers would allow the mapping of regional differences in P-gp expression levels in different tissues, such as the brain.

III.B Aims

In order to resolve this problem, a novel PET tracer should be designed that is capable to bind to P-gp at the BBB without being transported. By these means, the new tracer should enable a direct quantitative mapping of P-gp density at the BBB.

For this purpose, the third-generation P-gp inhibitor tariquidar was chosen as a candidate molecule. Tariquidar is one of the most potent and selective P-gp inhibitors known to date [Fox, 2007] which is amenable to radiolabelling with the PET radionuclide carbon-11 (^{11}C). Therefore the primary objective of this thesis was the synthesis of ^{11}C-labelled tariquidar ([^{11}C]tariquidar) as a PET-tracer for the imaging of P-gp at the BBB. Furthermore, the aim was to evaluate [^{11}C]tariquidar *in vivo* using small animal PET. Subsequently, an ^{18}F-labelled tariquidar derivative should have been synthesized, but this aim was not further pursued and replaced by the ^{11}C-labelling of the tariquidar derivative HM30181.

With these tracers at hand, a study to evaluate differences in brain P-gp expression levels in rats exhibiting status epilepticus should be started. By this study the connection of epilepsy and alterations of P-gp expression in the epileptic foci should be shown. In the case of promising results from the bioevaluation, the applicability of the new PET tracers in other diseases, especially drug resistant cancer, could be evaluated.

IV Design and Synthesis of Precursors and PET Tracers

IV.A General Considerations

IV.A.1 Selection of Tracer Candidates

When searching for suitable PET tracer candidates, attention must be paid to the general requirements a CNS PET tracer must fulfill [Pike, 2009]. These requirements are:

- *High affinity and selectivity*

  The affinity of a tracer to its desired target should be in the nanomolar range. In addition the tracer should not specifically interact with other molecular targets, particularly those that are anatomically located in the same region as the primary imaging target.

- *Ability to cross the BBB*

  For visualization of imaging targets inside the CNS, it is important that the PET tracer can cross the BBB in sufficiently high amounts to generate a specific imaging signal by binding to it molecular target. At the same time unspecific binding should be as low as possible (see below). For the visualization of P-gp, which protrudes into the capillary vascular lumen, this property may be less critical.

- *Metabolic stability*

  Effective PET tracers should ideally lack the generation of radiolabelled metabolites, which are taken up and retained in the same tissue where the imaging target is located (brain). Moreover, ^{18}F-labelled tracers should not be subject to *in vivo* defluorination as this will lead to imaging artefacts due to accumulation of ^{18}F in bone tissue.

- *Low degree of unspecific binding and proper range of lipophilicity*

  The degree of unspecific binding has a strong impact on the signal-to-noise ratio and thereby on the effectiveness of the PET tracer In general high lipophilicity is considered to favor unspecific binding. In addition, high lipophilicity may lead to high plasma protein binding of a PET tracer and thereby decrease BBB penetration. On the other hand, if the lipophilicity of a PET tracer is too low, it will not be able to cross the BBB by passive diffusion. A logP range from 1.5 to 3 is generally considered to be ideal for effective CNS PET tracers.

- *Good accessibility to radiochemical labelling and high specific activity*

  A very important point is good accessibility for radiolabelling. Due to the short half-life of commonly used PET radionuclides the radiolabel should ideally be incorporated into

the target molecule in the last step of a reaction sequence and proceed with high yields and in short reaction times. Especially for imaging of low-density molecular targets (e.g. receptor proteins in the brain) PET tracers should be synthesized at high specific activity (i.e. the ratio of radioactivity to mass, usually given in GBq/µmol). The masses associated with a PET tracer are usually in the range of only a few micrograms.

- *Density of target protein*

  The required affinity of a PET tracer for successful visualization of a given target protein depends on the density of the target protein in the tissue to be examined. It has generally been recognized that the ratio of the density of the target protein (B_{max}) and the equilibrium dissociation constant (K_D) of the radiotracer should exceed 5 for successful PET visualization. In other words low-density target proteins require higher affinities (lower K_D values) than high-density target proteins [Eckelman, 2006].

In search for a PET tracer to visualize P-gp density, the literature was searched for known P-gp inhibitors. P-gp inhibitors can be classified into three generations.

- *First generation P-gp inhibitors*

  The first identified inhibitors of P-gp were drugs for different therapeutic applications which additionally showed an ability to inhibit P-gp (e.g. verapamil, cyclosporine-A) [Chiba, 2004]. The problem associated with these compounds was that the doses needed for effective inhibition of P-gp were several times higher than their therapeutic doses and led to side effects. This limitation precluded the clinical use of first generation P-gp inhibitors.

- *Second generation P-gp inhibitors*

  The representatives of this group of agents were structurally based on inhibitors of the first generation. They show enhanced potency for P-gp inhibition with less side effects [Krishna, 2000]. (*R*)-Verapamil and valspodar were candidates of the second generation inhibitors. Nevertheless both compounds were not considered for clinical use as (*R*)-verapamil exhibited cardiotoxicity at P-gp-inhibiting doses [Wilson, 1995] and valspodar proved to inhibit cytochrome P450 3A4 mediated metabolism [Bates, 2001].

- *Third generation P-gp inhibitors*

  These compounds have been designed especially as inhibitors for P-gp. They generally display no toxicity and do not interact with cytochrome enzymes. These inhibitors exhibit high affinity and rather good selectivity for P-gp over other efflux pumps. Several members of this group of compounds (e.g. tariquidar, elacridar, laniquidar,

zosuquidar) have been investigated in clinical oncology trials, but were not further developed due to lack of efficacy.

For development of a PET tracer to visualize P-gp density the third-generation inhibitors elacridar (GF120918) and tariquidar (XR9576) were chosen as lead structures. Both compounds have been in phase III clinical trials and have therefore been well characterized in terms of pharmacokinetics and toxicity. They are generally considered as non-transported or non-competitive inhibitors of P-gp function, displaying a nanomolar affinity to their target. Moreover HM30181, a recently described tariquidar analogue [Bang, 2005; Kwak, 2010] was chosen as a further lead structure.

In this thesis the development of PET tracers based on tariquidar and HM30181 will be described. PET tracers based on elacridar were described in the doctoral thesis of Bernd Dörner [Dörner, 2009; Dörner, 2011; Dörner, 2012].

IV.A.2 Synthesis Strategy

^{11}C and ^{18}F are the most commonly used radionuclides in the synthesis of new PET radiotracers. A major advantage of ^{11}C is the possibility to synthesize structurally unchanged PET derivatives of known investigational drugs, as all organic compounds contain carbon. The pharmacokinetic properties of such ^{11}C-labelled drug compounds are identical to those of the unlabelled parent. So if a known investigational drug is labelled with ^{11}C, an estimation of the *in vitro* and *in vivo* behaviour of the tracer may be derived from existing preclinical and clinical studies of the unlabelled parent. A limitation of ^{11}C is the short half-life of 20.4 minutes, resulting in strict limitations in maximal allowable synthesis times for the labelling reaction (max. 3 half-lives ≈ 60 minutes) on the one hand and in restrictions in the clinical applicability, which is dependent on the availability of an onsite cyclotron on the other hand. A common alternative to ^{11}C is ^{18}F, which has a longer half-life time of 109.8 minutes. A drawback of ^{18}F is related to the fact that most drugs do not contain fluorine in their structure and ^{18}F-labelling will afford a new derivative, which needs to be toxicologically characterized for clinical PET applications in humans. On the other hand, ^{18}F allows multi-step syntheses and longer total synthesis times compared to ^{11}C.

Our first aim was to synthesize a radiolabelling precursor for [^{11}C]tariquidar. Tariquidar has four methoxy moieties (Fig. 3), which give straightforward access to ^{11}C-labelling by [^{11}C]methylation.

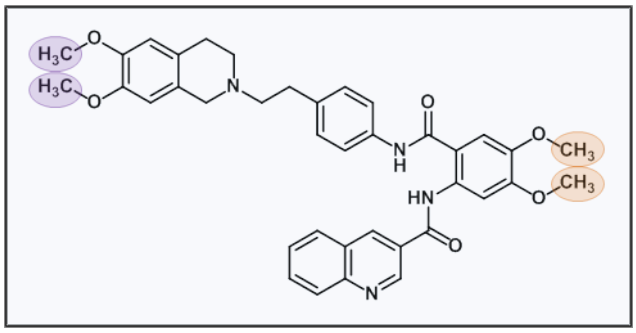

Fig. 3| Potential ^{11}C-labelling positions of tariquidar (methoxy moieties as red and violet circles)

To begin with, we had to decide whether we would try to demethylate one of the methoxy moieties in tariquidar or whether we would establish a total synthesis of a suitable precursor molecule.

The main advantage of the demethylation approach is that only one reaction step, starting from tariquidar, is necessary to synthesise an *O*-desmethyl tariquidar derivative. On the other hand by this type of reaction a mixture of various demethylated tariquidar derivatives is expected, requiring complex purification procedures. Besides it can be assumed that low yields would be achieved and that the structural characterisation of such a product would be difficult. A demethylation approach is also dependant on the availability of tariquidar. The total synthesis of *O*-desmethyl precursor is time consuming, but it allows to clearly defining the exact position of the methylation site. Due to limited access to unlabelled tariquidar the total synthesis access was favoured in this work. The demethylation approach to synthesize *O*-desmethyl tariquidar (Fig. 4) was pursued in parallel to our work by Kannan *et al.* [Kannan, 2011].

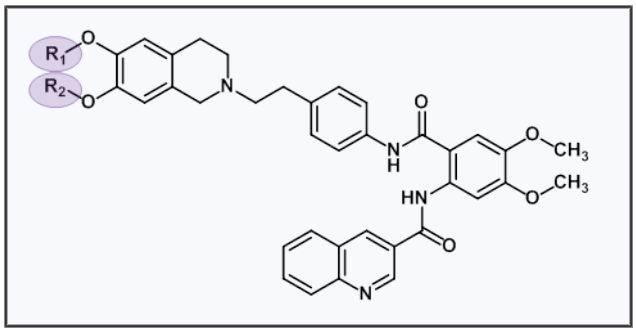

Fig. 4| *O*-Desmethyl tariquidar derivatives synthesized by Kannan *et al.* *via* demethylation "6-*O*-desmethyl tariquidar": R_1 = OCH_3, R2 = OH; "7-*O*-desmethyl tariquidar": R_1 = -OH, R_2 = -OCH_3

The next question was whether to label the isoquinoline or the anthranilic amide moiety. Initially the isoquinoline part was favoured, but for several reasons, which will be discussed in detail below, the anthranilic amide moiety was preferred.

After having performed a preliminary characterization of a [^{11}C]tariquidar, it was initially planned to develop a [^{18}F]derivative of tariquidar. However, because preliminary findings suggested that [^{11}C]tariquidar and [^{11}C]elacridar were not able to visualize P-gp density [Dörner, 2009; Dörner, 2011; Kawamura, 2011a; Kannan, 2011], the [^{18}F]tariquidar was not further pursued. Instead the ^{11}C-labelling and characterization of the tariquidar derivative HM30181 was undertaken.

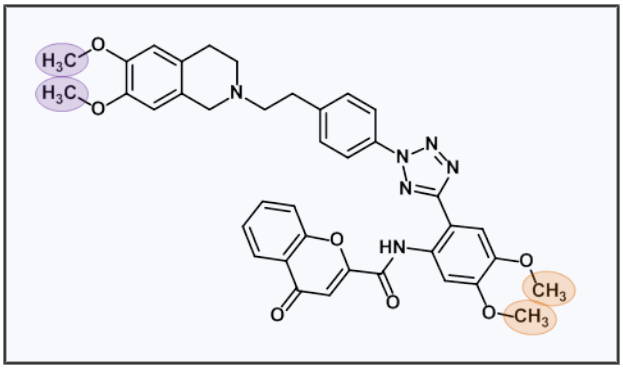

Fig. 5| Potential ^{11}C-labelling positions for HM30181 (methoxy moieties as red and violet circles)

As HM30181 is closely related to tariquidar, there are also several methoxy moieties suitable for substitution by [^{11}C]methylation (Fig. 5). Again, the aniline moiety, corresponding to the anthranilic amide moiety of tariquidar, was regarded to be best suited for [^{11}C]labelling.

IV.B Synthesis

IV.B.1 Reference compounds

The common synthesis pathway of tariquidar [Ryder, 1998; Sharp, 1998; Klinkhammer, 2006] starts from 6,7-dimethoxy-1,2,3,4-tetrahydroisoquinoline hydrochloride, which is coupled in a nucleophilic reaction (S_N2) with 4-nitrophenethylbromide. The resulting compound **1** is catalytically reduced with hydrogen, using palladium on carbon (Pd/C) as catalyst, to the corresponding aniline derivative **2** (Fig. 6).

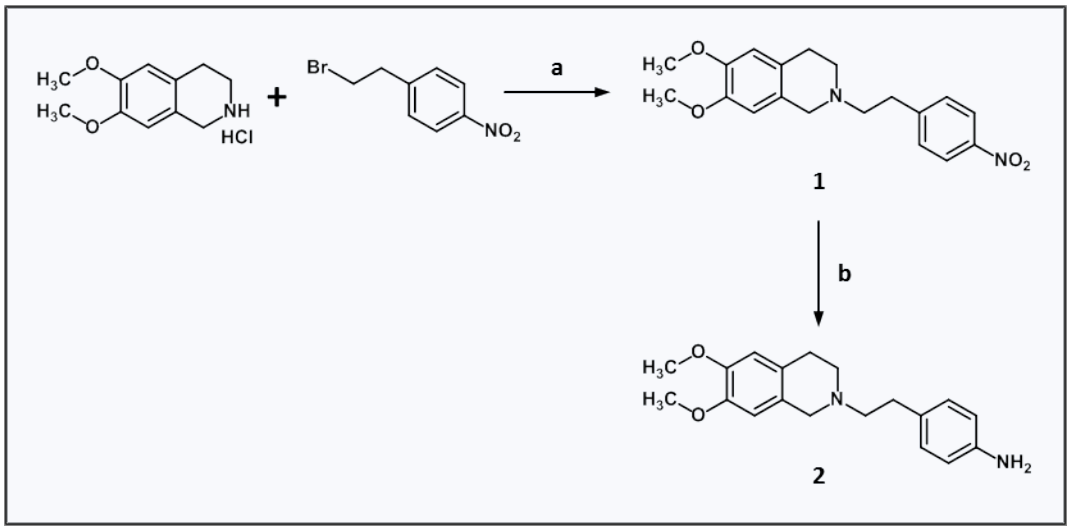

Fig. 6| Synthesis pathway for compound 2 (a) K_2CO_3, KI, DMF, 70 °C; (b) Pd/C, H_2, EtOH, rt;

Reacting compound **2** with 4,5-dimethoxy-2-nitrobenzoyl chloride yields the benzamide derivative **3**. Again, the nitro group is reduced by catalytic hydrogenation and the resulting benzamide derivative **4** (Fig. 7) is coupled with 3-quinolinecarbonyl chloride to obtain tariquidar, which was treated with methanesulfonic acid to form the corresponding bismesylate (Fig. 8). Especially the final steps often resulted in poor yields. Therefore, we attempted to develop an improved method to synthesize tariquidar during a diploma thesis, performed in our group [Mairinger, 2008].

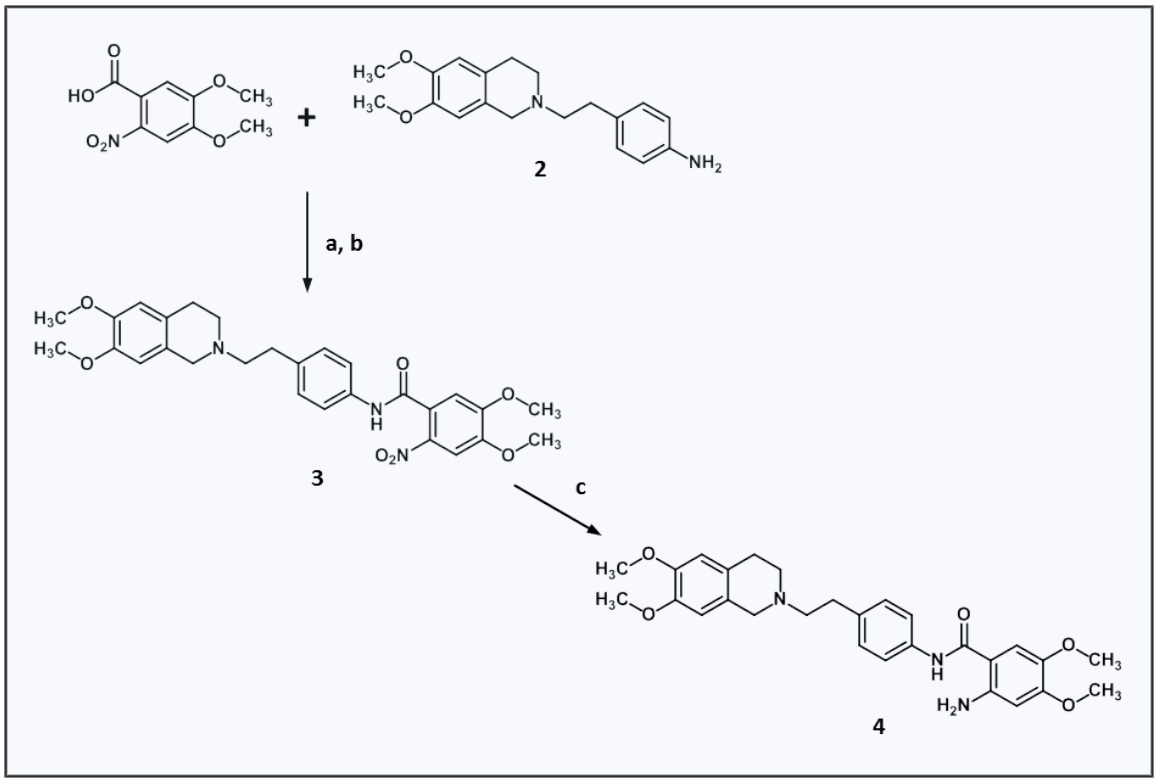

Fig. 7| Synthesis of compound 4 (a) $SOCl_2$, reflux; (b) TEA, THF, 0 °C → rt; (c) Pd/C, H_2, MeOH, rt;

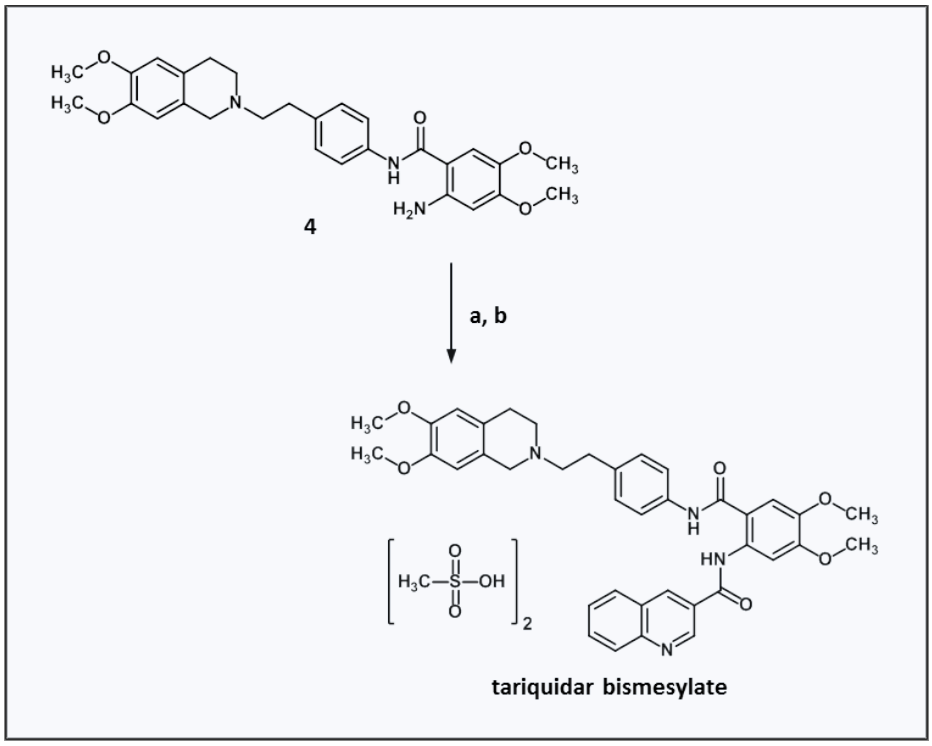

Fig. 8| Synthesis of tariquidar bismesylate (a) 3-quinolinecarbonyl chloride, TEA, THF, 0 °C → rt; (b) methanesulfonic acid, EtOH, H_2O, acetone;

In an attempt to increase the yields and to reduce the number of necessary consecutive reaction steps, a convergent synthesis scheme was developed [Mairinger, 2008]. Therefore the final product was split into two parts (Fig. 9), the "isoquinoline part" (compound **2**), which contains the tertiary amino group, and the "quinoline part" (4,5-dimethoxy-2-(quinoline-3-carboxamido)benzoic acid (**5**)).

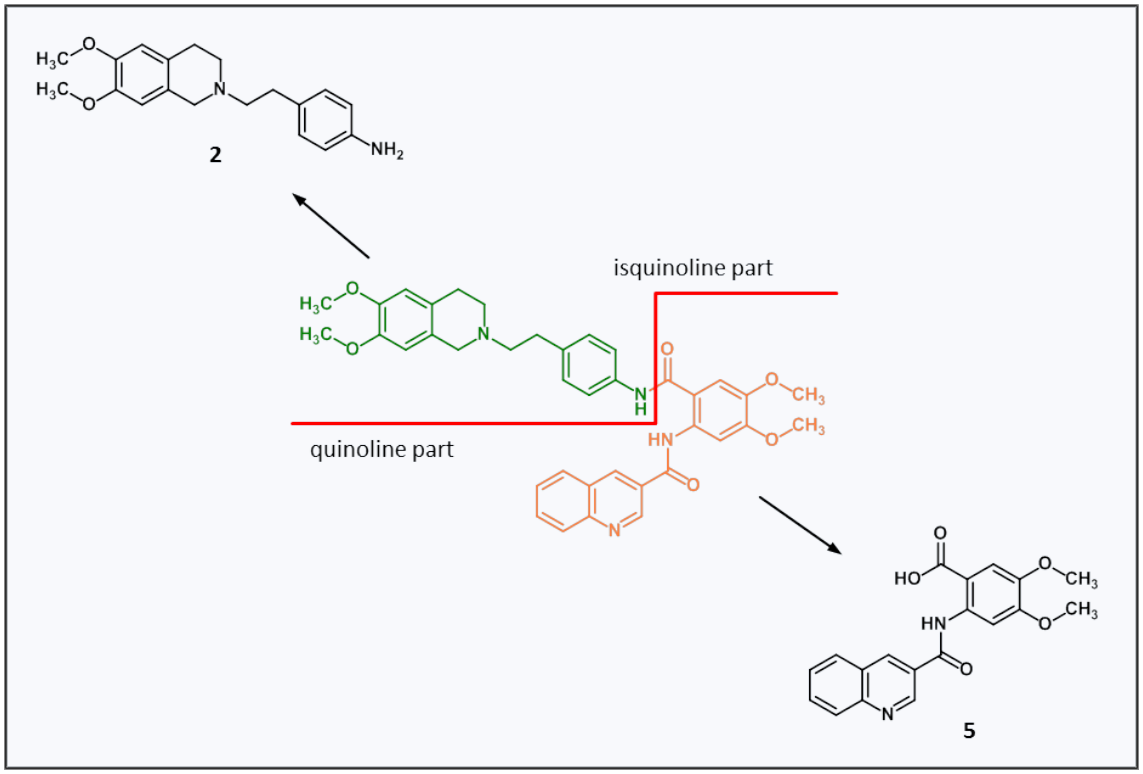

Fig. 9| Separation of tariquidar for convergent synthesis route

The synthesis of compound **5** starts from methyl 2-amino-4,5-dimethoxybenzoate, which is coupled with 3-quinolinecarbonyl chloride to obtain the methyl benzoate **6**. The methyl ester is cleaved with KOH in a mixture of water and methanol (Fig. 10).

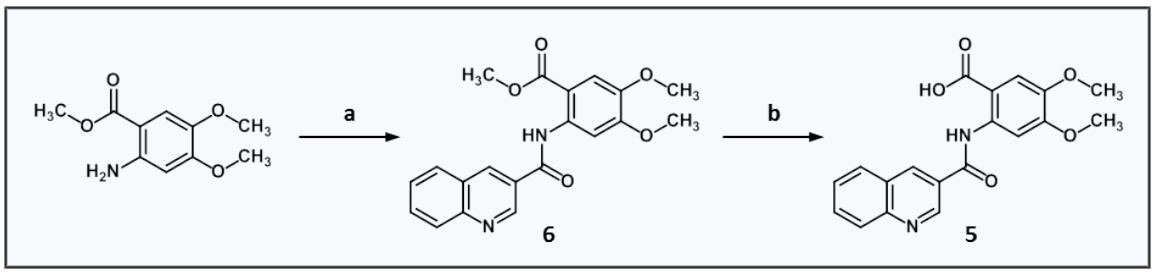

Fig. 10| Synthesis of compound 5 (a) 3-quinolinecarbonyl chloride, TEA, THF, 0 °C → rt; (b) KOH, H_2O, MeOH, reflux;

The deprotected derivative **5** should then be coupled to the aniline derivative **2** (Fig. 11). Unfortunately, upon activation of the acid moiety, compound **5** underwent an intramolecular cyclisation resulting in the formation of 6,7-dimethoxy-2-(quinolin-3-yl)-4*H*-benzo-[*d*][1,3]oxazin-4-one (**7**). This benzoxazinone derivative occurred as the main reaction product, independent of the method of acid activation. Neither by use of the corresponding acid chloride nor by utilizing coupling reagents was the desired product accessible.

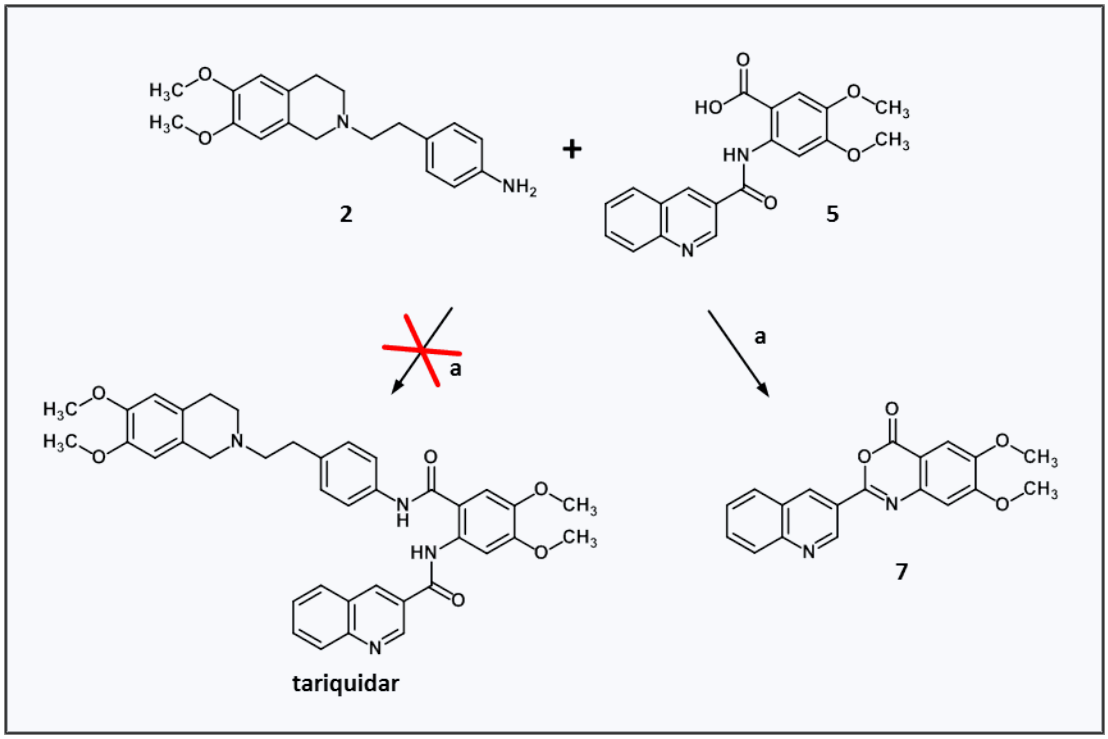

Fig. 11| Convergent synthesis pathway of tariquidar (a) coupling reagent or 1. $SOCl_2$, 2. TEA, THF, 0 °C → rt;

As a result of these experiments, the convergent synthesis approach was no longer pursued and the reference compound was synthesized following the already depicted classical pathway. The convergent synthesis pathway was described in greater detail in the diploma thesis of Severin Mairinger [Mairinger, 2008].

3-Quinolinecarboxylic acid (**8**) was synthesized starting from 3-bromoquinoline *via* 3-quinoline-carbonitrile. In a first attempt the carbonitrile should be introduced in position three by heating 3-bromoquinoline with $K_4[Fe(CN)_6]$ in the presence of CuI and 1-butylimidazole in toluene [Schareina, 2007], but following this pathway no product could be isolated. In an alternative approach [Weissman, 2005], $Pd(Oac)_2$ was used as catalyst, Na_2CO_3 was added as base and toluene was replaced by *N,N*-dimethylacetamide as solvent. Following these reaction conditions, 3-quinolinecarbonitrile (**9**) could be isolated in acceptable yields. For the hydrolysis to 3-quinolinecarboxylic acid three different approaches were tried: aqueous NaOH solution,

H_2SO_4 and hydrochloric acid. While the basic hydrolysis gave poor yields and in the H_2SO_4 catalyzed reaction no product could be detected at all, by the hydrolysis in aqueous hydrochloric acid 3-quinolinecarboxylic acid could be isolated in good yields (Fig. 12).

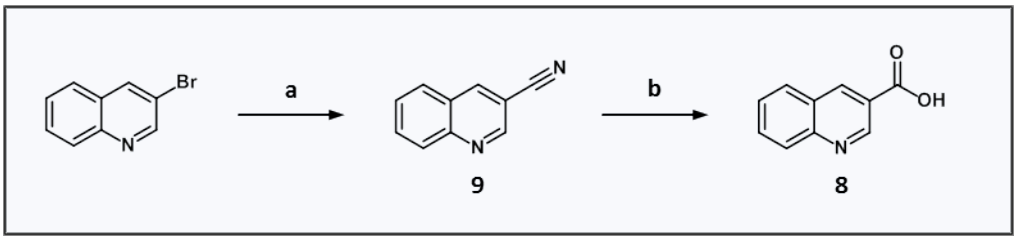

Fig. 12| Synthesis of 3-quinolinecarboylic acid (8) (a) $K_4[Fe(CN)_6]$, $Pd(Oac)_2$, Na_2CO_3, DMAc, 120 °C; (b) HCl (conc.), reflux;

Tariquidar was converted into the corresponding bismesylate by reaction of the free base with methanesulfonic acid in a mixture of water ethanol and subsequent precipitation by addition of acetone (Fig. 8) [Hayman, 2003].

The synthesis of HM30181 (**10**) [Bang, 2005] begins with the conversation of 6-nitro veratraldehyde and *p*-toluenesulfonyl hydrazide to (*E*)-*N*'-(4,5-dimethoxy-2-nitrobenzylidene)-4-methylbenzenesulfono-hydrazide (**11**) (Fig. 13).

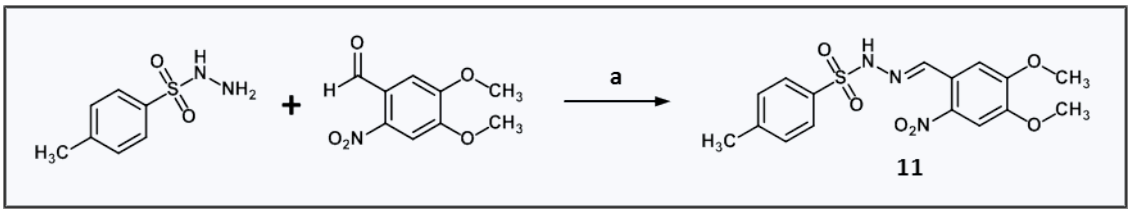

Fig. 13| Synthesis of compound 11 (a) EtOH, reflux → rt, H_2O;

The aniline derivative **2** is transformed into diazonium salt **12** by reaction with $NaNO_2$ and concentrated hydrochloric acid in ethanol and water. Adding the hydrazone **11** dissolved in pyridine to the diazonium salt **12** results in the formation of compound **13**, which is reduced, using Pd/C and hydrogen, to the aniline derivative **14** (Fig. 14).

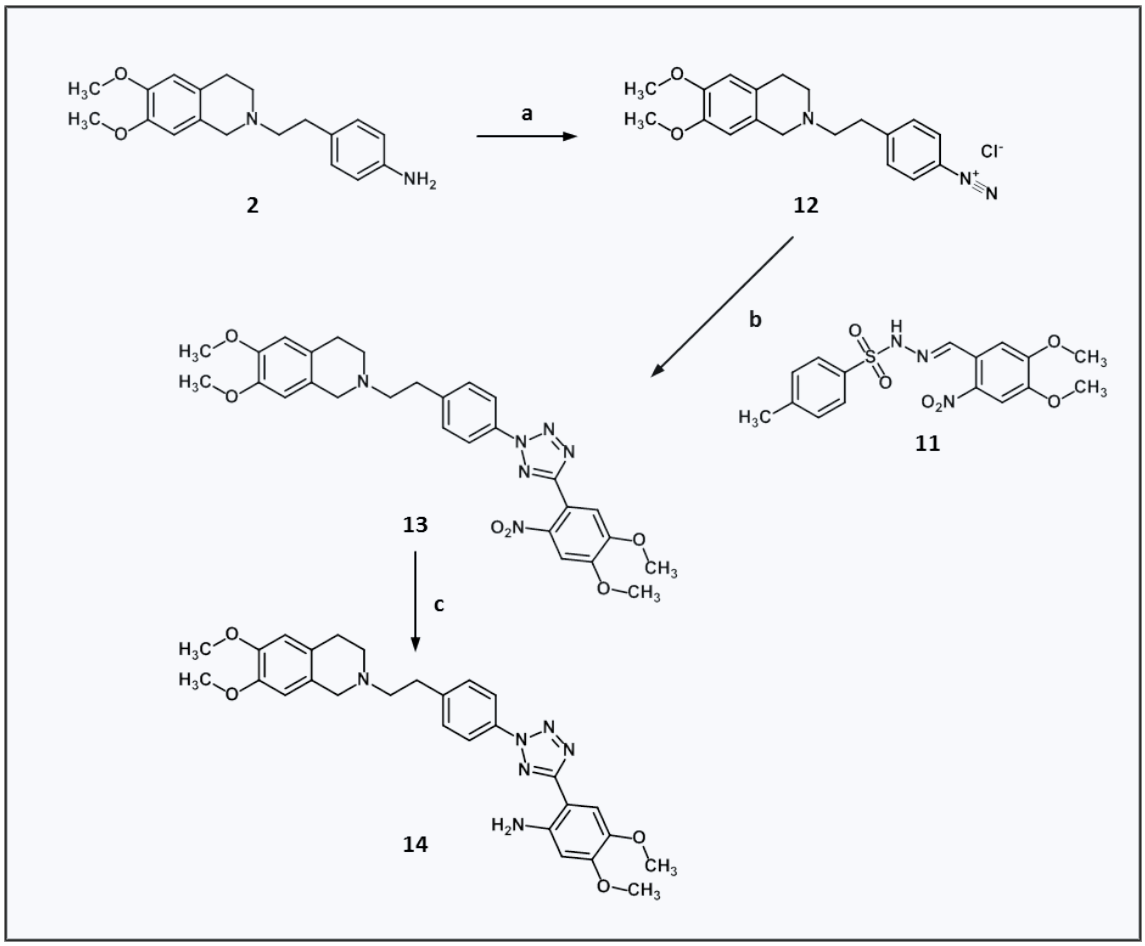

Fig. 14| Synthesis of compound 14 (a) $NaNO_2$, HCl, EtOH, H_2O, 0 °C; (b) pyridine, - 15 °C → rt; (c) Pd/C, H_2, EtOH, CH_2Cl_2, rt;

HM30181 is formed by an amide coupling of 4-oxo-4*H*-chromene-2-carboxylic acid and aniline derivative **14**, using *N*-(3-dimethylaminopropyl)-*N*'-ethylcarbodiimide hydrochloride (EDC•HCl) and 4-dimethylamionpyridine (4-DMAP). The mesylate of HM30181 is produced by reaction of the free base with methanesulfonic acid in methanol (Fig. 15).

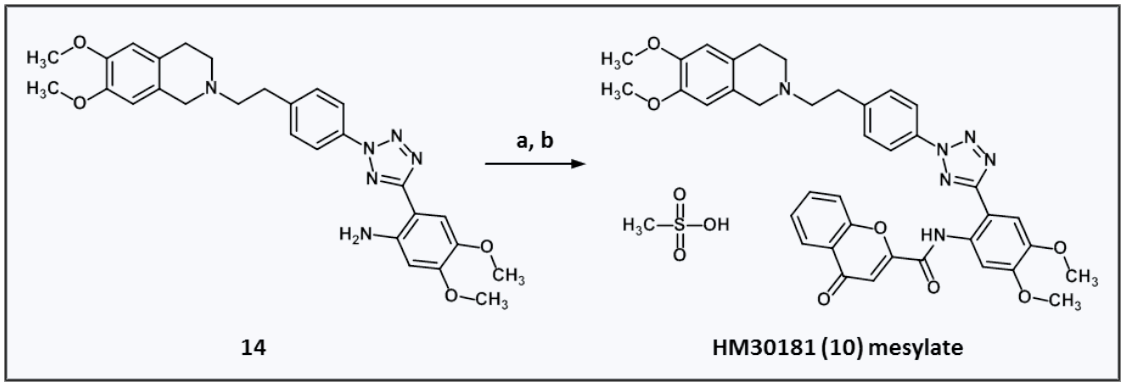

Fig. 15| Synthesis of HM30181 (10) mesylate (a) 4-oxo-4*H*-chromene-2-carboxylic acid, EDC•HCl, 4-DMAP, CH_2Cl_2, 0 °C → rt; (b) methanesulfonic acid, MeOH, rt;

IV.B.2 [^{11}C]Labelling Precursors

IV.B.2.a O-Desmethyl tariquidar

As described in chapter IV.A.2, a total synthesis approach for *O*-desmethyl tariquidar precursor was to be established. There are four potential positions for substitution of a methoxy moiety by a hydroxyl function, two in the "quinoline part" and two in the "isoquinoline part" of the molecule (Fig. 16).

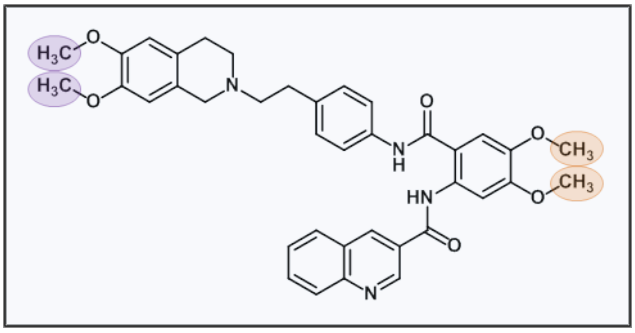

Fig. 16| Potential labelling positions in tariquidar (violet circles: labelling positions in "isoquinoline part", red circles: labelling positions in "quinoline part")

O-Desmethyl tetrahydroisoquinoline approach

Initially, an approach was followed to obtain a derivative with a free phenolic group in the "isoquinoline part" of the molecule. Therefore, starting from vanillin, an appropriate tetrahydroisoquinoline derivative should be synthesized. This approach was also pursued in a diploma thesis, which was performed earlier in our group [Poller, 2009]. In short, vanillin and aminoacetaldehyde dimethyl acetal were converted to compound **15** in a reductive amination reaction utilizing PtO_2 and hydrogen as catalyst and reductive agent, respectively. An acid-catalyzed ring closure yielded 7-methoxy-1,2,3,4-tetrahydroisoquinoline-4,6-diol hydrochloride (**16**·HCl), which was converted to 6-hydroxy-7-methoxy-1,2,3,4-tetrahydroisoquinoline hydrochloride (**17**·HCl) by catalytic hydrogenation with Pd/C as a catalyst in hydrochloric acid (Fig. 17) [Bobbit, 1965, Bobbit, 1968].

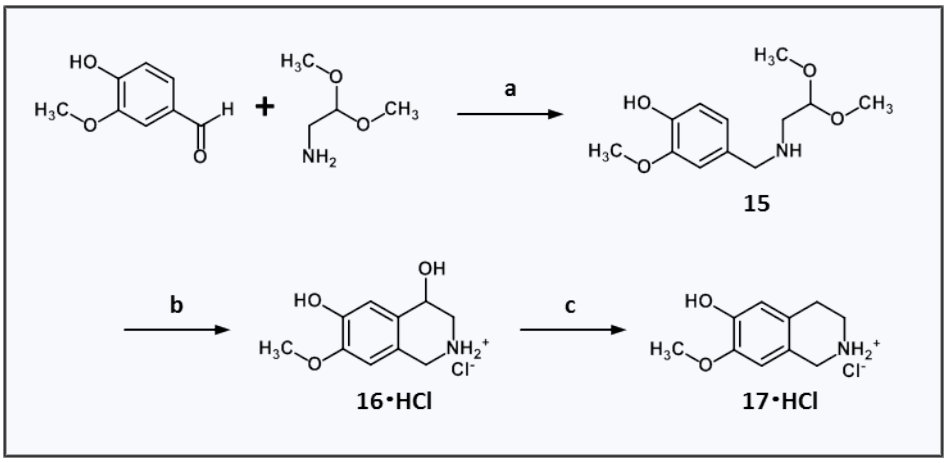

Fig. 17| Synthesis of Compound 17•HCl (a) PtO_2, H_2, EtOH, rt; (b) HCl, rt; (c) Pd/C, H_2, HCl, rt;

Subsequent reaction of **17**•HCl with 4-nitrophenethylbromide, K_2CO_3 and KI in *N,N*-dimethylformamide gave compound **18**, which was directly subjected to catalytic hydrogenation with Pd/C, hydrogen in ethanol to obtain the aniline derivative **19** (Fig. 18). The overall yield of these two steps was about 50 %, which corresponds to the value later published by Kawamura *et al.* [Kawamura, 2010], and implies a notable reduction of yield compared to the dimethoxy derivative **2**.

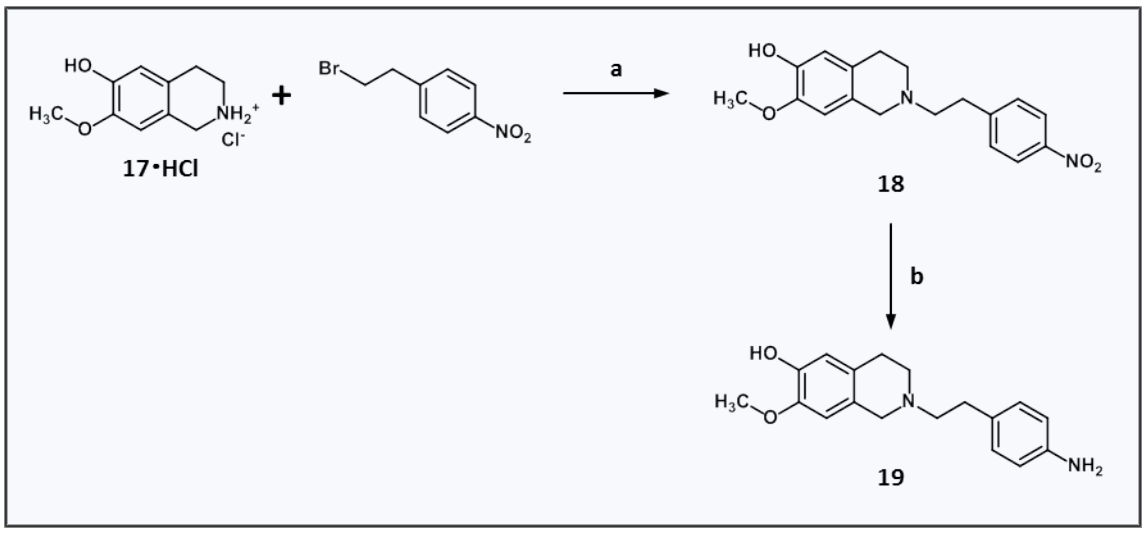

Fig. 18| Synthesis of Compound 19 (a) K_2CO_3, KI, DMF, 70 °C; (b) Pd/C, H_2, EtOH, rt;

Due to low yields at an early stage of this lengthy synthesis pathway and problems concerning the reliability of the synthesis of **17**•HCl, this synthesis approach was not further pursued. Further information regarding this synthesis can be found in the diploma thesis of Anna Poller [Poller, 2009].

O-Desmethyl anthranilic acid approach

An alternative position for the introduction of the required hydroxyl moiety is the anthranilic acid substructure in the "quinoline part" of tariquidar. A literature search soon revealed that a selective substitution of one methoxy moiety in 4,5-dimethoxy-2-nitrobenzoic acid by a hydroxyl group is possible [Joshi, 1986; Wéber, 2005]. For this purpose, 4,5-dimethoxy-2-nitrobenzoic acid was dissolved in 20 % aqueous KOH and was heated to reflux for 24 hours. Upon acidification of the cooled solution the desired product, 5-hydroxy-4-methoxy-2-nitrobenzoic acid (**20**), precipitated (Fig. 19).

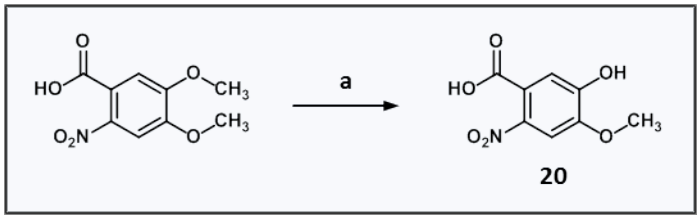

Fig. 19| Demethylation of 4,5-dimethoxy-2-nitrobenzoic acid (a) KOH, H_2O, reflux;

As attempts to directly couple **20** with **2** failed, the introduction of a suitable protective group for the phenolic moiety was pursued.

Acetyl protective group

The first strategy applied to protect the hydroxyl moiety was the introduction of an acetyl protective group at position five, by reacting **20** with acetic anhydride (Ac_2O) in pyridine (Fig. 20) [Joshi, 1986].

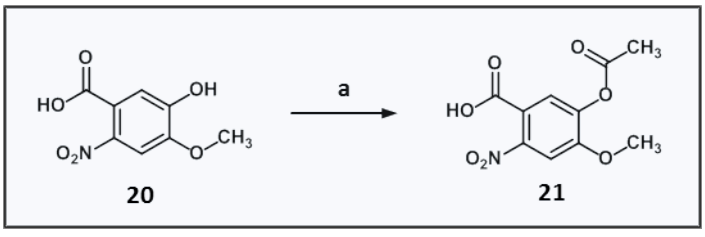

Fig. 20| Introduction of the acetyl protective group (a) Ac_2O, pyridine, 90 °C;

The acetyl-protected nitrobenzoic acid derivative **21** was then transformed to the corresponding acid chloride, by reaction with thionylchloride ($SOCl_2$). In the subsequent reaction, the acid chloride was coupled with aniline derivative **2** to obtain the benzamide derivative **22** in yields of about 68 %. In the following catalytic hydrogenation, first problems with this strategy became obvious, because deprotection of the acetyl protective group

occurred as a side reaction. Nevertheless, some product **23** could be isolated, which was directly reacted with 3-quinolinecarbonyl chloride to obtain an acetyl-protected *O*-desmethyl tariquidar derivative **24** (Fig. 21).

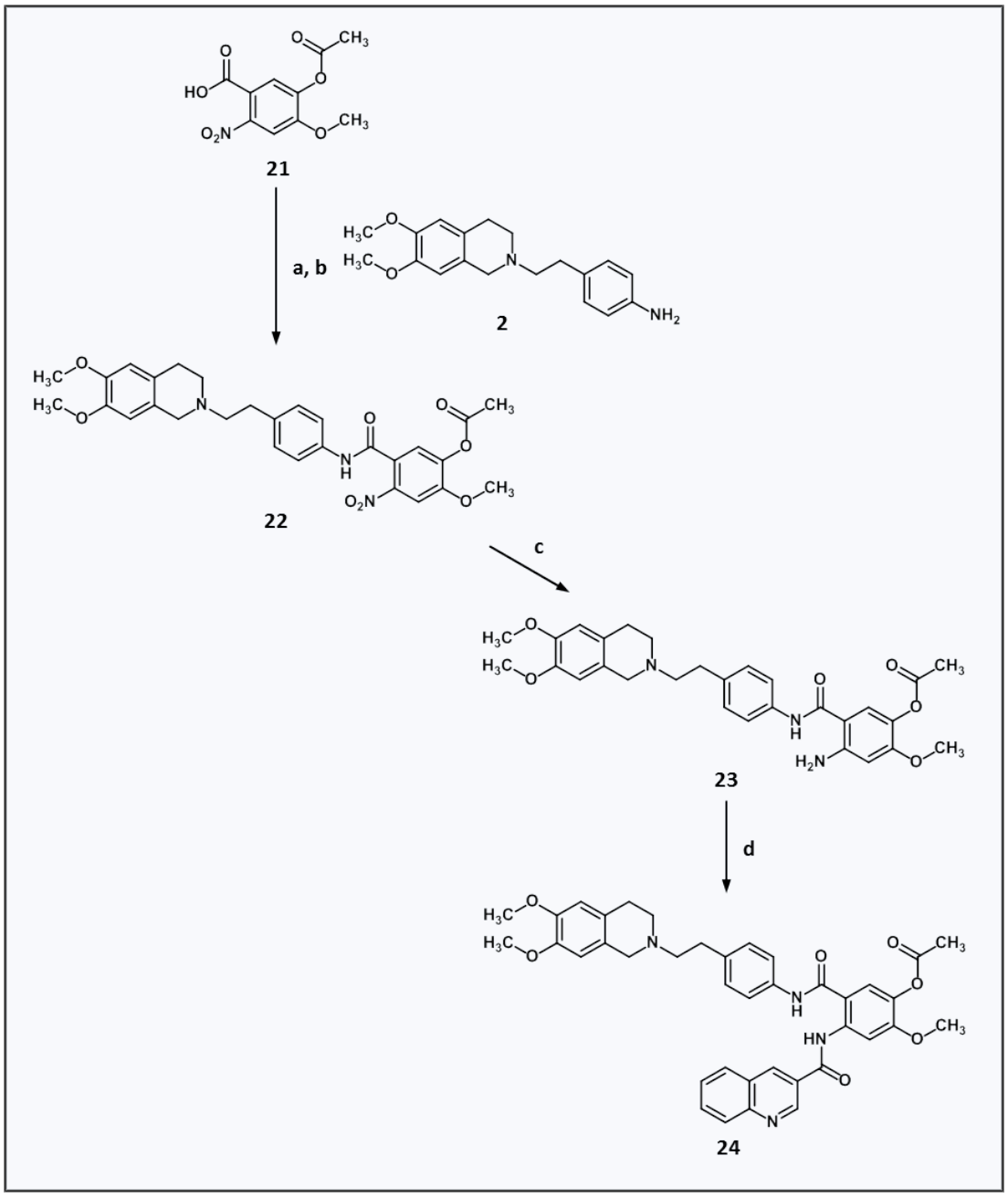

Fig. 21| Synthesis pathway for the acetyl-protected derivative of *O*-desmethyl tariquidar 24 (a) $SOCl_2$, reflux, (b) TEA, THF, 0 °C → rt; (c) Pd/C, H_2, MeOH, rt; (d) 3-quinolinecarbonyl chloride, TEA, THF, 0 °C → rt;

Experiments to deprotect compound **24** under basic conditions failed, but the protective group could be removed by heating the compound in a mixture of acetone and aqueous hydrochloric acid. Although the synthesis strategy, utilizing an acetyl protective group, initially looked very

promising, it proved to be ineffective due to the instability of the acetyl-protected anthranilic amide **23**.

Pivaloyl protective group

Regarding the instability of the acetyl protective group and the, by trend, beneficial influence of an ester-like protective group on the reactivity of the nitrobenzoic acid derivative, in an additional experiment, the acetyl protective group was to be replaced by a bulkier pivaloyl group.

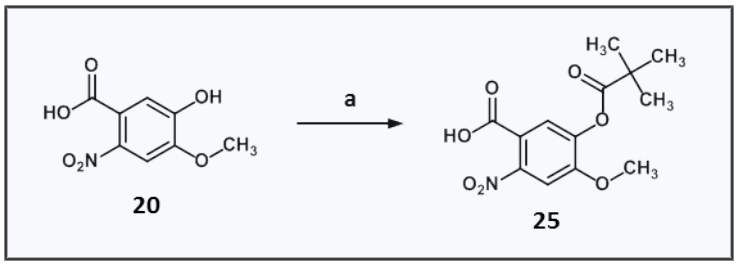

Fig. 22| Introduction of pivaloyl protective group (a) Piv_2O, Cs_2CO_3, DMF, 70 °C;

By reaction of compound **20** with pivalic anhydride and Cs_2CO_3 in anhydrous *N,N*-dimethyl-formamide , 4-methoxy-2-nitro-5-(pivaloyloxy)benzoic acid (**25**) was obtained (Fig. 22) [Choi, 2008]. Further reaction in $SOCl_2$ gave the corresponding acid chloride, which was then coupled with the aniline derivative **2** to generate the benzamide derivative **26**. Reduction of compound **26** with Pd/C and hydrogen gave the aniline derivative **27** in moderate yields. The pivaloyl-protected *O*-desmethyl tariquidar derivative **28** was obtained by reaction of compound **27** with 3-quinolinecarbonyl chloride (Fig. 23).

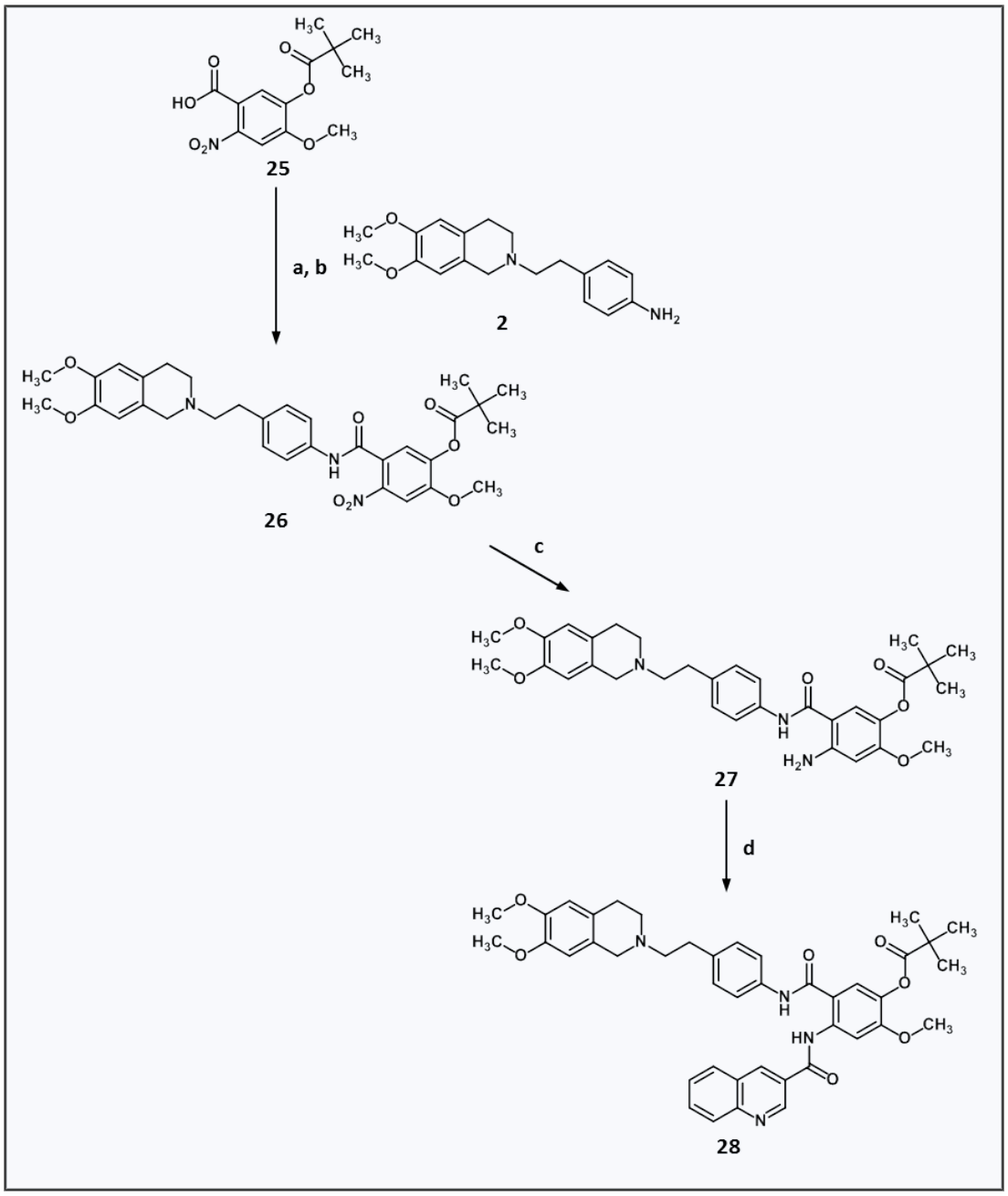

Fig. 23| Synthesis of pivaloyl-protected *O*-desmethyl tariquidar derivative 28 (a) $SOCl_2$, reflux, (b) TEA, THF, 0 °C → rt; (c) Pd/C, H_2, MeOH, rt; (d) 3-quinolinecarbonyl chloride, TEA, THF, 0 °C → rt;

In order to deprotect compound **28,** at first, similar conditions as for the deprotection of **24** were tried, but the removal of the protective group did not work properly using hydrochloric acid or several different basic reaction conditions ($NaOCH_3$, LiOH, and KOH). Instead, an aminolytic deprotection protocol was applied to remove the pivalic ester. Therefore, the protected *O*-desmethyl tariquidar derivative **28** was stirred in a 2M ethanolic solution of ammonia at 50°C (Fig. 24) until no starting material was observed on thin layer chromatography (TLC).

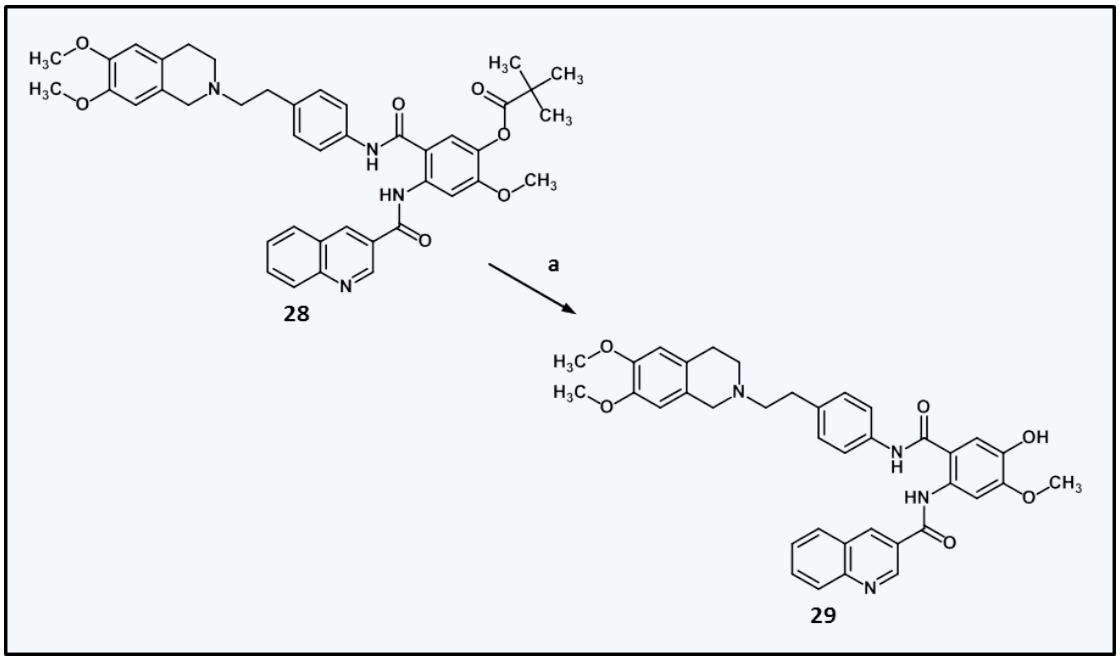

Fig. 24| Deprotection of compound 28 to obtain precursor 29 (a) NH_3 in EtOH, 50 °C;

By this approach sufficient amount of the precursor **29** was obtained to perform further experiments. Part of the precursor was converted to a sodium salt. To achieve this compound, **29** was suspended in water and dilute NaOH (0.053 M) was added until the solid had dissolved completely. Subsequently, the solvent was removed and the solid dried *in vacuo*.

Benzyl protective group

In order to optimize the synthesis of the tariquidar precursor **29,** efforts have been made later on, including the application of yet another protective group. This time a benzyl protective group was chosen. For the introduction of this protective group (Fig. 25), compound **20** was reacted with excess benzyl chloride (BnCl) and K_2CO_3 in DMF to obtain the dibenzylated derivative benzyl 5-(benzyloxy)-4-methoxy-2-nitrobenzoate (**30**) first, and then the benzyl ester was hydrolyzed with NaOH in ethanol and water [Bartolozzi, 2006] to obtain 5-(benzyloxy)-4-methoxy-2-nitrobenzoic acid (**31**).

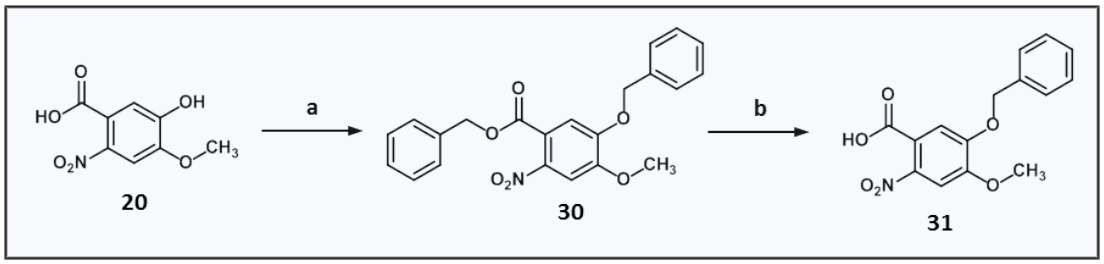

Fig. 25| Introduction of a benzylether as protective group (a) BnCl, K_2CO_3, DMF, 75 °C; (b) NaOH, EtOH, H_2O, rt;

By reaction with $SOCl_2$, compound **31** was converted to the corresponding acid chloride, which was subsequently reacted with aniline derivative **2** to obtain the benzamide derivative **32** (Fig. 26). The reduction of the nitro group was performed with Raney-Nickel as catalyst and hydrazine monohydrate as hydrogen source to prevent hydrogenolytic cleavage of the benzyl protective group [Batcho, 1985] and allow formation of the benzamide derivative **33** (Fig. 27). For the formation of *O*-benzyl tariquidar (**34**), two different approaches were tested. In a first variation, the anthranilamide derivative **33** was, like in previous experiments, reacted with 3-quinoline-carbonyl chloride to form an amide, resulting in yields of about 35 %. In a second experiment EDC•HCl was applied as a coupling reagent to form the benzyl-protected *O*-desmethyl tariquidar derivative **34** starting from 3-quinolinecarboxylic acid and **33** (Fig. 27). These reaction conditions led to a yield of about 64 %, which equals a nearly two-fold increase compared to the reaction with 3-quinolinecarbonyl chloride.

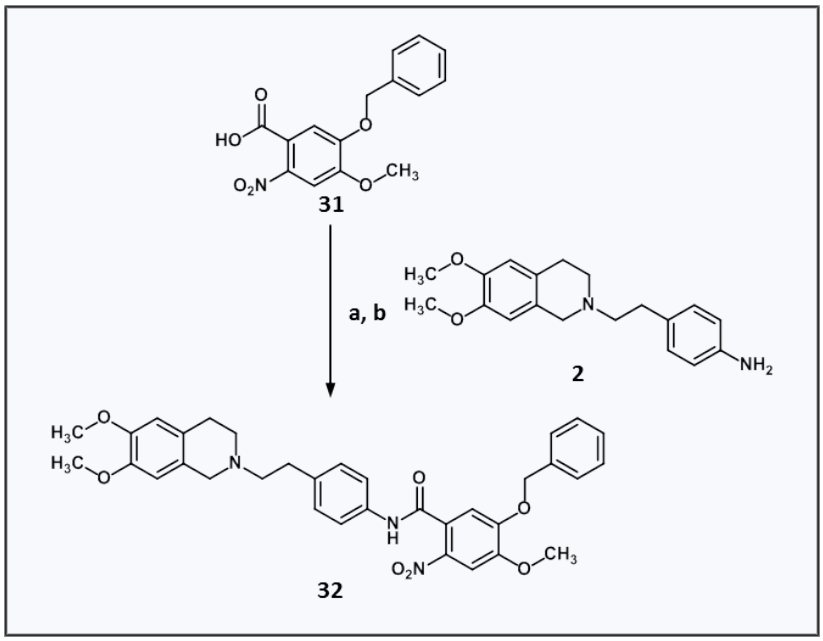

Fig. 26| Synthesis of compound 32 (a) $SOCl_2$, reflux, (b) TEA, THF, 0 °C → rt;

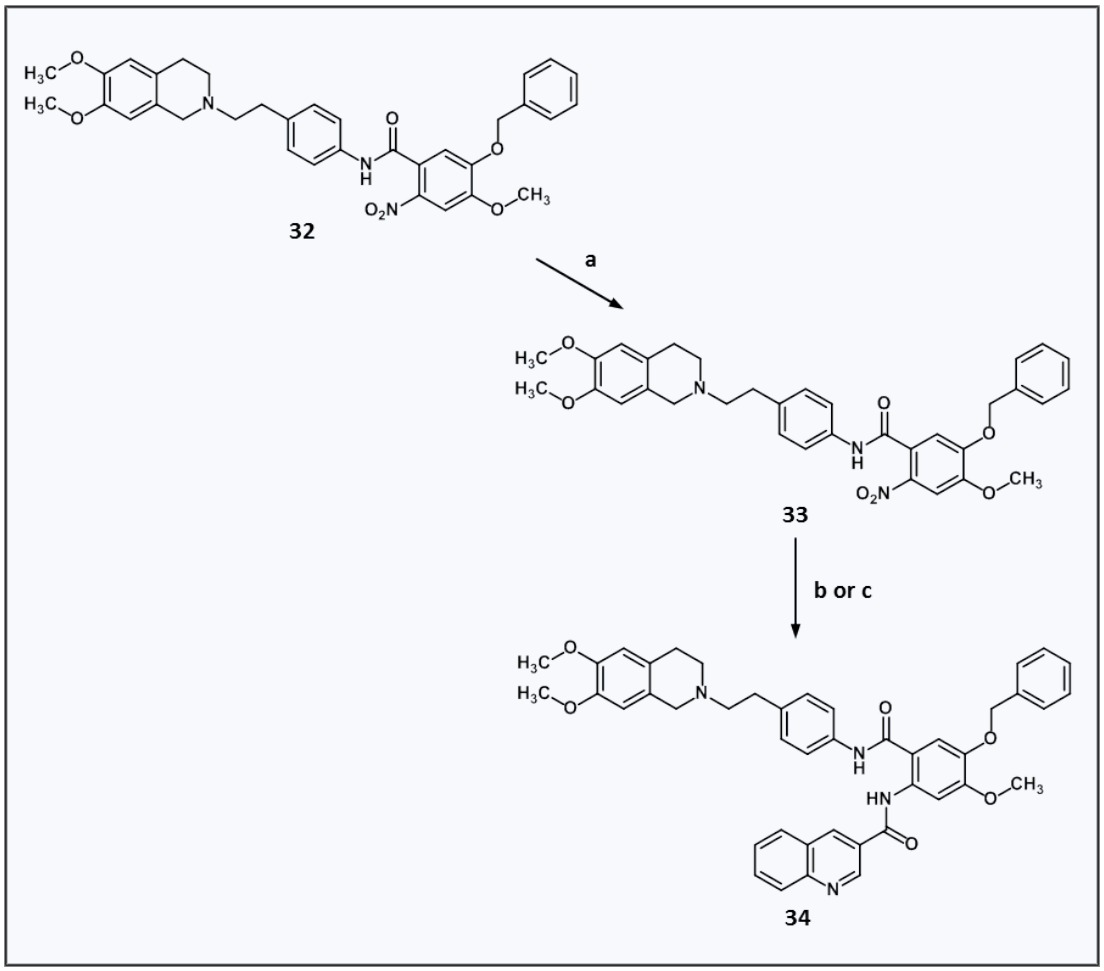

Fig. 27| Synthesis of benzyl-protected *O*-desmethyl tariquidar derivative 34 (a) Raney-Nickel, hydrazine•H_2O, EtOH, THF, reflux; (b) 3-quinolinecarbonyl chloride, TEA, THF, 0 °C → rt; (c) 3-quinolinecarboxylic acid, EDC•HCl, HOBt, 0 °C → rt;

Benzyl protective groups are generally cleaved by catalytic hydrogenation. Unexpectedly, the hydrogenolytic cleavage using common conditions (Pd/C and hydrogen) failed. Changing the catalyst to PtO_2 did not lead to the desired results either. In further experiments an acid catalyzed cleavage of the benzyl group, using trifluoroacetic acid and thioanisole [Kiso, 1980], was tried, but this strategy also did not yield the desired product **29**, although *O*-desmethyl HM30181 derivative **35** (Fig. 30) was obtained following this synthesis method (see chapter IV.B.2.b). Also, an attempt to cleave the benzyl ether by transfer hydrogenation using 1,4-cyclohexadiene as hydrogen source and Pd/C as catalyst [Felix, 1978] did not succeed.

IV.B.2.b O-Desmethyl HM30181

The synthesis of a radiolabelling precursor of HM30181 generally proceeded analogously to the synthesis of HM30181 with slight modifications of the reaction conditions.

In an initial step, 4-benzyloxy-5-methoxy-2-nirobenzaldehyde was reacted with toluenesulfonyl hydrazide to compound **36** (Fig. 28).

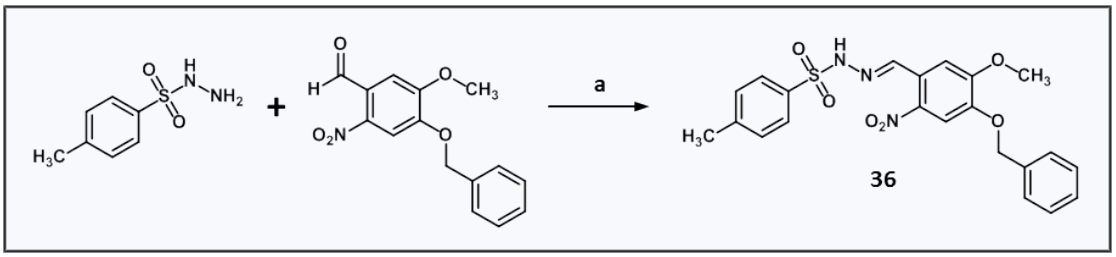

Fig. 28| Synthesis of compound 36 (a) EtOH, reflux → rt, H_2O;

In the following step, aniline derivative **2** was transformed to the corresponding diazonium salt **12**, which was further reacted with compound **36** to form the 2,5-disubstituted tetrazole derivative **37** (Fig. 29).

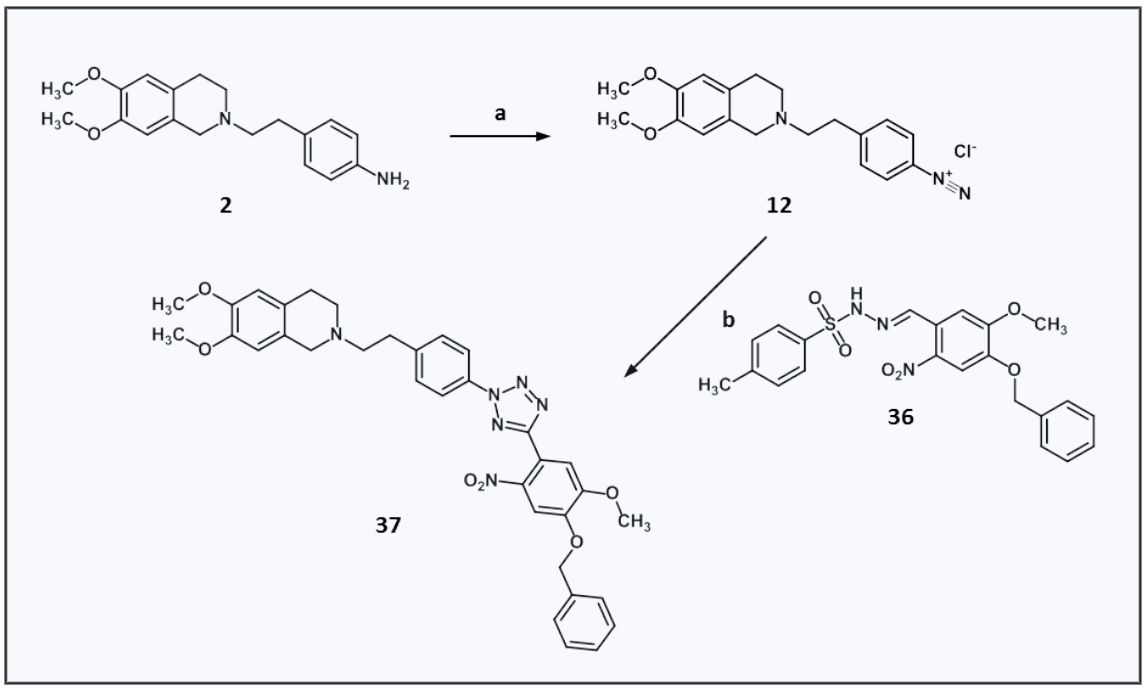

Fig. 29| Synthesis of compound 37 (a) $NaNO_2$, HCl, EtOH, H_2O, 0 °C; (b) pyridine, - 15 °C → rt;

Selective reduction of the nitrogroup, without cleavage of the benzyl ether, was accomplished by using Raney-Nickel as catalyst and hydrazine monohydrate as hydrogen source [Batcho, 1985], making compound **38** accessible. An amide coupling of compound **38** and 4-oxo-4*H*-chromene-2-carboxylic acid mediated by EDC•HCl and 1-hydroxybenzotriazole (HOBt) yielded *O*-benzyl HM30181 (**39**) (Fig. 30).

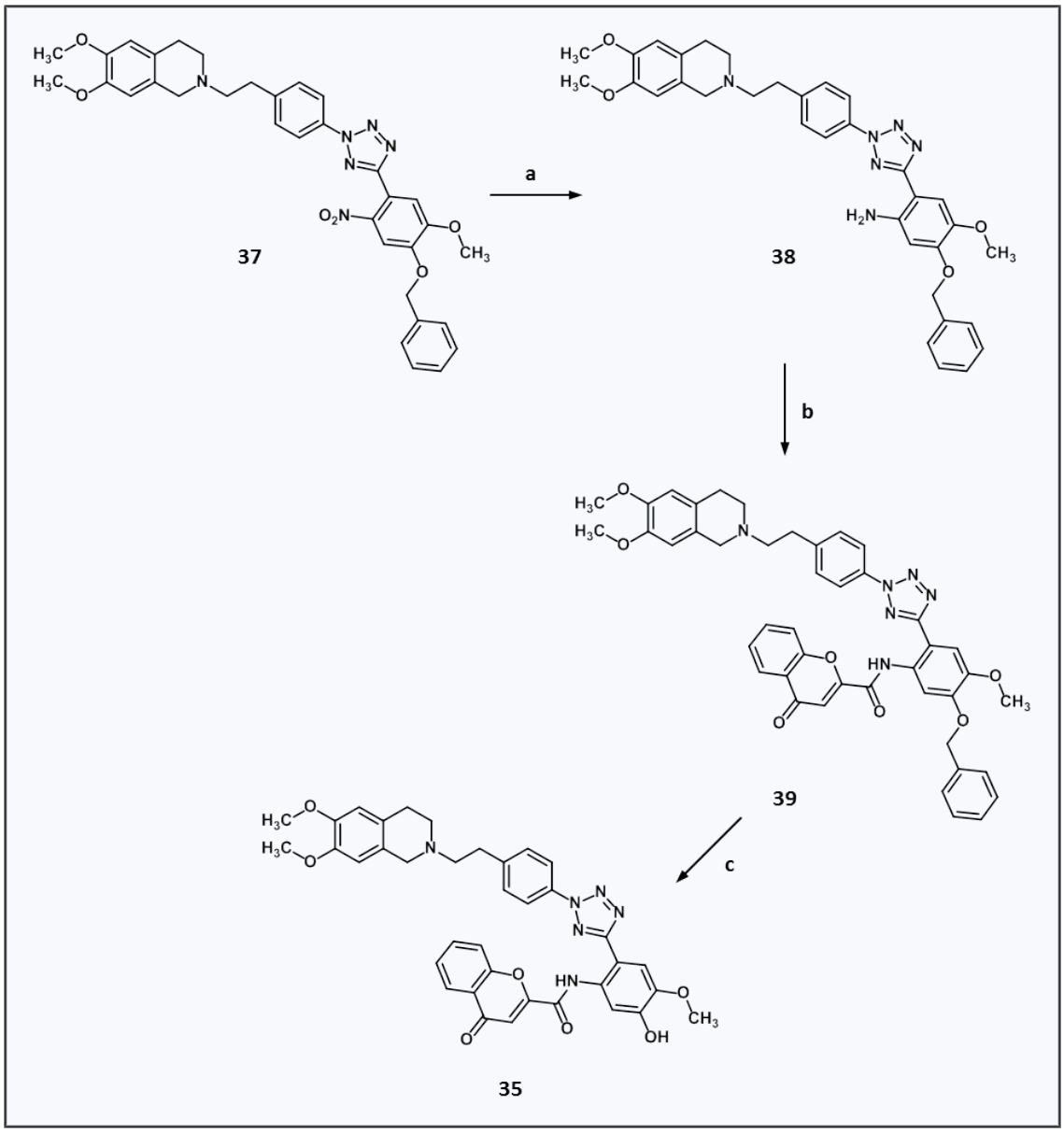

Fig. 30| Synthesis of O-Desmethyl HM30181 (35) (a) Raney-Nickel, hydrazine•H_2O, EtOH, THF, reflux; (b) 4-oxo-4*H*-chromene-2-carboxylic acid, EDC•HCl, HOBt, 0 °C → rt; (c) TFA, thioanisole, rt;

In a first approach, **39** was subjected to catalytic hydrogenation using Pd/C and hydrogen in an attempt to cleave the benzyl ether hydrogenolytically, but under these conditions no product could be isolated. In an alternative approach, the radiolabelling precursor *O*-desmethyl HM30181 **35** could be obtained by acid-catalyzed debenzylation with trifluoroacetic acid/thioanisole (Fig. 30) [Kiso, 1980].

IV.B.3 Additional derivatives

According to original plans, precursor molecules for ^{18}F-labelling of tariquidar were synthesized. Starting from the anthranilic amide derivative **4**, several fluorine-containing reference compounds and the appropriate radiolabelling precursors should be synthesized by reaction with different halogen-containing 3-quinolinecarboxylic acids or the corresponding acid chlorides.

Chlorotariquidar

The first candidate for an ^{18}F-labelling precursor of tariquidar was 2-chloro-3-quinoline-carboxylic acid (**40**). This quinoline derivative was synthesized starting form acetanilide *via* a Vilsmeier-Haack reaction (Fig. 31) [Meth-Cohn, 1981]. In brief, $POCl_3$ was slowly added to ice-cooled *N,N*-dimethylformamide, followed by the addition of acetanilide and heating for 16 hours. By pouring the reaction mixture on ice water, the intermediate was hydrolyzed to 2-chloroquinoline-3-carbaldehyde (**41**), which was subsequently oxidized to the desired carboxylic acid **40** using $AgNO_3$/KOH as oxidizing reagent.

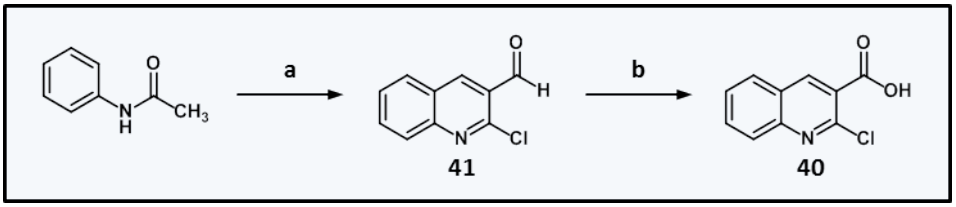

Fig. 31| Synthesis of compound 40 *via* Vilsmeier-Haack reaction and subsequent oxidation (a) DMF, $POCl_3$, 75 °C; (b) $AgNO_3$, KOH, EtOH, H_2O, rt;

Via reaction with $SOCl_2$, the acid **40** was converted into the corresponding carboxylic acid chloride, which was directly coupled with the antranilic amide derivative **4** to obtain the chlorotariquidar derivative **42** (Fig. 32).

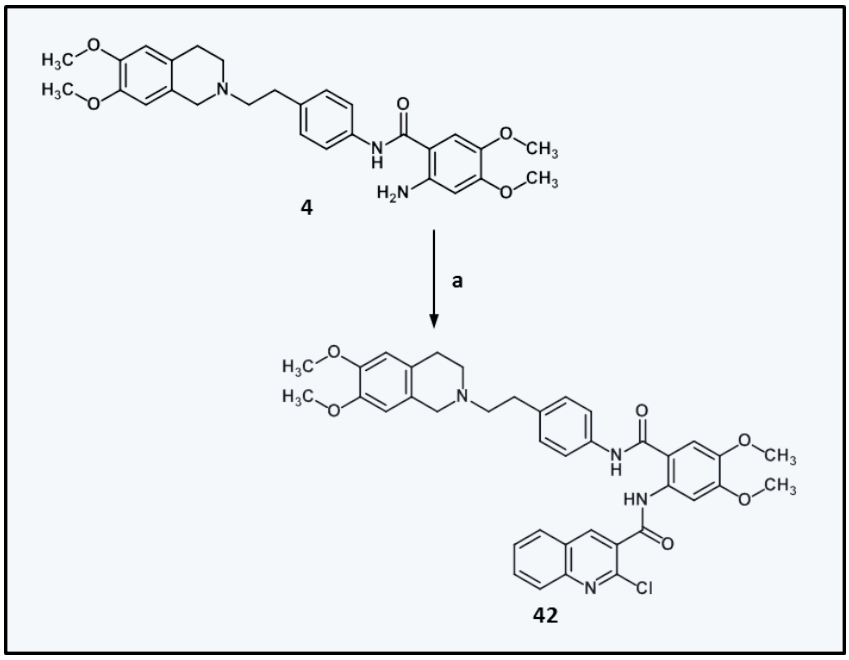

Fig. 32| Synthesis of compound 42 (a) 2-chloro-3-quinolinecarbonyl chloride, TEA, THF, 0 °C → rt;

N-Quarternized derivative of tariquidar

In a side project the impact of a positively charged group on the P-gp-inhibitory efficiency of tariquidar was investigated. The aim was to determine whether a tariquidar derivative containing a quaternary nitrogen function is still capable of inhibiting P-gp in order to possibly design a new series of non-absorbable P-gp inhibitors for topical medication.

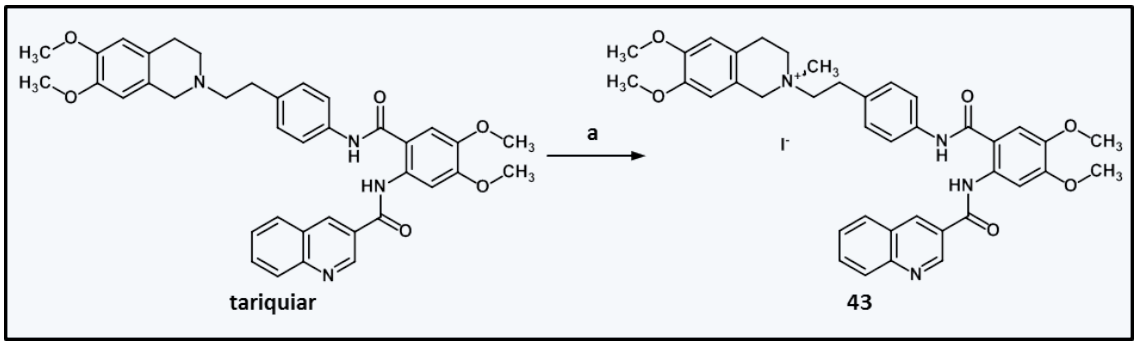

Fig. 33| Synthesis of compound 43, starting from tariquidar (a) MeI, acetone, 4 °C;

Therefore, iodomethane was added to a solution of tariquidar in dry acetone, which was kept at 4 °C until a white solid formed. The precipitate was collected and washed with acetone to obtain the quarternized tariquidar derivative **43** (Fig. 33).

IV.C Radiosynthesis

All radiosynthesis experiments for this thesis were performed at the Austrian Institute of Technology (AIT) in Seibersdorf (Austria) under supervision of Oliver Langer and with assistance of Johann Stanek and Severin Mairinger.

IV.C.1 General Remarks

Radiosynthesis was carried out in a TRACERlab FXC Pro synthesis module (GE Healthcare, Uppsala, Sweden) in a lead-shielded hot cell. The production of $[^{11}C]CH_4$ was achieved *via* the $^{14}N(p,\alpha)^{11}C$ nuclear reaction by irradiation of nitrogen gas containing 10% hydrogen using a PETtrace cyclotron equipped with a CH_4 target system (GE Healthcare, Uppsala, Sweden). $[^{11}C]CH_4$ was then converted, by transition through a heated I_2 column, to $[^{11}C]CH_3I$, which was further reacted to $[^{11}C]$methyl triflate by passage through a column containing silver-triflate impregnated graphitized carbon.

All radiochemical yields (RCY) are decay corrected and given in per cent relative to $[^{11}C]CH_4$, unless otherwise stated.

IV.C.2 [11C]Tariquidar

$[^{11}C]$Tariquidar was synthesized starting from the precursor **29** or the corresponding sodium salt by treatment with $[^{11}C]$methyl triflate (Fig. 34).

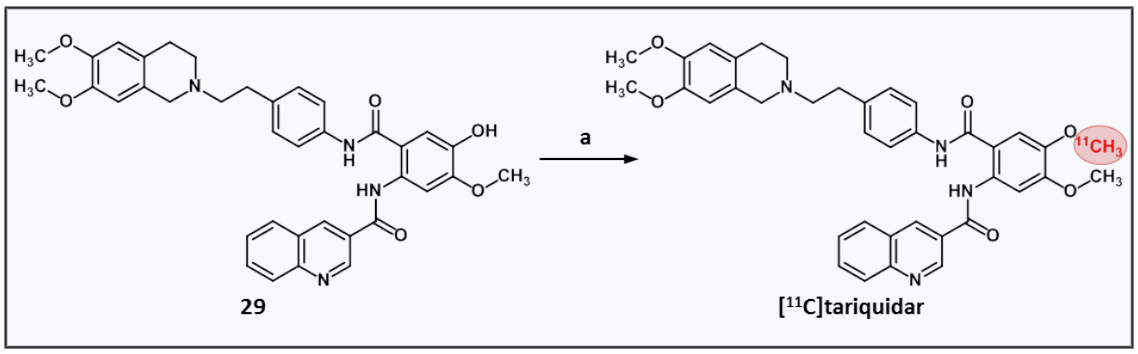

Fig. 34| Radiolabelling of precursor 29 to obtain [11C]tariquidar (a) $[^{11}C]$methyl triflate, NaOH, acetone, 60 °C;

In a first experiment, the sodium salt of **29** was dissolved in dimethylsulfoxide and the mixture was heated in the presence of $[^{11}C]$methyl triflate. Under these conditions, poor yields were obtained. In a second experiment, **29**·Na^+ was dissolved in acetone and aqueous NaOH and reacted with $[^{11}C]$methyl triflate at 60°C, resulting in a radiochemical yield of 9 %. To investigate the influence of the base on radiolabelling yield, one experiment was performed

without base, which gave no product at all. In the next experiment **29**·Na^+ was dissolved in dimethylsulfoxide and NaOH, which also afforded no product. After several reactions with the sodium salt of **29**, the corresponding free base was used in the reaction. Again the precursor was dissolved in acetone in the presence of NaOH. The resulting radiochemical yield was slightly lower than for the corresponding sodium salt. In the last experiment, a higher amount of NaOH was used, which led to a slight increase in radiochemical yield.

Experiment	Precursor[I]	Solvent	Base	Temperature	RCY [%][II]
1	compound **29** sodium salt	400 µL DMSO	-	60 °C	0.4
2	compound **29** sodium salt	500 µL acetone	10 µL 0.3 M NaOH	60 °C	9.0
3	compound **29** sodium salt	500 µL acetone	10 µL H_2O	60 °C	0
4	compound **29** sodium salt	500 µL DMSO	10 µL 0.3 M NaOH	60 °C	0
5	compound **29** free base	500 µL acetone	3 µL 0.3 M NaOH	60 °C	7.8 %
6	compound **29** free base	500 µL acetone	3 µL 0.6 M NaOH	60 °C	8.3 %

Tab. 1| Reaction conditions for the synthesis of [^{11}C]tariquidar [I] 0.3 – 0.7 mg; [II] decay-corrected, based on [^{11}C]CH_4

IV.C.3 [^{11}C]HM30181

Starting from *O*-desmethyl HM30181 ^{11}C-labelled HM30181 was synthesized by [^{11}C]methylation with [^{11}C]methyl triflate in presence of an appropriate base (Fig. 35). Different reaction conditions in terms of solvent composition, base and reaction temperature were applied in order to develop suitable radiolabelling conditions for [^{11}C]HM30181.

In a first attempt, precursor **35** was dissolved in a mixture of *N,N*-dimethylformamide and acetonitrile and tetrabutylammonium hydroxide (TBAH) in methanol was added as a base. After heating the reaction mixture to 50 °C for 5 minutes, the reaction was quenched with water and the mixture was subjected to purification on the built-in HPLC system, yielding 4.9 % radiochemical yield (decay-corrected).

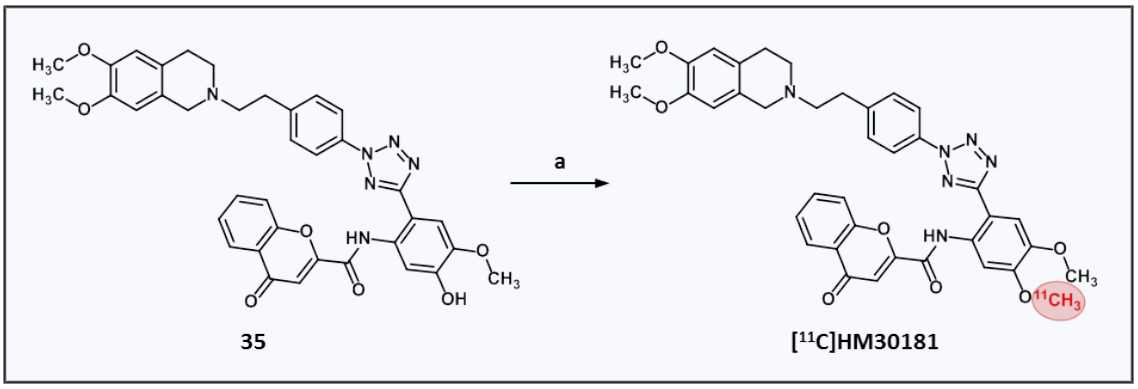

Fig. 35| Radiolabelling of precursor 35 to obtain [^{11}C]HM30181 (a) [^{11}C]methyl triflate, TBAH, DMF, MeCN, 75 °C;

In a next experiment, TBAH was replaced with NaOH, which gave no product at all. Replacing acetonitrile with acetone and increasing the amount of TBAH also resulted in decreased radiochemical yields. It was found that the initial conditions were almost ideal for the radiolabelling reaction, but slight improvements of the yield could be accomplished by reducing the amount of TBAH, elevating the reaction temperature to 75 °C and reducing the reaction time to 4 minutes. In a last experiment radiolabelling precursor was used as the hydrochloride salt instead of the free base, which resulted in a significantly reduced radiochemical yield.

Experiment	Precursor[I]	Solvent	Base	Temperature	RCY [%][II]
1	compound **35** free base	100 µL DMF + 400 µL MeCN	6 µL TBAH solution[III]	50 °C	4.9
2	compound **35** free base	100 µL DMF + 400 µL MeCN	10 µL 4M NaOH	50 °C	0
3	compound **35** free base	400 µL acetone + 100 µL DMF	10 µL TBAH solution[III]	50 °C	0.1
4	compound **35** free base	100 µL DMF + 400 µL MeCN	10 µL TBAH solution[IV]	75 °C	0.4
5	compound **35** free base	500 µL MeCN	10 µL TBAH solution[IV]	75 °C	0.2
6	compound **35** free base	100 µL DMF + 400 µL MeCN	5 µL TBAH solution[IV]	75 °C	5.6
7	compound **35** hydrochloride	100 µL DMF + 400 µL MeCN	5 µL TBAH solution[IV]	75 °C	1.2

Tab. 2| Different reaction conditions for the synthesis of [^{11}C]HM30181 [I] 0.3 – 0.7 mg; [II] decay-corrected, based on [^{11}C]CH_4; [III] 265 mg TBAH in 0.5 mL MeOH; [IV] 132 mg TBAH in 0.5 mL MeOH

V Bioevaluation

The bioevaluation studies presented in this thesis were performed at the AIT in Seibersdorf (Austria). The small-animal PET experiments were carried out by Claudia Kuntner, Thomas Wanek and Michael Sauberer. The experiments to determine the metabolism of [^{11}C]tariquidar and [^{11}C]HM30181 *in vivo* were performed by Severin Mairinger, Bernd Dörner and Florian Bauer.

V.A General

For the bioevaluation of the newly developed PET tracers, small-animal PET studies in female Sprague-Dawley rats and female transgenic FVB mice were performed. Paired PET scans before and after intravenous administration of a high dose of unlabelled P-gp inhibitor (tariquidar, 15 mg/kg, elacridar, 5 mg/kg) were performed in rats (Fig. 36) and single PET scans were performed in mice. As part of the small-animal PET studies, the metabolic stability of the tracers was determined in separate groups of animals. The biological evaluation of [^{11}C]tariquidar and [^{11}C]HM30181 has been described in greater detail in the thesis of Thomas Wanek [Wanek, 2013].

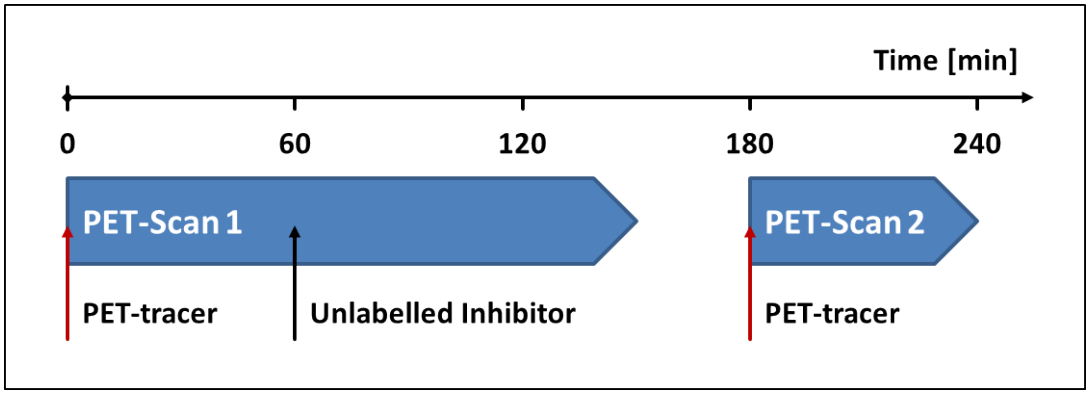

Fig. 36| General setup for small-animal PET scans in rats

V.B Results

V.B.1 [^{11}C]Tariquidar

The baseline scans for [^{11}C]tariquidar in female Sprague-Dawley rats revealed that the brain uptake of this tracer was very low. At 0.5 to 1.3 minutes after tracer injection a peak brain

activity uptake of 0.7 SUV (standardized uptake value) was reached, but at 25 minutes after tracer injection the brain activity uptake had reached a plateau at 0.2 SUV. This level remained steady until administration of a P-gp saturating dose of unlabelled inhibitor (Fig. 37), either tariquidar (15 mg/kg) or elacridar (5 mg/kg). The injection of the inhibitors led to an immediate steep increase in brain activity uptake of [^{11}C]tariquidar to 0.4 SUV for tariquidar and 0.7 SUV for elacridar. The second scan was started two hours after injection of the unlabelled inhibitors. Herein the brain activity uptake reached 2.9 times (tariquidar) and 4.3 times (elacridar) higher levels than in the baselinescan. Blood activity levels remained unchanged throughout the scans, regardless of the administration of unlabelled inhibitor.

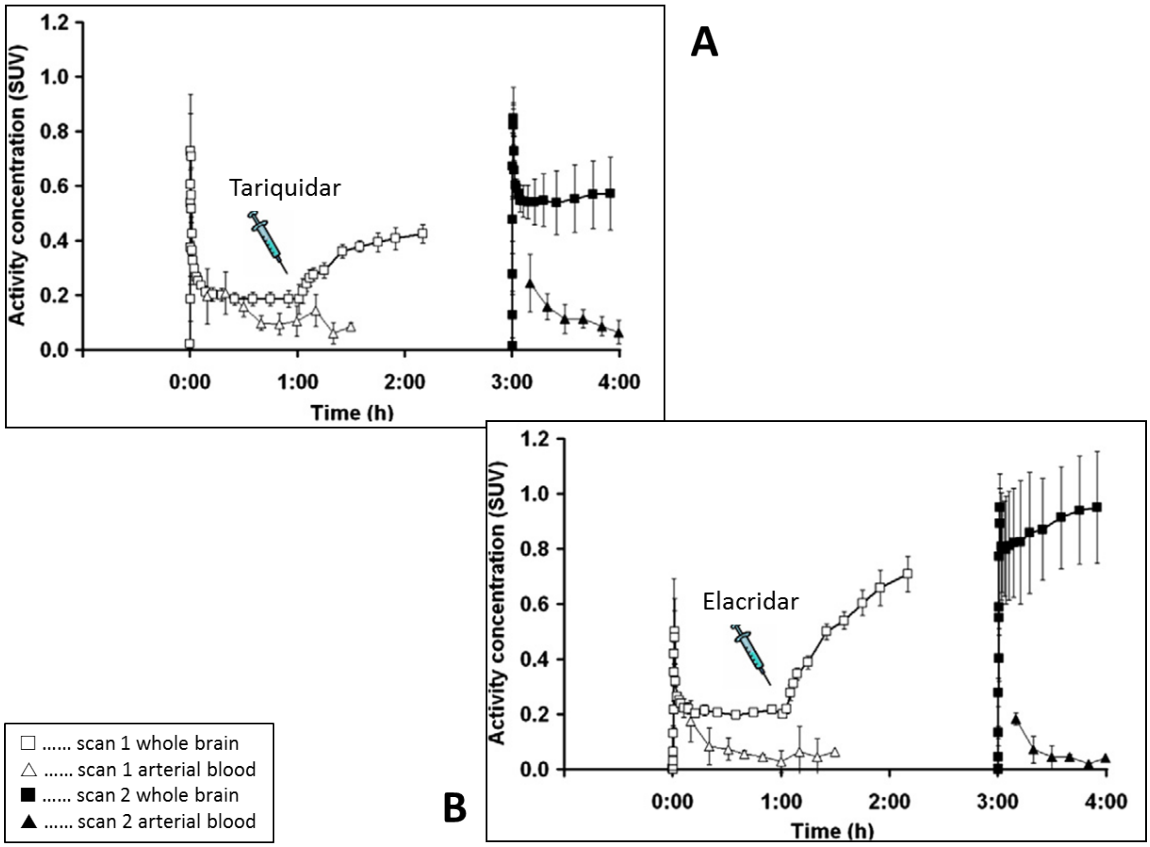

Fig. 37| Time-activity curves of [^{11}C]tariquidar in whole rat brain

The PET summation images reflect the low brain uptake of [^{11}C]tariquidar before and the increased brain activity uptake after injection of the unlabelled inhibitors (Fig. 38).

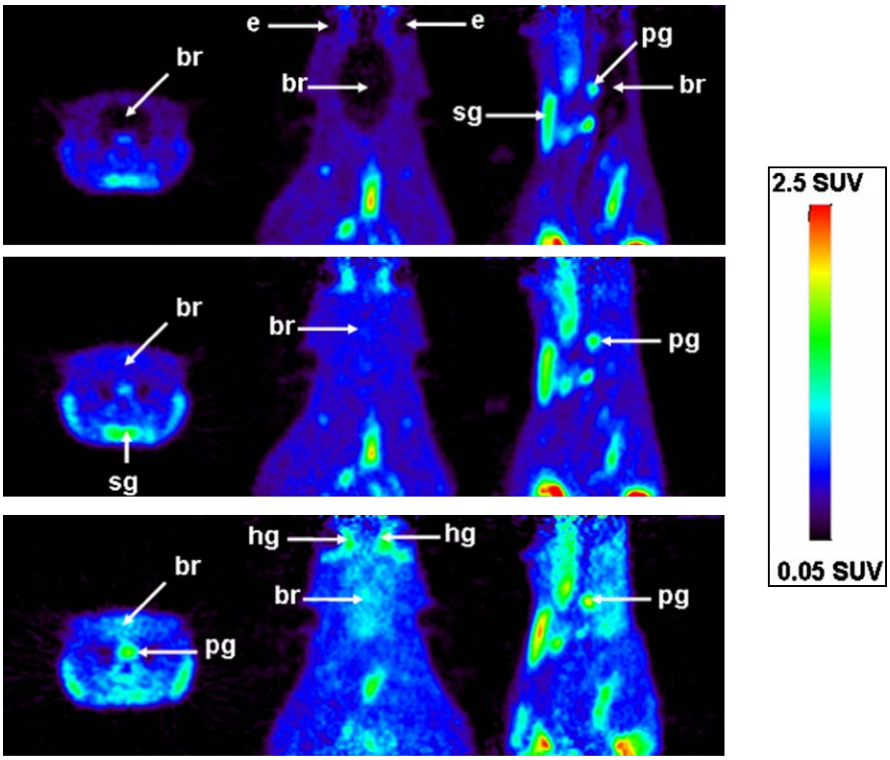

Fig. 38| PET summation images of [^{11}C]tariquidar in rats (upper row: baseline scan; middle row: after 15 mg/kg tariquidar; lower row: after 5 mg/kg elacridar). Anatomical structures are labelled with arrows (br, brain; e, eye; hg, haderian gland; pg, pituitary gland; sg, submandibular gland)

For the further evaluation of [^{11}C]tariquidar, single small-animal PET scans in female FVB mice (wild type, *Mdr1a/b*$^{(-/-)}$, *Bcrp1*$^{(-/-)}$ and *Mdr1a/b*$^{(-/-)}$*Bcrp1*$^{(-/-)}$) were performed. Blood activity levels were determined in a separate group of animals which did not undergo PET scanning. Brain activity uptake in transporter knockout mice was higher compared to wild type animals with highest increase seen in *Mdr1a/b*$^{(-/-)}$*Bcrp1*$^{(-/-)}$ mice (Fig. 39, Fig. 40). At 25 minutes after tracer injection the brain-to-blood activity ratios were 3.4 times higher in *Mdr1a/b*$^{(-/-)}$, 1.8 times higher in *Bcrp1*$^{(-/-)}$ and 14.5 times higher in *Mdr1a/b*$^{(-/-)}$*Bcrp1*$^{(-/-)}$ compared to wild type animals.

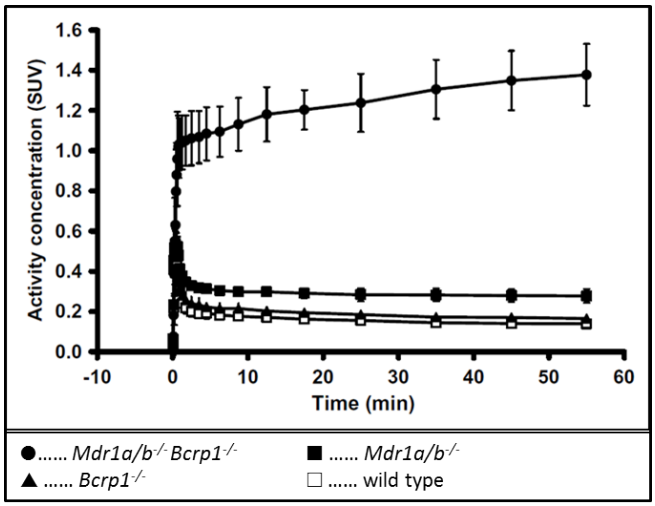

Fig. 39| Time-activity curves of [^{11}C]tariquidar in whole mouse brain

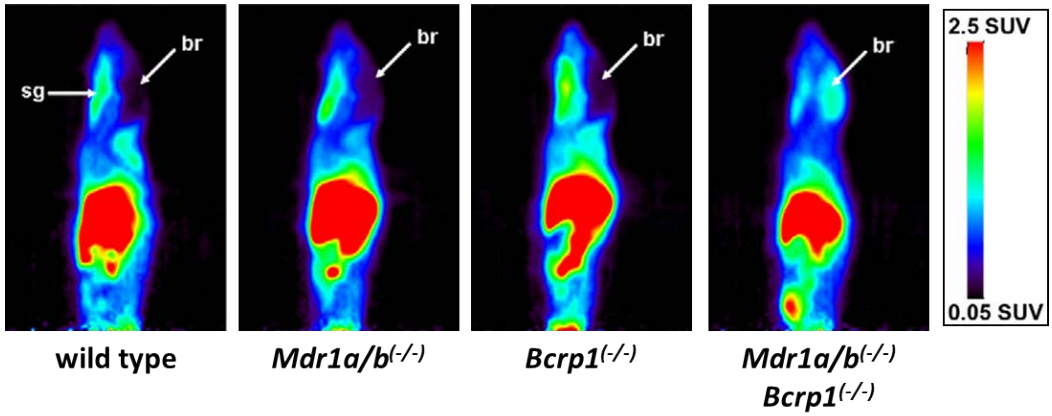

Fig. 40| PET summation images of [^{11}C]tariquidar in wild type and transporter knockout mice (br, brain; sg, submandibular gland)

For the analysis of radiometabolites of [^{11}C]tariquidar in rat plasma a previously described solid-phase extraction (SPE) assay [Abrahim, 2008] was used. At 20 minutes after tracer injection 4 ± 4 % of total plasma radioactivity was in the aqueous fractions of the SPE assay, corresponding to polar radiometabolites, while 96 ± 4 % were recovered in the methanol fraction. After 60 minutes 4 ± 5 % of the total activity were found in the aqueous phase and 96 ± 5 % in the methanol fraction. HPLC-analysis of the methanol fractions revealed that unchanged [^{11}C]tariquidar was the only radioactive species.

V.B.2 [^{11}C]HM30181

[^{11}C]HM30181 was only assessed in female FVB mice (wild type, *Mdr1a/b*$^{(-/-)}$, *Bcrp1*$^{(-/-)}$ and *Mdr1a/b*$^{(-/-)}$*Bcrp1*$^{(-/-)}$). Brain-to-blood activity ratios were 1.9 in wild type, 2.8 in *Mdr1a/b*$^{(-/-)}$and

2.6 in *Bcrp1*$^{(-/-)}$ mice. In *Mdr1a/b*$^{(-/-)}$*Bcrp1*$^{(-/-)}$ animals a brain-to-blood ratio of 8.9 was determined, which was significantly higher compared to wild type and single transporter knockout mice (Fig. 41, Fig. 42). Blood activity concentrations were determined at 60 minutes after tracer injection in a separate group of animals, which did not undergo small-animal PET scans. They were in a range of 0.1 to 0.2 SUV and did not differ significantly in the various mouse types.

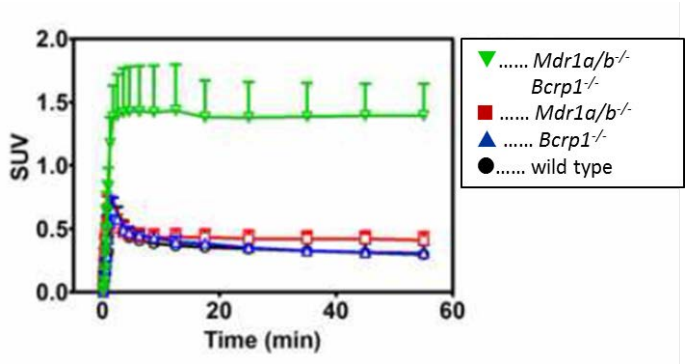

Fig. 41| Time-activity curves of [^{11}C]HM30181 in whole mouse brain

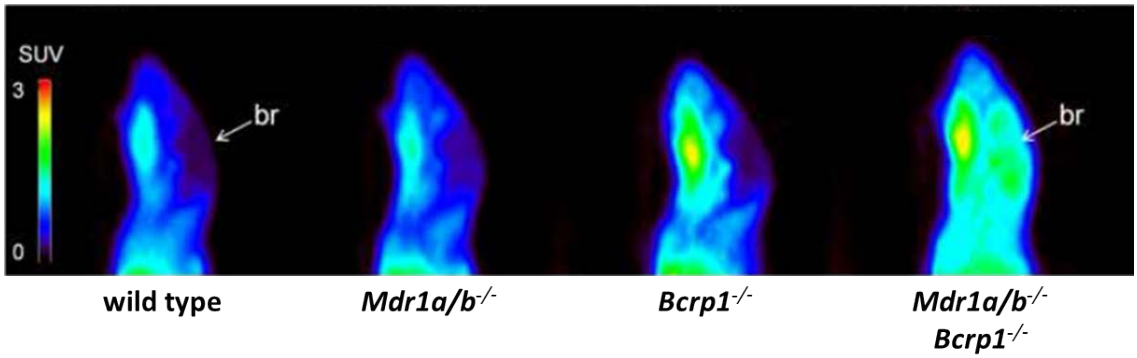

Fig. 42| PET summation images of [^{11}C]HM30181 in wild-type and transporter kncokout mice (br, brain)

To determine the metabolic stability of [^{11}C]HM30181, bloodsamples were collected in a separate group of animals, which did not undergo PET scanning. The analysis of the blood samples by the SPE assay and subsequent TLC showed that at 30 minutes after tracer injection 33 ± 4 % of the total plasma activity was in the form of polar radiometabolites of [^{11}C]HM30181.

V.B.3 Unlabelled HM30181

To investigate the ability of unlabelled HM30181 to inhibit cerebral P-gp, (*R*)-[^{11}C]verapamil PET scans in wild-type FVB mice were performed after pretreatment with different doses of

unlabelled HM30181 (10 mg/kg and 21 mg/kg) at three different time points before tracer injection (120, 60 and 10 minutes). These PET scans showed no significant difference in (*R*)-[^{11}C]verapamil brain uptake compared to untreated controls. In two animals the administration of 21 mg/kg HM30181 immediately led to death and therefore no further experiments with this dose group were performed.

VI Discussion

VI.A Chemistry

After choosing a promising tracer candidate, it was necessary to decide which labelling method would be the best choice for this molecule. The first objective was to develop a [^{11}C]tracer. Upon completion of this task it was planned to synthesize an ^{18}F-labelled derivative of the same molecule. The [^{18}F]tracer was not pursued any longer, because the results from the biological evaluation of [^{11}C]tariquidar did not meet our original expectations. Since tariquidar contains four methyl ether groups, it was decided to introduce the ^{11}C-label by [^{11}C]methylation. Initially, there have been preferences to introduce of the ^{11}C-label into the isoquinoline substructure of the molecule (Fig. 43), as this substructure is also part of elacridar, for which a [^{11}C]tracer was developed in parallel [Dörner, 2012].

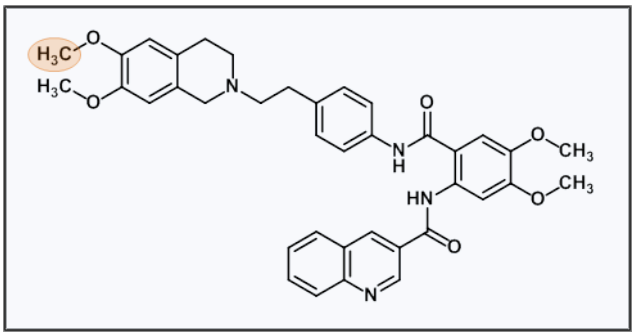

Fig. 43| Labelling position in isoquinoline substructure of tariquidar (red circle)

Therefore, the establishment of synthesis of the isoquinoline building block with a free phenolic OH group was of interest. On the other hand, this labelling strategy would have introduced changes into the well-established synthesis route of tariquidar early on in the synthesis scheme. Either the free phenol or some kind of protecting group would have been present during the whole course of the reaction. The experiments performed showed that the average yields for each of the first two synthesis steps were reduced by 20%, which gives an overall loss of yield of about a third for the first two steps of the common synthesis pathway. Additionally, the preparation of the isoquinoline derivative **17** requires three additional steps with poor overall yield. Due to these first results, an alternative approach for the synthesis of a precursor for [^{11}C]methylation was considered favorable.

The second possible position for the introduction of a hydroxyl moiety is the antranilic amide substructure of the molecule (Fig. 44). Research in literature revealed that it is possible to remove the methyl ester in position five of 4,5-dimethoxy-2-nitrobenzoic acid selectively by

treatment with potassium hydroxide [Joshi, 1986]. Access to this building block enabled a new approach to design the desired precursor molecule for the preparation of [^{11}C]tariquidar.

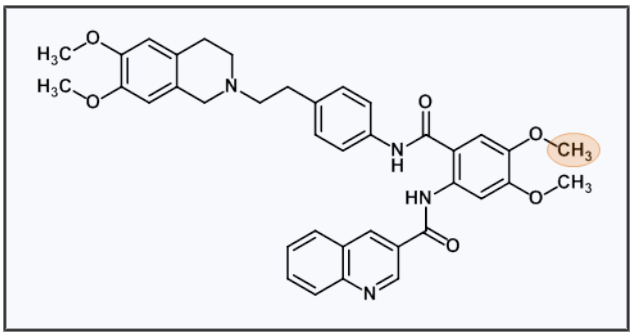

Fig. 44| Labelling position in anthranilic amide substructure of tariquidar (red circle)

Initially, there have been attempts to carry out the coupling of the phenolic nitrobenzoic acid derivative and the amine **2** to the appropriate amide without protecting the phenol moiety. It soon became obvious, that the free phenol had adverse effects on the reactivity of the benzoic acid derivative. It was, for example, not possible to isolate the desired product when reacting **20** with thionylchloride to the corresponding acid chloride and subsequent conversion to an amide with **2** (Fig. 45).

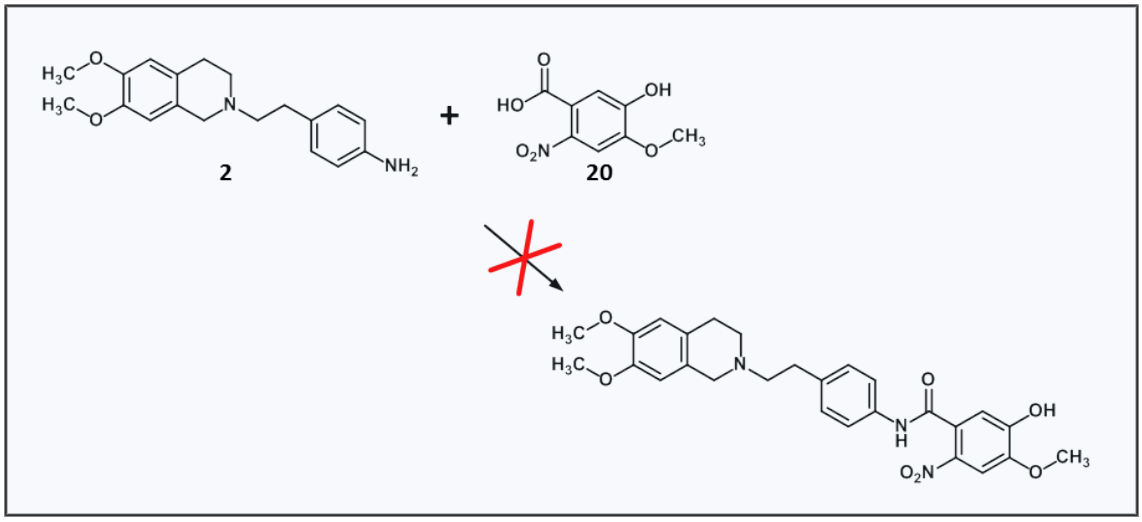

Fig. 45| Direct coupling of the compounds 2 and 20

Another potential pitfall is the possibility that the molecules might form inner salts due to the presence of the free phenol and a basic nitrogen atom in the side chain. This could lead to solubility issues and thus, to potential drawbacks in the synthesis and work-up procedures. Therefore, it was decided early on to use protective groups to avoid potential problems (Fig. 46).

Due to the diverse reaction conditions necessary to obtain the desired product, the choice of a suitable protective group was substantial. The protective group had to be stable in the presence of thionyl chloride and potential acidic conditions. It was also crucial that the protective group would not be cleaved during catalytic hydrogenation, either hydrogenolytically or by an amine, which was the product of the reduction.

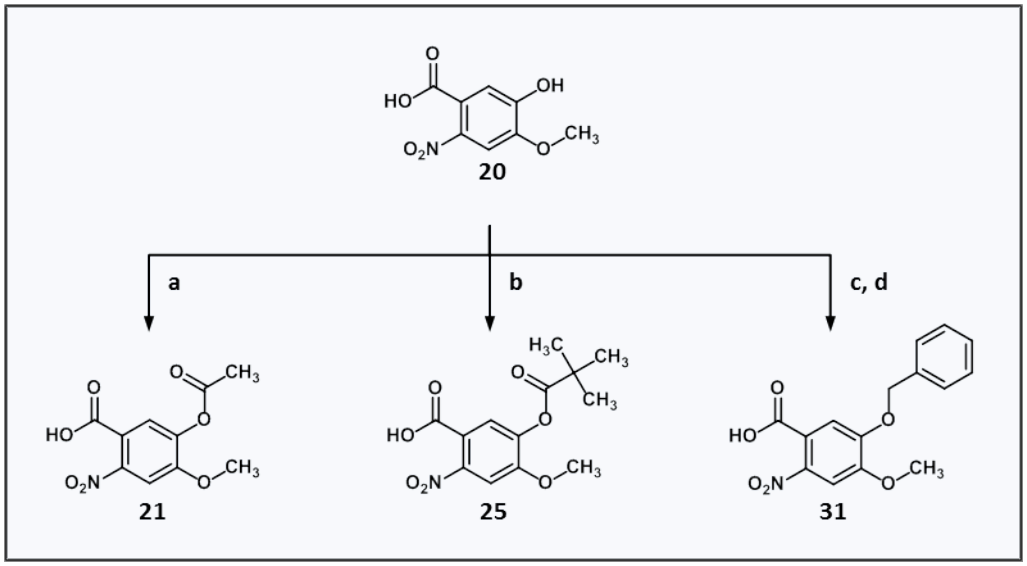

Fig. 46| Introduction of protective groups for phenol moiety of compound 20 (a) Ac_2O, pyridine, 90 °C; (b) Piv_2O, Cs_2CO_3, DMF, 70 °C; (c) BnCl, K_2CO_3, DMF, 75 °C; (d) NaOH, EtOH, H_2O, rt;

At first, the utilization of an acetyl protective group was considered (Fig. 46). Although this protective group is generally considered to be unstable under mild basic conditions, preliminary experiments with a fragment of the desired molecule revealed that in the given compound the acetyl protective group was actually stable under these conditions. It was possible to convert nitrobenzoic acid derivative **21** to the corresponding acetyl-protected benzoyl chloride derivative and react this compound with the amine **2** to the amide **22** in good yields. During the subsequent catalytic hydrogenation the acetyl protective group proved to be unstable in the presence of the primary aromatic amine formed during the course of the reaction. Therefore, hardly any pure amine **23** could be isolated. Additional observations suggested that, in solution, the acetyl protective group was readily cleaved by the amine moiety which rendered purification and even the measuring of a ^{13}C-NMR spectrum unfeasible. Nevertheless, the reactivity during the formation of the amide seemed to be slightly improved in comparison to the synthesis of the reference compound. For that reason it appeared to be rational to retain an ester as a protective group.

It was tried to enhance the stability of the protective group, especially against the aminolysis during the catalytic hydrogenation, by the introduction of a bulkier side chain. To achieve this, the pivalic ester **25** was prepared (Fig. 46). As expected, the stability of this protective group was markedly improved as compared to the previously used acetyl protective group. The pivalic ester proved to be stable during catalytic hydrogenation as well as during the synthesis of the pivaloyl-protected tariquidar derivative **28**. The pivaloyl protective group could not be cleaved by treatment with alkali carbonates or alkali hydroxides. It was also not possible to cleave the pivalic ester under acidic conditions. Heating the pivaloyl-protected tariquidar derivative **28** in an ethanolic ammonia solution finally gave the desired precursor molecule **29**.

There have also been experiments using benzyl ether as a protective group (Fig. 46). The most prominent obstacle in this synthesis pathway was the reduction of the nitro group to an amine by catalytic hydrogenation, as this type of reaction represents the most commonly used deprotection method for benzyl ethers. Besides this problem, the introduction of an ether protective group proved to be more time-consuming in this case because it was not possible to benzylate the phenol in nitrobenzoic acid derivate **20** selectively in the presence of the carboxylic acid function. This required an additional reaction step to cleave the formed benzyl ester, which was achieved by treating compound **30** with dilute NaOH solution [Bartolozzi, 2006]. Harsher conditions would have resulted in a cleavage of the benzyl ether as well, due to the nitro group in para position which allowed the selective demethylation of 4,5-dimethoxy-2-nitrobenzoic acid beforehand. The further reaction conditions had to be adapted with regard to the supposed instability of the protective group during catalytic hydrogenation using Pd/C and H_2. Research in literature showed that by inactivation or poisoning of Pd/C or by utilization of alternative catalysts, the reduction of a nitro group to an amine is possible in the presence of a benzyl ether without cleaving it. The further reactions provided moderate yields but the benzyl-protected tariquidar derivative **34** could be synthesized. However the deprotection of compound **34** to obtain the precursor **29** did not succeed (Fig. 47).

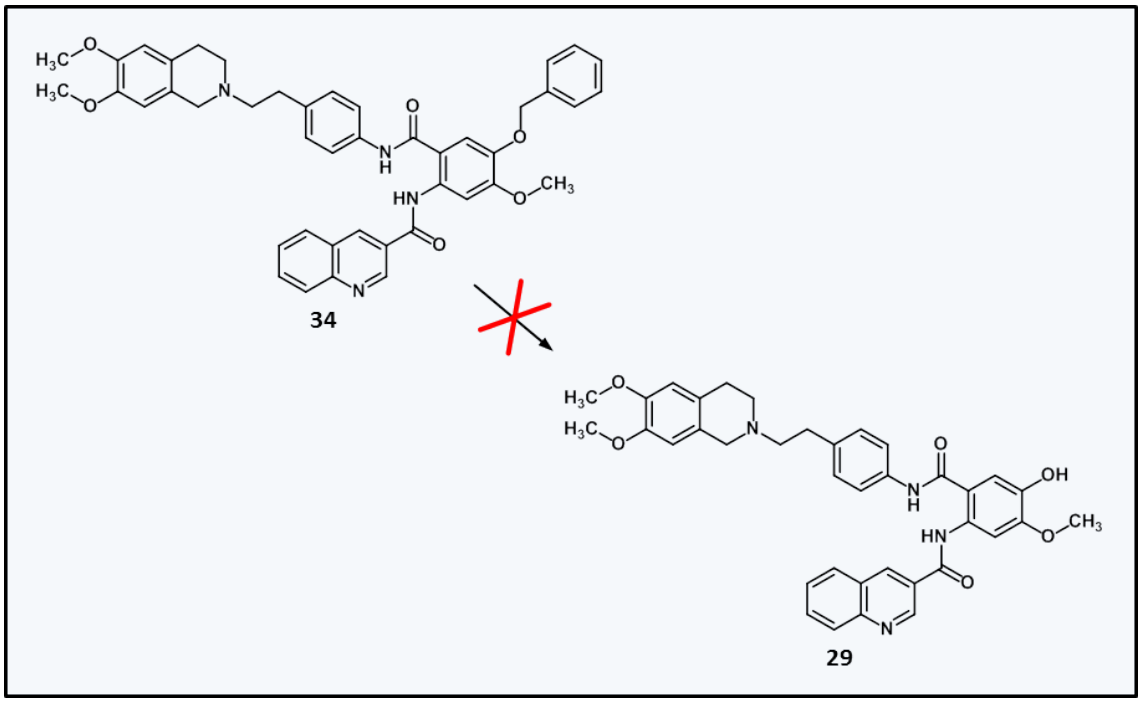

Fig. 47| Deprotection attempts of compound 34 did not yield isolatable radiolabelling precursor 29

Against expectations the benzyl ether remained stable under standard conditions (Pd/C and H_2). Using activated PtO_2 as an alternative catalyst could not solve this problem. Also, the attempt to cleave the protective group by transfer hydrogenation (1,4-cyclohexadiene and Pd/C) [Felix, 1978] did not succeed. As a last point it was tried to cleave the benzyl ether *via* treatment with trifluoroacetic acid and thioanisole [Kiso, 1980], but under these conditions no pure product could be isolated either. For this reason, the strategy to use a benzyl ether protective group was no longer pursued.

Another consideration was to synthesize a tariquidar derivative containing a dioxolane structure in the anthranilic amide substructure. This ring should further be cleaved at the end of the synthesis to generate an *O*-desmethyl derivative of tariquidar (Fig. 48). This strategy was not followed for two principal reasons. First, it did not seem possible to cleave the dioxolane ring in a manner to guarantee that only one specific synthesis product would be formed. And secondly, the strategy using a pivalic ester as a protection group, which was pursued simultaneously, showed promising results.

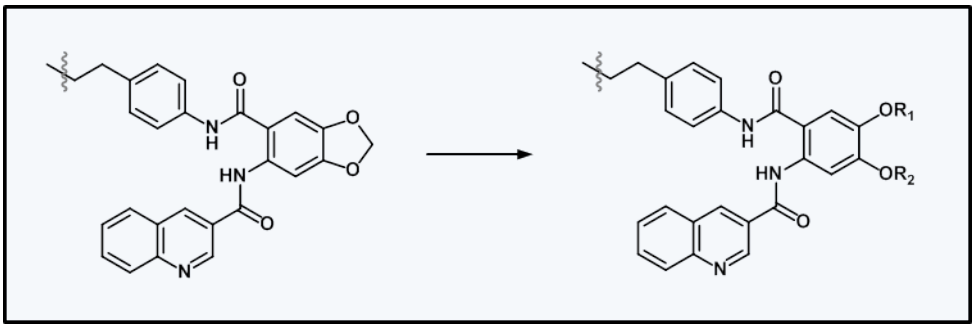

Fig. 48| Cleavage of dioxolane ring to obtain free phenol moiety (R_1 = -OH, R_2 = $-OCH_3$ or R_1 = $-OCH_3$, R_2 = -OH)

Similar to tariquidar, HM30181 possesses several methoxy moieties that could be used as sites for [^{11}C]methylation. Due to the experiences which were gathered with the synthesis of the tariquidar labelling precursor **29** it was decided not to label the isoquinoline substructure of HM30181. A benzyl-protected hydroxyl moiety was introduced into the molecule by replacement of 2-nitroveratraldehyde with 2-nitrobenzylvanillin. Because of the presence of the benzyl ether it was necessary to adapt the reaction conditions to preserve this protective group. For that purpose, the catalytic reduction with Pd/C and H_2 was replaced by Raney-Nickel and hydrazine [Batcho, 1985]. These conditions allowed the reduction of the nitro group in compound **37** to obtain the respective amine **38** without cleaving the benzyl ether.

In a first attempt, it was tried to cleave the benzyl ether by catalytic hydrogenation using Pd/C and H_2, which are the most commonly used conditions for deprotection for this kind of protective group. Surprisingly, reaction control *via* ^{1}H-NMR showed no conversion of the benzyl-protected derivative **39** to the desired precursor **35** (Fig. 49). In a second approach the benzyl ether **39** was treated with TFA and thioanisole [Kiso, 1980], resulting in a fast and specific cleavage of the protective group (Fig. 49). For purification the precursor **35** was converted to the corresponding hydrochloride after workup.

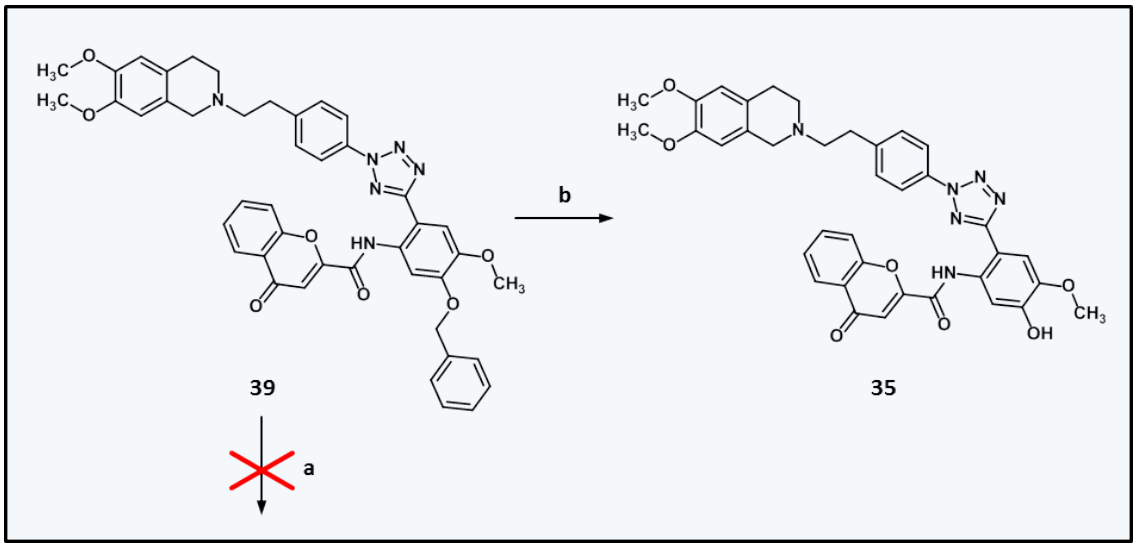

Fig. 49| Deprotection of compound 39 (a) Pd/C, H_2, rt; (b) TFA, thioanisole, rt;

Following the successful synthesis of the precursors **29** and **35**, the radiolabelling to obtain the desired PET-tracers [^{11}C]tariquidar and [^{11}C]HM30181 was performed at the AIT Seibersdorf. The first labelling experiments revealed that the hydroxyl moiety was not activated enough for direct methylation with [^{11}C]methyl triflate and that therefore, the addition of a base was necessary to enable successful labelling. Also, it became obvious that the choice of base depended on the precursor. For tariquidar precursor **29** addition of NaOH led to solubility in acetone and good yields in the [^{11}C]methylation. However, treatment of precursor **35** with NaOH led to the formation of a salt, which was insoluble in acetone, DMSO and MeCN. The substitution of NaOH with TBAH led to solubility of the precursor in a mixture of DMF and MeCN and enabled radiolabelling to obtain [^{11}C]HM30181. Additional experiments showed that the use of a hydrochloride of the precursors for radiolabelling resulted in a considerable loss of yield, most likely due to a competing reaction to generate volatile [^{11}C]methyl chloride. Therefore the free bases of the precursors were preferred for the methylation reaction to obtain [^{11}C]tariquidar and [^{11}C]HM30181.

VI.B Bioevaluation

The small-animal PET experiments with unlabelled HM30181, using (*R*)-[^{11}C]verapamil as radiotracer, showed that this compound was not able to inhibit P-gp at the BBB *in vivo*. This is an interesting observation as it had been shown *in vitro* that HM30181 had approximately the same P-gp inhibitory effect as tariquidar and elacridar [Kwak, 2010], which belong to the most potent P-gp inhibitors known to date. Furthermore, the experiments of Kwak *et al.*

demonstrated that, if HM30181 and paclitaxel were co-administered orally, the bioavailability of paclitaxel was increased in rats [Kwak, 2010]. This effect was attributed to an inhibition of intestinal P-gp. Thus, the question arises why HM30181 was not able to inhibit P-gp at the murine BBB.

One potential explanation would be the metabolic instability of HM30181. For [^{11}C]HM30181, it could be shown that at 30 minutes after tracer injection about a third of the administered radioactivity was present in the form of polar radiolabelled metabolites. To exclude that HM30181, by the time of the PET scan, had been metabolized completely, the pretreatment time was reduced to 60 and 10 minutes, respectively, in the PET experiments with (*R*)-[^{11}C]verapamil. Under all studied pretreatment conditions HM30181 showed no inhibition on P-gp at the BBB, so it can be excluded that the limited metabolic stability of HM30181 could explain the lack of inhibitory effect on P-gp at the BBB. The exact reasons for the observed discrepancies between the results of the *in vivo* and *in vitro* experiments remain unknown. However, the finding that HM30181 was not able to inhibit P-gp at the BBB may prove advantageous in that oral application of HM30181 will in all likelihood not lead to any side effects related to inhibition of P-gp in other tissues than in the intestine.

[^{11}C]Tariquidar as well as [^{11}C]HM30181 showed a similar behavior during small-animal PET evaluation. The results for tariquidar are consistent with the data obtained by Kawamura *et al.* in parallel to our study [Kawamura, 2010]. Likewise, the *in vivo* behavior of these two tracers was consistent with [^{11}C]elacridar [Dörner, 2009; Kawamura, 2011b] and [^{18}F]fluoroelacridar [Dörner, 2011; Kawamura, 2011a].

The first important observation was the low baseline uptake in untreated wild type mice and in rats. This behavior was contrary to our expectations, as it was assumed that a tracer based on a third generation inhibitor would bind to P-gp without being transported and thereby provide a higher baseline PET signal reflecting P-gp density. Consequently, the objective to develop PET tracers with enhanced baseline uptake compared to high-affinity substrates like (*R*)-[^{11}C]verapamil could not be achieved. This also limits the applicability of these novel tracers for the direct regional mapping of P-gp density at the BBB.

Treatment of rats with a high dose of unlabelled elacridar (5 mg/kg) or tariquidar (15 mg/kg) led to an immediate rise in the brain time-activity curve of [^{11}C]tariquidar and approximately three times increased brain uptake in the second PET scan as compared with the first PET scan (Fig. 33 and 34). A similar *in vivo* behavior was also observed for [^{11}C]elacridar, which had been

developed in parallel by our group [Dörner, 2009]. In wild type mice a similar behavior was observed as in rats, with low baseline brain uptake and a rise in brain activity uptake in response to tariquidar administration. In P-gp and/or BCRP knockout mice brain activity uptake was markedly increased compared with wild type mice, with largest increases seen in P-gp/BCRP combination knockout mice (Fig. 35 and 36). Similar observations were made for [^{11}C]HM30181 (Fig. 37 and 38). This *in vivo* behavior of [^{11}C]tariquidar and [^{11}C]HM30181 was consistent with that of dual P-gp/BCRP substrates, which were shown to only gain brain access when both P-gp or BCRP are knocked out [Agarwal, 2011].

However, other studies suggested that [^{11}C]tariquidar does not only act as a substrate for P-gp. In a P-gp expressing murine breast tumor model higher accumulation of [^{11}C]tariquidar was observed in the P-gp overexpressing as compared with the low P-gp expressing control tumor graft, which pointed to P-gp-specific binding of [^{11}C]tariquidar [Wanek, 2012a]. In another study, a significant negative correlation was found between regional uptake of [^{11}C]tariquidar and (*R*)-[^{11}C]verapamil in rat brain, which also pointed to some degree of P-gp binding of [^{11}C]tariquidar [Müllauer, 2013]. An *in vitro* study, performed by Kannan *et al*., showed higher binding of [^{3}H]tariquidar in P-gp overexpressing as compared with wild type cells [Kannan, 2011]. These contradicting data may be reconciled by the assumption that [^{11}C]tariquidar may both bind to P-gp and be effluxed by P-gp, possibly *via* different binding sites. It may thus depend on the P-gp expression levels of the tissue investigated, if P-gp efflux or P-gp binding of [^{11}C]tariquidar is observed. In the tumor model, in which P-gp expression levels were several times higher than at the BBB, a P-gp binding signal was observed [Wanek, 2012a], whereas in the brain the substrate properties of [^{11}C]tariquidar seemed to prevail. In fact, it has been suggested lately that for the mapping of the very low densities of P-gp at the BBB (1-2 nM), radiotracers with higher (i.e. picomolar) P-gp binding affinities than [^{11}C]tariquidar, [^{11}C]elacridar or [^{11}C]HM30181 might be needed [Kannan, 2013].

Despite the fact that the visualization of P-gp density with [^{11}C]tariquidar and [^{11}C]HM30181 has remained unsuccessful, [^{11}C]tariquidar might find future application as a PET tracer to measure the function of P-gp and BCRP at the BBB. This is currently of high interest, as several clinically used drugs (i.e. tyrosine kinase inhibitors for treatment of brain cancer) are excluded from the brain by concerted P-gp and BCRP efflux [Agarwal, 2011]. [^{11}C]Tariquidar may thus be used to measure functional activity of cerebral P-gp and BCRP in brain tumor patients and to study the inhibition of P-gp and BCRP in such patients by administration of dual inhibitors such as elacridar. Moreover, a recently developed novel PET protocol has shown that [^{11}C]tariquidar

can be used to selectively measure BCRP activity at the murine BBB when PET scans are performed at P-gp saturating tariquidar plasma levels [Wanek, 2012b]. This is of interest, as no PET tracer is currently available which allows for measuring BCRP function at the BBB.

VII Conclusion and Outlook

VII.A Conclusion

In summary, *O*-desmethyl precursors for ^{11}C-labelling of tariquidar and HM30181 have been successfully synthesized. Moreover, the radiosyntheses of [^{11}C]tariquidar and [^{11}C]HM30181 based on *O*-[^{11}C]methylation have been successfully developed, yielding both tracers in acceptable radiochemical yield, radiochemical purity and specific activity for PET experiments in rodents. The *O*-desmethyl tariquidar derivative **29** and *O*-desmethyl HM30181 **35** were each synthesized in six-step syntheses in overall yields of 26 % and 16 %, respectively, starting from 6,7-dimethoxy-1,2,3,4-tetrahydroisoquinoline hydrochloride.

[^{11}C]Tariquidar and [^{11}C]HM30181 have been evaluated with small-animal PET *in vivo* in rodent models. Against the original intention of this project, none of these two tracers was found to provide sufficiently high P-gp binding signals to allow for mapping the density of P-gp at the BBB with PET. It is suggested that compounds with higher P-gp binding affinities (i.e. picomolar) than tariquidar and HM30181 might be needed to visualize the very low density of P-gp at the BBB.

Our experiments revealed that [^{11}C]tariquidar and [^{11}C]HM30181 were effluxed at tracer doses by P-gp and/or BCRP at the BBB, which might make these compounds suitable as PET tracers to measure the functional activities of P-gp and BCRP at the BBB (e.g. in brain tumour patients).

VII.B Outlook

Although much effort has been made to develop suitable PET tracers for the mapping of P-gp density at the BBB, a lot of work remains to be done.

It will be necessary in the future to develop new compounds that, on the one hand, possess greater (i.e. picomolar) affinities to P-gp than existing substances and, on the other hand, show a high selectivity for P-gp without displaying interaction with other ABC transporters.

Of the two PET tracers described in this thesis [^{11}C]HM30181 will not be further pursued in the future, as it showed similar properties concerning interaction with transporters at the BBB as [^{11}C]tariquidar, while displaying poor metabolic stability and lower maximum brain uptake

when both P-gp and BCRP were knocked out. In contrast, [^{11}C]tariquidar may be used to measure P-gp expression levels in solid tumours or to measure P-gp and BCRP function at the human BBB. First human studies have already been initiated [Bauer, 2013]. Currently it is evaluated whether [^{11}C]tariquidar PET may contribute to improving our understanding of the cooperativity between P-gp and BCRP at the BBB both in the healthy and in the diseased brain.

VIII Experimental Part

VIII.A Chemistry

VIII.A.1 General Methods

Unless otherwise stated all chemicals and solvents were purchased from commercial suppliers (Sigma-Aldrich Chemie GmbH (Schnelldorf, Germany), Merck (Darmstadt, Germany), Apollo Scientific Ltd (Bredbury, UK), TCI Europe(Zwijndrecht, Belgium)) at analytical grade and were used without further purification.

The reactions were monitored by TLC on silica gel 60 F_{254} coated aluminium sheets from Merck (Darmstadt, Germany).

Silica gel 60 70-230 mesh ASTM from Merck (Darmstadt, Germany) was used as stationary phase in column chromatography.

Melting points were determined on a ThermoGalen Kofler hot stage microscope from Reichert (Vienna, Austria) and are uncorrected.

^{1}H- and ^{13}C-NMR spectra were recorded on a Bruker Advance DPx200 (200 and 50 MHz respectively). Chemical shifts are reported in δ units (ppm) relative to tetramethylsilane or solvent residual line as internal standard (br s, d, m, s, C_q for broad singlet, doublet, multiplet, singlet and quaternary carbon, respectively) and *J* values are reported in Hertz.

Mass spectra were recorded on a Shimadzu (GC-17A; MS-QP5050A) spectrometer. The peak intensity is specified in per cent relative to the most pronounced signal in the spectrum.

Elemental analysis was performed on a Perkin Elmer 2400 CHN Elemental Analyzer at the microanalytical laboratory of the University of Vienna, by Mag. Johannes Theiner and all encountered values are within ± 0.4 % of the calculated values.

The mass peaks of high resolution mass spectra were within ± 5 ppm of the calculated values.

HPLC was performed on LiChropher 100 RP 18-5µ EC (250 x 4 mm, Merck, Darmstadt, Germany) , Chromolith Performance RP18-e (100 – 4.6 mm, Merck KgaA, Darmstadt, Germany) and Nucleosil 100–3 C18 (3 µm, 3.00 x 125 mm, Macherey-Nagel, Düren, Germany) columns. Purity of the reference compounds and precursor molecules was established by analytical HPLC, confirming a purity >95%.

[^{11}C]CH_4 was produced *via* the $^{14}N(p,\alpha)^{11}C$ nuclear reaction by irradiation of nitrogen gas containing 10 % hydrogen using a PETtrace cyclotron equipped with a CH_4 target system (GE Healthcare, Uppsala, Sweden). [^{11}C]CH_3I was prepared in a TRACERRlab FXC Pro synthesis module (GE Healthcare) and converted into [^{11}C]methyl triflate by passage through a column containing silver-triflate impregnated graphitized carbon.

VIII.A.2 Characterization of synthesized compounds

VIII.A.2.a 6,7-Dimethoxy-2-(4-nitrophenethyl)-1,2,3,4-tetrahydroisoquinoline (1)

[Sharp, 1998; Wang, 2010]

Chemical structure:

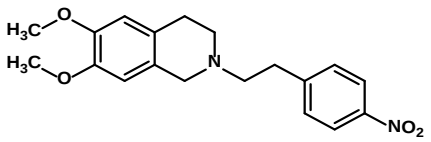

Molecular formula: $C_{19}H_{22}N_2O_4$

Molecular weight: 342.39 g/mol **Exact mass:** 342.16

Internal code: Fba1

6,7-Dimethoxy-1,2,3,4-thetrahydroisoquinoline hydrochloride (4.62 g, 20.11 mmol), 4-nitrophen-ethylbromide (4.64 g, 20.17 mmol), K_2CO_3 (3.11 g, 22.50 mmol) and KI (0.87 g, 5.24 mmol) were suspended in dry DMF (32 mL) under argon atmosphere. The mixture was heated to 70 °C overnight until completion of the reaction and was subsequently cooled down slowly. At 50 °C MeOH (11 mL) was added and after cooling to 30 °C, the solution was slowly diluted with H_2O (60 mL). The mixture was stirred at 0 °C for one hour. The resulting precipitate was filtered off, washed with water and recrystallized from EtOH to obtain the title compound as yellow solid.

Yield: 5.97 g (86.7 %)

Melting point: 107 – 110 °C lit. 108 – 109 °C [Wang, 2010]

^{1}H-NMR (200 MHz, $CDCl_3$)

C**H** (aromatic)	AB system	δ = 8.15 ppm, A part of an AB system, J_{AB} = 8.7 Hz	2H
C**H** (aromatic)	AB system	δ = 7.40 ppm, B part of an AB system, J_{AB} = 8.7 Hz	2H
C**H** (aromatic)	s	δ = 6.60 ppm	1H
C**H** (aromatic)	s	δ = 6.53 ppm	1H
OC**H**$_3$	s	δ = 3.85 ppm	3H

O**C**$\mathbf{H}_3$	s	δ = 3.84 ppm	3H
C$\mathbf{H}_2$	s	δ = 3.64 ppm	2H
C$\mathbf{H}_2$	m	δ = 3.08 – 2.72 ppm	8H

^{13}C-NMR (50 MHz, $CDCl_3$)

$\mathbf{C}_q$	δ = 148.4	1C
$\mathbf{C}_q$	δ = 147.5	1C
$\mathbf{C}_q$	δ = 147.2	1C
$\mathbf{C}_q$	δ = 146.4	1C
CH (aromatic)	δ = 129.5	2C
$\mathbf{C}_q$	δ = 126.2	1C
$\mathbf{C}_q$	δ = 126.0	1C
CH (aromatic)	δ = 123.6	2C
CH (aromatic)	δ = 111.3	1C
CH (aromatic)	δ = 109.3	1C
CH_2	δ = 59.1	1C
O**C**H_3	δ = 55.9	1C
O**C**H_3	δ = 55.8	1C
CH_2	δ = 55.6	1C
CH_2	δ = 50.9	1C
CH_2	δ = 33.8	1C
CH_2	δ = 28.6	1C

Mass spectrum

m/z	342	(0.46 %, M^+)
	207	(12 %)
	206	(100 %)
	77	(10 %)
	57	(11 %)
	42	(31 %)

VIII.A.2.b 6,7-Dimethoxy-2-(4-aminophenethyl)-1,2,3,4-tetrahydroisoquinoline (2) [Sharp, 1998; Klinkhammer, 2009]

Chemical structure:

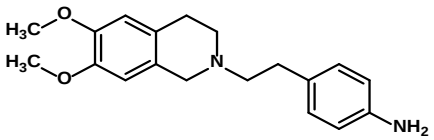

Molecular formula: $C_{19}H_{24}N_2O_2$

Molecular weight: 312.41 g/mol **Exact mass:** 312.18

Internal code: Fba6

Compound **1** (2.07 g, 6.05 mmol) was suspended in EtOH (130 mL) and purged with argon. Pd/C (10% *w/w*, 0.21 g) was suspended in EtOH (20 mL) under argon atmosphere and added to the reaction mixture. Compound **1** was hydrogenated at atmospheric pressure until hydrogen consumption stopped. The catalyst was filtered off, washed thoroughly with EtOH and the solvent was evaporated *in vacuo*. The crude product was recrystallized from EtOH to gain title compound as white solid.

Yield: 1.77 g (93.6 %)

Melting point: 129 – 132 °C lit.: 129 °C [Klinkhammer, 2009]

^{1}H-NMR (200 MHz, $CDCl_3$)

C**H** (aromatic)	AB system	δ = 7.03 ppm, A part of an AB system, J_{AB} = 8.3 Hz	2H
C**H** (aromatic)	m	δ = 6.69 – 6.57 ppm	3H
C**H** (aromatic)	s	δ = 6.53 ppm	1H
OC**H**$_3$	s	δ = 3.84 ppm	3H
OC**H**$_3$	s	δ = 3.83 ppm	3H
C**H**$_2$	s	δ = 3.63 ppm	2H
N**H**$_2$	br s	δ = 3.57 ppm	2H
C**H**$_2$	m	δ = 2.91 – 2.62 ppm	8H

^{13}C-NMR (50 MHz, $CDCl_3$)

C$_q$	δ = 147.4 ppm	1C
C$_q$	δ = 147.1 ppm	1C
C$_q$	δ = 144.4 ppm	1C
C$_q$	δ = 130.2 ppm	1C
CH (aromatic)	δ = 129.4 ppm	2C

C$_q$	δ = 126.6 ppm	1C
C$_q$	δ = 126.1 ppm	1C
CH (aromatic)	δ = 115.2 ppm	2C
CH (aromatic)	δ = 111.3 ppm	1C
CH (aromatic)	δ = 109.4 ppm	1C
CH$_2$	δ = 60.6 ppm	1C
O**C**H$_3$	δ = 55.8 ppm	1C
O**C**H$_3$	δ = 55.8 ppm	1C
CH$_2$	δ = 55.7 ppm	1C
CH$_2$	δ = 51.0 ppm	1C
CH$_2$	δ = 33.1 ppm	1C
CH$_2$	δ = 28.6 ppm	1C

Mass spectrum

m/z	312	(0.83 %, M^+)
	207	(14 %)
	206	(100 %)
	106	(8.5 %)
	42	(10 %)

VIII.A.2.c 3-Quinolinecarboxylic acid (8) [Uhle, 1945]

Chemical structure:

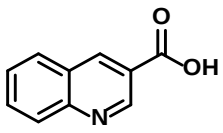

Molecular formula: $C_{10}H_7NO_2$

Molecular weight: 173.17 g/mol **Exact mass:** 173.05

Internal code: Fba8

A suspension of compound **8** (5.01 g, 32.50 mmol) in 51 mL aqueous HCl (conc.) was heated to reflux until TLC indicated complete depletion of the starting material. Subsequently the reaction mixture was cooled to room temperature, adjusted to a pH of about 5-6 and extracted with EtOAc. After removal of the solvent the crude product was recrystallized from EtOH to obtain title compound as a white solid.

Yield: 4.54 g (80.7 %)

Melting point: 253 – 257 °C lit.: 273 – 275 °C [Uhle, 1945]

^{1}H-NMR (200 MHz, d_6-DMSO)

COO**H**	br s	δ = 13.52 ppm	1H
C**H** (aromatic)	m	δ = 9.44 – 9.24 ppm	1H
C**H** (aromatic)	s	δ = 8.96 ppm	1H
C**H** (aromatic)	m	δ = 8.25 – 8.05 ppm	2H
C**H** (aromatic)	m	δ = 7.99 – 7.82 ppm	1H
C**H** (aromatic)	m	δ = 7.79 – 7.62 ppm	1H

^{13}C-NMR (50 MHz, d_6-DMSO)

COOH	δ = 166.4 ppm	1C
CH (aromatic)	δ = 149.9 ppm	1C
C_q	δ = 149.1 ppm	1C
CH (aromatic)	δ = 138.5 ppm	1C
CH (aromatic)	δ = 131.9 ppm	1C
CH (aromatic)	δ = 129.6 ppm	1C
CH (aromatic)	δ = 128.8 ppm	1C
CH (aromatic)	δ = 127.5 ppm	1C
C_q	δ = 126.6 ppm	1C
C_q	δ = 123.8 ppm	1C

VIII.A.2.d 3-Quinolinecarbonitrile (9) [Zymalkowski, 1966]

Chemical structure:

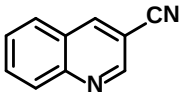

Molecular formula: $C_{10}H_6N_2$

Molecular weight: 154.17 g/mol **Exact mass:** 154.05

Internal code: Fba7

A stirred mixture of 3-bromoquinoline (6.35 g, 30.52 mmol), powdered $K_4[Fe(CN)_6]\cdot 3\ H_2O$ (3.01 g, 7.13 mmol), Na_2CO_3 (3.67 g, 34.63 mmol) and $Pd(Oac)_2$ (0.11 g, 0.47 mmol) in DMAc (50 mL) under argon atmosphere was heated to 120 °C. The conversion to the desired product was monitored by TLC (T/EtOAc – 4/1). Upon completion of the reaction the mixture was cooled to room temperature, EtOAc (100 mL) was added and the resulting slurry filtered. The

filtrate was washed with H_2O and $NaHCO_3$ (5 %, aqueous solution), dried over Na_2SO_4 and evaporated *in vacuo*. The crude product was recrystallized from EtOH to obtain title compound as an off-white solid.

Yield: 3.45 g (73.3 %)

Melting point: 105 – 107 °C lit.: 105 – 107 °C [Zymalkowski, 1966]

^{1}H-NMR (200 MHz, $CDCl_3$)

C**H** (aromatic)	d	δ = 9.04 ppm, *J* = 2.0 Hz	1H
C**H** (aromatic)	d	δ = 8.55 ppm, *J* = 2.0 Hz	1H
C**H** (aromatic)	AB system	δ = 8.18 ppm, A part of an AB system, *J* = 8.9 Hz	1H
C**H** (aromatic)	m	δ = 7.96 – 7.85 ppm	2H
C**H** (aromatic)	m	δ = 7.76 – 7.65 ppm	1H

^{13}C-NMR (50 MHz, $CDCl_3$)

CH (aromatic)	δ = 149.8 ppm	1C
C$_q$	δ = 148.9 ppm	1C
CH (aromatic)	δ = 141.6 ppm	1C
CH (aromatic)	δ = 132.9 ppm	1C
CH (aromatic)	δ = 130.0 ppm	1C
CH (aromatic)	δ = 128.6 ppm	1C
CH (aromatic)	δ = 128.4 ppm	1C
C$_q$	δ = 126.3 ppm	1C
CN	δ = 117.2 ppm	1C
C$_q$	δ = 106.7 ppm	1C

VIII.A.2.e HM30181 (10) [Bang, 2005]

Chemical structure:

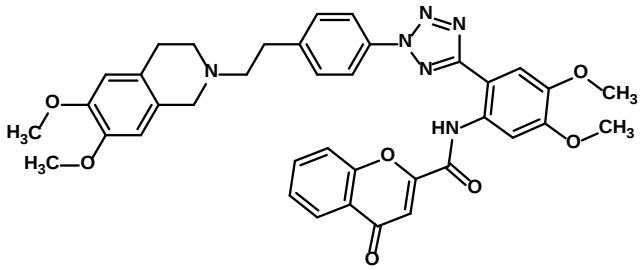

Molecular formula: $C_{38}H_{36}N_6O_7$

Molecular weight: 688.73 g/mol **Exact mass:** 688.26

Internal code: Fba85

EDC•HCl (0.55 g, 2.87 mmol) and 4-DMAP (0.01 g, 0.08 mmol) were added to an ice-cooled solution of compound **14** (0.41 g, 0.79 mmol) and 4-oxo-4*H*-chromene-2-carboxylic acid (0.34 g, 1.79 mmol). The mixture was warmed to room temperature and stirred overnight until TLC indicated full conversion of the starting material. Following the addition of H_2O (100 mL) the mixture was extracted with CH_2Cl_2. The combined organic layers were washed with 5 % aqueous $NaHCO_3$ solution and H_2O, dried over Na_2SO_4 and evaporated *in vacuo*. The crude product was subjected to column chromatography (toluene/EtOAc/TEA – 8/1/1) to obtain title compound as a yellow solid.

Yield: 0.15 g (27.6 %)

Melting point: 145 – 148 °C

^{1}H-NMR (200 MHz, $CDCl_3$)

CON**H**	s	δ = 12.45 ppm	1H
C**H** (aromatic)	s	δ = 8.50 ppm	1H
C**H** (aromatic)	AB system	δ = 8.16 ppm, A part of an AB system, J_{AB} = 7.7 Hz	1H
C**H** (aromatic)	AB system	δ = 8.08 ppm, A part of an AB system, J_{AB} = 8.5 Hz	2H
C**H** (aromatic)	m	δ = 7.76 – 7.66 ppm	2H
C**H** (aromatic)	s	δ = 7.62 ppm	1H
C**H** (aromatic)	AB system	δ = 7.45 ppm, B part of an AB system, J_{AB} =8.5 Hz	2H
C**H** (aromatic)	m	δ = 7.23 – 7.14 ppm	2H
C**H** (aromatic)	s	δ = 6.62 ppm	1H
C**H** (aromatic)	s	δ = 6.56 ppm	1H
OC**H**$_3$	s	δ = 3.96 ppm	3H
OC**H**$_3$	s	δ = 3.94 ppm	3H
OC**H**$_3$	s	δ = 3.86 ppm	6H
C**H**$_2$	s	δ = 3.69 ppm	2H
C**H**$_2$	m	δ = 3.09 – 2.79 ppm	8H

^{13}C-NMR (50 MHz, $CDCl_3$)

CO	δ = 178.3 ppm	1C
CNN	δ = 164.2 ppm	1C

CONR	δ = 157.4 ppm	1C
$\mathbf{C}_q$	δ = 155.3 ppm	1C
$\mathbf{C}_q$	δ = 155.1 ppm	1C
$\mathbf{C}_q$	δ = 151.4 ppm	1C
$\mathbf{C}_q$	δ = 147.8 ppm	1C
$\mathbf{C}_q$	δ = 147.5 ppm	1C
$\mathbf{C}_q$	δ = 145.9 ppm	1C
$\mathbf{C}_q$	δ = 143.4 ppm	1C
$\mathbf{C}_q$	δ = 134.8 ppm	1C
CH (aromatic)	δ = 134.6 ppm	1C
$\mathbf{C}_q$	δ = 131.3 ppm	1C
CH (aromatic)	δ = 130.2 ppm	2C
$\mathbf{C}_q$	δ = 126.5 ppm	1C
$\mathbf{C}_q$	δ = 126.2 ppm	1C
CH (aromatic)	δ = 126.0 ppm	2C
$\mathbf{C}_q$	δ = 124.3 ppm	1C
CH (aromatic)	δ = 120.4 ppm	2C
CH (aromatic)	δ = 118.6 ppm	1C
CH (aromatic)	δ = 112.1 ppm	1C
CH (aromatic)	δ = 111.6 ppm	1C
CH (aromatic)	δ = 110.1 ppm	1C
CH (aromatic)	δ = 109.7 ppm	1C
$\mathbf{C}_q$	δ = 106.8 ppm	1C
CH (aromatic)	δ = 104.4 ppm	1C
$\mathbf{C}H_2$	δ = 59.7 ppm	1C
O$\mathbf{C}H_3$	δ = 56.2 ppm	1C
O$\mathbf{C}H_3$	δ = 56.2 ppm	1C
O$\mathbf{C}H_3$	δ = 56.1 ppm	1C
O$\mathbf{C}H_3$	δ = 56.1 ppm	1C
$\mathbf{C}H_2$	δ = 55.9 ppm	1C
$\mathbf{C}H_2$	δ = 51.2 ppm	1C
$\mathbf{C}H_2$	δ = 33.8 ppm	1C
$\mathbf{C}H_2$	δ = 28.8 ppm	1C

Mass spectrum

m/z	688	(M^+, signal missing)
	120	(34 %)
	63	(25 %)
	57	(26 %)
	55	(23 %)
	44	(100 %)
	43	(30 %)

Elemental analysis ($C_{38}H_{36}N_6O_7 \cdot 0.5\ C_4H_8O_2 \cdot 1\ H_2O$)

Calculated:	C (63.99 %)	H (5.64 %)	N (11.19 %)
Found:	C (64.01 %)	H (5.00 %)	N (10.59 %)

VIII.A.2.f (E)-N'-(4,5-Dimethoxy-2-nitrobenzylidene)-4-methylbenzenesulfono-hydrazide (11) [Bang, 2005]

Chemical structure:

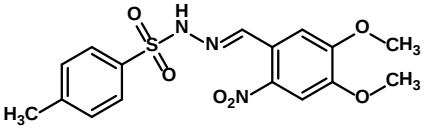

Molecular formula: $C_{16}H_{17}N_3O_6S$

Molecular weight: 379.39 g/mol **Exact mass:** 379.08

Internal code: Fba71

To a stirred suspension of 4-methylbenzenesulfonohydrazide (0.66 g, 3.54 mmol) in EtOH (7 mL), 4,5-dimethoxy-2-nitrobenzaldehyde (0.74 g, 3.50 mmol) suspended in EtOH (23 mL) was added. The resulting mixture was heated to reflux for two hours. After cooling to room temperature, H_2O (100 mL) was added and the solid was collected by vacuum filtration to obtain title compound as yellow solid.

Yield: 1.20 g (90.4 %)

Melting point: 172 – 176 °C decomposition

^{1}H-NMR (200 MHz, d_6-DMSO)

SO_2NH	br s	δ = 11.74 ppm	1H
CHN	s	δ = 8.34 ppm	1H
CH (aromatic)	AB system	δ = 7.79 ppm, A part of an AB system, J_{AB} = 8.2 Hz	2H

C**H** (aromatic)	s	δ = 7.56 ppm	1H
C**H** (aromatic)	AB system	δ = 7.42 ppm, B part of an AB system, J_{AB} = 8.2 Hz	2H
C**H** (aromatic)	s	δ = 7.12 ppm	1H
OC**H**$_3$	m	δ = 3.97 – 3.81 ppm	6H
C**H**$_3$	s	δ = 2.36 ppm	3H

^{13}C-NMR (50 MHz, d$_6$-DMSO)

C$_q$	δ = 152.7 ppm	1C
C$_q$	δ = 149.6 ppm	1C
C$_q$	δ = 143.7 ppm	1C
CH (aromatic)	δ = 142.8 ppm	1C
C$_q$	δ = 140.7 ppm	1C
C$_q$	δ = 136.0 ppm	1C
CH (aromatic)	δ = 129.7 ppm	2C
CH (aromatic)	δ = 127.3 ppm	2C
C$_q$	δ = 122.8 ppm	1C
CH (aromatic)	δ = 108.2 ppm	1C
CH (aromatic)	δ = 107.6 ppm	1C
O**C**H$_3$	δ = 56.2 ppm	1C
O**C**H$_3$	δ = 56.1 ppm	1C
CH$_3$	δ = 21.0 ppm	1C

Mass spectrum

m/z	379	(M^+, signal missing)
	136	(86 %)
	91	(63 %)
	65	(100 %)
	63	(76%)
	51	(68 %)

Elemental analysis (C$_{16}$H$_{17}$N$_3$O$_6$S)

Calculated:	C (50.65 %)	H (4.52 %)	N (11.08 %)
Found:	C (50.61 %)	H (4.54 %)	N (11.13 %)

VIII.A.2.g 2-(4-(5-(4,5-Dimethoxy-2-nitrophenyl)-2H-tetrazol-2-yl)phenethyl)-6,7-dimethoxy-1,2,3,4-tetrahydroisoquinoline (13) [Bang, 2005]

Chemical structure:

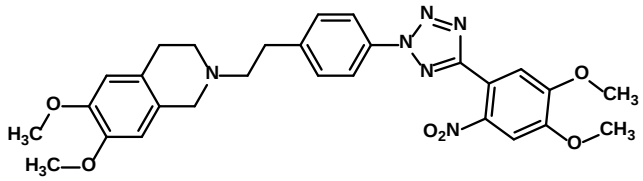

Molecular formula: $C_{28}H_{30}N_6O_6$

Molecular weight: 546.57 g/mol **Exact mass:** 546.22

Internal code: Fba73

To a cooled (0 °C) suspension of compound **2** (2.66 g, 8.51 mmol) in 50 % aqueous EtOH (14.4 mL) 36 % HCl (2.25 mL) was added dropwise. After addition of $NaNO_2$ (0.66 g, 9.57 mmol) in H_2O (3.56 mL) the resulting mixture was stirred at 0 °C for 30 minutes and then cooled to -15 °C. Compound **11** (3.20 g, 8.43 mmol) in pyridine (49.5 mL) was added over a period of ten minutes. The reaction mixture was stirred at -15 °C for 3.5 hours and then at room temperature overnight. The slurry was acidified with 1 M hydrochloric acid (650 mL) and extracted with CH_2Cl_2. The organic phase was washed with 1 M hydrochloric acid, H_2O, saturated aqueous $NaHCO_3$-solution and brine, dried over Na_2SO_4 and concentrated under reduced pressure. The crude product was purified by column chromatography (toluene/EtOAc/TEA – 7/2/1) and subsequent recrystallization from toluene to obtain title compound as a red solid.

Yield: 2.63 g (57.0 %)

Melting point: 162 – 165 °C

^{1}H-NMR (200 MHz, $CDCl_3$)

C**H** (aromatic)	AB system	δ = 8.07 ppm, A part of an AB system, J_{AB} = 8.4 Hz	2H
C**H** (aromatic)	s	δ = 7.57 ppm	1H
C**H** (aromatic)	AB system	δ = 7.44 ppm, B part of an AB system, J_{AB} = 8.4 Hz	2H
C**H** (aromatic)	s	δ = 7.31 ppm	1H
C**H** (aromatic)	s	δ = 6.62 ppm	1H
C**H** (aromatic)	s	δ = 6.55 ppm	1H
OC**H**$_3$	s	δ = 4.02 ppm	6H
OC**H**$_3$	s	δ = 3.85 ppm	3H
OC**H**$_3$	s	δ = 3.85 ppm	3H

C**H**$_2$	s	δ = 3.71 ppm	2H
C**H**$_2$	m	δ = 3.12 – 2.77 ppm	8H

^{13}C-NMR (50 MHz, CDCl$_3$)

CNN	δ = 162.1 ppm	1C
C$_q$	δ = 152.4 ppm	1C
C$_q$	δ = 150.4 ppm	1C
C$_q$	δ = 147.8 ppm	1C
C$_q$	δ = 147.5 ppm	1C
C$_q$	δ = 142.7 ppm	1C
C$_q$	δ = 142.2 ppm	1C
C$_q$	δ = 135.1 ppm	1C
CH (aromatic)	δ = 130.1 ppm	2C
C$_q$	δ = 126.0 ppm	2C
CH (aromatic)	δ = 120.2 ppm	2C
C$_q$	δ = 115.7 ppm	1C
CH (aromatic)	δ = 112.9 ppm	1C
CH (aromatic)	δ = 111.5 ppm	1C
CH (aromatic)	δ = 109.6 ppm	1C
CH (aromatic)	δ = 108.0 ppm	1C
CH$_2$	δ = 59.5 ppm	1C
O**C**H$_3$	δ = 56.8 ppm	1C
O**C**H$_3$	δ = 56.7 ppm	1C
O**C**H$_3$	δ = 56.1 ppm	1C
O**C**H$_3$	δ = 56.0 ppm	1C
CH$_2$	δ = 55.6 ppm	1C
CH$_2$	δ = 51.1 ppm	1C
CH$_2$	δ = 33.6 ppm	1C
CH$_2$	δ = 28.5 ppm	1C

Mass spectrum

m/z	546	(M^+, signal missing)
	206	(100 %)
	164	(26 %)

91 (50.3 %)

51 (29 %)

50 (28 %)

Elemental analysis ($C_{28}H_{30}N_6O_6$)

Calculated:	C (61.53 %)	H (5.53 %)	N (15.38 %)
Found:	C (61.52 %)	H (5.54 %)	N (15.33 %)

VIII.A.2.h 2-(2-(4-(2-(6,7-Dimethoxy-3,4-dihydroisoquinolin-2(1H)-yl)ethyl)-phenyl)-2H-tetrazol-5-yl)-4,5-dimethoxyaniline (14) [Bang, 2005]

Chemical structure:

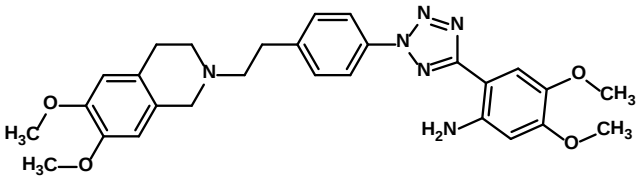

Molecular formula: $C_{28}H_{32}N_6O_4$

Molecular weight: 516.59 g/mol **Exact mass:** 516.25

Internal code: Fba79

A solution of compound **13** (1.04 g, 1.90 mmol) in EtOH (15 mL) and CH_2Cl_2 (25 mL) was purged with argon. Pd/C catalyst (10% *w/w*, 100 mg) was suspended in EtOH (10 mL) under argon atmosphere and added to the reaction mixture. Compound **13** was hydrogenated in a Parr-apparatus at 2.5 bar until hydrogen consumption stopped. The catalyst was filtered off and the solvent was evaporated *in vacuo* to obtain title compound as off-white solid. Analytical samples were purified by column chromatography (toluene/EtOAc/TEA – 7/2/1).

Yield: 0.45 g (45.8 %)

Melting point: 168 – 172 °C

^{1}H-NMR (200 MHz, $CDCl_3$)

C**H** (aromatic)	AB system	δ = 8.08 ppm, A part of an AB system, J_{AB} = 8.5 Hz	2H
C**H** (aromatic)	s	δ = 7.70 ppm	1H
C**H** (aromatic)	AB system	δ = 7.44 ppm, B part of an AB system, J_{AB} = 8.5 Hz	2H
C**H** (aromatic)	s	δ = 6.61 ppm	1H
C**H** (aromatic)	s	δ = 6.54 ppm	1H
C**H** (aromatic)	s	δ = 6.35 ppm	1H

N**H**$_2$	br s	δ = 5.31 ppm	2H
OC**H**$_3$	s	δ = 3.93 ppm	3H
OC**H**$_3$	s	δ = 3.90 ppm	3H
OC**H**$_3$	s	δ = 3.85 ppm	3H
OC**H**$_3$	s	δ = 3.84 ppm	3H
C**H**$_2$	s	δ = 3.75 ppm	2H
C**H**$_2$	m	δ = 3.12 – 2.84 ppm	8H

^{13}C-NMR (50 MHz, CDCl$_3$)

CNN	δ = 165.1 ppm	1C
C$_q$	δ = 152.4 ppm	1C
C$_q$	δ = 147.9 ppm	1C
C$_q$	δ = 147.6 ppm	1C
C$_q$	δ = 141.9 ppm	1C
C$_q$	δ = 141.8 ppm	1C
C$_q$	δ = 141.5 ppm	1C
C$_q$	δ = 135.3 ppm	1C
CH (aromatic)	δ = 130.0 ppm	2C
C$_q$	δ = 125.7 ppm	1C
C$_q$	δ = 125.4 ppm	1C
CH (aromatic)	δ = 120.0 ppm	2C
CH (aromatic)	δ = 111.5 ppm	1C
CH (aromatic)	δ = 111.3 ppm	1C
CH (aromatic)	δ = 109.6 ppm	1C
C$_q$	δ = 101.2 ppm	1C
CH (aromatic)	δ = 100.4 ppm	1C
CH$_2$	δ = 59.3 ppm	1C
O**C**H$_3$	δ = 56.7 ppm	1C
O**C**H$_3$	δ = 56.1 ppm	1C
O**C**H$_3$	δ = 56.0 ppm	1C
O**C**H$_3$	δ = 55.9 ppm	1C
CH$_2$	δ = 55.4 ppm	1C
CH$_2$	δ = 50.9 ppm	1C
CH$_2$	δ = 33.3 ppm	1C
CH$_2$	δ = 28.2 ppm	1C

Mass spectrum

m/z	516	(0.26 %, M^+)
	207	(14 %)
	206	(100 %)
	178	(8.0 %)
	164	(9.1 %)
	77	(8.0 %)
	42	(13 %)

Elemental analysis ($C_{28}H_{32}N_6O_4$ • 0.25 toluene • 0.75 H_2O)

Calculated:	C (64.60 %)	H (6.47 %)	N (15.19 %)
Found:	C (64.83 %)	H (6.37 %)	N (14.91 %)

VIII.A.2.i 5-Hydroxy-4-methoxy-2-nitrobenzoic acid (20) [Joshi, 1986; Wéber, 2005]

Chemical structure:

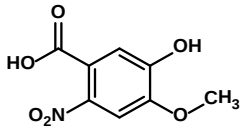

Molecular formula: $C_8H_7NO_6$

Molecular weight: 213.14 g/mol **Exact mass:** 213.03

Internal code: Fba22

4,5-Dimethoxy-2-nitrobenzoic acid (6,11 g, 26,89 mmol) and KOH (6,02 g, 107,29 mmol) were dissolved in H_2O (30 mL). The resulting solution was heated to reflux for 24 hours. After cooling to room temperature, the mixture was acidified with 2M HCl to pH 1-2. The precipitate was filtered off and recrystallized from H_2O to afford compound **18** as yellow solid.

Yield: 5.39 g (94.5 %)

Melting point: 179 – 183 °C lit.: 182 – 183 °C [Wéber, 2005]
lit.: 181 – 182 °C [Joshi, 1986]

^{1}H-NMR (200 MHz, d_6-DMSO)

C**H** (aromatic)	s	δ = 7.36 ppm	1H
C**H** (aromatic)	s	δ = 6.93 ppm	1H

O**C**H$_3$	s	δ = 3.80 ppm	3H

^{13}C-NMR (50 MHz, d$_6$-DMSO)

COOH	δ = 169.1	1C
C$_q$	δ = 152.4	1C
C$_q$	δ = 147.5	1C
C$_q$	δ = 138.2	1C
C$_q$	δ = 130.6	1C
CH (aromatic)	δ = 114.8	1C
CH (aromatic)	δ = 107.6	1C
O**C**H$_3$	δ = 56.5	1C

VIII.A.2.j 5-(Acetyloxy)-4-methoxy-2-nitrobenzoic acid (21) [Joshi, 1986]

Chemical structure:

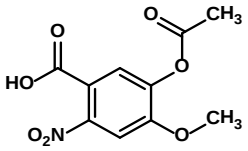

Molecular formula: C$_{10}$H$_9$NO$_7$

Molecular weight: 255.18 g/mol **Exact mass:** 255.04

Internal code: Fba23

Compound **20** (6.57 g, 30.82 mmol) was suspended in Ac$_2$O (50 mL). After addition of pyridine (5.5 mL) the reaction mixture was heated to 90 °C for 2 hours. The solution was poured on crushed ice and acidified to pH 1 with 2M HCl. The resulting precipitate was filtered off and recrystallized from EtOAc to obtain compound **21** as brown solid.

Yield: 4.03 g (51.2 %)

Melting point: 212 – 214 °C lit.: 213 – 214 °C [Joshi, 1986]

^{1}H-NMR (200 MHz, d$_6$-DMSO)

C**H** (aromatic)	s	δ = 7.76 ppm	1H
C**H** (aromatic)	s	δ = 7.70 ppm	1H
OC**H**$_3$	s	δ = 3.92 ppm	3H
C**H**$_3$	s	δ = 2.31 ppm	3H

^{13}C-NMR (50 MHz, d_6-DMSO)

COOH	δ = 168.2 ppm	1C
COOR	δ = 164.3 ppm	1C
$\mathbf{C}_q$	δ = 153.9 ppm	1C
$\mathbf{C}_q$	δ = 148.1 ppm	1C
$\mathbf{C}_q$	δ = 140.8 ppm	1C
CH (aromatic)	δ = 124.9 ppm	1C
$\mathbf{C}_q$	δ = 117.9 ppm	1C
CH (aromatic)	δ = 108.6 ppm	1C
O**C**H$_3$	δ = 57.1 ppm	1C
CH$_3$	δ = 20.4 ppm	1C

Mass spectrum

m/z	255	(2.6 %, M^+)
	213	(52 %)
	195	(6.5 %)
	111	(8.3 %)
	51	(13 %)
	50	(10 %)
	43	(100 %)

VIII.A.2.k 5-((4-(2-(6,7-Dimethoxy-3,4-dihydroisoquinolin-2(1H)-yl)ethyl)-phenyl)carbamoyl)-2-methoxy-4-nitrophenyl acetate hydrochloride (22)

Chemical structure:

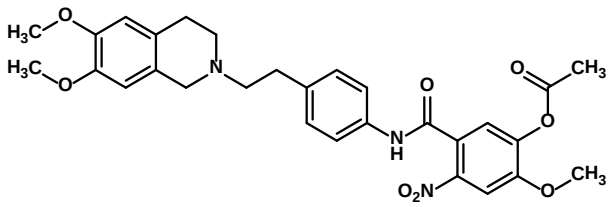

Molecular formula: $C_{29}H_{31}N_3O_8$

Molecular weight: 549.57 g/mol **Exact mass:** 549.21

Internal code: Fba24

Compound **21** (3.33 g, 13.05 mmol) was refluxed in $SOCl_2$ (4 mL, 54.84 mmol) for 3 hours. Excess $SOCl_2$ was evaporated and the resulting acid chloride was dissolved in THF and slowly added to a solution of compound **2** (4.01 g, 12.84 mmol) in THF. The reaction mixture was

stirred overnight and then evaporated. The residue was treated with 1 M NaOH, extracted with EtOAc and evaporated *in vacuo*. The crude product was recrystallized in EtOH/MeOH to afford title compound as yellow solid.

Yield: 4.88 g (68.0 %)

Melting point: 156 – 160 °C

^{1}H-NMR (200 MHz, $CDCl_3$)

CON**H**	s	δ = 8.31 ppm	1H
C**H** (aromatic)	s	δ = 7.54 ppm	1H
C**H** (aromatic)	AB system	δ = 7.48 ppm, A part of an AB system, J_{AB} = 8.3 Hz	2H
C**H** (aromatic)	s	δ = 7.25 ppm	1H
C**H** (aromatic)	AB system	δ = 7.18 ppm, B part of an AB system, J_{AB} = 8.3 Hz	2H
C**H** (aromatic)	s	δ = 6.57 ppm	1H
C**H** (aromatic)	s	δ = 6.51 ppm	1H
OC**H**$_3$	s	δ = 3.88 ppm	3H
OC**H**$_3$	s	δ = 3.82 ppm	3H
OC**H**$_3$	s	δ = 3.81 ppm	3H
C**H**$_2$	s	δ = 3.64 ppm	2H
C**H**$_2$	m	δ = 2.98 – 2.67 ppm	8H
C**H**$_3$	s	δ = 2.31 ppm	3H

^{13}C-NMR (50 MHz, $CDCl_3$)

CONH	δ = 168.1 ppm	1C
C$_q$	δ = 163.5 ppm	1C
C$_q$	δ = 152.3 ppm	1C
C$_q$	δ = 147.6 ppm	1C
C$_q$	δ = 147.2 ppm	1C
C$_q$	δ = 144.4 ppm	1C
C$_q$	δ = 143.4 ppm	1C
C$_q$	δ = 137.0 ppm	1C
C$_q$	δ = 135.8 ppm	1C
CH (aromatic)	δ = 129.4 ppm	2C
C$_q$	δ = 126.2 ppm	1C

C$_q$	δ = 126.0 ppm	1C
C$_q$	δ = 126.0 ppm	1C
CH (aromatic)	δ = 123.1 ppm	1C
CH (aromatic)	δ = 120.8 ppm	2C
CH (aromatic)	δ = 111.4 ppm	1C
CH (aromatic)	δ = 109.5 ppm	1C
CH (aromatic)	δ = 108.7 ppm	1C
CH$_2$	δ = 60.0 ppm	1C
O**C**H$_3$	δ = 56.7 ppm	1C
O**C**H$_3$	δ = 55.9 ppm	1C
O**C**H$_3$	δ = 55.9 ppm	1C
CH$_2$	δ = 55.5 ppm	1C
CH$_2$	δ = 51.1 ppm	1C
CH$_2$	δ = 33.3 ppm	1C
CH$_2$	δ = 28.5 ppm	1C
CH$_3$	δ = 20.6 ppm	1C

Mass spectrum

m/z	549	(0.20 %, M^+)
	203	(100 %)
	105	(87 %)
	91	(23 %)
	77	(38 %)
	56	(21 %)

VIII.A.2.l 4-Amino-5-((4-(2-(6,7-dimethoxy-3,4-dihydroisoquinolin-2(1H)-yl)-ethyl)phenyl)carbamoyl)-2-methoxyphenyl acetate (23)

Chemical structure:

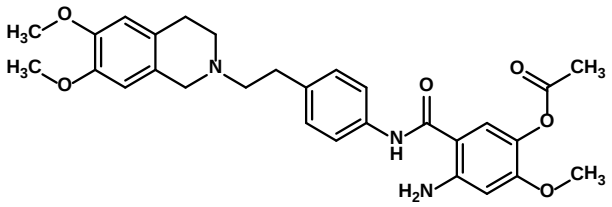

Molecular formula: $C_{29}H_{33}N_3O_6$

Molecular weight: 519.59 g/mol **Exact mass:** 519.24

Internal code: Fba25

Compound **22** (2.01 g, 3.66 mmol) was suspended in MeOH (130 mL) and purged with argon. Pd/C (10% w/w, 0.20 g) was suspended in MeOH (20 mL) and added to the reaction mixture. **22** was then hydrogenated at atmospheric pressure until hydrogen consumption stopped. The catalyst was filtered off and the solution was concentrated *in vacuo* until title compound precipitated as brown solid.

Yield: 0.53 g (27.9 %)

Melting point: n/a (compound not stable)

^{1}H-NMR (200 MHz, $CDCl_3$)

CON**H**	s	δ = 7.65 ppm	1H
C**H** (aromatic)	AB system	δ = 7.44 ppm, A part of an AB system, J_{AB} = 8.4 Hz	2H
C**H** (aromatic)	AB system	δ = 7.21 ppm, B part of an AB system, J_{AB} = 8.4 Hz	2H
C**H** (aromatic)	s	δ = 7.14 ppm	1H
C**H** (aromatic)	s	δ = 6.60 ppm	1H
C**H** (aromatic)	s	δ = 6.54 ppm	1H
C**H** (aromatic)	s	δ = 6.18 ppm	1H
N**H**$_2$	br s	δ = 5.72 ppm	2H
OC**H**$_3$	m	δ = 3.87 – 3.82 ppm	6H
OC**H**$_3$	s	δ = 3.76 ppm	3H
C**H**$_2$	s	δ = 3.65 ppm	2H
C**H**$_2$	m	δ = 2.96 – 2.69 ppm	8H
C**H**$_3$	s	δ = 2.30 ppm	3H

Due to the instability of the compound only ^{1}H-NMR could be recorded.

VIII.A.2.m 5-((4-(2-(6,7-Dimethoxy-3,4-dihydroisoquinolin-2(1H)-yl)ethyl)-phenyl)carbamoyl)-2-methoxy-4-(quinoline-3-carboxamido)phenyl acetate (24)

Chemical structure:

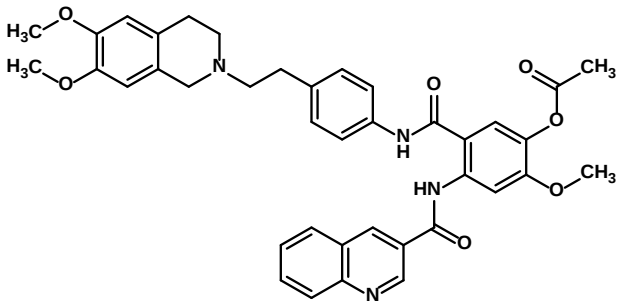

Molecular formula: $C_{39}H_{38}N_4O_7$

Molecular weight: 674.74 g/mol **Exact mass:** 674.27

Internal code: Fba26

3-Quinolinecarboxilic acid (0.27 g, 1.56 mmol) was refluxed in $SOCl_2$ for 3 hours. Excess $SOCl_2$ was evaporated. Compound **23** (0.53 g, 1.02 mmol) was suspended in THF and TEA was added. The acid chloride was suspended in THF and slowly added to the suspension of **23**. The reaction mixture was stirred overnight and then poured on ice water. The precipitate was filtered off and dried to obtain title compound as an off-white solid.

Yield: 0.35 g (50.9 %)

Melting point: n/a

^{1}H-NMR (200 MHz, d_6-DMSO)

CON**H**	s	δ = 12.47 ppm	1H
CON**H**	s	δ = 10.48 ppm	1H
C**H** (aromatic)	d	δ = 9.37 ppm, *J* = 2.2 Hz	1H
C**H** (aromatic)	d	δ = 8.93 ppm, *J* = 2.2 Hz	1H
C**H** (aromatic)	s	δ = 8.37 ppm	1H
C**H** (aromatic)	m	δ = 8.20 – 8.10 ppm	2H
C**H** (aromatic)	m	δ = 7.97 – 7.88 ppm	1H
C**H** (aromatic)	s	δ = 7.86 ppm	1H
C**H** (aromatic)	m	δ = 7.78 – 7.67 ppm	3H
C**H** (aromatic)	AB system	δ = 7.31 ppm, B part of an AB system, J_{AB} = 8.5 Hz	2H
C**H** (aromatic)	s	δ = 6.83 ppm	1H
C**H** (aromatic)	s	δ = 6.79 ppm	1H
C**H**$_2$	s	δ = 4.35 ppm	2H

OC**H**$_3$	s	δ = 3.91 ppm	3H
OC**H**$_3$	s	δ = 3.75 ppm	3H
OC**H**$_3$	s	δ = 3.74 ppm	3H
C**H**$_2$	m	δ = 3.35 – 2.89 ppm	8H
C**H**$_3$	s	δ = 2.33 ppm	3H

^{13}C-NMR (50 MHz, d$_6$-DMSO)

COOR	δ = 168.6 ppm	1C
CONR	δ = 166.4 ppm	1C
CONR	δ = 163.5 ppm	1C
C$_q$	δ = 153.7 ppm	1C
C$_q$	δ = 148.7 ppm	1C
C$_q$	δ = 148.4 ppm	1C
CH (aromatic)	δ = 148.3 ppm	1C
C$_q$	δ = 147.4 ppm	1C
C$_q$	δ = 138.7 ppm	1C
C$_q$	δ = 137.2 ppm	1C
CH (aromatic)	δ = 136.0 ppm	1C
C$_q$	δ = 134.4 ppm	1C
C$_q$	δ = 132.9 ppm	1C
CH (aromatic)	δ = 131.8 ppm	1C
CH (aromatic)	δ = 129.4 ppm	1C
CH (aromatic)	δ = 129.0 ppm	2C
CH (aromatic)	δ = 128.9 ppm	1C
CH (aromatic)	δ = 127.8 ppm	1C
C$_q$	δ = 127.3 ppm	1C
C$_q$	δ = 126.6 ppm	1C
C$_q$	δ = 123.4 ppm	1C
CH (aromatic)	δ = 123.3 ppm	1C
CH (aromatic)	δ = 121.6 ppm	2C
C$_q$	δ = 120.1 ppm	1C
C$_q$	δ = 114.4 ppm	1C
CH (aromatic)	δ = 111.5 ppm	1C
CH (aromatic)	δ = 109.7 ppm	1C
CH (aromatic)	δ = 105.6 ppm	1C

O**C**H$_3$	δ = 56.1 ppm	1C
CH$_2$	δ = 56.0 ppm	1C
O**C**H$_3$	δ = 55.6 ppm	1C
O**C**H$_3$	δ = 55.6 ppm	1C
CH$_2$	δ = 51.5 ppm	1C
CH$_2$	δ = 49.0 ppm	1C
CH$_2$	δ = 29.2 ppm	1C
CH$_2$	δ = 24.6 ppm	1C
CH$_3$	δ = 20.4 ppm	1C

Due to instability of the compound during purification attempts only ^{1}H- and ^{13}C-NMR of the raw product could be recorded.

VIII.A.2.n 4-Methoxy-2-nitro-5-(pivaloyloxy)benzoic acid (25)

Chemical structure:

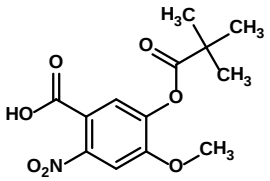

Molecular formula: C$_{13}$H$_{15}$NO$_7$

Molecular weight: 297.26 g/mol **Exact mass:** 297.08

Internal code: Fba35

Compound **20** (0.22 g, 1.03 mmol) was suspended in anhydrous DMF (4 mL) and purged with argon. After addition of Cs$_2$CO$_3$ (0.22 g, 0.68 mmol) and Piv$_2$O (0.22 mL, 1.1 mmol) the reaction mixture was stirred at 70°C until completion of the reaction. The solution was evaporated and the residue was dissolved in aqueous 2M HCl (5 mL). The product was extracted with EtOAc and purified by column chromatography (toluene/EtOAc, 4/1 + 1% AcOH) and recrystallization from EtOAc to give the title compound as a white solid.

Yield: 0.24 g (78.4 %)

Melting point: 213 – 215 °C decomposition

^{1}H-NMR (200 MHz, d$_6$-DMSO)

COO**H**	br s	δ = 13.82 ppm	1H

C**H** (aromatic)	s	δ = 7.75 ppm	1H
C**H** (aromatic)	s	δ = 7.66 ppm	1H
OC**H**$_3$	s	δ = 3.91 ppm	3H
C**H**$_3$	s	δ = 1.32 ppm	9H

^{13}C-NMR (50 MHz, CDCl$_3$)

COOR	δ = 175.3 ppm	1C
COOH	δ = 164.3 ppm	1C
C$_q$	δ = 153.8 ppm	1C
C$_q$	δ = 148.0 ppm	1C
C$_q$	δ = 141.2 ppm	1C
CH (aromatic)	δ = 124.6 ppm	1C
C$_q$	δ = 117.9 ppm	1C
CH (aromatic)	δ = 108.5 ppm	1C
O**C**H$_3$	δ = 57.2 ppm	1C
C$_q$	δ = 38.6 ppm	1C
CH$_3$	δ = 26.7 ppm	3C

Mass spectrum

m/z	297	(0.73 %, M^+)
	213	(17 %)
	85	(15 %)
	57	(100 %)
	41	(20 %)

Elemental analysis (C$_{13}$H$_{15}$NO$_7$)

Calculated:	C (52.53 %)	H (5.09 %)	N (4.71 %)
Found:	C (52.45 %)	H (4.99 %)	N (4.59 %)

VIII.A.2.o 5-((4-(2-(6,7-Dimethoxy-3,4-dihydroisoquinolin-2(1H)-yl)ethyl)-phenyl)-carbamoyl)-2-methoxy-4-nitrophenyl pivalate (26)

Chemical structure:

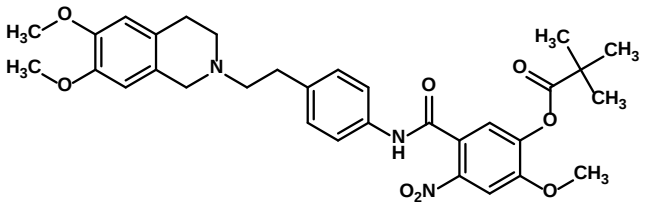

Molecular formula: $C_{32}H_{37}N_3O_8$

Molecular weight: 591.65 g/mol **Exact mass:** 591.26

Internal code: Fba40

Compound **25** (0.68 g, 2.29 mmol) was refluxed in $SOCl_2$ (4 mL) for 3 hours. Excess $SOCl_2$ was evaporated. The acid chloride was dissolved in THF and slowly added at 0 °C to a solution of **2** (0.68 g, 2.17 mmol) and TEA (1 mL) in THF. The reaction mixture was stirred overnight at room temperature and then poured on ice H_2O. The precipitate was filtered off and dried to afford the title compound as a yellow solid.

Yield: 1.21 g (94 %)

Melting point: 142 – 145 °C

^{1}H-NMR (200 MHz, d_6-DMSO)

CON**H**	s	δ = 10.57 ppm	1H
C**H** (aromatic)	s	δ = 7.84 ppm	1H
C**H** (aromatic)	s	δ = 7.61 ppm	1H
C**H** (aromatic)	AB system	δ = 7.55 ppm, A part of an AB system, J_{AB} = 8.5 Hz	2H
C**H** (aromatic)	AB system	δ = 7.23 ppm, B part of an AB system, J_{AB} = 8.5 Hz	2H
C**H** (aromatic)	m	δ = 6.68 – 6.61 ppm	2H
OC**H**$_3$	s	δ = 3.93 ppm	3H
OC**H**$_3$	s	δ = 3.69 ppm	6H
C**H**$_2$	s	δ = 3.56 ppm	2H
C**H**$_2$	m	δ = 2.82 – 2.64 ppm	8H
C**H**$_3$	s	δ = 1.32 ppm	9H

^{13}C-NMR (50 MHz, d_6-DMSO)

COOR	δ = 175.2 ppm	1C
CONR	δ = 162.7 ppm	1C
$\mathbf{C}_q$	δ = 152.1 ppm	1C
$\mathbf{C}_q$	δ = 147.6 ppm	1C
$\mathbf{C}_q$	δ = 147.2 ppm	1C
$\mathbf{C}_q$	δ = 145.2 ppm	1C
$\mathbf{C}_q$	δ = 142.7 ppm	1C
$\mathbf{C}_q$	δ = 137.1 ppm	1C
$\mathbf{C}_q$	δ = 134.8 ppm	1C
CH (aromatic)	δ = 129.0 ppm	2C
$\mathbf{C}_q$	δ = 125.3 ppm	1C
$\mathbf{C}_q$	δ = 125.0 ppm	1C
CH (aromatic)	δ = 123.6 ppm	1C
CH (aromatic)	δ = 119.8 ppm	1C
CH (aromatic)	δ = 111.7 ppm	2C
CH (aromatic)	δ = 109.8 ppm	1C
CH (aromatic)	δ = 108.9 ppm	1C
$\mathbf{C}H_2$	δ = 58.3 ppm	1C
O$\mathbf{C}H_3$	δ = 57.1 ppm	1C
O$\mathbf{C}H_3$	δ = 55.5 ppm	1C
O$\mathbf{C}H_3$	δ = 55.5 ppm	1C
$\mathbf{C}H_2$	δ = 53.7 ppm	1C
$\mathbf{C}H_2$	δ = 50.0 ppm	1C
$\mathbf{C}_q$	δ = 38.7 ppm	1C
$\mathbf{C}H_2$	δ = 31.3 ppm	1C
$\mathbf{C}H_2$	δ = 26.9 ppm	1C
$\mathbf{C}H_3$	δ = 26.7 ppm	3C

Mass spectrum

m/z	591	(0.05 %), M^+)
	206	(59 %)
	164	(44 %)
	57	(100 %)
	41	(33 %)

Elemental analysis ($C_{32}H_{37}N_3O_8 \cdot 0.5\ H_2O$)

Calculated:	C (63.99 %)	H (6.38 %)	N (7.00 %)
Found:	C (63.79 %)	H (6.04 %)	N (6.89 %)

VIII.A.2.p 4-Amino-5-((4-(2-(6,7-dimethoxy-3,4-dihydroisoquinolin-2(1H)-yl)-ethyl)-phenyl)carbamoyl)-2-methoxyphenyl pivalate (27)

Chemical structure:

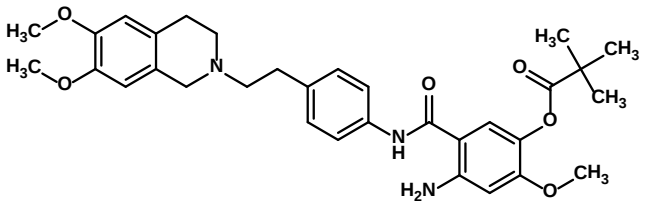

Molecular formula: $C_{32}H_{39}N_3O_6$

Molecular weight: 561.67 g/mol **Exact mass:** 561.28

Internal code: Fba41

A solution of compound **26** (1.15 g, 1.94 mmol) in a mixture of MeOH and EtOAc (1/1, 90 mL) was purged with argon and Pd/C catalyst (10%, w/w, 0.12 g) suspended in MeOH and EtOAc (1/1, 15 mL) was added. The compound was hydrogenated under atmospheric pressure until hydrogen uptake was complete. The catalyst was filtered off and the solvent was evaporated to obtain title compound as a white solid. Analytical samples were purified by column chromatography (toluene/EtOAc/TEA – 7/2/1).

Yield: 0.94 g (86.3 %)

Melting point: 157 – 160 °C

^{1}H-NMR (200 MHz, $CDCl_3$) :

CON**H**	s	δ = 8.02 ppm	1H
C**H** (aromatic)	AB system	δ = 7.57 ppm, A part of an AB system, J_{AB} = 8.4 Hz	2H
C**H** (aromatic)	AB system	δ = 7.29 ppm, B part of an AB system, J_{AB} = 8.4 Hz	2H
C**H** (aromatic)	s	δ = 7.20 ppm	1H
C**H** (aromatic)	s	δ = 6.70 ppm	1H
C**H** (aromatic)	s	δ = 6.64 ppm	1H
C**H** (aromatic)	s	δ = 6.20 ppm	1H
N**H**$_2$	br s	δ = 5.83 ppm	2H

O**C**H$_3$	s	δ = 3.94 ppm	2H
O**C**H$_3$	s	δ = 3.93 ppm	2H
CH$_2$	s	δ = 3.75 ppm	2H
O**C**H$_3$	s	δ = 3.68 ppm	3H
CH$_2$	m	δ = 3.05 – 2.79 ppm	8H
CH$_3$	s	δ = 1.46 ppm	9H

^{13}C-NMR (50 MHz, CDCl$_3$)

COOR	δ = 177.8 ppm	1C
CONR	δ = 166.9 ppm	1C
C$_q$	δ = 154.7 ppm	1C
C$_q$	δ = 149.6 ppm	1C
C$_q$	δ = 147.6 ppm	1C
C$_q$	δ = 147.3 ppm	1C
C$_q$	δ = 136.4 ppm	1C
C$_q$	δ = 136.1 ppm	1C
C$_q$	δ = 130.5 ppm	1C
CH (aromatic)	δ = 129.1 ppm	2C
C$_q$	δ = 126.6 ppm	1C
C$_q$	δ = 126.2 ppm	1C
CH (aromatic)	δ = 121.5 ppm	1C
CH (aromatic)	δ = 120.7 ppm	2C
CH (aromatic)	δ = 111.4 ppm	1C
CH (aromatic)	δ = 109.5 ppm	1C
C$_q$	δ = 107.2 ppm	1C
CH (aromatic)	δ = 100.0 ppm	1C
CH$_2$	δ = 60.4 ppm	1C
O**C**H$_3$	δ = 56.0 ppm	1C
O**C**H$_3$	δ = 56.0 ppm	1C
CH$_2$	δ = 55.8 ppm	1C
O**C**H$_3$	δ = 55.6 ppm	1C
CH$_2$	δ = 51.2 ppm	1C
C$_q$	δ = 39.1 ppm	1C
CH$_2$	δ = 33.5 ppm	1C
CH$_2$	δ = 28.8 ppm	1C

CH$_3$	δ = 27.3 ppm	3C

Mass spectrum

m/z	561	(0.46 %, M^+)
	207	(16 %)
	206	(100 %)
	166	(11 %)
	57	(17 %)

Elemental analysis ($C_{32}H_{39}N_3O_6 \cdot 0.75\ SiO_2$)

Calculated:	C (63.35 %)	H (6.48 %)	N (6.93 %)
Found:	C (63.35 %)	H (6.43 %)	N (6.93 %)

VIII.A.2.q 5-((4-(2-(6,7-Dimethoxy-3,4-dihydroisoquinolin-2(1H)-yl)ethyl)-phenyl)carbamoyl)-2-methoxy-4-(quinoline-3-carboxamido)phenyl pivalate (28)

Chemical structure:

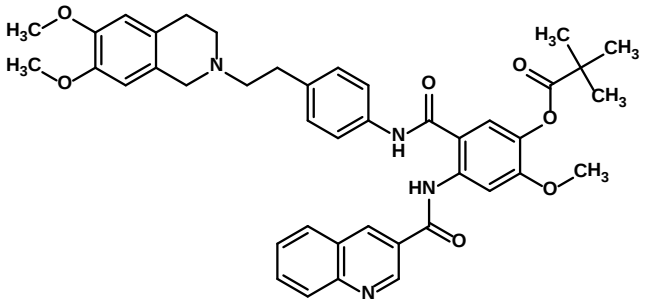

Molecular formula: $C_{42}H_{44}N_4O_7$

Molecular weight: 716.82 g/mol **Exact mass:** 716.32

Internal code: Fba42

3-Quinolinecaboxilic acid (0.26 g, 1.50 mmol) was refluxed in $SOCl_2$ (4 mL) for 3 hours, followed by evaporation of excess $SOCl_2$. The acid chloride was then suspended in THF and added at 0 °C to a solution of **27** (0.39 g, 0.69 mmol) and TEA (0.75 mL) in THF. The reaction mixture was stirred at room temperature overnight and then poured on ice H_2O. The precipitate was filtered off and dried to afford title compound as an off-white solid.

Yield: 0.36 g (72.8 %)

Melting point:

^{1}H-NMR (200 MHz, $CDCl_3$)

CON**H**	s	δ = 13.01 ppm	1H
C**H** (aromatic)	d	δ = 9.39 ppm, *J* = 2.2 Hz	1H
CON**H**	s	δ = 8.67 ppm	1H
C**H** (aromatic)	d	δ = 8.57 ppm, *J* = 2.2 Hz	1H
C**H** (aromatic)	s	δ = 8.54 ppm	1H
C**H** (aromatic)	AB system	δ = 8.04 ppm, A part of an AB system, J_{AB} = 8.6 Hz	1H
C**H** (aromatic)	m	δ = 7.82 – 7.71 ppm	2H
C**H** (aromatic)	AB system	δ = 7.66 ppm, A part of an AB system, J_{AB} = 8.4 Hz	2H
C**H** (aromatic)	m	δ = 7.58 – 7.49 ppm	1H
C**H** (aromatic)	s	δ = 7.39 ppm	1H
C**H** (aromatic)	AB system	δ = 7.27 ppm, B part of an AB system, J_{AB} = 8.4 Hz	2H
C**H** (aromatic)	s	δ = 6.61 ppm	1H
C**H** (aromatic)	s	δ = 6.55 ppm	1H
OC**H**$_3$	s	δ = 3.85 ppm	6H
C**H**$_2$	s	δ = 3.73 ppm	2H
OC**H**$_3$	s	δ = 3.61 ppm	3H
C**H**$_2$	m	δ = 3.05 – 2.76 ppm	8H
C**H**$_3$	s	δ = 1.40 ppm	9H

^{13}C-NMR (50 MHz, $CDCl_3$)

COOR	δ = 177.9 ppm	1C
CONR	δ = 166.7 ppm	1C
CONR	δ = 163.8 ppm	1C
C$_q$	δ = 154.6 ppm	1C
C$_q$	δ = 149.3 ppm	1C
CH (aromatic)	δ = 148.7 ppm	1C
C$_q$	δ = 147.9 ppm	1C
C$_q$	δ = 147.5 ppm	1C
C$_q$	δ = 140.7 ppm	1C
C$_q$	δ = 136.6 ppm	1C
C$_q$	δ = 134.6 ppm	1C
CH (aromatic)	δ = 131.5 ppm	1C
CH (aromatic)	δ = 129.4 ppm	1C
CH (aromatic)	δ = 129.3 ppm	2C

CH (aromatic)	δ = 129.3 ppm	1C
CH (aromatic)	δ = 129.2 ppm	1C
CH (aromatic)	δ = 127.4 ppm	1C
$\mathbf{C}_q$	δ = 126.9 ppm	1C
$\mathbf{C}_q$	δ = 126.8 ppm	1C
$\mathbf{C}_q$	δ = 125.9 ppm	1C
CH (aromatic)	δ = 121.7 ppm	1C
CH (aromatic)	δ = 121.1 ppm	2C
CH (aromatic)	δ = 111.5 ppm	1C
$\mathbf{C}_q$	δ = 111.5 ppm	1C
CH (aromatic)	δ = 109.6 ppm)	1C
CH (aromatic)	δ = 104.8 ppm	1C
$\mathbf{C}H_2$	δ = 59.9 ppm	1C
O$\mathbf{C}H_3$	δ = 56.1 ppm)	1C
O$\mathbf{C}H_3$	δ = 56.0 ppm	1C
O$\mathbf{C}H_3$	δ = 56.0 ppm	1C
$\mathbf{C}H_2$	δ = 55.5 ppm	1C
$\mathbf{C}H_2$	δ = 51.0 ppm	1C
$\mathbf{C}_q$	δ = 39.3 ppm	1C
$\mathbf{C}H_2$	δ = 33.3 ppm	1C
$\mathbf{C}H_2$	δ = 28.4 ppm	1C
$\mathbf{C}H_3$	δ = 27.4 ppm	3C

Two $\mathbf{C}_q$ could not be detected in ^{13}C-NMR.

High resolution mass spectrum (ESI/MS)

m/z calculated for $C_{45}H_{44}N_4O_7 + H^+$: 717.3288

Found : 717.3285

VIII.A.2.r N-(2-((4-(2-(6,7-Dimethoxy-3,4-dihydroisoquinolin-2(1H)-yl)ethyl)-phenyl)carbamoyl)-4-hydroxy-5-methoxyphenyl)quinoline-3-carboxamide (29)

Chemical structure:

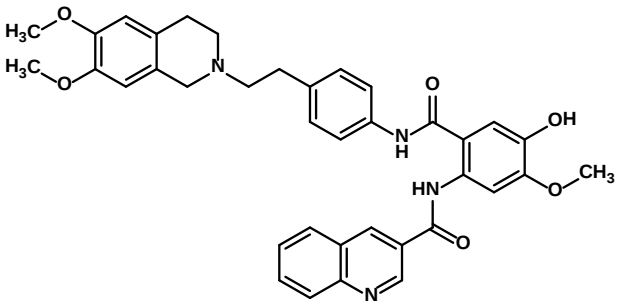

Molecular formula: $C_{37}H_{36}N_4O_6$

Molecular weight: 632.70 g/mol **Exact mass:** 632.26

Internal code: Fba27

Compound **28** (0.21 g, 0.29 mmol) was suspended in a solution of NH_3 in EtOH (2M, 30 mL) and stirred at 50°C for 24 hours. The mixture was then evaporated and the product was purified by column chromatography (EtOAc/EtOH, 4/1) to afford the title compound as an off-white solid.

Yield: 0.10 g (55 %)

Melting point: 184 – 190 °C

^{1}H-NMR (200 MHz, d_6-DMSO)

CON**H**	s	δ = 12.14 ppm	1H
CON**H**	s	δ = 10.32 ppm	1H
C**H** (aromatic)	m	δ = 9.44 – 9.27 ppm	2H
C**H** (aromatic)	d	δ = 8.87 ppm, J = 2.2 Hz	1H
C**H** (aromatic)	s	δ = 8.21 ppm	1H
C**H** (aromatic)	m	δ = 8.18 – 8.09 ppm	2H
C**H** (aromatic)	m	δ = 7.96 – 7.86 ppm	1H
C**H** (aromatic)	m	δ = 7.76 – 7.67 ppm	1H
C**H** (aromatic)	AB system	δ = 7.64 ppm, A part of an AB system, J_{AB} = 8.4 Hz	2H
C**H** (aromatic)	s	δ = 7.44 ppm	1H
C**H** (aromatic)	AB system	δ = 7.23 ppm, B part of an AB system, J_{AB} = 8.4 Hz	2H
C**H** (aromatic)	s	δ = 6.65 ppm	1H
C**H** (aromatic)	s	δ = 6.63 ppm	1H
OC**H**$_3$	s	δ = 3.92 ppm	3H

O**C**H$_3$	s	δ = 3.70 ppm	6H
C**H**$_2$	s	δ = 3.53 ppm	2H
C**H**$_2$	m	δ = 2.87 – 2.60 ppm	8H

^{13}C-NMR (50 MHz, d$_6$-DMSO)

CONR	δ = 167.1 ppm	1C
CONR	δ = 162.9 ppm	1C
C$_q$	δ = 150.3 ppm	1C
C$_q$	δ = 148.6 ppm	1C
CH (aromatic)	δ = 148.3 ppm	1C
C$_q$	δ = 147.1 ppm	1C
C$_q$	δ = 146.9 ppm	1C
C$_q$	δ = 142.2 ppm	1C
C$_q$	δ = 136.5 ppm	1C
C$_q$	δ = 136.2 ppm	1C
CH (aromatic)	δ = 135.5 ppm	1C
C$_q$	δ = 132.1 ppm	1C
CH (aromatic)	δ = 131.6 ppm	1C
CH (aromatic)	δ = 129.3 ppm	1C
CH (aromatic)	δ = 128.8 ppm	2C
CH (aromatic)	δ = 127.6 ppm	1C
C$_q$	δ = 127.6 ppm	1C
CH (aromatic)	δ = 127.4 ppm	1C
C$_q$	δ = 126.6 ppm	1C
C$_q$	δ = 126.6 ppm	1C
C$_q$	δ = 125.9 ppm	1C
CH (aromatic)	δ = 121.1 ppm	2C
CH (aromatic)	δ = 115.5 ppm	1C
C$_q$	δ = 115.2 ppm	1C
CH (aromatic)	δ = 111.8 ppm	1C
CH (aromatic)	δ = 110.0 ppm	1C
CH (aromatic)	δ = 105.5 ppm	1C
CH$_2$	δ = 59.6 ppm	1C
O**C**H$_3$	δ = 55.7 ppm	1C
O**C**H$_3$	δ = 55.5 ppm	1C

O**C**H$_3$	δ = 55.5 ppm	1C
CH$_2$	δ = 55.1 ppm	1C
CH$_2$	δ = 50.6 ppm	1C
CH$_2$	δ = 32.5 ppm	1C
CH$_2$	δ = 28.3 ppm	1C

Mass spectrum

m/z		
	633	(M^+, signal missing)
	128	(35 %)
	119	(48 %)
	57	(43 %)
	55	(42 %)
	44	(100 %)
	43	(48 %)
	41	(31 %)

High resolution mass spectrum (ESI/MS)

m/z calculated for $C_{37}H_{36}N_4O_6 + H^+$:	633.2713
Found :	633.2715

VIII.A.2.s Benzyl 5-(benzyloxy)-4-methoxy-2-nitrobenzoate (30) [Matsuno, 2003]

Chemical structure:

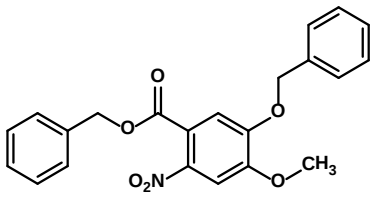

Molecular formula: $C_{22}H_{19}NO_6$

Molecular weight: 393.39 g/mol **Exact mass:** 393.12

Internal code: Fba64

To stirred solution of **20** (2.34 g, 10.98 mmol) and K_2CO_3 (3.30 g, 23.88 mmol) in dry DMF (20 mL) BnCl (2.8 mL, 24.33 mmol) was added under vigorous stirring. The mixture was heated to 75 °C for five hours followed by addition of H_2O (200 mL). The resulting solution was extracted with EtOAc and the combined organic phases were washed with 1 M NaOH, H_2O and brine, dried over Na_2SO_4 and evaporated *in vacuo*. Remaining DMF was removed by

vacuum-flash chromatography, using toluene for washing and EtOAc for elution of the product, to obtain title compound as yellow oil.

Yield: 3.92 g (90.8 %)

Melting point: oil

^{1}H-NMR (200 MHz, $CDCl_3$)

C**H** (aromatic)	m	δ = 7.45 – 7.31 ppm	11H
C**H** (aromatic)	s	δ = 7.14 ppm	1H
C**H**$_2$ (benzylic)	s	δ = 5.30 ppm	2H
C**H**$_2$ (benzylic)	s	δ = 5.17 ppm	2H
OC**H**$_3$	s	δ = 3.92 ppm	3H

^{13}C-NMR (50 MHz, $CDCl_3$)

COOR	δ = 165.6 ppm	1C
C$_q$	δ = 151.6 ppm	1C
C$_q$	δ = 151.1 ppm	1C
C$_q$	δ = 141.6 ppm	1C
C$_q$	δ = 135.2 ppm	1C
C$_q$	δ = 135.0 ppm	1C
CH (aromatic)	δ = 128.9 ppm	2C
CH (aromatic)	δ = 128.7 ppm	2C
CH (aromatic)	δ = 128.6 ppm	4C
CH (aromatic)	δ = 127.6 ppm	2C
C$_q$	δ = 121.3 ppm	1C
CH (aromatic)	δ = 112.8 ppm	1C
CH (aromatic)	δ = 107.3 ppm	1C
CH$_2$ (benzylic)	δ = 71.5 ppm	1C
CH$_2$ (benzylic)	δ = 68.4 ppm	1C
O**C**H$_3$	δ = 56.7 ppm	1C

Mass spectrum

m/z	393	(0.14 %, M^+)
	181	(8.9 %)
	91	(100 %)
	65	(13 %)

VIII.A.2.t 5-(Benzyloxy)-4-methoxy-2-nitrobenzoic acid (31) [Althuis, 1977; Bartolozzi, 2006; Li, 2008]

Chemical structure:

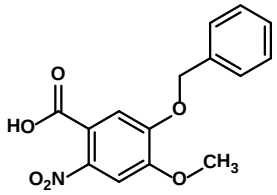

Molecular formula: $C_{15}H_{13}NO_6$

Molecular weight: 303.27 g/mol **Exact mass:** 303.07

Internal code: Fba66

A suspension of **30** (3.32 g, 8.44 mmol) in EtOH (25 mL) and 1 M NaOH (aq., 10 mL) was stirred at room temperature for one hour, after which another 10 mL of 1M NaOH (aq.) was added. The resulting mixture was stirred overnight at room temperature. After completion of the reaction, H_2O (50 mL) was added and the solution was washed three times with CH_2Cl_2. The aqueous layer was acidified to a pH of about 2 with 0.5 M HCl and extracted with EtOAc. The organic layer was dried over Na_2SO_4 and evaporated *in vacuo* to obtain title compound as pale yellow solid. Analytical samples were recrystallized from EtOAc.

Yield: 1.91 g (74.6 %)

Melting point: 192 – 195 °C lit.: 192 °C [Li, 2008]

lit.: 195.5 °C [Althuis, 1977]

^{1}H-NMR (200 MHz, d_4-MeOH)

C**H** (aromatic)	m	δ = 7.50 – 7.31 ppm	7H
C**H**$_2$ (benzylic)	s	δ = 5.20 ppm	2H
OC**H**$_3$	s	δ = 3.93 ppm	3H

^{13}C-NMR (50 MHz, d_4-MeOH)

COOH	δ = 168.5 ppm	1C
C$_q$	δ = 152.6 ppm	1C
C$_q$	δ = 152.5 ppm	1C
C$_q$	δ = 143.5 ppm	1C
C$_q$	δ = 137.4 ppm	1C
CH (aromatic)	δ = 129.6 ppm	2C
CH (aromatic)	δ = 129.3 ppm	1C
CH (aromatic)	δ = 128.9 ppm	2C
C$_q$	δ = 122.4 ppm	1C
CH (aromatic)	δ = 114.2 ppm	1C
CH (aromatic)	δ = 108.4 ppm	1C
CH$_2$ (benzylic)	δ = 72.3 ppm	1C
O**C**H$_3$	δ = 57.0 ppm	1C

Mass spectrum

m/z	303	(1.3 %, M^+)
	91	(100 %)
	65	(17 %)
	51	(8.8 %)

VIII.A.2.u 5-(Benzyloxy)-N-(4-(2-(6,7-dimethoxy-3,4-dihydroisoquinolin-2(1H)-yl)ethyl)phenyl)-4-methoxy-2-nitrobenzamide (32)

Chemical structure:

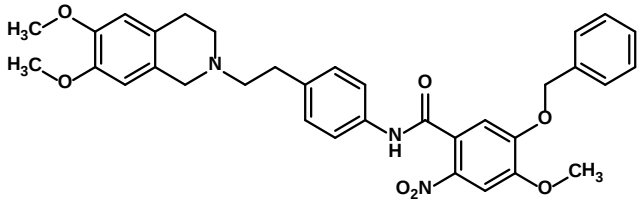

Molecular formula: $C_{34}H_{35}N_3O_7$

Molecular weight: 597.66 g/mol **Exact mass:** 597.25

Internal code: Fba67

Compound **31** (0.63 g, 2.08 mmol) was suspended in $SOCl_2$ (5 mL) containing DMF (2 drops) and heated to reflux for five hours. Excess $SOCl_2$ was removed *in vacuo* and the obtained acid chloride was dissolved in dry THF (7.5 mL). The resulting solution was added to a cooled (0 °C) solution of **2** (0.60 g, 1.92 mmol) and TEA (0.32 mL, 2.30 mmol) in dry THF (7.5 mL). After

stirring at 0 °C for 10 minutes the reaction mixture was warmed to room temperature and stirred overnight before pouring it on ice H_2O (250 mL) and adjusting to pH > 7 with TEA. The precipitate was filtered off, washed with H_2O and purified by column chromatography (toluene/EtOAc/TEA – 7/2/1) obtain title compound as a yellow solid.

Yield: 0.96 g (83.7 %)

Melting point: 122 – 125 °C

^{1}H-NMR (200 MHz, $CDCl_3$)

C**H** (aromatic)	s	δ = 7.94 ppm	1H
C**H** (aromatic)	s	δ = 7.53 ppm	1H
C**H** (aromatic), CON**H**	m	δ = 7.49 – 7.33 ppm	7H
C**H** (aromatic)	m	δ = 7.22 – 7.14 ppm	2H
C**H** (aromatic)	s	δ = 6.98 ppm	1H
C**H** (aromatic)	s	δ = 6.58 ppm	1H
C**H** (aromatic)	s	δ = 6.51 ppm	1H
CH_2 (benzylic)	s	δ = 5.14 ppm	2H
OCH_3	s	δ = 3.90 ppm	3H
OCH_3	s	δ = 3.82 ppm	3H
OCH_3	s	δ = 3.81 ppm	3H
CH_2	s	δ = 3.62 ppm	2H
CH_2	m	δ = 2.97 – 2.64 ppm	8H

^{13}C-NMR (50 MHz, $CDCl_3$)

CONR	δ = 164.7 ppm	1C
C_q	δ = 152.8 ppm	1C
C_q	δ = 149.9 ppm	1C
C_q	δ = 147.6 ppm	1C
C_q	δ = 147.3 ppm	1C
C_q	δ = 138.7 ppm	1C
C_q	δ = 137.2 ppm	1C
C_q	δ = 135.8 ppm	1C
C_q	δ = 135.2 ppm	1C
CH (aromatic)	δ = 129.4 ppm	2C

CH (aromatic)	δ = 128.9 ppm	2C
CH (aromatic)	δ = 128.7 ppm	1C
CH (aromatic)	δ = 127.7 ppm	2C
$\mathbf{C}_q$	δ = 127.1 ppm	1C
$\mathbf{C}_q$	δ = 126.6 ppm	1C
$\mathbf{C}_q$	δ = 126.2 ppm	1C
CH (aromatic)	δ = 120.7 ppm	2C
CH (aromatic)	δ = 111.8 ppm	1C
CH (aromatic)	δ = 111.4 ppm	1C
CH (aromatic)	δ = 109.5 ppm	1C
CH (aromatic)	δ = 107.5 ppm	1Ci
$\mathbf{C}H_2$ (benzylic)	δ = 71.5 ppm	1C
$\mathbf{C}H_2$	δ = 60.3 ppm	1C
O$\mathbf{C}H_3$	δ = 56.6 ppm	1C
O$\mathbf{C}H_3$	δ = 56.0 ppm	1C
O$\mathbf{C}H_3$	δ = 56.0 ppm	1C
$\mathbf{C}H_2$	δ = 55.8 ppm	1C
$\mathbf{C}H_2$	δ = 51.2 ppm	1C
$\mathbf{C}H_2$	δ = 33.6 ppm	1C
$\mathbf{C}H_2$	δ = 28.8 ppm	1C

Mass spectrum

m/z	597	(M^+, signal missing)
	206	(28 %)
	164	(27 %)
	91	(100 %)
	77	(13 %)
	65	(21 %)

Elemental analysis ($\mathbf{C_{34}H_{35}N_3O_7}$)

Calculated:	C (68.33 %)	H (5.90 %)	N (7.03 %)
Found:	C (68.62 %)	H (5.75 %)	N (6.79 %)

VIII.A.2.v 2-Amino-5-(benzyloxy)-N-(4-(2-(6,7-dimethoxy-3,4-dihydroisoquinolin-2-(1H)-yl)ethyl) phenyl)-4-methoxybenzamide (33)

Chemical structure:

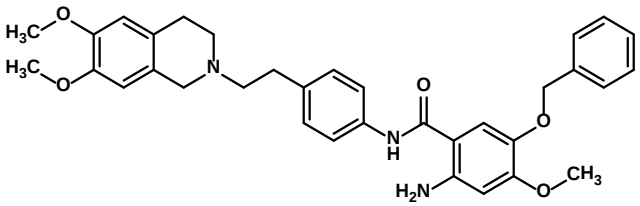

Molecular formula: $C_{34}H_{37}N_3O_5$

Molecular weight: 567.67 g/mol **Exact mass:** 567.27

Internal code: Fba86

To a stirred solution of compound **32** (1.51 g, 2.53 mmol) in EtOH (30 mL) and THF (30 mL) under argon atmosphere, Raney-Nickel (W.R. Grace and Co. Raney®2800 slurry in H_2O, 1mL) was added. After addition of hydrazine monohydrate (65% aq. Solution, 1 mL), the mixture was heated to reflux until no starting material was observed in TLC. After cooling to room temperature the catalyst was filtered off and the solvent was evaporated. The crude product was purified by column chromatography (toluene/EtOAc/TEA, 5/4/1) to afford title compound as white solid.

Yield: 1.04 g (73.8 %)

Melting point: 173 – 177 °C

^{1}H-NMR (200 MHz, $CDCl_3$)

CON**H**	s	δ = 7.49 ppm	1H
C**H** (aromatic)	m	δ = 7.45 – 7.12 ppm	9H
C**H** (aromatic)	s	δ = 6.94 ppm	1H
C**H** (aromatic)	s	δ = 6.60 ppm	1H
C**H** (aromatic)	s	δ = 6.54 ppm	1H
C**H** (aromatic)	s	δ = 6.20 ppm	1H
N**H**$_2$	br s	δ = 5.40 ppm	2H
C**H**$_2$ (benzylic)	s	δ = 5.02 ppm	2H
OC**H**$_3$	s	δ = 3.86 ppm	3H
OC**H**$_3$	s	δ = 3.84 ppm	3H
OC**H**$_3$	s	δ = 3.83 ppm	3H
C**H**$_2$	s	δ = 3.64 ppm	2H
C**H**$_2$	m	δ = 2.95 – 2.68 ppm	8H

^{13}C-NMR (50 MHz, $CDCl_3$)

CONH	δ = 167.1 ppm	1C
$\mathbf{C}_q$	δ = 154.9 ppm	1C
$\mathbf{C}_q$	δ = 147.6 ppm	1C
$\mathbf{C}_q$	δ = 147.3 ppm	1C
$\mathbf{C}_q$	δ = 146.1 ppm	1C
$\mathbf{C}_q$	δ = 139.4 ppm	1C
$\mathbf{C}_q$	δ = 137.4 ppm	1C
$\mathbf{C}_q$	δ = 136.4 ppm	1C
$\mathbf{C}_q$	δ = 136.2 ppm	1C
CH (aromatic)	δ = 129.3 ppm	2C
CH (aromatic)	δ = 128.6 ppm	2C
CH (aromatic)	δ = 128.1 ppm	1C
CH (aromatic)	δ = 128.0 ppm	2C
$\mathbf{C}_q$	δ = 126.7 ppm	1C
$\mathbf{C}_q$	δ = 126.3 ppm	1C
CH (aromatic)	δ = 120.7 ppm	2C
CH (aromatic)	δ = 116.0 ppm	1C
CH (aromatic)	δ = 111.5 ppm	1C
CH (aromatic)	δ = 109.6 ppm	1C
$\mathbf{C}_q$	δ = 107.4 ppm	1C
CH (aromatic)	δ = 100.9 ppm	1C
$\mathbf{C}H_2$ (benzylic)	δ = 73.3 ppm	1C
$\mathbf{C}H_2$	δ = 60.4 ppm	1C
O$\mathbf{C}H_3$	δ = 56.0 ppm	1C
O$\mathbf{C}H_3$	δ = 56.0 ppm	1C
O$\mathbf{C}H_3$	δ = 55.9 ppm	1C
$\mathbf{C}H_2$	δ = 55.8 ppm	1C
$\mathbf{C}H_2$	δ = 51.2 ppm	1C
$\mathbf{C}H_2$	δ = 33.6 ppm	1C
$\mathbf{C}H_2$	δ = 28.8 ppm	1C

Mass spectrum

m/z	567	(0.48 %, M^+)
	207	(19 %)
	206	(100 %)
	164	(19 %)
	91	(20 %)

Elemental analysis ($C_{34}H_{37}N_3O_5 \cdot 0.25\ H_2O$)

Calculated:	C (71.37 %)	H (6.61 %)	N (7.34 %)
Found:	C (71.43 %)	H (6.36 %)	N (7.11 %)

VIII.A.2.w N-(4-(Benzyloxy)-2-((4-(2-(6,7-dimethoxy-3,4-dihydroisoquinolin-2-(1H)-yl)ethyl)-phenyl) carbamoyl)-5-methoxyphenyl)quinoline-3-carboxamide (34)

Chemical structure:

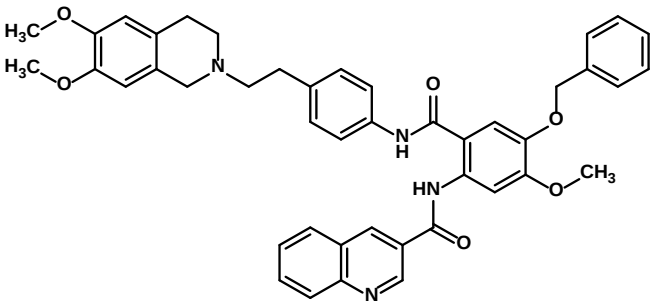

Molecular formula: $C_{44}H_{42}N_4O_6$

Molecular weight: 722.83 g/mol **Exact mass:** 722.31

Internal code: Fba87

Method A:

3-Quinolinecarboxylic acid (0.35 g, 2.02 mmol) was refluxed in $SOCl_2$ (4.5 mL) containing DMF (3 drops) for four hours. Excess $SOCl_2$ was removed and the resulting solid was suspended in CH_2Cl_2 (7 mL). The resulting suspension was added to a cooled (0°C) solution of **33** (0.95 g, 1.67 mmol) and TEA (0.60 mL, 4.30 mmol) in CH_2Cl_2 (10 mL). After ten minutes the reaction mixture was warmed to room temperature and stirred overnight. After diluting with CH_2Cl_2 (40 mL) the mixture was washed three times with 2 M K_2CO_3 solution (aq.) and brine, dried over Na_2SO_4 and concentrated *in vacuo*. The crude product was subjected to column chromatography (EtOAc/EtOH – 9/1) and washed with EtOH to obtain title compound as a white solid.

Method B:

To a cooled (0°C) solution of **33** (281 mg, 0.49 mmol), 3-quinolinecarboxylic acid (92 mg, 0.53 mmol) and HOBt.xH_2O (~14% H_2O, 90 mg, 0.57 mmol) in DMF (3 mL) EDC•HCl (191 mg, 1.00 mmol) was added. After 15 minutes the mixture was warmed to room temperature and stirred for 24 hours. After addition of H_2O (15 mL) and 1 M NaOH (0.75 mL) the reaction mixture was extracted with CH_2Cl_2, the organic layer was washed with 1 M NaOH dried over Na_2SO_4 and evaporated *in vacuo*. The resulting crude product was recrystallized from CH_2Cl_2/n-hexane to afford title compound as a white solid.

Yield:	***method A:***	0.43 g (35.5 %)
	method B:	0.23 g (64.4 %)
Melting point:	191 – 195 °C	

^{1}H-NMR (200 MHz, $CDCl_3$)

CON**H**	s	δ = 12.48 ppm	1H
C**H** (aromatic)	d	δ = 9.53 ppm, *J* = 2.2 Hz	1H
C**H** (aromatic)	d	δ = 8.74 ppm, *J* = 2.2 Hz	1H
C**H** (aromatic)	s	δ = 8.57 ppm	1H
C**H** (aromatic)	d	δ = 8.15 ppm, *J* = 8.4 Hz	1H
CON**H**	m	δ = 8.05 – 7.91 ppm	2H
C**H** (aromatic)			
C**H** (aromatic)	m	δ = 7.85 – 7.75 ppm	1H
C**H** (aromatic)	m	δ = 7.66 – 7.49 ppm	3H
C**H** (aromatic)	m	δ = 7.37 – 7.22 ppm	7H
C**H** (aromatic)	s	δ = 7.09 ppm	1H
C**H** (aromatic)	s	δ = 6.61 ppm	1H
C**H** (aromatic)	s	δ = 6.55 ppm	1H
C**H**$_2$ (benzylic)	s	δ = 5.01 ppm	2H
OC**H**$_3$	s	δ = 3.94 ppm	3H
OC**H**$_3$	s	δ = 3.84 ppm	3H
OC**H**$_3$	s	δ = 3.83 ppm	3H
C**H**$_2$	s	δ = 3.66 ppm	2H
C**H**$_2$	m	δ = 2.98 – 2.70 ppm	8H

^{13}C-NMR (50 MHz, $CDCl_3$)

CONR	δ = 167.4 ppm	1C
CONR	δ = 164.0 ppm	1C
$\mathbf{C}_q$	δ = 153.9 ppm	1C
$\mathbf{C}_q$	δ = 149.5 ppm	1C
CH (aromatic)	δ = 148.9 ppm	1C
$\mathbf{C}_q$	δ = 147.6 ppm	1C
$\mathbf{C}_q$	δ = 147.3 ppm	1C
$\mathbf{C}_q$	δ = 143.3 ppm	1C
$\mathbf{C}_q$	δ = 137.4 ppm	1C
$\mathbf{C}_q$	δ = 136.7 ppm	1C
$\mathbf{C}_q$	δ = 136.4 ppm	1C
CH (aromatic)	δ = 135.9 ppm	1C
$\mathbf{C}_q$	δ = 135.6 ppm	1C
CH (aromatic)	δ = 131.5 ppm	1C
CH (aromatic)	δ = 129.5 ppm	3H
CH (aromatic)	δ = 129.3 ppm	1H
CH (aromatic)	δ = 128.7 ppm	2H
CH (aromatic)	δ = 128.3 ppm	1H
CH (aromatic)	δ = 127.7 ppm	2H
CH (aromatic)	δ = 127.5 ppm	1H
$\mathbf{C}_q$	δ = 127.3 ppm	1H
$\mathbf{C}_q$	δ = 127.0 ppm	1H
$\mathbf{C}_q$	δ = 126.6 ppm	1C
$\mathbf{C}_q$	δ = 126.2 ppm	1C
CH (aromatic)	δ = 121.0 ppm	2C
CH (aromatic)	δ = 114.0 ppm	1C
$\mathbf{C}_q$	δ = 112.1 ppm	1C
CH (aromatic)	δ = 111.4 ppm	1C
CH (aromatic)	δ = 109.6 ppm	1C
CH (aromatic)	δ = 105.3 ppm	1C
$\mathbf{C}H_2$ (benzylic)	δ = 72.2 ppm	1C
$\mathbf{C}H_2$	δ = 60.2 ppm	1C
O$\mathbf{C}H_3$	δ = 56.2 ppm	1C
O$\mathbf{C}H_3$	δ = 56.0 ppm	1C
O$\mathbf{C}H_3$	δ = 56.0 ppm	1C

CH$_2$	δ = 55.8 ppm	1C
CH$_2$	δ = 51.1 ppm	1C
CH$_2$	δ = 33.6 ppm	1C
CH$_2$	δ = 28.8 ppm	1C

Mass spectrum

m/z	722	(M^+, signal missing)
	167	(63 %)
	122	(62 %)
	69	(67 %)
	68	(61 %)
	57	(100 %)
	55	(90 %)
	43	(76 %)

Elemental analysis ($C_{44}H_{42}N_4O_6 \cdot 0.5\ H_2O$)

Calculated:	C (72.21 %)	H (5.92 %)	N (7.66 %)
Found:	C (72.20 %)	H (5.87 %)	N (7.77 %)

VIII.A.2.x N-(2-(2-(4-(2-(6,7-Dimethoxy-3,4-dihydroisoquinolin-2(1H)-yl)ethyl)-phenyl)-2H-tetrazol-5-yl)-5-hydroxy-4-methoxyphenyl)-4-oxo-4H-chromene-2-carboxamide (35)

Chemical structure:

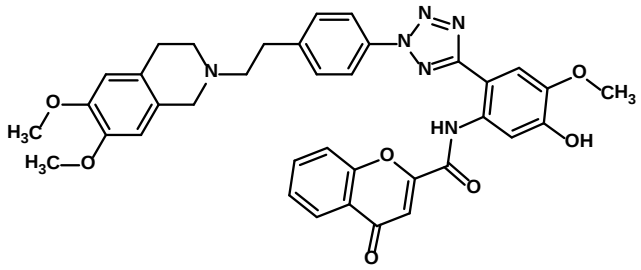

Molecular formula: $C_{37}H_{34}N_6O_7$

Molecular weight: 674.70 g/mol **Exact mass:** 674.25

Internal code: Fba80

To a suspension of **39** (0.42 g, 0.55 mmol) in thioanisole (4 mL), TFA (13 mL) was added slowly under stirring. The reaction mixture was kept at room temperature during the course of the reaction. Upon complete conversion of the starting material (TLC monitoring) the reaction was

neutralized with aqueous $NaHCO_3$-solution. The resulting solid was filtered off and washed with H_2O and toluene. The product was suspended in THF and 1M HCl in Et_2O was added. After keeping the solution at 4°C overnight the formed solid was collected by filtration to obtain the dihydrochloride of title compound as a green solid (0.33 g, 80.3 %).

Yield:	0.33 g (80.3 %)
Melting point (•2 HCl):	165 – 168 °C

^{1}H-NMR (200 MHz, d_6-DMSO) dihydrochloride

CON**H, H**Cl	m	δ = 11.80 – 11.49 ppm	2H
HCl	br s	δ = 10.04 ppm	1H
C**H** (aromatic)	m	δ = 8.24 – 7.97 ppm	4H
C**H** (aromatic)	m	δ = 7.93 – 7.75 ppm	1H
C**H** (aromatic)	m	δ = 7.67 – 7.47 ppm	5H
C**H** (aromatic)	m	δ = 6.95 – 6.74 ppm	3H
C**H**$_2$, O**H**	m	δ = 4.60 – 4.19 ppm	3H
OC**H**$_3$	s	δ = 3.83 ppm	3H
OC**H**$_3$	s	δ = 3.75 ppm	3H
OC**H**$_3$	s	δ = 3.74 ppm	3H
C**H**$_2$	m	δ = 3.52 – 2.82 ppm	8H

^{13}C-NMR (50 MHz, d_6-DMSO) dihydrochloride

CO	δ = 177.1 ppm	1C
CNN	δ = 163.5 ppm	1C
CONR	δ = 156.9 ppm	1C
C$_q$	δ = 155.1 ppm	1C
C$_q$	δ = 154.8 ppm	1C
C$_q$	δ = 149.5 ppm	1C
C$_q$	δ = 148.3 ppm	1C
C$_q$	δ = 147.7 ppm	1C
C$_q$	δ = 145.2 ppm	1C
C$_q$	δ = 139.8 ppm	1C
CH (aromatic)	δ = 135.0 ppm	1C

C$_q$	δ = 134.7 ppm	1C
CH (aromatic)	δ = 130.3 ppm	2C
C$_q$	δ = 129.7 ppm	1C
CH (aromatic)	δ = 126.2 ppm	1C
CH (aromatic)	δ = 125.0 ppm	1C
C$_q$	δ = 123.6 ppm	1C
C$_q$	δ = 123.4 ppm	1C
CH (aromatic)	δ = 120.5 ppm	2C
CH (aromatic)	δ = 120.2 ppm	1C
C$_q$	δ = 120.0 ppm	1C
CH (aromatic)	δ = 118.4 ppm	1C
CH (aromatic)	δ = 111.5 ppm	1C
CH (aromatic)	δ = 111.1 ppm	1C
CH (aromatic)	δ = 110.9 ppm	1C
CH (aromatic)	δ = 109.7 ppm	1C
C$_q$	δ = 107.0 ppm	1C
O**C**H$_3$	δ = 55.7 ppm	1C
O**C**H$_3$	δ = 55.6 ppm	1C
O**C**H$_3$	δ = 55.5 ppm	1C
CH$_2$	δ = 55.3 ppm	1C
CH$_2$	δ = 51.2 ppm	1C
CH$_2$	δ = 48.8 ppm	1C
CH$_2$	δ = 29.1 ppm	1C
CH$_2$	δ = 24.5 ppm	1C

Mass spectrum

m/z	674	(M^+, signal missing)
	207	(25 %)
	206	(100 %)
	189	(40 %)
	164	(70 %)
	77	(23 %)

Elemental analysis ($C_{37}H_3N_6O_7 \cdot 2\ HCl \cdot 0.5\ H_2O$)

Calculated:	C (58.73 %)	H (4.93 %)	N (11.11 %)
Found:	C (58.91 %)	H (4.95 %)	N (10.93 %)

VIII.A.2.y I-N'-(4-(Benzyloxy)-5-methoxy-2-nitrobenzylidene)-4-methylbenzene-sulfonohydrazide (36)

Chemical structure:

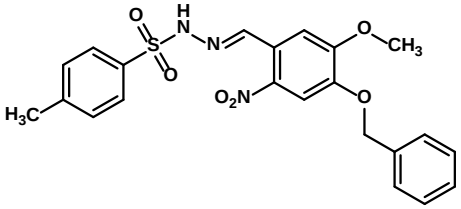

Molecular formula: $C_{22}H_{21}N_3O_6S$

Molecular weight: 455.48 g/mol **Exact mass:** 455.12

Internal code: Fba75

To a stirred suspension of 4-methylbenzenesulfonohydrazide (0.64 g, 3.44 mmol) in EtOH (7 mL), 4-(benzyloxy)-5-methoxy-2-nitrobenzaldehyde (1.01 g, 3.52 mmol) suspended in EtOH (23 mL) was added. The resulting mixture was heated to reflux for one hour. After cooling to room temperature H_2O (100 mL) was added. The precipitate was collected by vacuum filtration and washed with EtOH to obtain title compound as yellow solid.

Yield: 1.37 g (87.5 %)

Melting point: 165 – 167 °C

^{1}H-NMR (200 MHz, d_6-DMSO)

SO_2NH	br s	δ = 11.77 ppm	1H
CHN	s	δ = 8.35 ppm	1H
CH (aromatic)	AB system	δ = 7.80 ppm , A part of an AB system, J_{AB} = 8.1 Hz	2H
CH (aromatic)	s	δ = 7.72 ppm	1H
CH (aromatic)	m	δ = 7.54 – 7.30 ppm	7H
CH (aromatic)	s	δ = 7.16 ppm	1H
CH_2 (benzylic)	s	δ = 5.22 ppm	2H
OCH_3	s	δ = 3.89 ppm	3H
CH_3	s	δ = 2.36 ppm	3H

^{13}C-NMR (50 MHz, d_6-DMSO)

C$_q$	δ = 153.0 ppm	1C
C$_q$	δ = 148.5 ppm	1C
C$_q$	δ = 143.7 ppm	1C
CH (aromatic)	δ = 142.9 ppm	1C
C$_q$	δ = 140.6 ppm	1C
C$_q$	δ = 135.9 ppm	1C
C$_q$	δ = 135.9 ppm	1C
CH (aromatic)	δ = 129.8 ppm	2C
CH (aromatic)	δ = 128.5 ppm	2C
CH (aromatic)	δ = 128.2 ppm	1C
CH (aromatic)	δ = 128.1 ppm	2C
CH (aromatic)	δ = 127.4 ppm	2C
C$_q$	δ = 123.0 ppm	1C
CH (aromatic)	δ = 109.0 ppm	1C
CH (aromatic)	δ = 108.5 ppm	1C
CH$_2$ (benzylic)	δ = 70.4 ppm	1C
O**C**H$_3$	δ = 56.1 ppm	1C
CH$_3$	δ = 21.0 ppm	1C

Mass spectrum

m/z	455	(M^+, signal missing)
	107	(7.3 %)
	92	(14 %)
	91	(100 %)
	65	(30 %)
	63	(11 %)
	51	(9.3 %)

Elemental analysis ($C_{22}H_{21}N_3O_6S$)

Calculated:	C (58.01 %)	H (4.65 %)	N (9.23 %)
Found:	C (57.82 %)	H (4.44 %)	N (9.11 %)

VIII.A.2.z 2-(4-(5-(4-(Benzyloxy)-5-methoxy-2-nitrophenyl)-2H-tetrazol-2-yl)-phenethyl)-6,7-dimethoxy-1,2,3,4-tetrahydroisoquinoline (37)

Chemical structure:

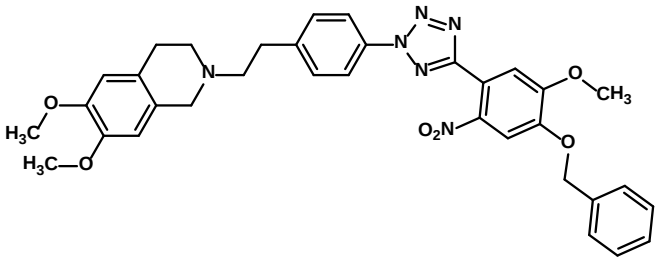

Molecular formula: $C_{34}H_{34}N_6O_6$

Molecular weight: 622.67 g/mol **Exact mass:** 622.25

Internal code: Fba76

To a cooled (0 °C) suspension of compound **2** (0.65 g, 2.08 mmol) in 50 % aqueous EtOH (3.5 mL) 36 % HCl (0.56 mL) was added dropwise. After addition of $NaNO_2$ (0.17 g, 2.42 mmol) in H_2O (0.88 mL) the resulting mixture was stirred at 0 °C for 15 minutes and then cooled to -15 °C. Compound **36** (0.95 g, 2.07 mmol) in pyridine (12 mL) was added over a period of five minutes. The reaction mixture was stirred at -15 °C for three hours and then at room temperature overnight. The slurry was acidified with hydrochloric acid (1 M, 170 mL) and extracted with CH_2Cl_2. The organic phase was washed with hydrochloric acid (1 M), H_2O, saturated aqueous $NaHCO_3$-solution and brine, dried over Na_2SO_4 and concentrated under reduced pressure. The crude product was purified by recrystallization from toluene to obtain title compound as an orange solid.

Yield: 1.11 g (85.6 %)

Melting point: 174 – 178 °C

^{1}H-NMR (200 MHz, $CDCl_3$)

C**H** (aromatic)	AB system	δ = 8.05 ppm, A part of an AB system, J_{AB} = 8.5 Hz	2H
C**H** (aromatic)	s	δ = 7.61 ppm	1H
C**H** (aromatic)	m	δ = 7.51 – 7.34 ppm	7H
C**H** (aromatic)	s	δ = 7.31 ppm	1H
C**H** (aromatic)	s	δ = 6.61 ppm	1H
C**H** (aromatic)	s	δ = 6.54 ppm	1H
C**H**$_2$ (benzylic)	s	δ = 5.25 ppm	2H
OC**H**$_3$	s	δ = 4.00 ppm	3H
OC**H**$_3$	s	δ = 3.84 ppm	3H
OC**H**$_3$	s	δ = 3.84 ppm	3H

C**H**$_2$	s	δ = 3.66 ppm	2H
C**H**$_2$	m	δ = 3.07 – 2.73 ppm	8H

^{13}C-NMR (50 MHz, CDCl$_3$)

CNN	δ = 162.1 ppm	1C
C$_q$	δ = 152.9 ppm	1C
C$_q$	δ = 149.3 ppm	1C
C$_q$	δ = 147.6 ppm	1C
C$_q$	δ = 147.3 ppm	1C
C$_q$	δ = 142.9 ppm	1C
C$_q$	δ = 141.8 ppm	1C
C$_q$	δ = 135.3 ppm	1C
C$_q$	δ = 135.0 ppm	1C
CH (aromatic)	δ = 130.0 ppm	2C
CH (aromatic)	δ = 128.9 ppm	2C
CH (aromatic)	δ = 128.6 ppm	1C
CH (aromatic)	δ = 127.7 ppm	2C
C$_q$	δ = 126.4 ppm	1C
C$_q$	δ = 126.2 ppm	1C
CH (aromatic)	δ = 120.1 ppm	2C
C$_q$	δ = 115.9 ppm	1C
CH (aromatic)	δ = 113.1 ppm	1C
CH (aromatic)	δ = 111.4 ppm	1C
CH (aromatic)	δ = 109.9 ppm	1C
CH (aromatic)	δ = 109.5 ppm	1C
CH$_2$ (benzylic)	δ = 71.5 ppm	1C
CH$_2$	δ = 59.7 ppm	1C
O**C**H$_3$	δ = 56.7 ppm	1C
O**C**H$_3$	δ = 56.0 ppm	1C
O**C**H$_3$	δ = 56.0 ppm	1C
CH$_2$	δ = 55.8 ppm	1C
CH$_2$	δ = 51.1 ppm	1C
CH$_2$	δ = 33.7 ppm	1C
CH$_2$	δ = 28.8 ppm	1C

Mass spectrum

m/z	622	(M^+, signal missing)
	206	(100 %)
	189	(35 %)
	164	(47 %)
	146	(36 %)
	91	(99 %)
	77	(21 %)

Elemental analysis ($C_{34}H_{34}N_6O_6$)

Calculated:	C (65.58 %)	H (5.50 %)	N (13.50 %)
Found:	C (65.24 %)	H (5.23 %)	N (13.22 %)

VIII.A.2.aa 5-(Benzyloxy)-2-(2-(4-(2-(6,7-dimethoxy-3,4-dihydroisoquinolin-2-(1H)-yl)-ethyl)phenyl)-2H-tetrazol-5-yl)-4-methoxyaniline (38)

Chemical structure:

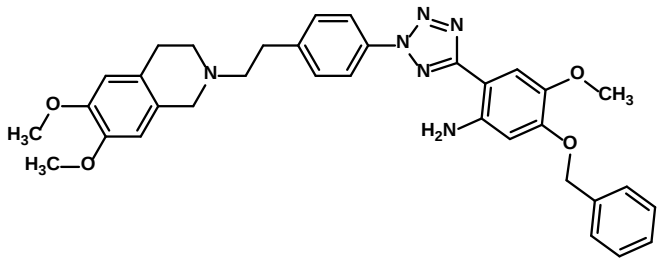

Molecular formula: $C_{34}H_{36}N_6O_4$

Molecular weight: 592.69 g/mol **Exact mass:** 592.28

Internal code: Fba77

To a stirred solution of compound **37** (1.30 g, 2.09 mmol) in EtOH (30 mL) and THF (30 mL) under argon atmosphere Raney-Nickel (W.R. Grace and Co. Raney®2800 slurry in H_2O, 1mL) was added. After addition of hydrazine monohydrate (65 % aq. Solution; 0 h, 5 h, 7.5 h; 1 mL each) the mixture was heated to reflux until no starting material was observed in TLC. The catalyst was filtered off and rinsed with CH_2Cl_2. Evaporation of the solvent afforded the title compound as off-white solid.

Yield: 0.94 g (76.0 %)

Melting point: 165 – 167 °C

^{1}H-NMR (200 MHz, $CDCl_3$)

C**H** (aromatic)	AB system	δ = 8.08 ppm, A part of an AB system, J_{AB} = 8.4 Hz	2H
C**H** (aromatic)	s	δ = 7.74 ppm	1H
C**H** (aromatic)	m	δ = 7.51 – 7.29 ppm	7H
C**H** (aromatic)	s	δ = 6.61 ppm	1H
C**H** (aromatic)	s	δ = 6.54 ppm	1H
C**H** (aromatic)	s	δ = 6.36 ppm	1H
N**H**$_2$	br s	δ = 5.25 ppm	2H
C**H**$_2$ (benzylic)	s	δ = 5.18 ppm	2H
OC**H**$_3$	s	δ = 3.93 ppm	3H
OC**H**$_3$	s	δ = 3.85 ppm	3H
OC**H**$_3$	s	δ = 3.84 ppm	3H
C**H**$_2$	s	δ = 3.72 ppm	2H
C**H**$_2$	m	δ = 3.11 – 2.79 ppm	8H

^{13}C-NMR (50 MHz, $CDCl_3$)

CNN	δ = 165.0 ppm	1C
C$_q$	δ = 151.7 ppm	1C
C$_q$	δ = 147.9 ppm	1C
C$_q$	δ = 147.5 ppm	1C
C$_q$	δ = 142.3 ppm	1C
C$_q$	δ = 142.1 ppm	1C
C$_q$	δ = 141.4 ppm	2C
C$_q$	δ = 136.8 ppm	1C
C$_q$	δ = 135.3 ppm	1C
CH (aromatic)	δ = 130.0 ppm	2C
CH (aromatic)	δ = 128.7 ppm	2C
CH (aromatic)	δ = 128.1 ppm	1C
CH (aromatic)	δ = 127.3 ppm	2C
C$_q$	δ = 125.9 ppm	1C
CH (aromatic)	δ = 120.0 ppm	2C
CH (aromatic)	δ = 112.2 ppm	1C
CH (aromatic)	δ = 111.5 ppm	1C
CH (aromatic)	δ = 109.6 ppm	1C
CH (aromatic)	δ = 102.6 ppm	1C

C$_q$	δ = 101.9 ppm	1C
CH$_2$ (benzylic)	δ = 70.8 ppm	1C
CH$_2$	δ = 59.5 ppm	1C
O**C**H$_3$	δ = 57.0 ppm	1C
O**C**H$_3$	δ = 56.1 ppm	1C
O**C**H$_3$	δ = 56.0 ppm	1C
CH$_2$	δ = 55.6 ppm	1C
CH$_2$	δ = 51.0 ppm	1C
CH$_2$	δ = 33.5 ppm	1C
CH$_2$	δ = 28.4 ppm	1C

Mass spectrum

m/z	592	(0.03 %, M^+)
	207	(16 %)
	206	(100 %)
	91	(13 %)
	42	(12 %)

Elemental analysis ($C_{34}H_{36}N_6O_4$)

Calculated:	C (68.90 %)	H (6.12 %)	N (14.18 %)
Found:	C (68.63 %)	H (5.85 %)	N (13.97 %)

VIII.A.2.bb N-(5-(Benzyloxy)-2-(2-(4-(2-(6,7-dimethoxy-3,4-dihydroisoquinolin-2-(1H)-yl)ethyl)phenyl)-2H-tetrazol-5-yl)-4-methoxyphenyl)-4-oxo-4H-chromene-2-carboxamide (39)

Chemical structure:

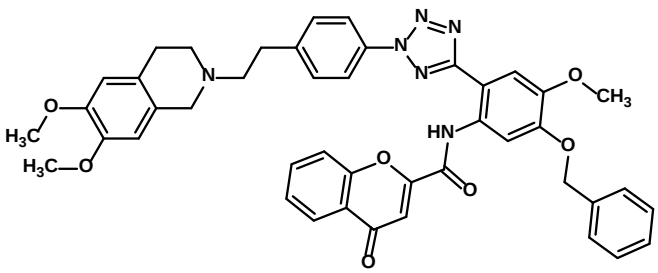

Molecular formula: $C_{44}H_{40}N_6O_7$

Molecular weight: 764.82 g/mol **Exact mass:** 764.30

Internal code: Fba78

Compound **38** (0.87 g, 1.47 mmol), 4-oxo-4*H*-chromene-2-carboxylic acid (0.29 g, 1.53 mmol) and HOBt.xH_2O (~14% H_2O, 0.25 g, 1.59 mmol) were dissolved in DMF (12 mL) and the resulting mixture was cooled to 0 °C. After addition of EDC•HCl (0.42 g, 2.19 mmol) the reaction mixture was stirred at room temperature. More EDC•HCl was added to the reaction mixture at 22 hours (0.20 g, 1.04 mmol) and at 29 hours (0.40 g, 2.08 mmol) after start of the reaction. After two more days H_2O (48 mL) was added to the solution and the resulting mixture was extracted with CH_2Cl_2. The combined organic layers were washed with 5 % aqueous $NaHCO_3$ solution and H_2O, dried over Na_2SO_4 and evaporated *in vacuo*. The crude product was subjected to column chromatography (toluene/EtOAc/TEA – 7/2/1) to obtain title compound as a yellow solid.

Yield: 0.44 g (39.1 %)

Melting point: 85 – 89 °C

^{1}H-NMR (200 MHz, $CDCl_3$)

CON**H**	s	δ = 12.45 ppm	1H
C**H** (aromatic)	s	δ = 8.66 ppm	1H
C**H** (aromatic)	AB system	δ = 8.19 ppm, A part of an AB system, J_{AB} = 7.9 Hz	1H
C**H** (aromatic)	AB system	δ = 8.11 ppm, A part of an AB system, J_{AB} = 8.5 Hz	2H
C**H** (aromatic)	m	δ = 7.77 – 7.70 ppm	3H
C**H** (aromatic)	m	δ = 7.59 – 7.31 ppm	8H
C**H** (aromatic)	s	δ = 7.21 ppm	1H
C**H** (aromatic)	s	δ = 6.62 ppm	1H
C**H** (aromatic)	s	δ = 6.56 ppm	1H
C**H**$_2$ (benzylic)	s	δ = 5.23 ppm	2H
OC**H**$_3$	s	δ = 3.97 ppm	3H
OC**H**$_3$	s	δ = 3.86 ppm	3H
OC**H**$_3$	s	δ = 3.85 ppm	3H
C**H**$_2$	s	δ = 3.68 ppm	2H
C**H**$_2$	m	δ = 3.09 – 2.76 ppm	8H

^{13}C-NMR (50 MHz, $CDCl_3$)

CO	δ = 178.4 ppm	1C

CNN	δ = 164.3 ppm	1C
CONR	δ = 157.4 ppm	1C
$\mathbf{C}_q$	δ = 155.4 ppm	1C
$\mathbf{C}_q$	δ = 155.2 ppm	1C
$\mathbf{C}_q$	δ = 150.7 ppm	1C
$\mathbf{C}_q$	δ = 147.8 ppm	1C
$\mathbf{C}_q$	δ = 147.5 ppm	1C
$\mathbf{C}_q$	δ = 146.5 ppm	1C
$\mathbf{C}_q$	δ = 143.4 ppm	1C
$\mathbf{C}_q$	δ = 136.3 ppm	1C
$\mathbf{C}_q$	δ = 134.9 ppm	1C
CH (aromatic)	δ = 134.7 ppm	1C
$\mathbf{C}_q$	δ = 131.2 ppm	1C
CH (aromatic)	δ = 130.2 ppm	2C
CH (aromatic)	δ = 128.7 ppm	2C
CH (aromatic)	δ = 128.3 ppm	1C
CH (aromatic)	δ = 128.0 ppm	2C
$\mathbf{C}_q$	δ = 126.5 ppm	1C
$\mathbf{C}_q$	δ = 126.2 ppm	1C
CH (aromatic)	δ = 126.0 ppm	2C
$\mathbf{C}_q$	δ = 124.4 ppm	1C
CH (aromatic)	δ = 120.5 ppm	2C
CH (aromatic)	δ = 118.6 ppm	1C
CH (aromatic)	δ = 112.2 ppm	1C
CH (aromatic)	δ = 111.5 ppm	1C
CH (aromatic)	δ = 110.8 ppm	1C
CH (aromatic)	δ = 109.6 ppm	1C
$\mathbf{C}_q$	δ = 107.2 ppm	1C
CH (aromatic)	δ = 106.1 ppm	1C
$\mathbf{C}H_2$ (benzylic)	δ = 70.9 ppm	1C
$\mathbf{C}H_2$	δ = 59.7 ppm	1C
O$\mathbf{C}H_3$	δ = 56.4 ppm	1C
O$\mathbf{C}H_3$	δ = 56.1 ppm	1C
O$\mathbf{C}H_3$	δ = 56.1 ppm	1C
$\mathbf{C}H_2$	δ = 55.9 ppm	1C
$\mathbf{C}H_2$	δ = 51.2 ppm	1C

CH$_2$	δ = 33.8 ppm	1C
CH$_2$	δ = 28.9 ppm	1C

Mass spectrum

m/z	764	(M^+, signal missing)
	207	(21 %)
	206	(100 %)
	164	(35 %)
	91	(99 %)
	65	(17 %)

Elemental analysis ($C_{44}H_{40}N_6O_7$)

Calculated:	C (69.10 %)	H (5.27 %)	N (10.99 %)
Found:	C (68.78 %)	H (5.11 %)	N (10.67 %)

VIII.A.2.cc 2-Chloro-3-quinolinecarboxylic acid (40) [Cale, 1986]

Chemical structure:

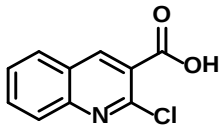

Molecular formula: $C_{10}H_6ClNO_2$

Molecular weight: 207.61 g/mol **Exact mass:** 207.01 / 209.01

Internal code: Fba19

To a suspension of compound **41** (2.00 g, 10.44 mmol) in EtOH (2 mL), $AgNO_3$ (5.00 g, 29.43 mmol) in H_2O (10 mL) and KOH (3.53 g, 62.91 mmol) in H_2O (10 mL) were added consecutively. The resulting mixture was stirred at room temperature for four hours, and filtered afterwards. Upon acidification to pH 5 with 2M H_2SO_4 a solid crushed out, which was collected by filtration and recrystallized from EtOH to obtain title compound as a white solid.

Yield: 1.89 g (87.2 %)

Melting point: 185 – 188 °C lit.: 190 – 210 °C [Cale, 1986]

^{1}H-NMR (200 MHz, d_6-DMSO)

COO**H**	br s	δ = 13.79 ppm	1H
C**H** (aromatic)	s	δ = 8.93 ppm	1H
C**H** (aromatic)	AB system	δ = 8.16 ppm, A part of an AB system, J_{AB} = 8.0 Hz	1H
C**H** (aromatic)	AB system	δ = 7.99 ppm, A part of an AB system, J_{AB} = 8.2 Hz	1H
C**H** (aromatic)	m	δ = 7.96 – 7.84 ppm	1H
C**H** (aromatic)	m	δ = 7.78 – 7.65 ppm	1H

^{13}C-NMR (50 MHz, d_6-DMSO)

COOH	δ = 165.8 ppm	1C
C$_q$	δ = 147.4 ppm	1C
C$_q$	δ = 146.5 ppm	1C
CH (aromatic)	δ = 141.4 ppm	1C
CH (aromatic)	δ = 132.8 ppm	1C
CH (aromatic)	δ = 129.0 ppm	1C
CH (aromatic)	δ = 128.1 ppm	1C
CH (aromatic)	δ = 127.7 ppm	1C
C$_q$	δ = 125.9 ppm	1C
C$_q$	δ = 125.5 ppm	1C

VIII.A.2.dd 2-Chloroquinoline-3-carbaldehyde (41) [Meth-Cohn, 1981]

Chemical structure:

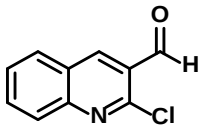

Molecular formula: $C_{10}H_6ClNO$

Molecular weight: 191.61 g/mol **Exact mass:** 191.01 / 193.01

Internal code: Fba18

To ice-cooled dry DMF (9.94 g, 136.00 mmol) $POCl_3$ (32.2 mL, 345.46 mmol) was slowly added under stirring. Subsequently acetanilide (6.86 g, 50.75 mmol) was added and the reaction mixture was heated to 75 °C for 19 hours. After cooling to room temperature the mixture was poured on ice-water and stirred for 30 minutes. The precipitate was filtered off, washed with water and recrystallized from EtOAc to obtain title compound as pale yellow solid.

Yield: 5.68 g (58.4 %)

Melting point: 147 – 148 °C 148 – 149 °C [Meth-Cohn, 1981]

^{1}H-NMR (200 MHz, $CDCl_3$)

C**H**O	s	δ = 10.56 ppm	1H
C**H** (aromatic)	s	δ = 8.75 ppm	1H
C**H** (aromatic)	AB system	δ = 8.07 ppm, A part of an AB system, J_{AB} = 8.4 Hz	1H
C**H** (aromatic)	AB system	δ = 7.99 ppm, B part of an AB system, J_{AB} = 8.1 Hz	1H
C**H** (aromatic)	m	δ = 7.94 – 7.84 ppm	1H
C**H** (aromatic)	m	δ = 7.71 – 7.60 ppm	1H

^{13}C-NMR (50 MHz, $CDCl_3$)

CHO	δ = 189.6 ppm	1C
C$_q$	δ = 150.5 ppm	1C
C$_q$	δ = 150.0 ppm	1C
CH (aromatic)	δ = 140.7 ppm	1C
CH (aromatic)	δ = 134.0 ppm	1C
CH (aromatic)	δ = 130.1 ppm	1C
CH (aromatic)	δ = 129.0 ppm	1C
CH (aromatic)	δ = 128.6 ppm	1C
C$_q$	δ = 126.9 ppm	1C
C$_q$	δ = 126.8 ppm	1C

VIII.A.2.ee 2-Chloro-N-(2-((4-(2-(6,7-dimethoxy-3,4-dihydroisoquinolin-2-(1H)-yl) ethyl)phenyl)carbamoyl)-4,5-dimethoxyphenyl)quinoline-3-carboxamide (42)

Chemical structure:

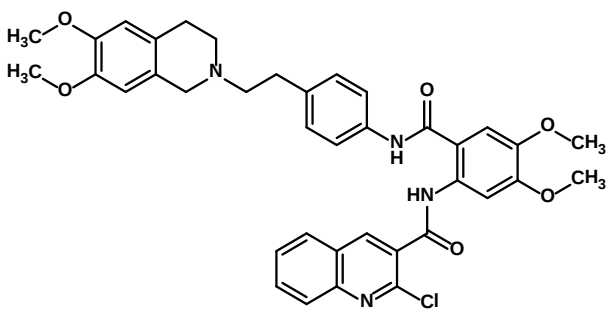

Molecular formula: $C_{38}H_{37}ClN_4O_6$

Molecular weight: 681.18 g/mol **Exact mass:** 680.24 / 682.24

Internal code: Fba20

2-Chloro-3-quinolinecarboxylic acid (0.21 g, 1.01 mmol) was refluxed in $SOCl_2$ (3 mL) for six hours. After removing excess $SOCl_2$ the residue was dissolved in THF (5 mL) and added to a cooled (0 °C) solution of the aniline derivative **4** (0.25 g, 0.51 mmol) and TEA (0.5 mL) in THF (10 mL). After ten minutes the mixture was warmed to room temperature and stirred overnight. Upon pouring the reaction mixture on ice water (150 mL) the product crushed out and was filtered off. Purification by column chromatography (toluene/EtOAc/TEA – 7/2/1) yielded the title compound as off white solid.

Yield: 0.17 g (48.9 %)

Melting point: 162 – 165 °C

^{1}H-NMR (200 MHz, $CDCl_3$)

CON**H**	s	δ = 11.76 ppm	1H
C**H** (aromatic)	s	δ = 8.51 ppm	1H
C**H** (aromatic)	s	δ = 8.41 ppm	1H
CON**H,** C**H** (aromatic)	m	δ = 8.16 – 7.99 ppm	2H
C**H** (aromatic)	m	δ = 7.92 – 7.76 ppm	2H
C**H** (aromatic)	m	δ = 7.68 – 7.55 ppm	1H
C**H** (aromatic)	AB system	δ = 7.43 ppm , A part of an AB system, J_{AB} = 8.4 Hz	2H
C**H** (aromatic)	m	δ = 7.24 – 7.17 ppm	2H
C**H** (aromatic)	s	δ = 7.12 ppm	1H
C**H** (aromatic)	s	δ = 6.59 ppm	1H
C**H** (aromatic)	s	δ = 6.52 ppm	1H
OC**H**$_3$	s	δ = 3.99 ppm	3H
OC**H**$_3$	s	δ = 3.88 ppm	3H
OC**H**$_3$	s	δ = 3.83 ppm	3H
OC**H**$_3$	s	δ = 3.82 ppm	3H
C**H**$_2$	s	δ = 3.62 ppm	2H
C**H**$_2$	m	δ = 2.94 – 2.64 ppm	8H

^{13}C-NMR (50 MHz, $CDCl_3$)

CONR	δ = 167.2 ppm	1C
CONR	δ = 164.1 ppm	1C
$\mathbf{C}_q$	δ = 152.8 ppm	1C
$\mathbf{C}_q$	δ = 148.0 ppm	1C
$\mathbf{C}_q$	δ = 147.6 ppm	1C
$\mathbf{C}_q$	δ = 147.3 ppm	1C
$\mathbf{C}_q$	δ = 146.6 ppm	1C
$\mathbf{C}_q$	δ = 145.0 ppm	1C
CH (aromatic)	δ = 138.4 ppm	1C
$\mathbf{C}_q$	δ = 137.6 ppm	1C
$\mathbf{C}_q$	δ = 135.2 ppm	1C
$\mathbf{C}_q$	δ = 135.2 ppm	1C
CH (aromatic)	δ = 132.1 ppm	1C
$\mathbf{C}_q$	δ = 130.3 ppm	1C
CH (aromatic)	δ = 129.5 ppm	2C
CH (aromatic)	δ = 128.6 ppm	1C
CH (aromatic)	δ = 128.4 ppm	1C
CH (aromatic)	δ = 127.9 ppm	1C
$\mathbf{C}_q$	δ = 126.5 ppm	1C
$\mathbf{C}_q$	δ = 126.3 ppm	1C
$\mathbf{C}_q$	δ = 126.2 ppm	1C
CH (aromatic)	δ = 121.5 ppm	2C
$\mathbf{C}_q$	δ = 112.8 ppm	1C
CH (aromatic)	δ = 111.4 ppm	1C
CH (aromatic)	δ = 109.8 ppm	1C
CH (aromatic)	δ = 109.5 ppm	1C
CH (aromatic)	δ = 105.3 ppm	1C
$\mathbf{C}H_2$	δ = 60.2 ppm	1C
O$\mathbf{C}H_3$	δ = 56.6 ppm	1C
O$\mathbf{C}H_3$	δ = 56.4 ppm	1C
O$\mathbf{C}H_3$	δ = 56.0 ppm	1C
O$\mathbf{C}H_3$	δ = 56.0 ppm	1C
$\mathbf{C}H_2$	δ = 55.8 ppm	1C
$\mathbf{C}H_2$	δ = 51.1 ppm	1C
$\mathbf{C}H_2$	δ = 33.5 ppm	1C

CH$_2$	δ = 28.8 ppm	1C

Mass spectrum

m/z	682 / 680	(M^+, signal missing)
	207	(18 %)
	206	(100 %)
	180	(63 %)
	164	(25 %)
	57	(12 %)
	42	(13 %)

Elemental analysis ($C_{38}H_{37}ClN_4O_6 \cdot 1\,H_2O$)

Calculated:	C (65.28 %)	H (5.62 %)	N (8.01 %)
Found:	C (65.43 %)	H (5.47 %)	N (7.74 %)

VIII.A.2.ff 2-(4-(4,5-Dimethoxy-2-(quinoline-3-carboxamido)benzamido)phenethyl)-6,7-dimethoxy-2-methyl-1,2,3,4-tetrahydroisoquinolin-2-ium iodide (43)

Chemical structure:

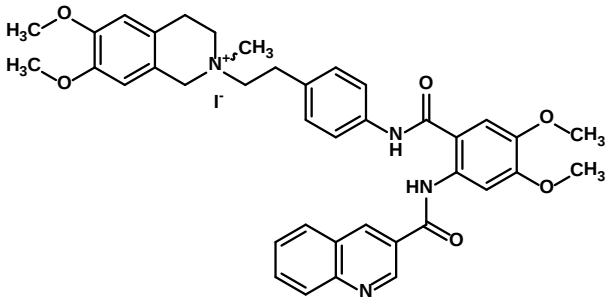

Molecular formula: $C_{39}H_{41}N_4O_6^+ \cdot I^-$

Molecular weight: 788.21 g/mol **Exact mass (cation):** 661.30

Internal code: Fba21

To a solution of tariquidar (0.78 g, 1.21 mmol) in dry acetone (170 mL) MeI (0.2 mL, 3.21 mmol) was added. Upon keeping the mixture at 4 °C for about a week a white solid formed, which was filtered off and washed with acetone to obtain title compound as white powder.

Yield: 0.76 g (79.7 %)

Melting point: 228 – 232 °C decomposition

^{1}H-NMR (200 MHz, d_6-DMSO)

CON**H**	s	δ = 12.24 ppm	1H
CON**H**	s	δ = 10.37 ppm	1H
C**H** (aromatic)	s	δ = 9.32 ppm	1H
C**H** (aromatic)	s	δ = 8.86 ppm	1H
C**H** (aromatic)	m	δ = 8.27 – 8.05 ppm	3H
C**H** (aromatic)	m	δ = 7.97 – 7.84 ppm	1H
C**H** (aromatic)	m	δ = 7.79 – 7.62 ppm	3H
C**H** (aromatic)	s	δ = 7.50 ppm	1H
C**H** (aromatic)	AB system	δ = 7.34 ppm, B part of an AB system, J_{AB} = 8.0 Hz	2H
C**H** (aromatic)	s	δ = 6.89 ppm	1H
C**H** (aromatic)	s	δ = 6.78 ppm	1H
C**H**$_2$	m	δ = 4.85 – 4.41 ppm	2H
OC**H**$_3$	m	δ = 3.98 – 3.85 ppm	6H
OC**H**$_3$	m	δ = 3.80 – 3.72 ppm	6H
C**H**$_2$	m	δ = 3.70 – 3.54 ppm	2H
NC**H**$_3$	s	δ = 3.36 ppm	3H
C**H**$_2$	m	δ = 3.27 – 3.06 ppm	6H

^{13}C-NMR (50 MHz, d_6-DMSO)

CONR	δ = 167.1 ppm	1C
CONR	δ = 163.0 ppm	1C
C$_q$	δ = 151.5 ppm	1C
C$_q$	δ = 148.7 ppm	1C
C$_q$	δ = 148.6 ppm	1C
CH (aromatic)	δ = 148.2 ppm	1C
C$_q$	δ = 147.9 ppm	1C
C$_q$	δ = 144.4 ppm	1C
C$_q$	δ = 137.3 ppm	1C
CH (aromatic)	δ = 135.7 ppm	1C
C$_q$	δ = 133.7 ppm	1C
C$_q$	δ = 132.0 ppm	1C
CH (aromatic)	δ = 131.6 ppm	1C
CH (aromatic)	δ = 129.3 ppm	1C
CH (aromatic)	δ = 129.2 ppm	2C

CH (aromatic)	δ = 128.8 ppm	1C
CH (aromatic)	δ = 127.7 ppm	1C
$\mathbf{C}_q$	δ = 127.4 ppm	1C
$\mathbf{C}_q$	δ = 126.5 ppm	1C
CH (aromatic)	δ = 121.9 ppm	2C
$\mathbf{C}_q$	δ = 121.6 ppm	1C
$\mathbf{C}_q$	δ = 118.4 ppm	1C
$\mathbf{C}_q$	δ = 114.2 ppm	1C
CH (aromatic)	δ = 111.9 ppm	1C
CH (aromatic)	δ = 111.6 ppm	1C
CH (aromatic)	δ = 109.9 ppm	1C
CH (aromatic)	δ = 105.3 ppm	1C
$\mathbf{C}H_2$	δ = 63.4 ppm	1C
$\mathbf{C}H_2$	δ = 60.9 ppm	1C
$\mathbf{C}H_2$	δ = 57.1 ppm	1C
O$\mathbf{C}H_3$	δ = 56.1 ppm	1C
O$\mathbf{C}H_3$	δ = 55.6 ppm	2C
O$\mathbf{C}H_3$	δ = 55.6 ppm	1C
N$\mathbf{C}H_3$	δ = 46.5 ppm	1C
$\mathbf{C}H_2$	δ = 27.3 ppm	1C
$\mathbf{C}H_2$	δ = 22.9 ppm	1C

Mass spectrum

m/z	661	(M^+, signal missing)
	206	(100 %)
	189	(34 %)
	164	(97 %)
	136	(46 %)
	103	(33 %)
	77	(32 %)

Elemental analysis ($\mathbf{C_{39}H_{41}IN_4O_6 \cdot 0.25\ H_2O}$)

Calculated:	C (59.06 %)	H (5.27 %)	N (7.06 %)
Found:	C (58.92 %)	H (5.07 %)	N (7.02 %)

VIII.B Biological Evaluation

VIII.B.1 Animals

The *in vivo* experiments for this thesis were performed in adult female Sprague Dawley rats from Harlan Netherlands (Horst, Netherlands) and in female wild type, *Mdr1a/b*$^{(-/-)}$, *Bcrp1*$^{(-/-)}$ and *Mdr1a/b*$^{(-/-)}$*Bcrp1*$^{(-/-)}$ FVB mice from Taconic Inc. (Germantown, USA) or Charles River (Sulzfeld, Germany). The studies were approved by the local animal welfare committee and all study procedures were performed in accordance with the Austrian Animal Experiments Act. All efforts were undertaken to minimize the suffering and the number of animal used in the studies.

Before the experiments the animals were placed in an induction box and anesthetized with 2.5 % isoflurane and were kept under anesthesia with 1 -2 % isoflurane administered by a cone mask during the course of the experiments. The animals were kept warm during the experiments at about 38 °C.

For the small-animal PET experiments the rats were implanted with a catheter in the femoral artery. In mice the tracer was applied *via* the lateral tail vain.

VIII.B.2 Technical Equipment

The small-animal PET scans were performed on a microPET Focus220 (Siemens Medical Solutions, Knoxville, USA).

Blood samples and solutions of the metabolite assays were counted for activity in a Wallac gamma counter (Perkin Elmer Instruments, Wellesley, USA).

VIII.B.3 Experimental Setup

In rats paired scans were performed, consisting of a 150-minutes baseline scan, during which unlabelled inhibitor (tariquidar: 15 mg/kg or elacridar: 5 mg/kg) was administered intravenously over 1 minute at 1 hour after radiotracer injection and a second 60-minutes PET scan starting two hours after administration of unlabelled inhibitor. For the small-animal PET evaluation in mice 60-minutes single scans in wild type and transporter KO mice were carried out.

For the determination of the metabolic stability of the evaluated PET tracers blood samples were collected at 20 and 60 minutes or at 30 minutes after tracer injection. After centrifugation at 10000 rpm for four to five minutes plasma was added to 0.5 mL H_2O containing 20 µL reference solution (10 mg/mL unlabelled inhibitor in DMSO) and 80 µL 5M HCl. The mixture was vortexed and applied to a Sep-Pak tC18 cartridge, which has been preactivated with 3 mL MeOH and 5 mL H_2O. Following elution with 4 mL H_2O and 4 mL MeOH the collected samples were counted in a gamma counter for activity and subjected to HPLC or TLC analysis.

IX Bibliography

Abrahim, A.; Luurtsema, G; Bauer, M; Karch, R.; Lubberink, M.; Pataraia, E.; Loukhadar, C.; Kletter, K.; Lammertsmaa, A.A.; Baumgartner, C.; Müller, M.; Langer, O.: Peripheral metabolism of (*R*)-[^{11}C]verapamil in epilepsy patients. *Eur. J. Nucl. Med. Mol. Imaging* **2008**, *35*, 116-123.

Agarwal, S.; Hartz, A.M.; Elmquist, W.F.; Bauer, B.: Breast Cancer Resistance Protein and P-glycoprotein in Brain Cancer: Two Gatekeepers Team Up. *Curr. Pharm. Des.* **2011**, *17*, 2793-2802.

Althuis, T.H. and Hess, H.-J.: Synthesis and Identification of the Major Metabolites of Prazosin Formed in Dog and Rat. *J. Med. Chem.* **1977**, *20*, 146-149.

Ambudkar, S.V.; Dey, S.; Hrycyna, C.A.; Ramachandra, M.; Pastan, I.; Gottesman, M.M.: Biochemical, cellular, and pharmacological aspects of the multidrug transporter. *Annu. Rev. Pharmacol. Toxicol.* **1999**, *39*, 361-398.

Ambudkar, S.V.; Kimchi-Sarfaty, C.; Sauna, Z.E.; Gottesman, M.M.: P-glycoprotein: from genomics to mechanism. *Oncogene* **2003**, *22*, 7468-7485.

Aronica, E; Gorter, J.A.; Ramkema, M.; Redeker, S.; Ozbas-Gerçeker, F.; van Vliet, E.A.; Scheffer, G.L.; Scheper, R.J.; van der Valk, P.; Baayen, J.C.; Troost, D.: Expression and cellular distribution of multidrug resistance-related proteins in the hippocampus of patients with mesial temporal lobe epilepsy. *Epilepsia* **2004**, *45*, 441-451.

Van Assema, D.M.E.; Lubberink, M.; Bauer, M.; van der Flier, W.M.; Schuit, R.C.; Windhorst, A.D.; Comans, E.F.I.; Hoetjes, N.J.; Tolboom, N.; Langer, O.; Müller, M.; Scheltens, P.; Lammertsma, A.A.; Berckel, B.N.M.: Blood-brain barrier P-glycoprotein function in Alzheimer's disease. *Brain* **2012**, *135*, 181-189.

Bang, 2005 Bang, K.C.; Cha, M.Y.; Ahn, Y.G.;Ham, Y.J.; Kim, M.S.; Lee, G.S.: P-glycoprotein Inhibitor, Method for Preparing the Same and Pharmaceutical Composition Comprising the Same. *PCT Int. Appl.* **2005**, WO 2005/033097 A1.

Bankstahl, J.P.; Kuntner, C.; Abrahim, A.; Karch, R.; Stanek, J.; Wanek, T.; Wadsak, W.; Kletter, K.; Müller, M.; Löscher, W.; Langer, O.: Tariquidar-induced P-glycoprotein inhibition at the

rat blood-brain barrier studied with (*R*)-^{11}C-verapamil and PET. *J. Nucl. Med.* **2008**, *49*, 1328-1335.

Bartolozzi, A.; Sweetnam, P.; Campbell, S.; Foudoulakis, H.; Kirk, B.; Ram, S.: Pharmacokinetically improved compounds. *PCT Int. Appl.* **2006**, WO 2006/105081 A2.

Batcho, A.D. and Leimgruber, W.: Indoles from 2-methylnitrobenzenes by condensation with formamide acetals followed by reduction: 4-Benzyloxyindole. *Org. Synth.* **1985**, *63*, 214.

Bates, S.; Kang, M.; Meadows, B.; Bakke, S.; Choyke, P.; Merino, M.; Goldspiel, B.; Chico, I.; Smith, T.; Chen, C.; Robey, R.; Bergan, R.; Figg, W.D.; Fojo, T. A: Phase I study of infusional vinblastine in combination with the P-Glykoprotein antagonist PSC 833 (valspodar). *Cancer* **2001**, *92*, 1577-1590.

Bauer, M.; Karch, R.; Zeitlinger, M.; Stanek, J.; Philippe, C.; Wadsak, W.; Mitterhauser, M.; Jäger, W.; Haslacher, H.; Müller, M.; Langer, O.: Interaction of ^{11}C-tariquidar and ^{11}C-elacridar with P-glycoprotein and breast cancer resistance protein at the human blood-brain barrier. *J. Nucl. Med.* **2013**, *54*, 1181-1187.

Bobbit, J.M.; Winter, D.P.; Kiely, J.M.: Synthesis of Isoquinolines. IV. 4-Benzylisoquinolines. *J. Org. Chem.* **1965**, *30*, 2459-2460.

Bobbit, J.M. and Sih, J.C.: Synthesis of Isoquinolines. VII. 4-Hydroxy-1,2,3,4-tetrahydroisoquinolines. *J. Org. Chem.* **1968**, *33*, 856-858.

Bradbury, M.W.: The blood-brain barrier. Transport across the cerebral endothelium. *Circ. Res.* **1985**, *57*, 213-222.

Cale, A.D.: Fused aromatic oxazepinones, thiazepinones, diazepinones and their sulfur analogs. *US Patent* **1986**, US 4 592 866 (A).

Chiba, P. and Ecker, G.F.: Inhibitors of ABC-type drug efflux pumps: an overview of the current patent situation. *Expert Opin. Ther. Patents*, **2004**, *14*, 499-508.

Choi, M.G.; Ryu, D.H.; Jeon, H.L.; Cha, S.; Cho, J.; Joo, H.H.; Hong, K.S.; Lee, C.; Ahn, S.; Chang, S.-K.: Chemodosiometric Hg-Selective Signaling by Mercuration of Dichlorofluorescein Derivatives. *Org. Lett.* **2008**, *10*, 3717-3720.

Cole, S.P.; Bhardwaj, G.; Gerlach, J.H.; Mackie, J.E.; Grant, C.E.; Almquist, K.C.; Steward, A.J.; Kurz, E.U.; Duncan, A.M.; Deeley, R.G.: Overexpression of a transporter gene in a multidrug-resistant human lung cancer cell line. *Science* **1992**, *258*, 1650-1654.

Cordon-Cardo, C.; O'Brien, J.P.; Boccia, J.; Casals, D.; Bertino, J.R.; Melamed, M.R.: Expression of the multidrug resistance gene product (P-glycoprotein) in human normal tissues. *J. Histochem. Cytochem.* **1990**, *38*, 1277-1287.

Dean, M.; Hamon, Y.; Chimini, G.: The human ATP-binding cassette (ABC) transporter superfamily. *J. Lipid Res.* **2001a**, *42*, 1007-1017.

Dean, M.; Rzhetsky, A.; Allikmets, R.: The Human ATP-Binding Cassette (ABC) Transporter Superfamiliy. *Genome Res.* **2001b**, *11*, 1156-1166.

Dörner, B.; Kuntner, C.; Bankstahl, J.P.; Bankstahl, M.; Stanek, J.; Wanek, T.; Stundner, G.; Mairinger, S.; Löscher, W.; Müller, M.; Langer, O.; Erker, T.: Synthesis and Small-Animal Positron Emission Tomography Evaluation of [^{11}C]-Elacridar as a Radiotracer to Assess the Distribution of P-Glycoprotein at the Blood-Brain Barrier. *J. Med. Chem.* **2009**, *52*, 6073-6082.

Dörner, B.; Kuntner, C.; Bankstahl, J.P.; Wanek, T.; Bankstahl, M.; Stanek, J.; Müllauer, J.; Bauer, F.; Mairinger, S.; Löscher, W.; Miller, D.W.; Chiba, P.; Müller, M.; Erker, T.; Langer, O.: Radiosynthesis and *in vivo* evaluation of 1-[^{18}F]fluoroelacridar as a positron emission tomography tracer for P-glycoprotein and breast cancer resistance protein. *Bioorg. Med. Chem.* **2011**, *19*, 2190-2198.

Dörner, B.: Synthesis and biological evaluation of PET radiotracers for determination of P-glycoprotein at the blood-brain barrier. *Doctoral thesis*, University of Vienna, **2012**.

Doyle, L.A.; Yang, W.; Abruzzo, L.V.; Krogmann, T.; Gao, Y.; Rishi, A.K.; Ross, D.D.: A multidrug resistance transporter from human MCF-7 breast cancer cells. *Proc. Natl.Acad.Sci. USA* **1998**, *95*, 15665-15670.

Eckelman, W.C. and Mathis, C.A.: Targeting proteins *in vivo*: *in vitro* guidelines. *Nucl. Med. Biol.* **2006**, *33*, 161–164.

Engelhardt, B.: Molecular mechanisms involved in T cell migration across the blood-brain barrier. *J. Neural Transm.* **2006**, *113*, 477-485.

Felix, A.M.; Heimer, E.P.; Lambros, T.J.; Tzougraki, C.; Meienhofer, J.: Rapid Removal of Protecting Groups from Peptides by Catalytic Transfer Hydrogenation with 1,4-Cyclohexadiene. *J. Org. Chem.* **1978**, *43*, 4194-4196.

Fox, E. and Bates, S.E.: Tariquidar (XR9576): a P-glycoprotein drug efflux pump inhibitor. *Expert Rev. Anticancer Ther.* **2007**, *7*, 447–459.

Hall, M.D.; Handley, M.D.; Gottesman, M.M.: Is resistance useless? Multidrug resistance and collateral sensitivity. *Trends Pharmacol. Sci.* **2009**, *30*, 546-556.

Hayman, D.F. and Wright, M.: Process for the preparation of a hydrate of an anthranilic acid derivative. *PCT Int. Appl.* **2003**, WO 03/095447 A1.

Jin, M. S.; Oldham, M.L.; Zhang, Q.; Chen, J.: Crystal structure of the multidrug transporter P-glycoprotein from *Caenorhabditis elegans*. *Nature* **2012**, *490*, 566-569.

Joshi, B.S.; Desai, H.K.; Pelletier, S.W.: Synthesis of Pratorimine. *J. Nat. Prod.* **1986**, *49*, 445-448.

Juliano, R.L. and Ling, V.: A surface glycoprotein modulating drug permeability in Chinese hamster ovary cell mutants. *Biochim. Biophys. Acta* **1976**, *455*, 152-162.

Kamiie, J.; Ohtsuki, S.; Iwase, R.; Ohmine, K.; Katsukura, Y.; Yanai, K.; Sekine, Y.; Uchida, Y.; Ito, S.; Terasaki, T.: Quantitative Atlas of Membrane Transporter Proteins: Development and Application of a Highly Sensitive Simultaneous LC/MS/MS Method Combined with Novel *In-silico* Peptide Selection Criteria. *Pharmaceutical Research* **2008**, *25*, 1469-1483.

Kannan, P.; John, C.; Zoghbi, S.S.; Halldin, C.; Gottesman, M.M.; Innis, R.B.; Hall, M.D.: Imaging the Function of P-Glycoprotein With Radiotracers: Pharmacokinetics and *In Vivo* Applications. *Clin. Pharmacol. Ther.* **2009**, *86*, 368-377.

Kannan, P.; Telu, S.; Shukla, S.; Ambudkar, S.V.; Pike, V.W.; Halldin, C.; Gottesman, M.M.; Innis, R.B.; Hall, M.D.: The ”specific” P-glycoprotein inhibitor tariquidar is also a substrate and an inhibitor for breast cancer resistance protein (BCRP/ABCG2), *ACS Chem. Neurosci.* **2011**, *2*, 82–89.

Kannan, P.; Pike, V.W.; Halldin, C.; Langer, O.; Gottesman, M.M.; Innis, R.B.; Hall, M.D.: Factors That Limit Positron Emission Tomography Imaging of P-Glycoprotein Density at the Blood-Brain Barrier. *Mol. Pharmaceutics* **2013**, *10*, 2222-2229.

Kawamura, K.; Konno, F.; Yui, J.; Yamasaki, T.; Hatori, A.; Yanamoto, K.; Wakizaka, H.; Takei, M.; Nengaki, N.; Fukumura, T. Zhang, M.-R.: Synthesis and evaluation of [^{11}C]XR9576 to assess the function of drug efflux transporters using PET. *Ann. Nucl. Med.* **2010**, *24*, 403-412.

Kawamura, K.; Yamasaki, T.; Konno, F.; Yui, J.; Hatori, A.; Yanamoto, K.; Wakizaka, H.; Ogawa, M.; Yoshida, Y.; Nengaki, N.; Fukumura, T.; Zhang, M.-R.: Synthesis and *in vivo* evaluation of ^{18}F-fluoroethyl GF120918 and XR9576 as positron emission tomography probes for assessing the function of drug efflux transporters. *Bioorg. Med. Chem.* **2011a**, *19*, 861-870.

Kawamura, K.; Yamasaki, T.; Konno, F.; Yui, J.; Hatori, A.; Yanamoto, K.; Wakizaka, H.; Takei, M.; Kimura, Y.; Fukumura, T.; Zhang, M.-R.: Evaluation of Limiting Brain Penetration Related to P-glycoprotein and Breast Cancer Resistance Protein Using [^{11}C]GF120918 by PET in Mice. *Mol. Imaging Biol.* **2011b**, *13*, 152-160.

Kiso, Y.; Ukawa, K.; Nakamura, S.; Ito, K.; Akita, T.: Efficient Removal of Protecting Groups by a "Push-Pull" Mechanism. II. Deprotection of *O*-Benzyltyrosine with Thioanisole-Trifluoroacetic acid System without *O*-to-*C* Rearrangements. *Chem. Pharm. Bull.* **1980**, *28*, 673-676.

Klinkhammer, W.: Design, Synthese und 3D-QSAR neuartiger P-gp-Modulatoren. *Doctoral thesis*, Rheinische Friedrich-Wilhelms-Universität Bonn, **2006**.

Klinkhammer, W.; Müller, H.; Globisch, C.; Pajeva, I.K.; Wiese, M.: Synthesis and biological evaluation of a small molecule library of 3rd generation multidrug resistance modulators. *Bioorg. Med. Chem.* **2009**, *17*, 2524-2535.

Krishna, R. and Mayer L.D.: Multidrug resistance (MDR) in cancer. Mechanisms, reversal using modulators of MDR and the role of MDR modulators in influencing the pharmacokinetics of anticancer drugs. *Eur. J. Pharm. Sci.* **2000**, *11*, 265-283.

Kwak, J.-O.; Lee, S.H.; Lee, G.S.; Kim, M.S.; Ahn,Y.-G.; Lee, J.H.; Kim, S.W.; Kim, K.H.; Lee, M.G.: Selective inhibition of MDR1 (ABCB1) by HM30181 increases oral bioavailability and therapeutic efficacy of paclitaxel. *Eur.J.Pharmacol.* **2010**, *627*, 92–98.

Lam, F.C.; Liu, R.; Lu, P.; Shapiro, A.B.; Renoir, J.-M.; Sharom, F.J.; Reiner, P.B.: β-Amyloid efflux mediated by P-glycoprotein. *J. Neurochem.* **2001**, *76*, 1121-1128.

Lazarova, N.; Zoghbi, S.S.; Hong, J.; Seneca, N.; Tuan, E.; Gladding, R.L.; Liow, J.-S.; Taku, A.; Innis, R.B.; Pike, V.W.: Synthesis and Evaluation of [*N*-methyl-^{11}C]*N*-Desmethyl-loperamide as

a New and Improved PET Radiotracer for Imaging P-gp Function. *J. Med. Chem.* **2008**, *51*, 6034-6043.

Lee, G. and Bendayan, R.: Functional expression and localization of P-glycoprotein in the central nervous system: relevance to the pathogenesis and treatment of neurological disorders. *Pharm. Res.* **2004**, *21*, 1313-1330.

Li, H.-H.; Huang, H.; Zhang, X.-H.; Luo, X.-M.; Lin, L.-P.; Jiang, H.-L.; Ding, J.; Chen, K.-X.; Liu, H.: Discovering novel 3-nitroquinolines as a new class of anticancer agents. *Acta Pharmacol. Sin.* **2008**, *29*, 1529-1538.

Liu, J.Y.W.; Thom, M.; Catarino, C.B.; Martinian, L.; Figarella-Branger, D.; Bartolomei, F.; Koepp, M.; Sisodiya, S.M.: Neuropathology of the blood-brain barrier and pharmaco-resistance in human epilepsy. *Brain* **2012**, *135*, 3115-3133.

Löscher, W. and Potschka, H.: Role of drug efflux transporters in the brain for drug disposition and treatment of brain diseases. *Prog. Neurobiol.* **2005a**, *76*, 22-76.

Löscher, W., Potschka, H.: Drug resistance in brain diseases and the role of drug efflux transporters. *Nat. Rev. Neurosci.* **2005b**, *6*, 591-602.

Löscher, W.; Luna-Tortós, C.; Römermann, K.; Fedrowitz, M.: Do ATP-Binding Cassette Transporters Cause Pharmacoresistance in Epilepsy? Problems and Approaches in Determining which Antiepileptic drugs are Affected. *Curr. Pharm. Des.* **2011**, *17*, 2808-2828.

Luurtsema, G.; Molthoff, C.F.M.; Windhorst, A.D.; Smit, J.W.; Keizer, H.; Boellaard, R.; Lammertsma, A.A.; Franssen, E.J.F.: (*R*)- and (*S*)-[^{11}C]Verapamil as PET-tracers for measuring P-glycoprotein function: *in vitro* and *in vivo* evaluation. *Nucl. Med. Biol.* **2003**, *30*, 747-751.

Mairinger, S.; Tariquidar Analogues as PET Precursors for Functional Imaging of P-glycoprotein. *Diploma thesis*, FH Campus Wien, **2008**.

Mairinger, S.; Erker, T.; Müller, M.; Langer, O.: PET and SPECT Radiotracers to Assess Function and Expression of ABC Transporters *in Vivo*. *Curr. Drug Metab.* **2011**, *12*, 774-792.

Matsuno, K.; Ushiki, J.; Seishi, T.; Ichimura, M.; Giese, N.A.; Yu, J.-C.; Takahashi, S.; Oda, S.; Nomoto, Y.: Potent and Selective Inhibitors of Platelet-Derived Growth Factor Receptor Phosphorylation. 3. Replacement of Quinazoline Moiety and Improvement of Metabolic

Polymorphism of 4-[4-(*N*-Substituted(thio)carbamoyl)-1-piperazinyl]-6,7-dimethoxy-quinazoline Derivatives. *J. Med. Chem.* **2003**, *46*, 4910-4925.

Meth-Cohn, O.; Narine, B.; Tarnowski, B.: A Versatile New Synthesis of Quinolines and Related Fused Pyridines Part 5. The Synthesis of 2-Chloroquinoline-3-carbaldehydes. *J. Chem. Soc. Perkin Trans. 1* **1981**, 1520-1530.

Müllauer, J.; Karch, R.; Bankstahl, J.P.; Bankstahl, M.; Stanek, J.; Wanek, T.; Mairinger, S.; Müller, M.; Löscher, W.; Langer, O.; Kuntner, C.: Assessment of cerebral P-glycoprotein expression and function with PET by combined [^{11}C]inhibitor and [^{11}C]substrate scans in rats. *Nucl. Med. Biol.* **2013**, *40*, 755-763.

Ni, Z.; Bikadi, Z.; Rosenberg, M.F.; Mao, Q.: Structure and Function of the Human Breast Cancer Resistance Protein (BCRP/ABCG2). *Curr. Drug. Metab.* **2010**, *11*, 603-617.

Ohtsuki, S.: New Aspects of the Blood-Brain Barrier Transporters; Its Physiological Roles in the Central Nervous System. *Biol. Pharm. Bull.* **2004**, *27*, 1489-1496.

Oldendorf, W.H.: Lipid solubility and drug penetration of the Blood-brain barrier. *Proc. Soc. Exp. Biol. Med.* **1974**, *147*, 813-816.

Pike, V.W.: PET Radiotracers: crossing the blood-brain barrier and surviving metabolism. *Trends Pharmacol. Sci.* **2009**, *30*, 431-440.

Poller, A.M.: Elacridar Analogue as PET Precursor for Functional Imaging of P-glycoprotein and Breast Cancer Resistance Protein. *Diploma thesis*, FH Campus Wien, **2009**.

Qu, J.; Zhou, B.-T.; Yin, J.-Y.; Xu, X.-J.; Zhao, Y.-C.; Lei, G.H.; Tang, Q.; Zhou, H.-H.; Liu, Z.-Q.: ABCC2 Polymorphisms and Haplotype are Associated with Drug Resistance in Chinese Epileptic Patients. *CNS Neurosci. Ther.* **2012**, *18*, 647-651.

Remy, S. and Beck, H.: Molecular and cellular mechanisms of pharmacoresistance in epilepsy. *Brain* **2006**, *129*, 18-35.

Ryder, H.; Ashworth, P.A.; Roe, M.J.; Brumwell, J.E.; Hunjan, S.; Folkes, A.J.; Sanderson, J.T.; Williams, S.; Maximen, L.M: Anthranilic acid derivatives as multi drug resistance modulators. *PCT Int. Appl.* **1998**, WO 98/17648 A1.

Schareina, T.; Zapf, A.; Mägerlein, W.; Müller, N.; Beller, M.: A State-of-the-Art Cyanation of Aryl Bromides: A Novel and Versatile Copper Catalyst System Inspired by Nature. *Chem. Eur. J.* **2007**, *13*, 6249-6254.

Seelig, A.: A general pattern for substrate recognition by P-glycoprotein. *Eur. J. Biochem.* **1998**, *251*, 252-261.

Sharp, M.J.; Mader, C.J.; Strachan, C.: Synthesis of Acridine Derivate Multidrug-Resistant Inhibitors. *PCT Int. Appl.* **1998**, WO 98/52923 A1.

Stockner, T.; de Vries, S.J.; Bonvin, A.M.J.J.; Ecker, G.F.; Chiba, P.: Data-driven homology modelling of P-glycoprotein in the ATP-bound state indicates flexibility of the transmembrane domains. *FEBS J.* **2009**, *276*, 964-972.

Thiebaut, F.; Tsuro, T.; Hamada, H.; Gottesman, M.M.; Pastan, I.; Willingham, M.C.: Cellular localization of the multidrug-resistance gene product in normal human tissues. *Proc. Natl. Acad. Sci. USA* **1987**, *84*, 7735-7738.

Tishler, D.M.; Weinberg, K.I.; Hinton, D.R.; Barbaro, N.; Annett, G.M.; Raffel, C.: *MDR1* Gene Expression in Brain of Patients with Medically Intractable Epilepsy. *Epilepsia* **1995**, *36*, 1-6.

Uchida, Y.; Ohtsuki, S.; Katsukura, Y.; Ikeda, C.; Suzuki, T.; Kamiie, J.; Terasaki, T.: Quantitative targeted absolute proteomics of human blood-brain barrier transporters and receptors. *J. Neurochem.* **2011**, *117*, 333-345.

Uhle, F.C. and Jacobs, W.A.: The ergot alkaloids. XX. The synthesis of dihydro-*dl*-lysergic acid. A new synthesis of 3-substituted quinolones. *J. Org. Chem.* **1945**, *10*, 76-86.

Vlaming, M.L.H.; Lagas, J.S.; Schinkel, A.H.: Physiological and pharmacological roles of ABCG2 (BCRP): Recent findings in Abcg2 knockout mice. *Adv. Drug Deliv. Rev.* **2009**, *61*, 14-25.

De Vries, H.E.; Kuiper, J.; de Boer, A.G.; van Berkel, T.J.C.; Breimer, D.D.: The Blood-Brain Barrier in Neuroinflammatory Diseases. *Pharmacol. Rev.* **1997**, *49*, 143-155.

Wanek, T.; Kuntner, C.; Bankstahl, J.P.; Bankstahl, M.; Stanek, J.; Sauberer, M.; Mairinger, S.; Strommer, S.; Wacheck, V.; Löscher, W.; Erker, T.; Müller, M.; Langer, O.: A Comparative small-animal PET evaluation of [^{11}C]tariquidar, [^{11}C]elacridar and (*R*)-[^{11}C]verapamil for detection of P-glycoprotein-expressing murine breast cancer. *Eur. J. Nucl. Med. Mol. Imaging* **2012a**, *39*, 149-159.

Wanek, T.; Kuntner, C.; Bankstahl, J.P.; Mairinger, S.; Bankstahl, M.; Stanek, J.; Sauberer, M.; Filip, T.; Erker, T.; Müller, M.; Löscher, W.; Langer, O.: A novel PET protocol for visualization of breast cancer resistance protein function at the blood-brain barrier. *J. Cereb. Blood Flow Metab.* **2012b**, *32*, 2002-2011.

Wanek, T.: Imaging of ABC transporters with positron emission tomography – new insights from the development of new radiotracers. *Doctoral thesis*, Medical University of Vienna, **2013**.

Wang, M.; Zheng, D.X.; Luo, M.B.; Gao, M.; Miller, K.D.; Hutchins, G.D.; Zheng, Q.-H.: Synthesis of carbon-11-labeled tariquidar derivatives as new PET agents for imaging breast cancer resistance protein (ABCG2). *Appl. Radiat. Isot.* **2010**, *68*, 1098-1103.

Wéber, C.; Bielik, A.; Demeter, Á.; Borza, I.; Szendrei, G.I.; Keserű, G.M.; Greiner, I.: Solid-phase synthesis of 6-hydroxy-2,4-diaminoquinazolines. *Tetrahedron* **2005**, *61*, 9375-9380.

Weissman, S.A.; Zewge, D.; Chen,. C.: Ligand-Free Palladium-Catalyzed Cyanation of Aryl Halides. *J. Org. Chem.* **2005**, *70*, 1508-1510.

Wilson, W.H.; Bates, S.E.; Fojo, A.; Bryant, G.; Zhan, Z.; Regis, J.; Wittes, R.E.; Jaffe, E.S.; Steinberg, S.M.; Herdt, J.; *et al.*: Controlled trial of dexverapamil, a modulator of multidrug resistance, in lymphomas refractory to EPOCH chemotherapy. *J. Clin. Oncol.* **1995**, *13*, 1995-2004.

Wolf, S.; Seehaus, B.; Minol, K.; Gassen, H.G.: Die Blut-Hirn-Schranke: Eine Besonderheit des cerebralen Mikrozirkulationssystems. *Naturwissenschaften* **1996**, *83*, 302-311.

Woodward, O.M.; Köttgen, A.; Coresh, J.; Boerwinkle, E.; Guggino, W.B.; Köttgen, M.: Identification of a urate transporter, ABCG2, with a common functional polymorphism causing gout. *Proc. Natl. Acad. Sci. USA* **2009**, *106*, 10338-10342.

Woodward, O.M.; Tukaye, D.N.; Cui, J.; Greenwell, P.; Constantoulakis, L.M.; Parker, B.S.; Rao, A.; Köttgen, M.; Maloney, P.C.; Guggino, W.B.: Gout-causing Q141K mutation in ABCG2 leads to instability of the nucleotide-binding domain and can be corrected with small molecules. *Proc. Natl. Acad. Sci. USA* **2013**, *110*, 5223-5228.

Tamaki, A.; Ierano, C.; Szakacs, G.; Robey, R.W.; Bates, S.E.: The controversial role of ABC transporters in clinical oncology. *Essays Biochem.* **2011**, *50*, 209-232.

Zlokovic, B.V.: Neurovascular mechanisms of Alzheimer's neurodegeneration. *Trends Neurosci.* **2005**, *28*, 202-208.

Zymalkowski, F. and Tinapp, P.: Chemistry of 3-quinolinecarboxaldehyde. *Liebigs Ann. Chem.* **1966**, *699*, 98-106.

X Appendix

X.A Abbreviations

ABC	.....	ATP binding cassette
Ac_2O	.....	acetic anhydride
AcOH	.....	acetic acid
ADMET	.....	absorption, distribution, metabolism, excretion and toxicity
AED	.....	anti-epileptic drug
ATP	.....	adenosine triphosphate
BBB	.....	blood-brain barrier
BCRP	.....	breast cancer resistance protein
BHS	.....	Blut-Hirn-Schranke
BnCl	.....	benzyl chloride
br s	.....	broad singlet
CFTR	.....	cystic fibrosis transmembrane regulator
CNS	.....	central nervous system
C_q	.....	quaternary carbon
d	.....	doublet
DMAc	.....	*N,N*-dimethylacetamide
4-DMAP	.....	4-dimethylaminopyridine
DMF	.....	*N,N*-dimethylformamide
EDC•HCl	.....	*N*-(3-dimethylaminopropyl)-*N*′-ethylcarbodiimide hydrochloride
EtOAc	.....	ethyl acetate
EtOH	.....	ethanol
GLUT1	.....	glucose transporter
HCl	.....	hydrochloric acid
HOBt	.....	1-hydroxybenzotriazole

LAT1	……	amino acid transporter
m	……	multiplet
MDR	……	multidrug resitance
MeCN	……	acetonitrile
MeI	……	iodomethane
MeOH	……	methanol
MRP	……	multidrug resistance-associated protein
NBD	……	nucleotide binding domain
OAT3	……	organic anion transporter
Pd/C	……	palladium on carbon
PET	……	positron emission tomography
P-gp	……	p-glycoprotein
Piv_2O	……	pivalic anhydride
ROI	……	region of interest
rpm	……	revolutions per minute
rt	……	room temperature
s	……	singlet
SNP	……	single nucleotide polymorphism
$SOCl_2$	……	thionyl chloride
SUR	……	sulfonylurea receptor
SUV	……	standardized uptake value
TBAH	……	tetrabutylammonium hydroxide
TEA	……	triethylamine
TFA	……	trifluoroacetic acid
THF	……	tetrahydrofuran
TLC	……	thin layer chromatography
TMD	……	transmembrane domain

X.B Figures and Tables

Figures:

Tables:

X.C Spectral Data

Compound **1**, ^{1}H-NMR (200 MHz, $CDCl_3$)

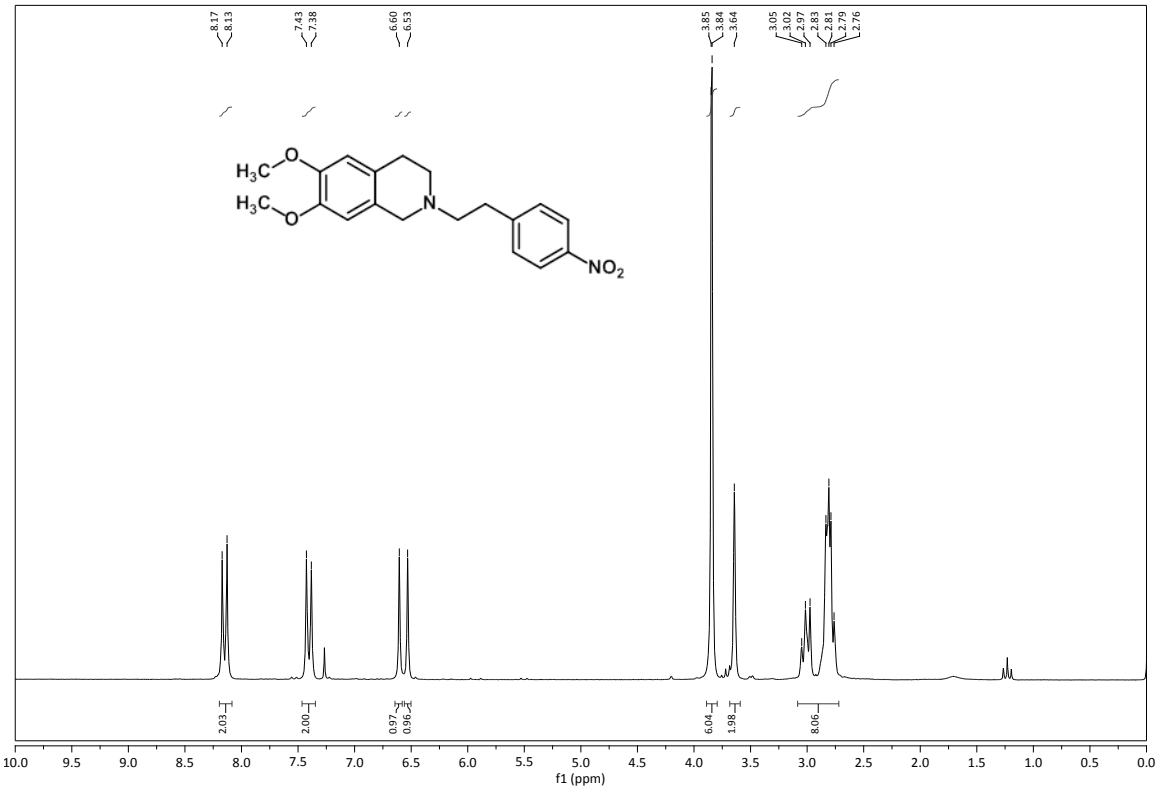

Compound **1**, ^{13}C-NMR (50 MHz, $CDCl_3$)

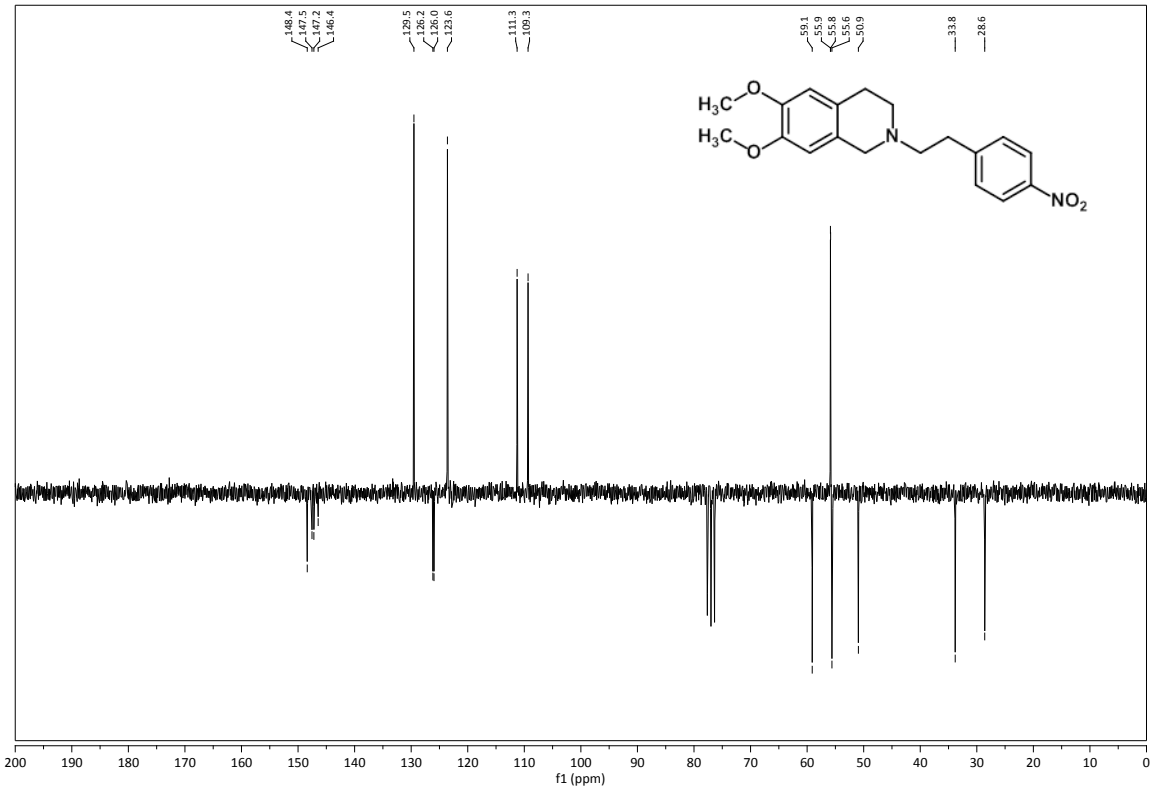

Compound **1**, mass spectrum

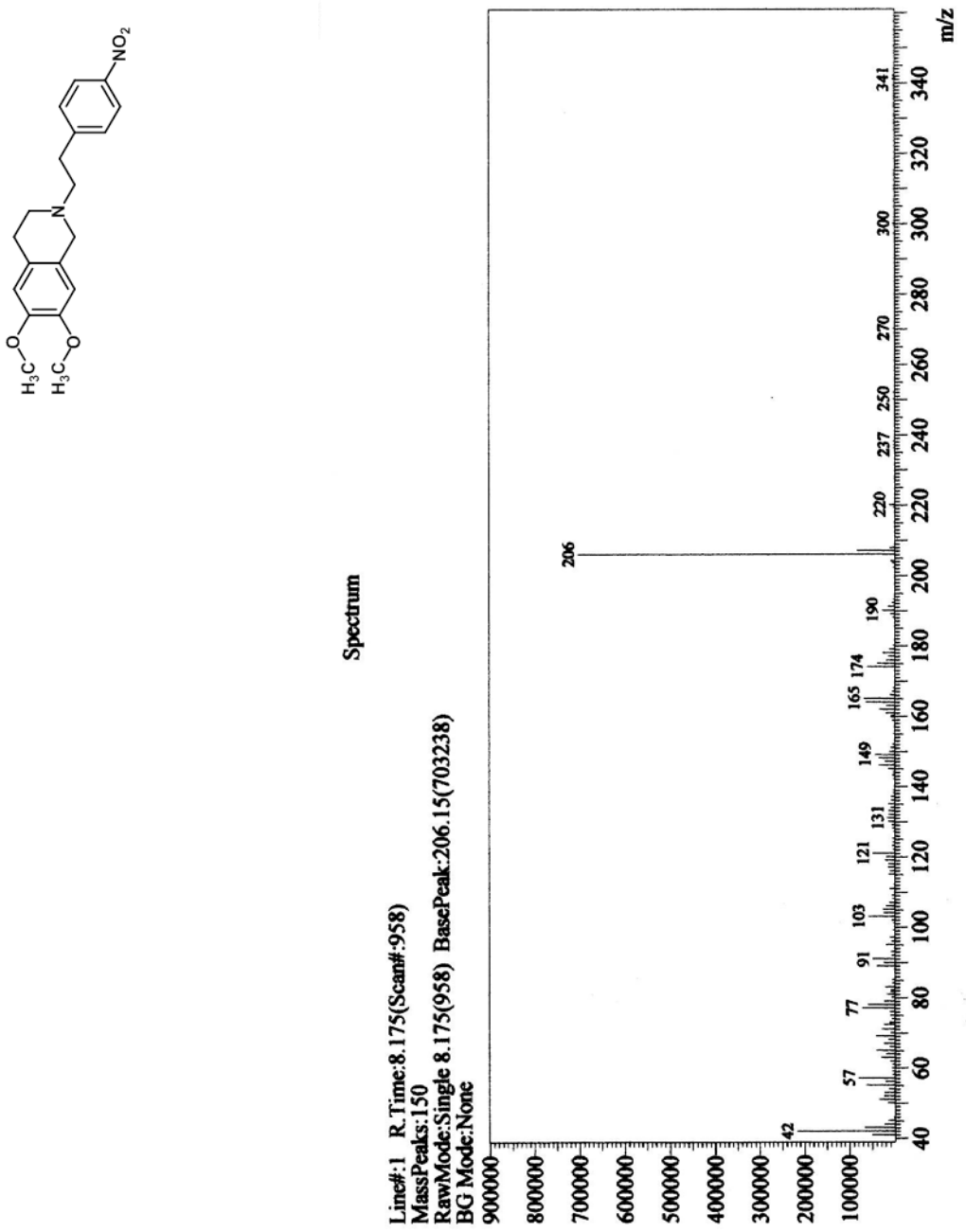

Compound **2**, ^{1}H-NMR (200 MHz, $CDCl_3$)

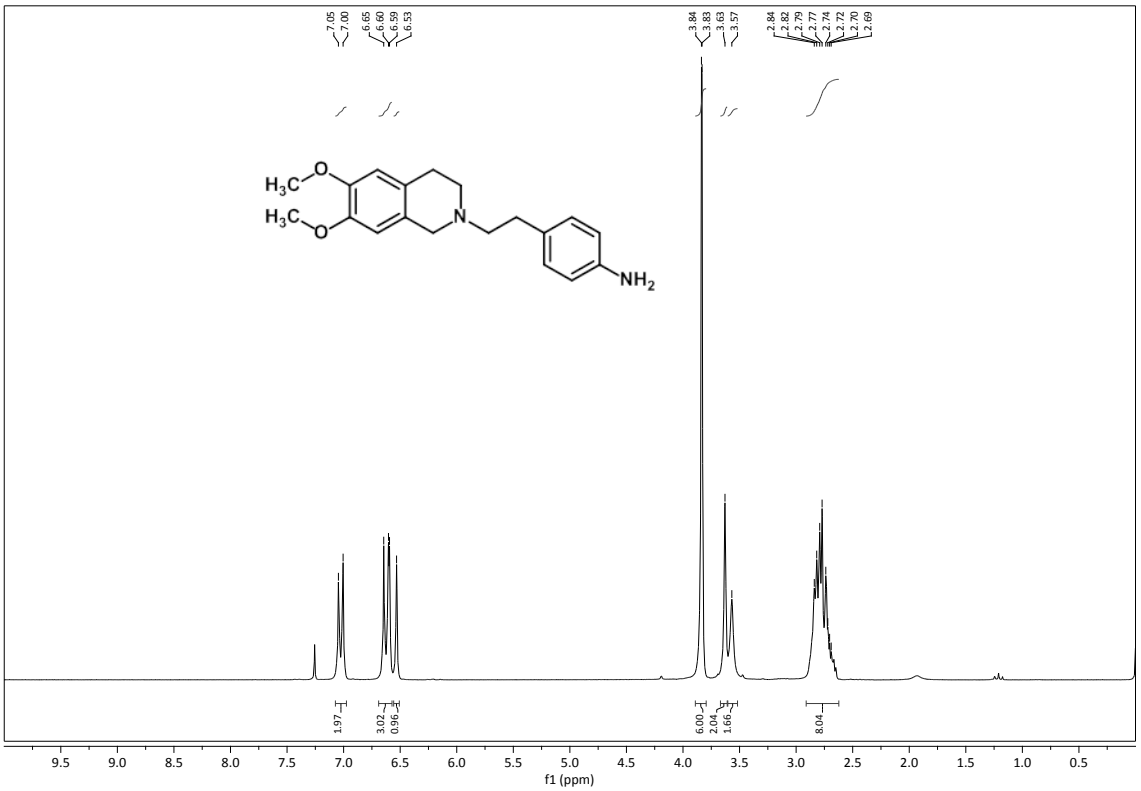

Compound **2**, ^{13}C-NMR (50 MHz, $CDCl_3$)

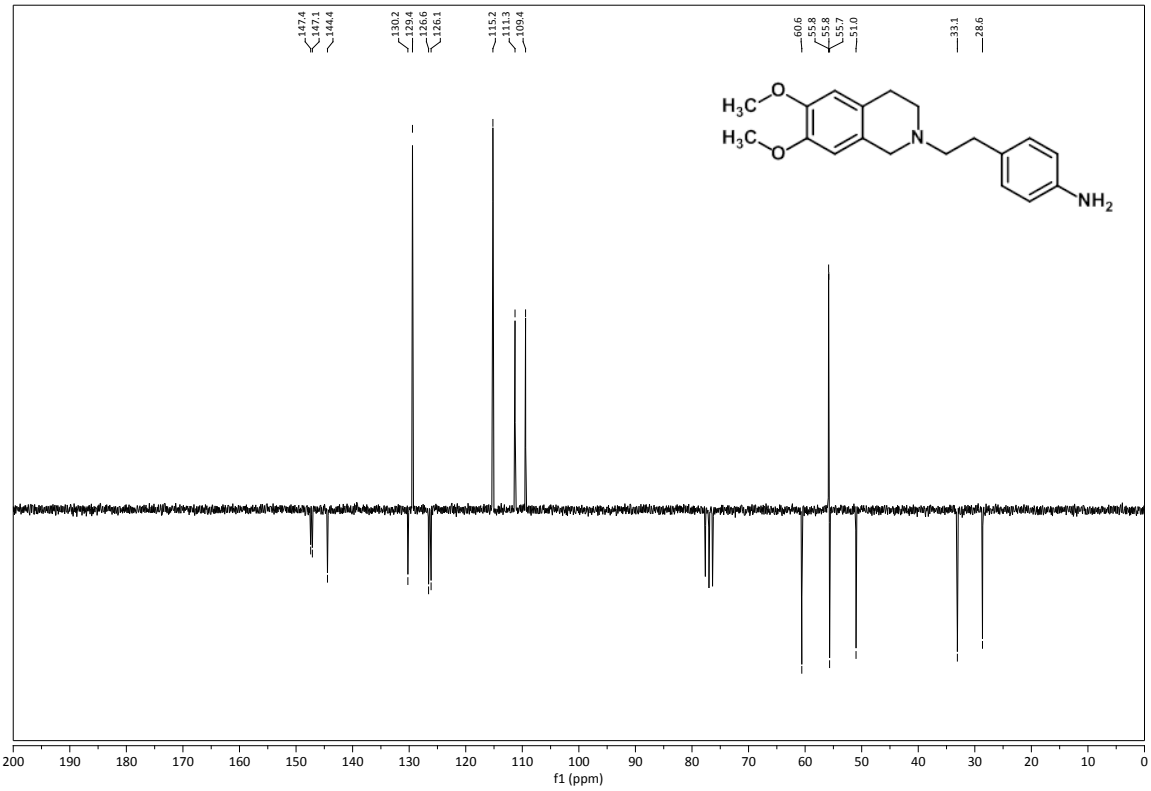

Compound **2**, mass spectrum

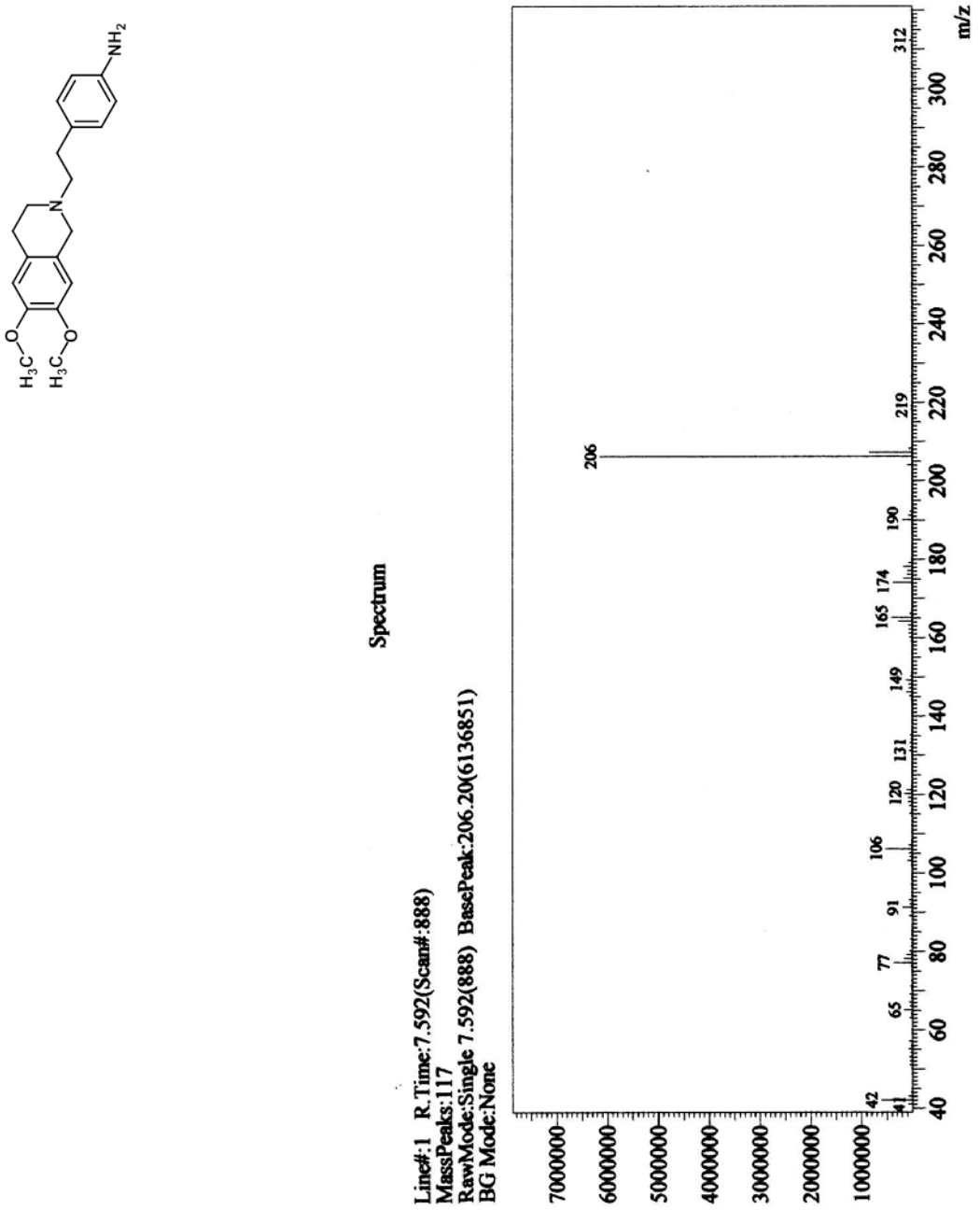

Compound **8**, ^{1}H-NMR (200 MHz, d_6-DMSO)

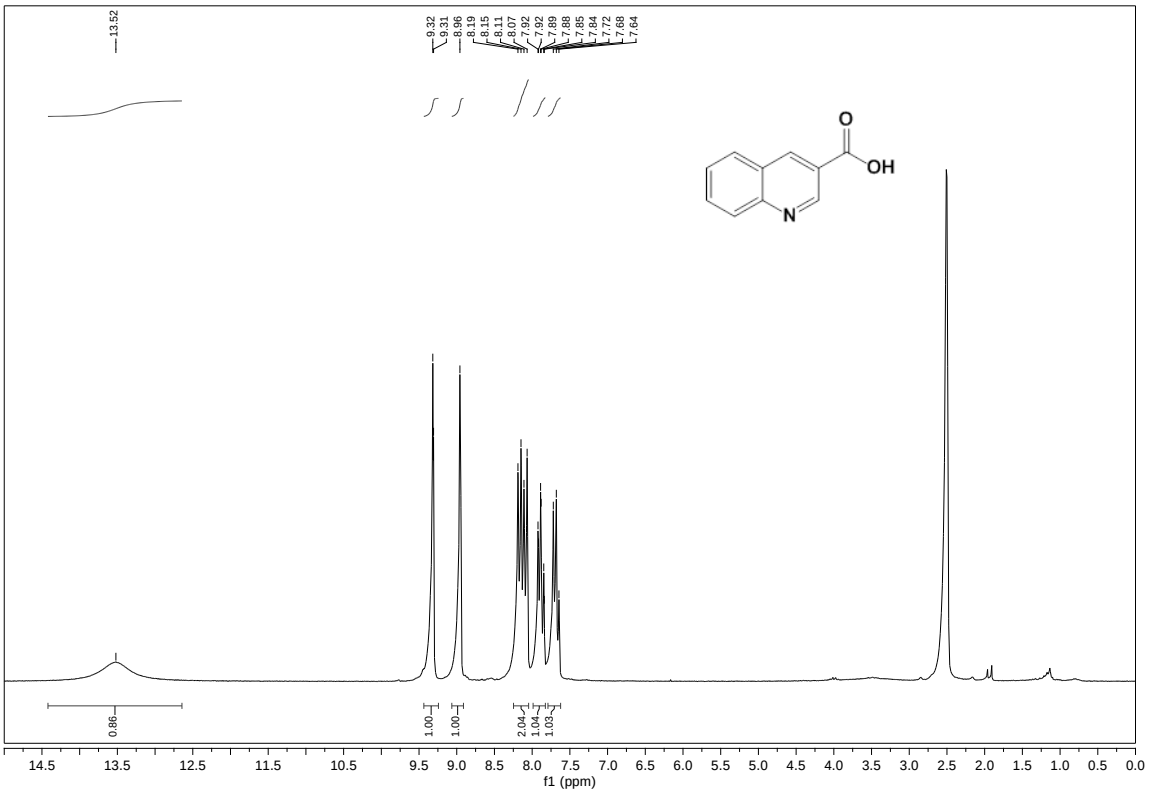

Compound **8**, ^{13}C-NMR (50 MHz, d_6-DMSO)

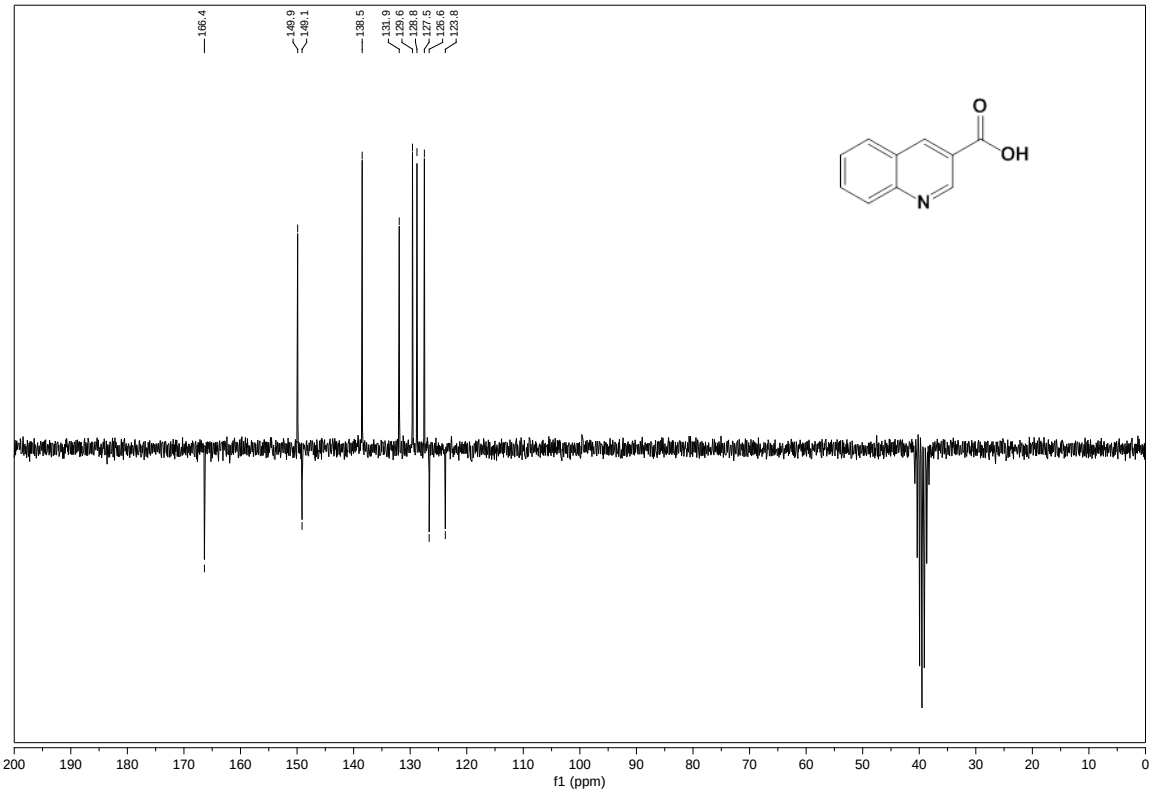

Compound **9**, ^{1}H-NMR (200 MHz, $CDCl_3$)

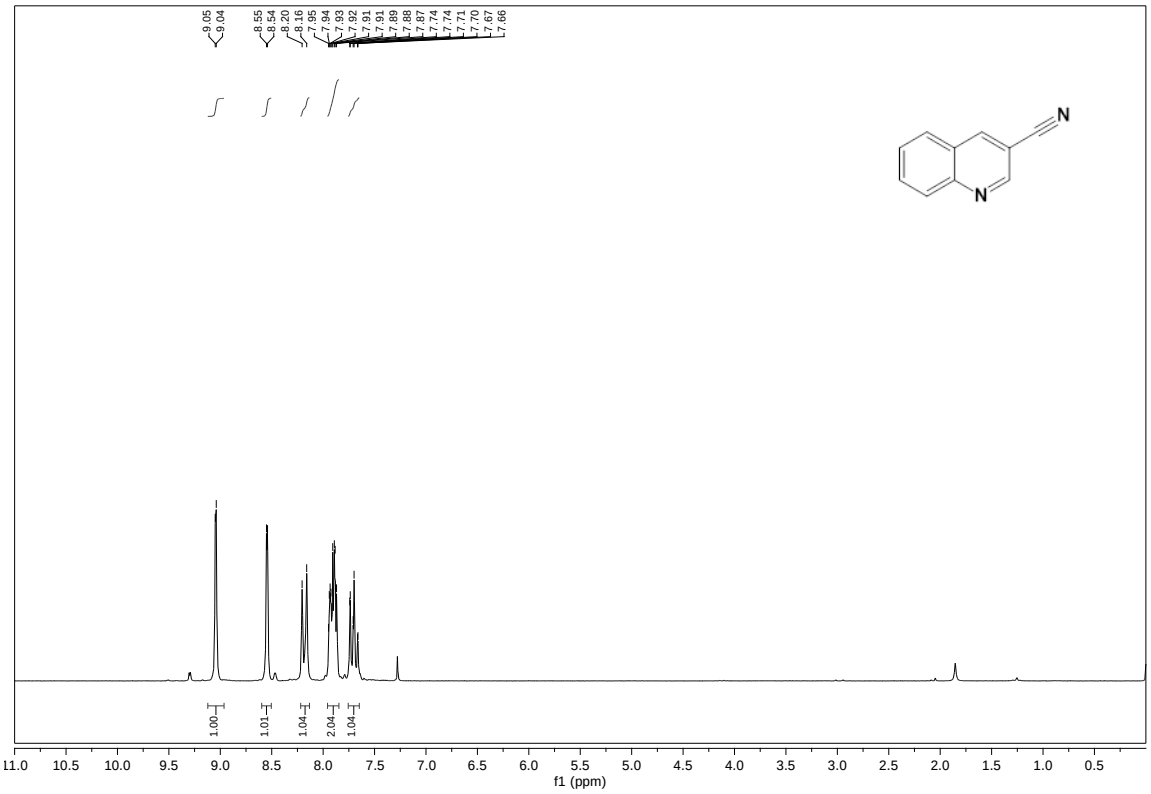

Compound **9**, ^{13}C-NMR (50 MHz, $CDCl_3$)

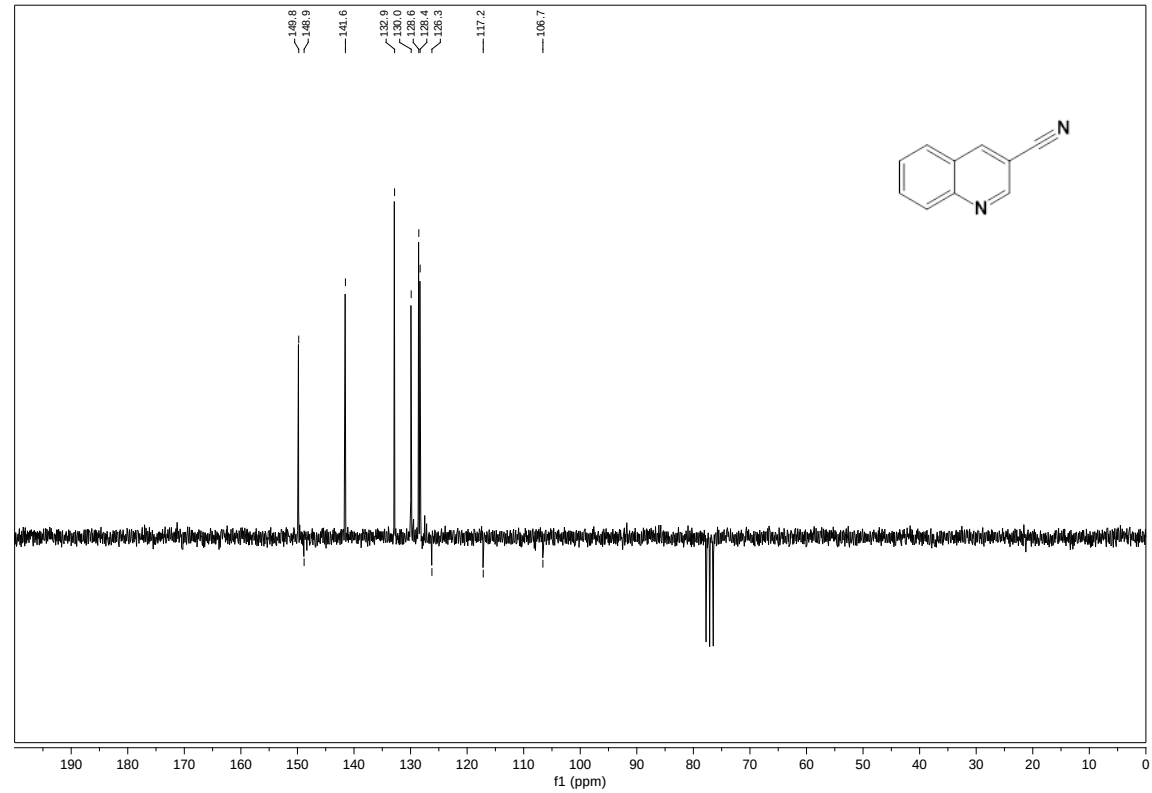

HM30181 (**10**), ^{1}H-NMR (200 MHz, $CDCl_3$)

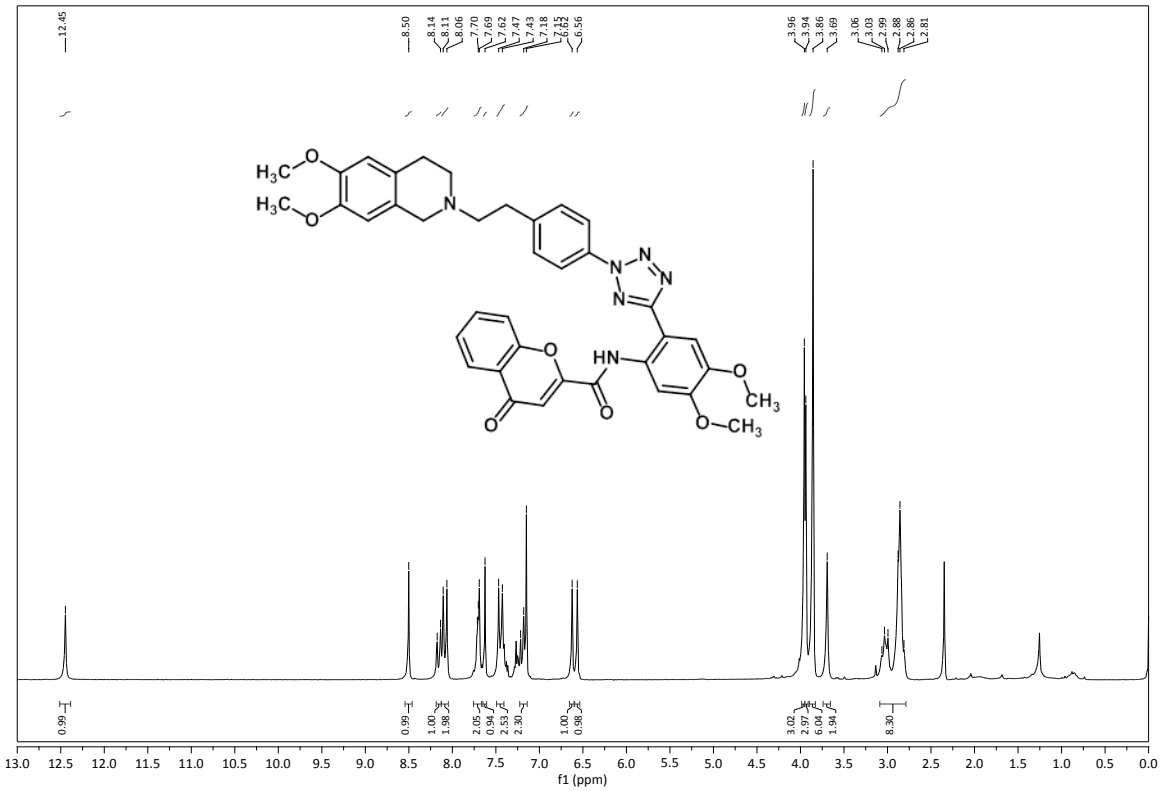

HM30181 (**10**), ^{13}C-NMR (50 MHz, $CDCl_3$)

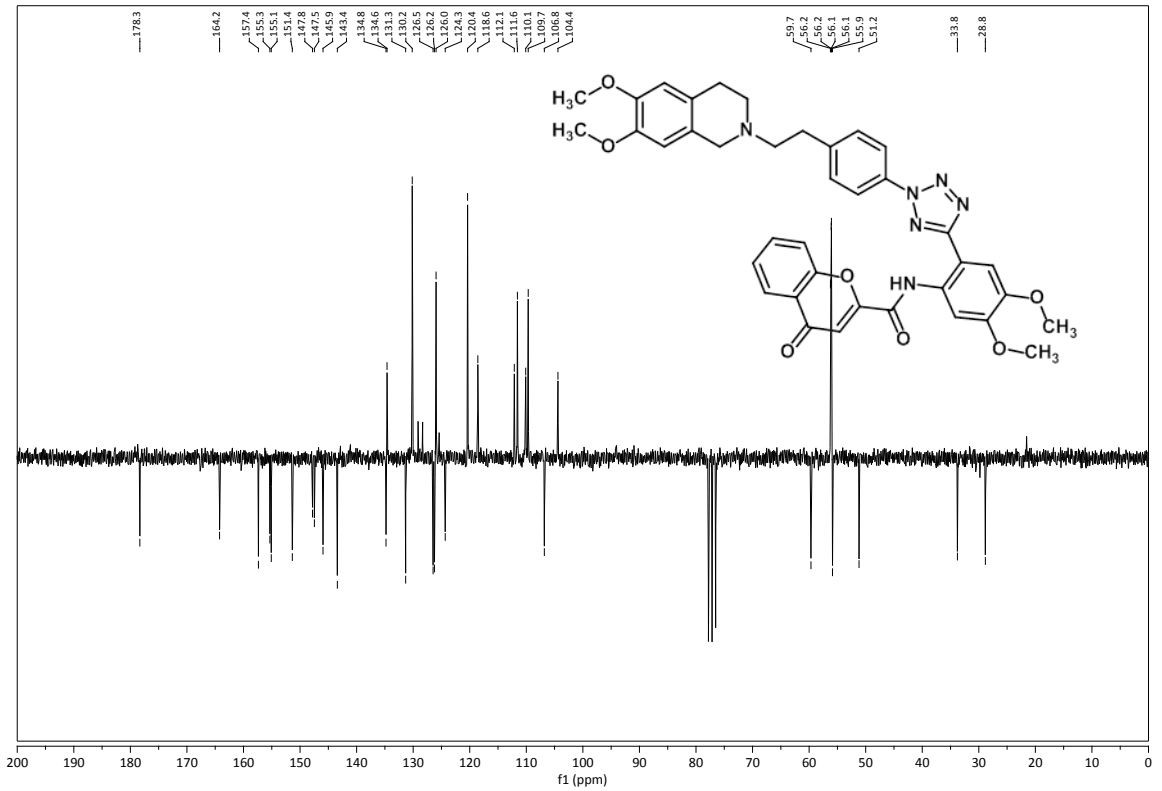

HM30181 (**10**), mass spectrum

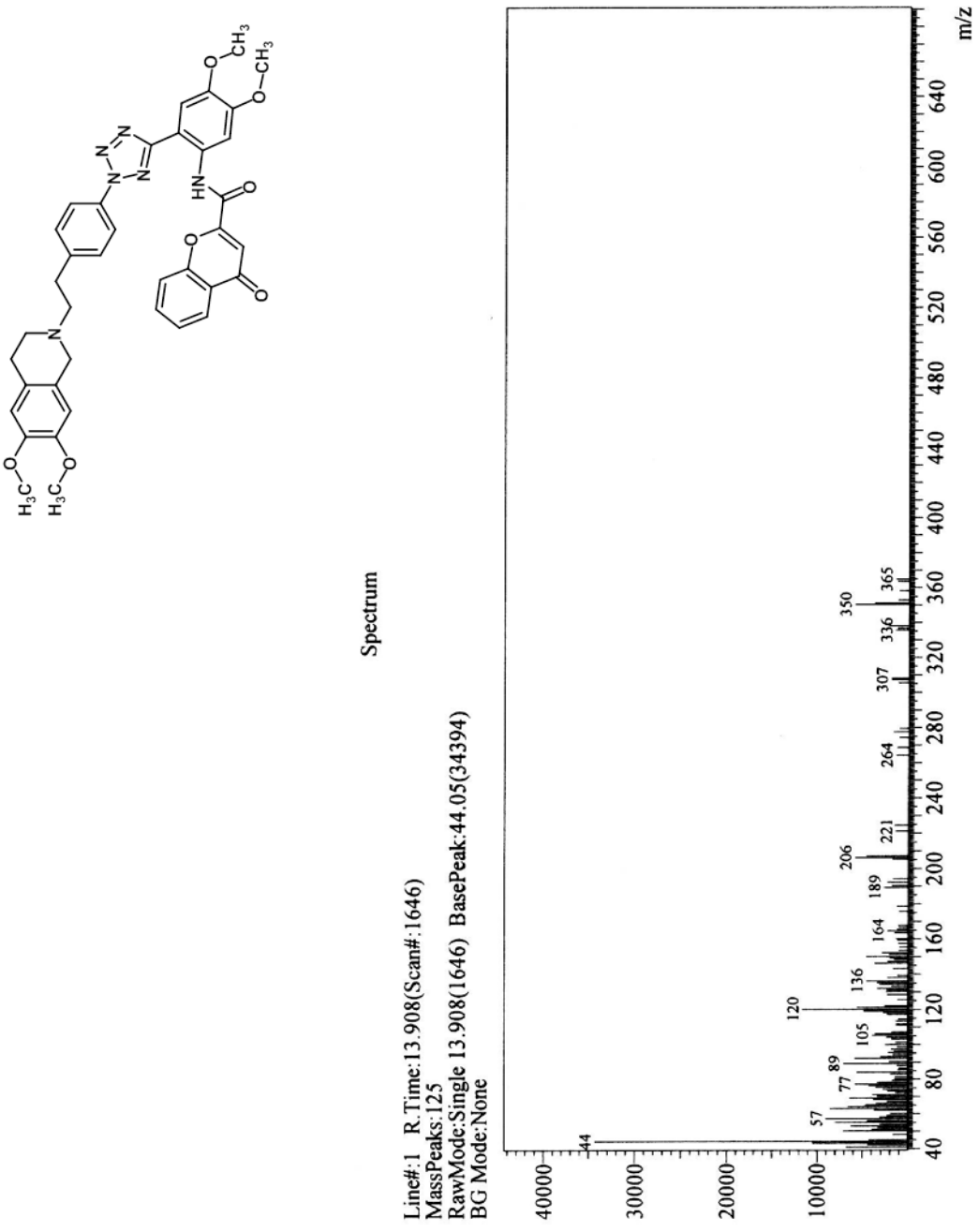

Compound **11**, ^{1}H-NMR (200 MHz, d$_6$-DMSO)

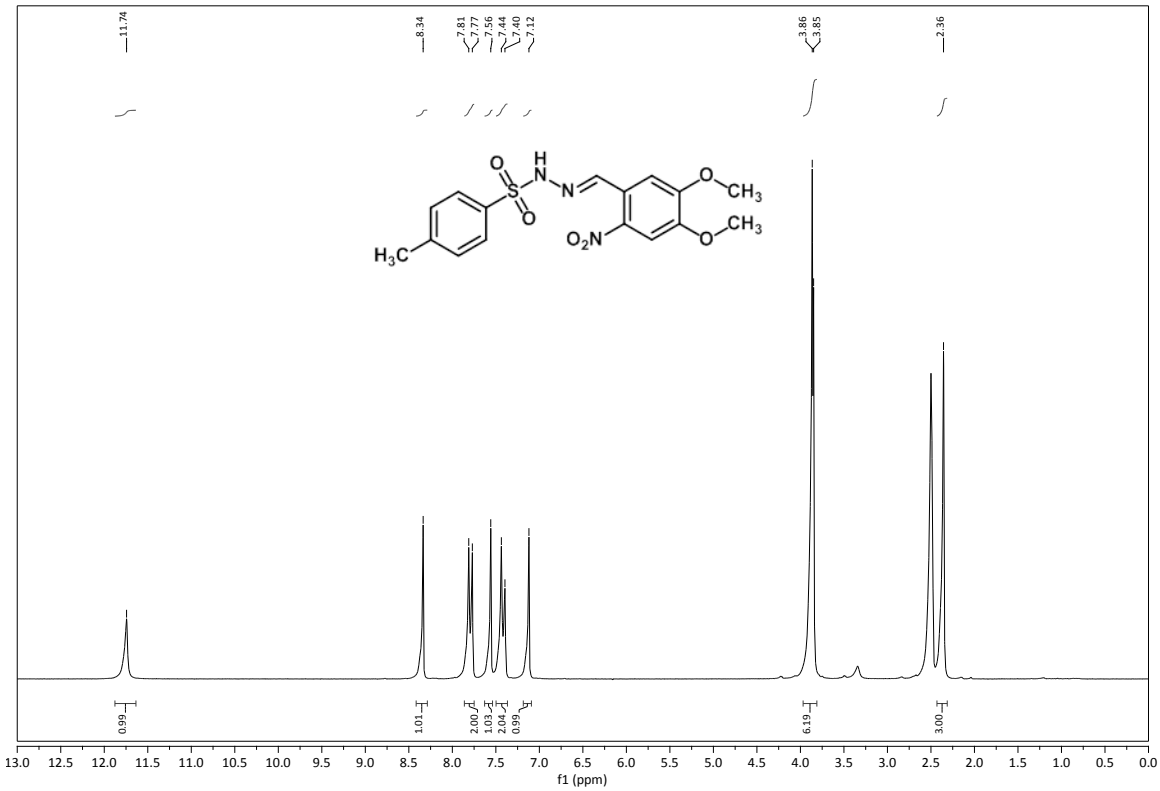

Compound **11**, ^{13}C-NMR (50 MHz, d$_6$-DMSO)

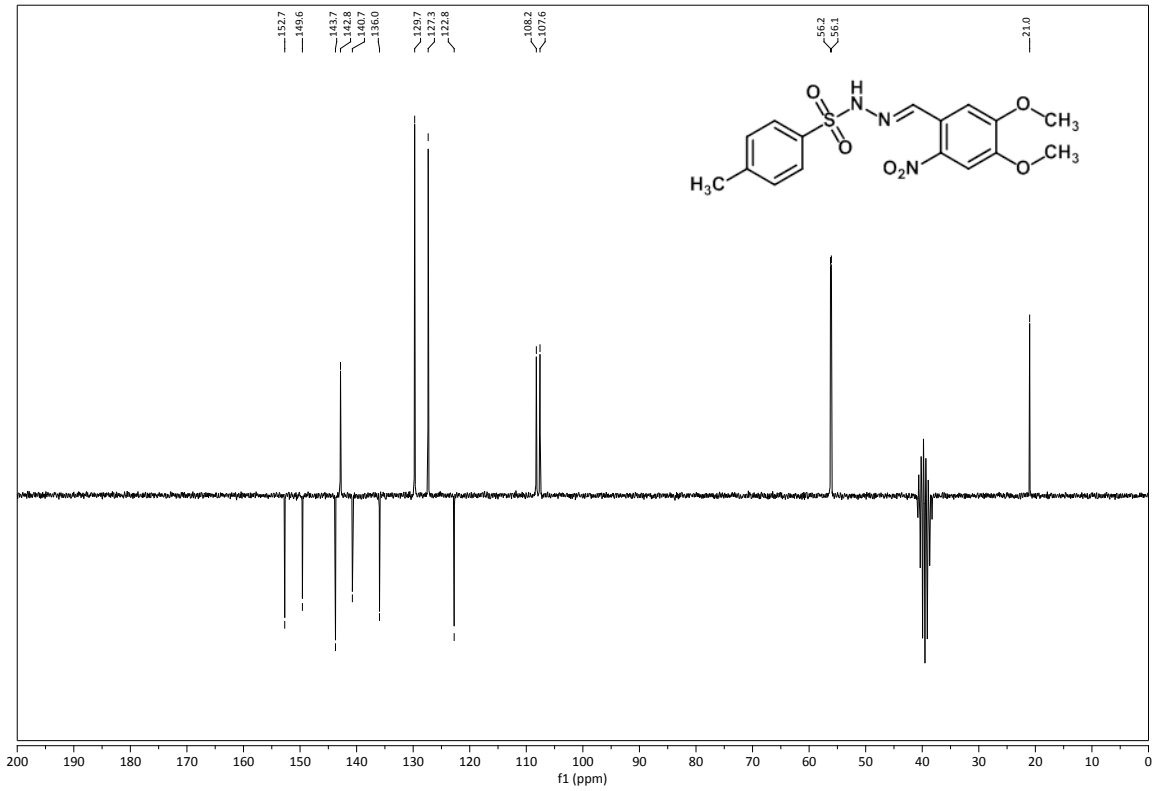

Compound **11**, mass spectrum

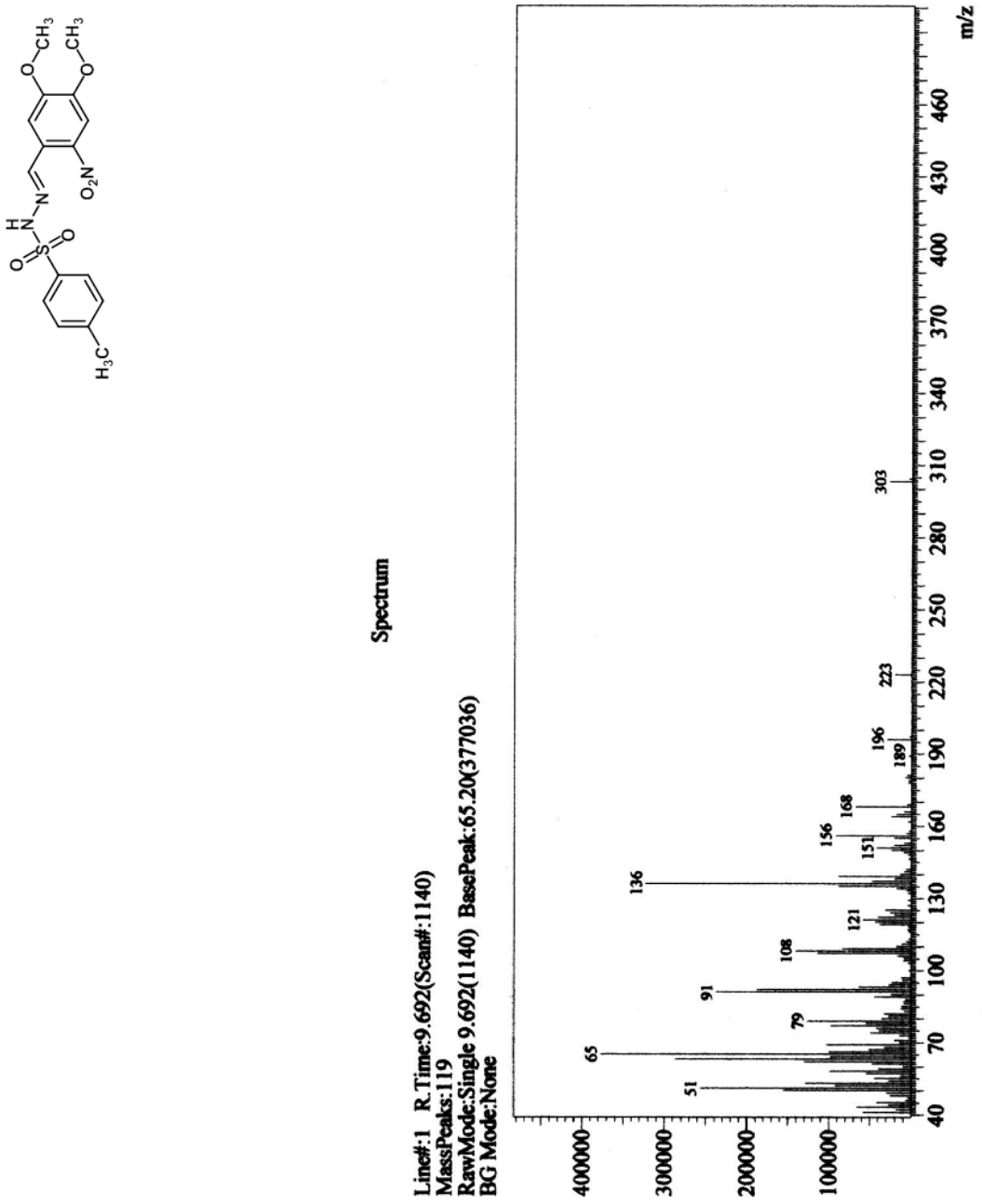

Compound **13**, ^{1}H-NMR (200 MHZ, $CDCl_3$)

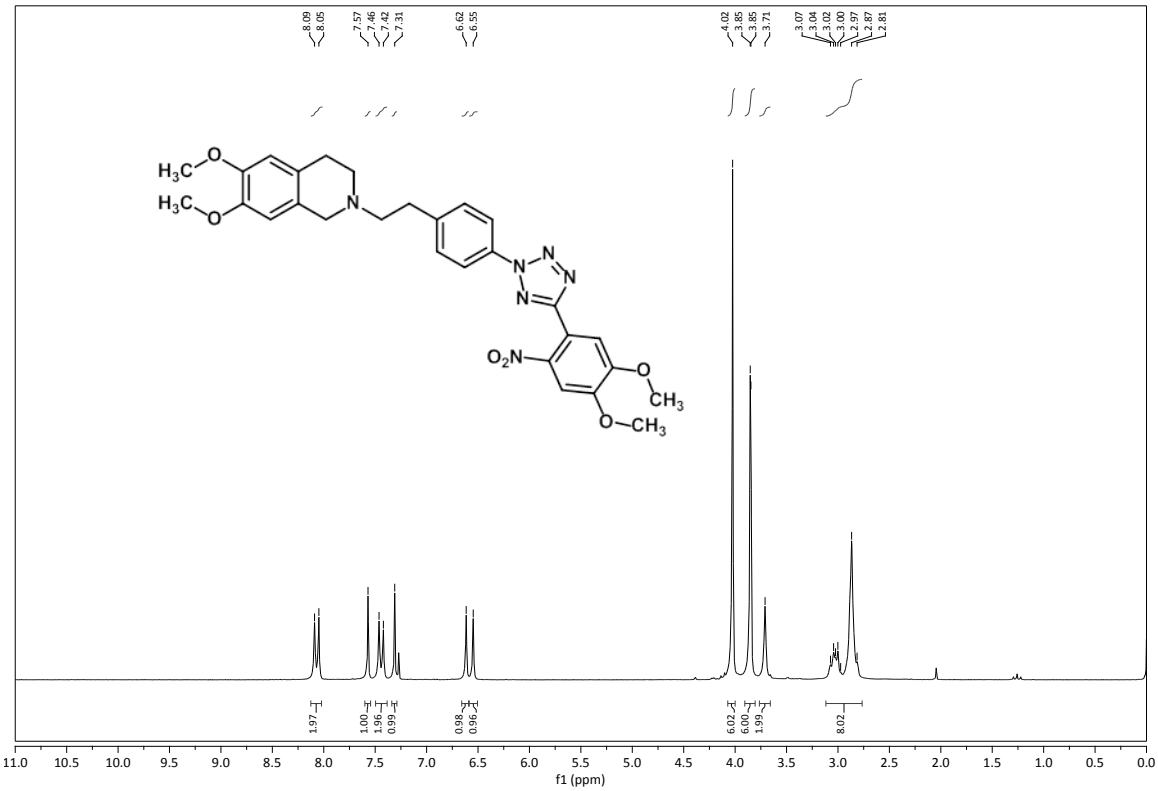

Compound **13**, ^{13}C-NMR (50 MHz, $CDCl_3$)

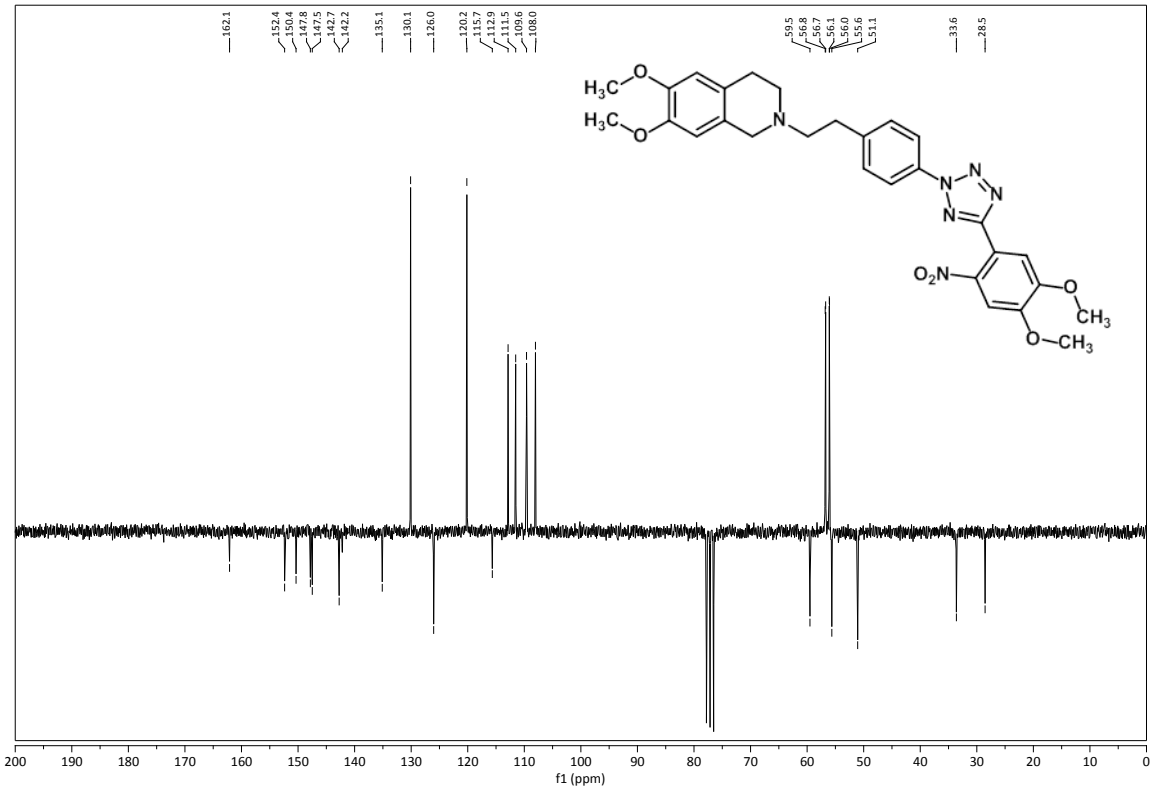

Compound **13**, mass spectrum

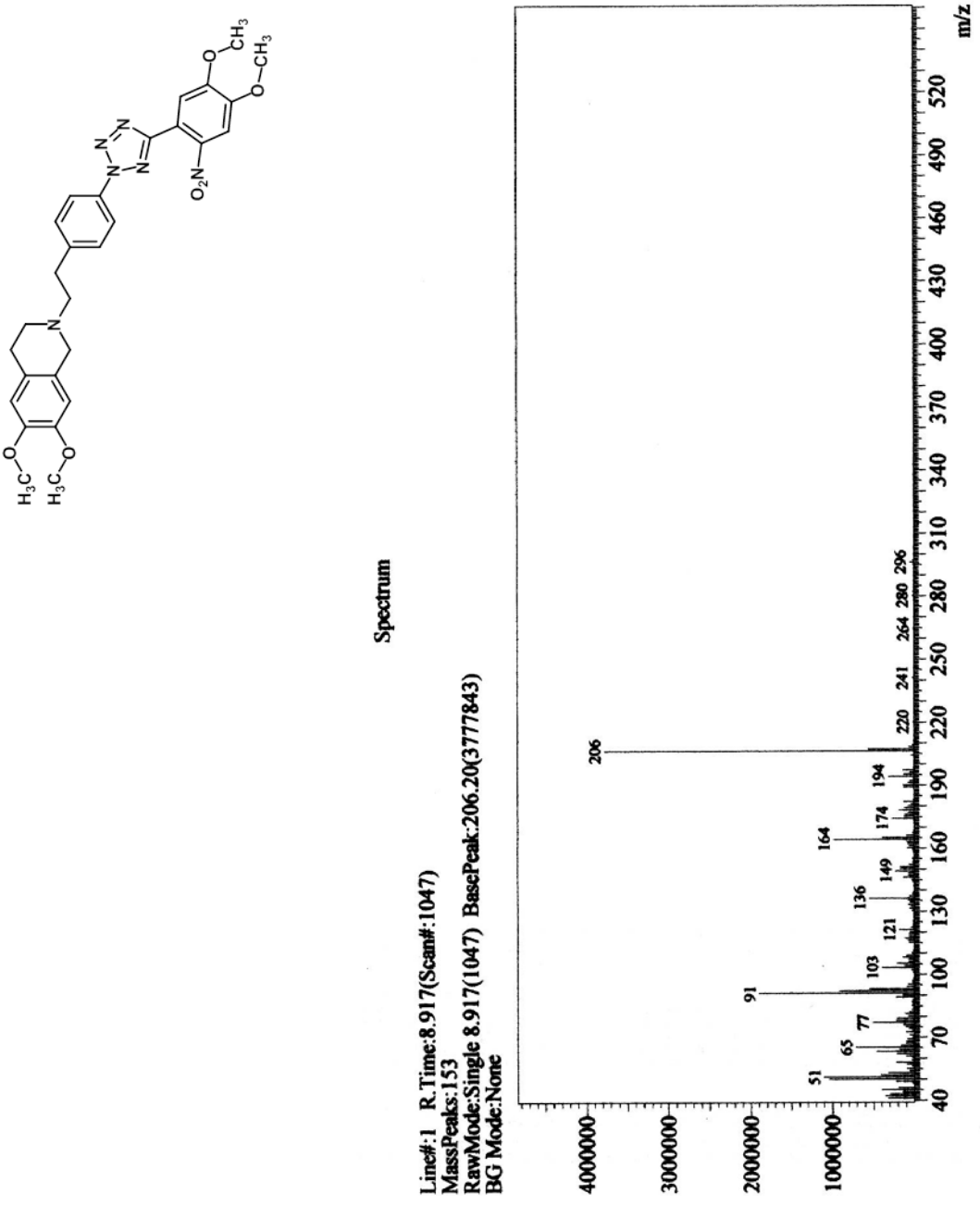

Compound **14**, ^{1}H-NMR (200 MHz, $CDCl_3$)

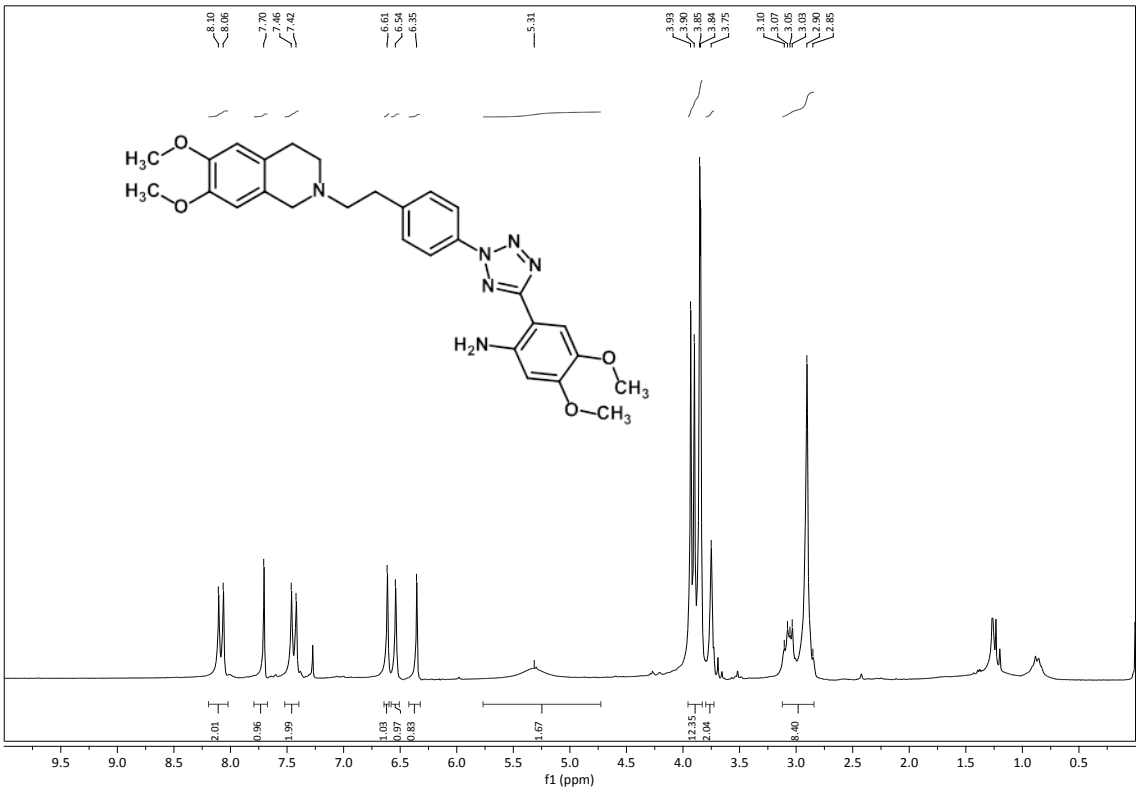

Compound **14**, ^{13}C-NMR (50 MHz, $CDCl_3$)

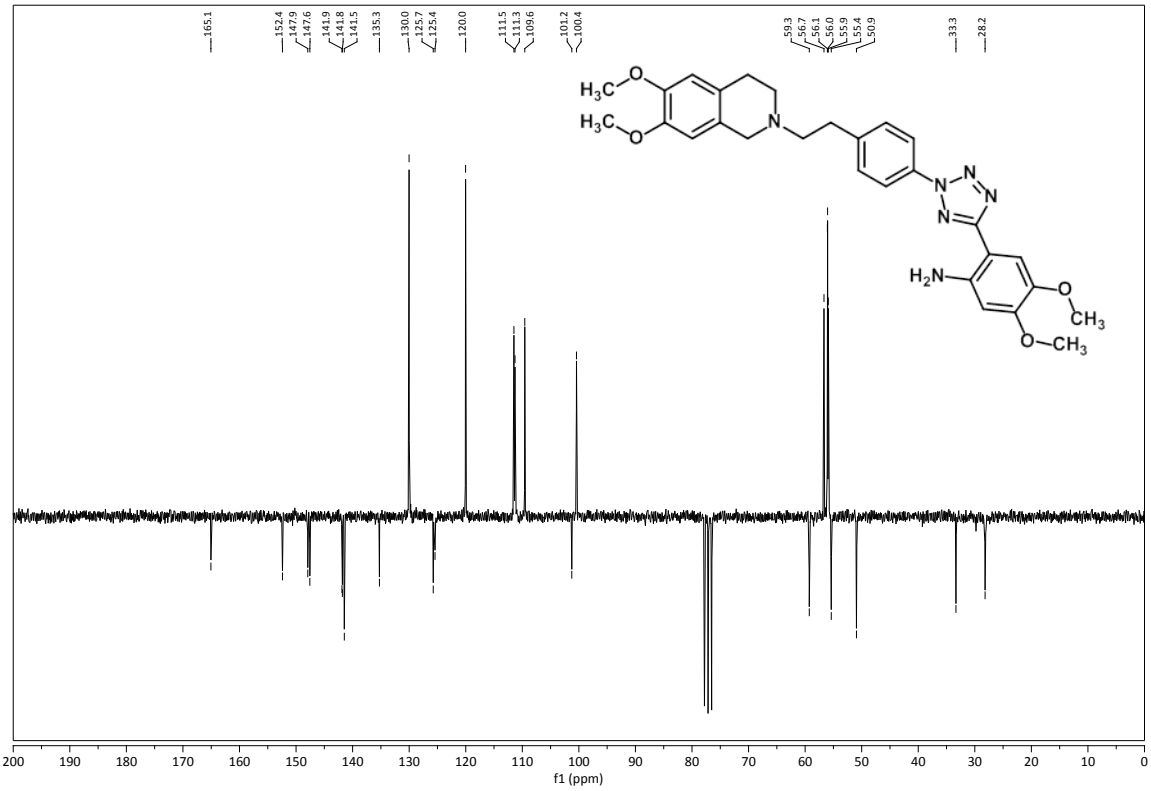

Compound **14**, mass spectrum

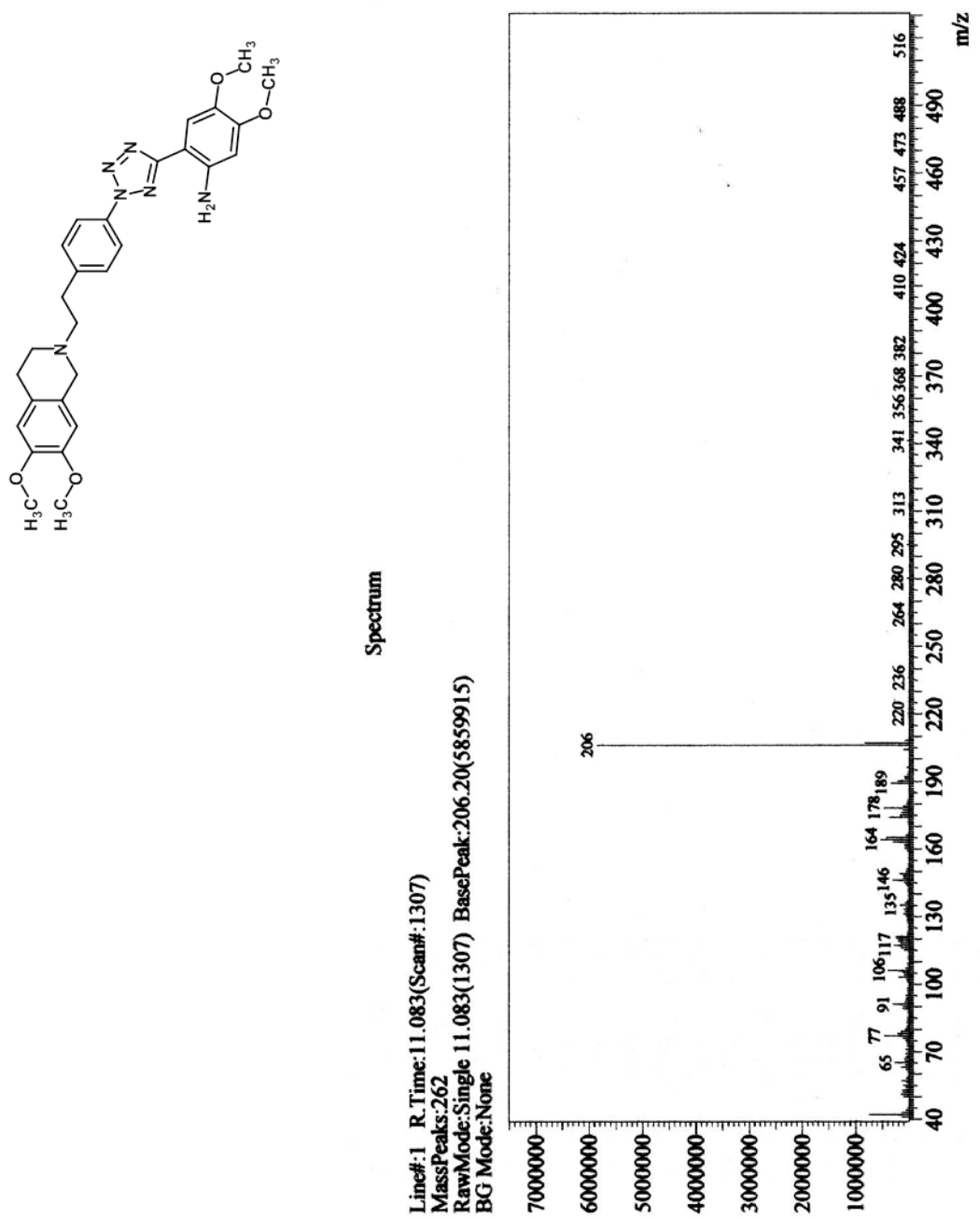

Compound **20**, ^{1}H-NMR (200 MHz, d$_6$-DMSO)

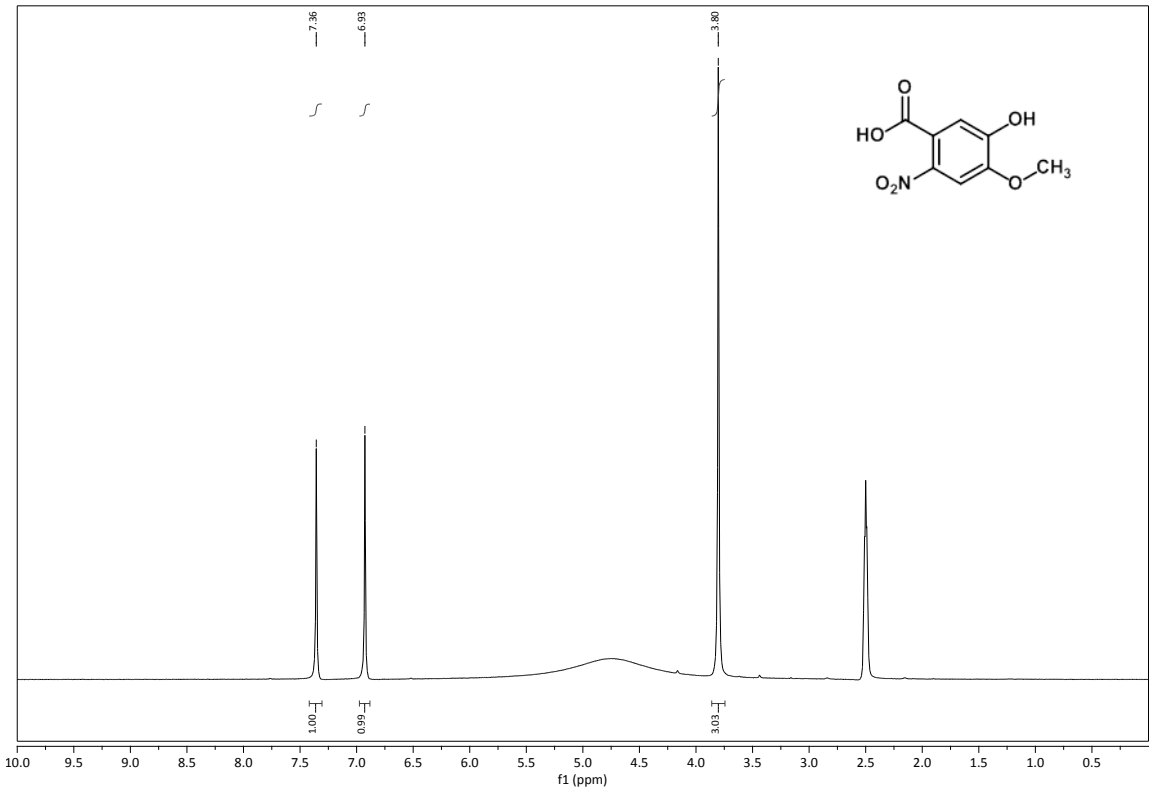

Compound **20**, ^{13}C-NMR (50 MHz, d$_6$-DMSO)

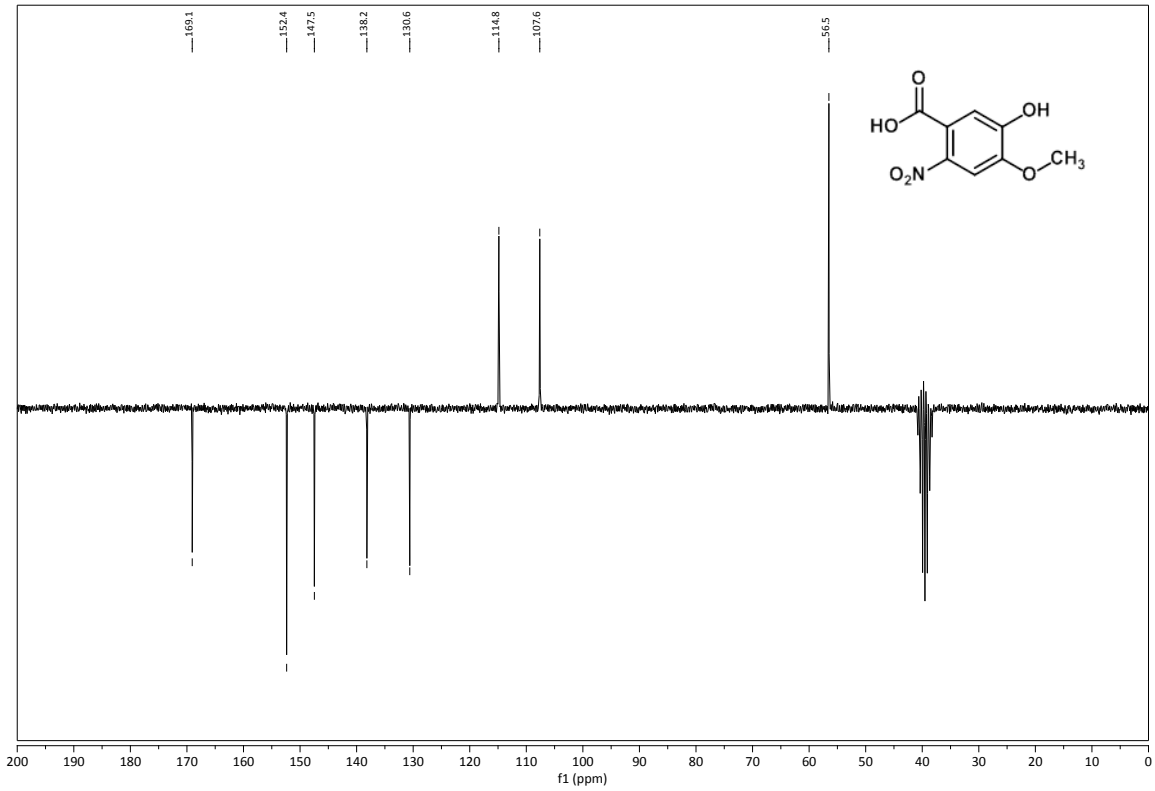

Compound **21**, ^{1}H-NMR (200 MHz, d_6-DMSO)

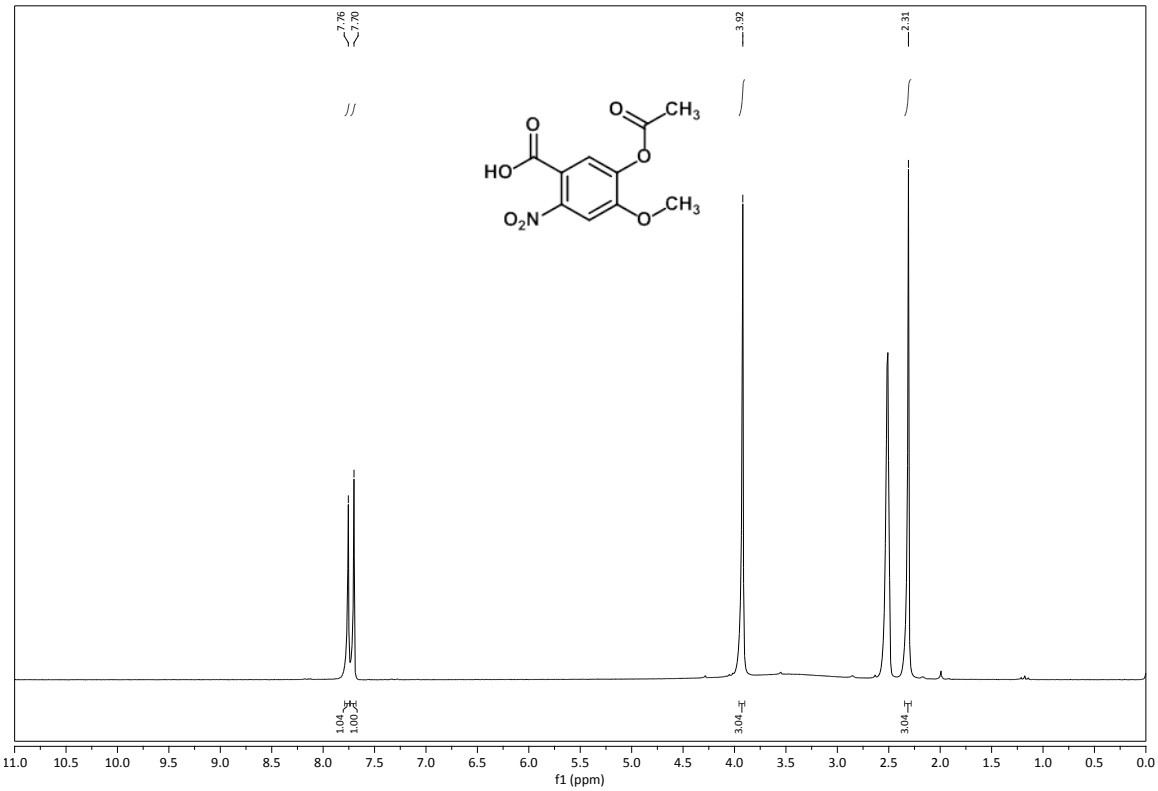

Compound **21**, ^{13}C-NMR (50, MHz, d_6-DMSO)

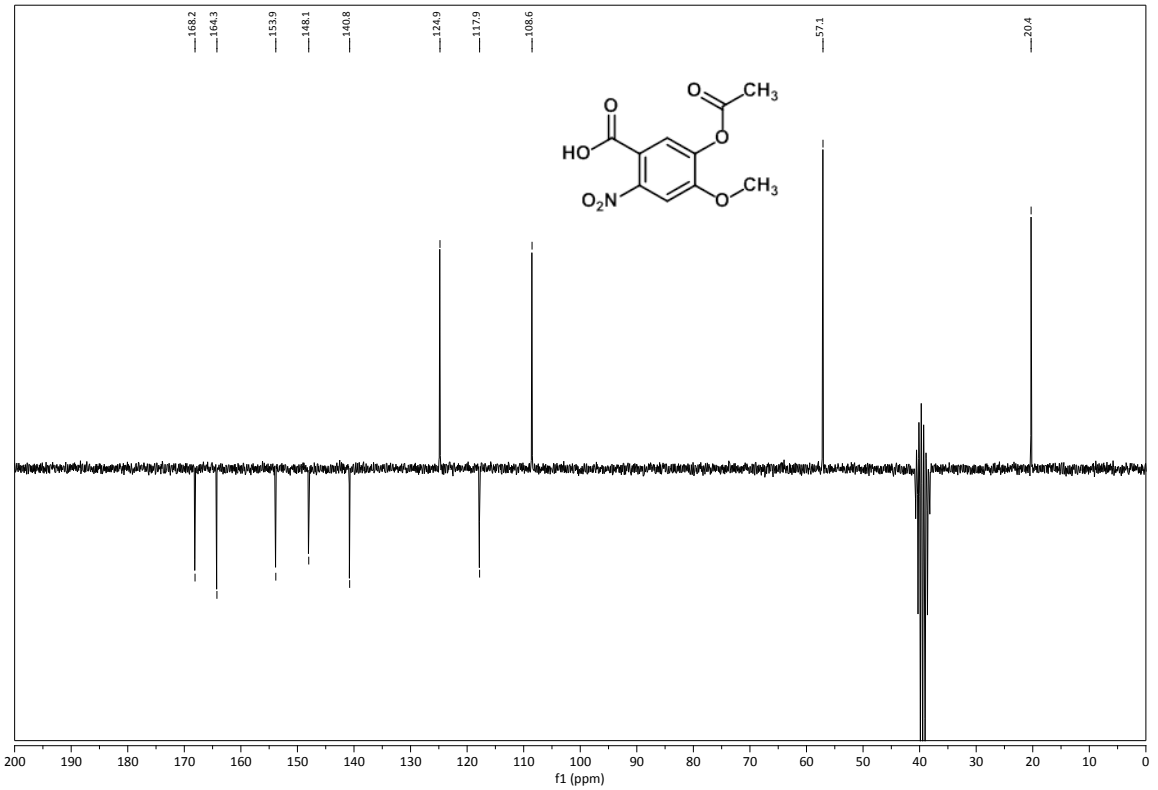

Compound **21**, mass spectrum

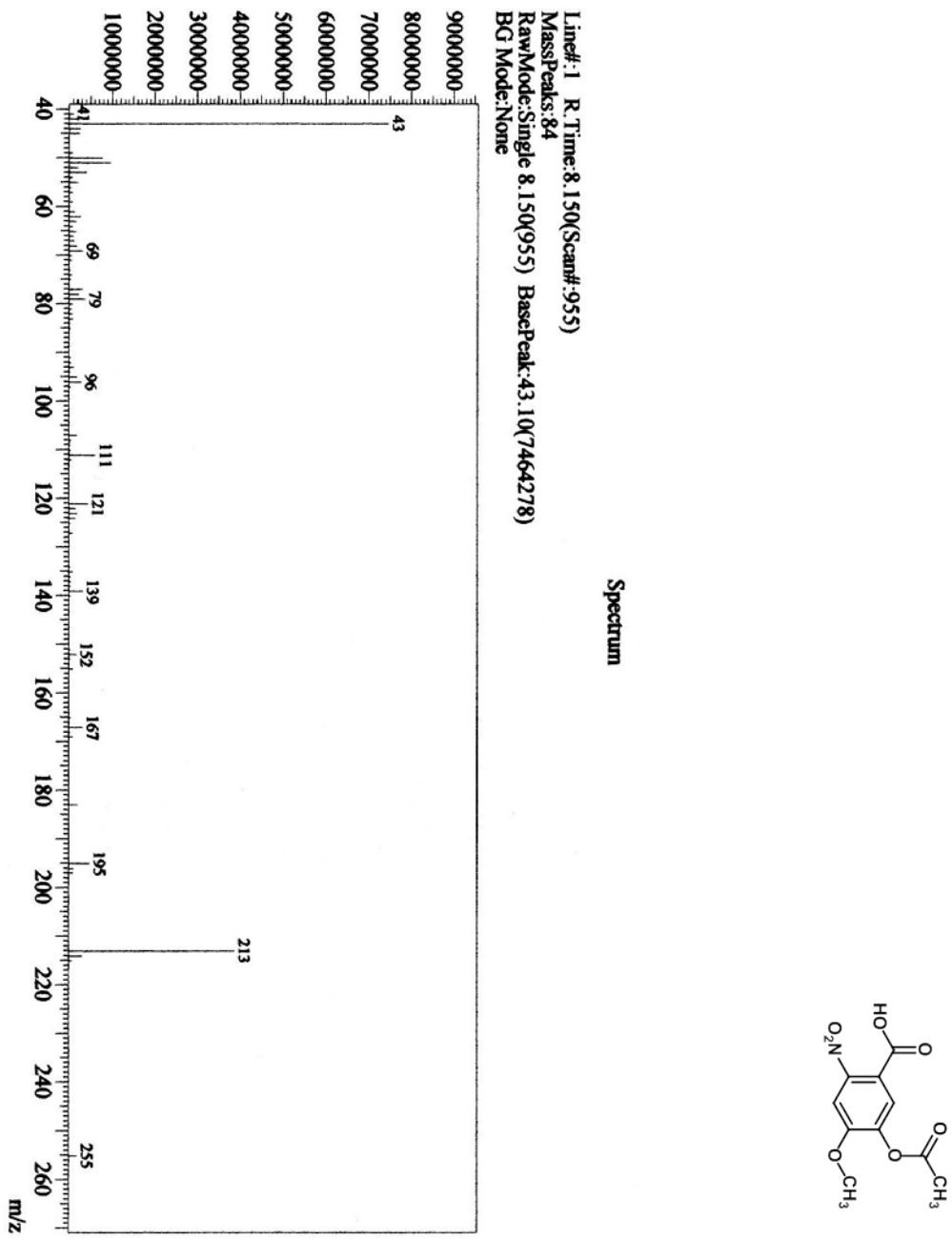

Compound **22**, ^{1}H-NMR (200 MHz, $CDCl_3$)

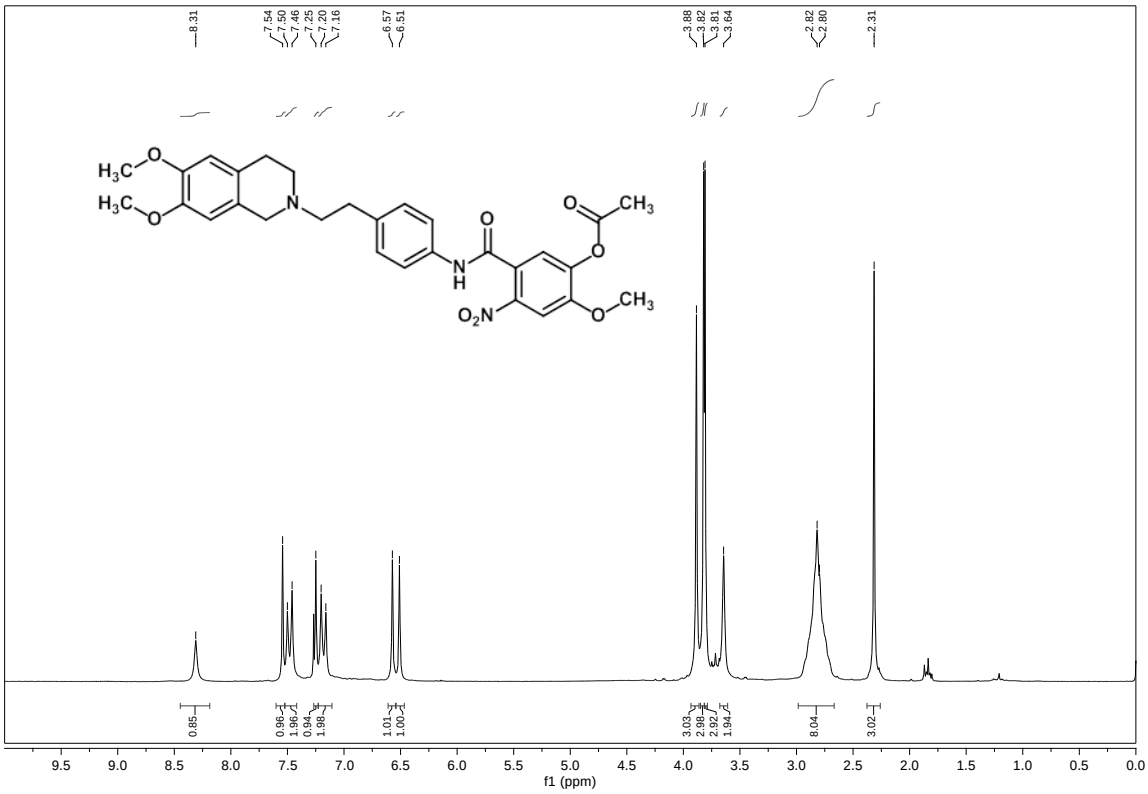

Compound **22**, ^{13}C-NMR (50 MHz, $CDCl_3$)

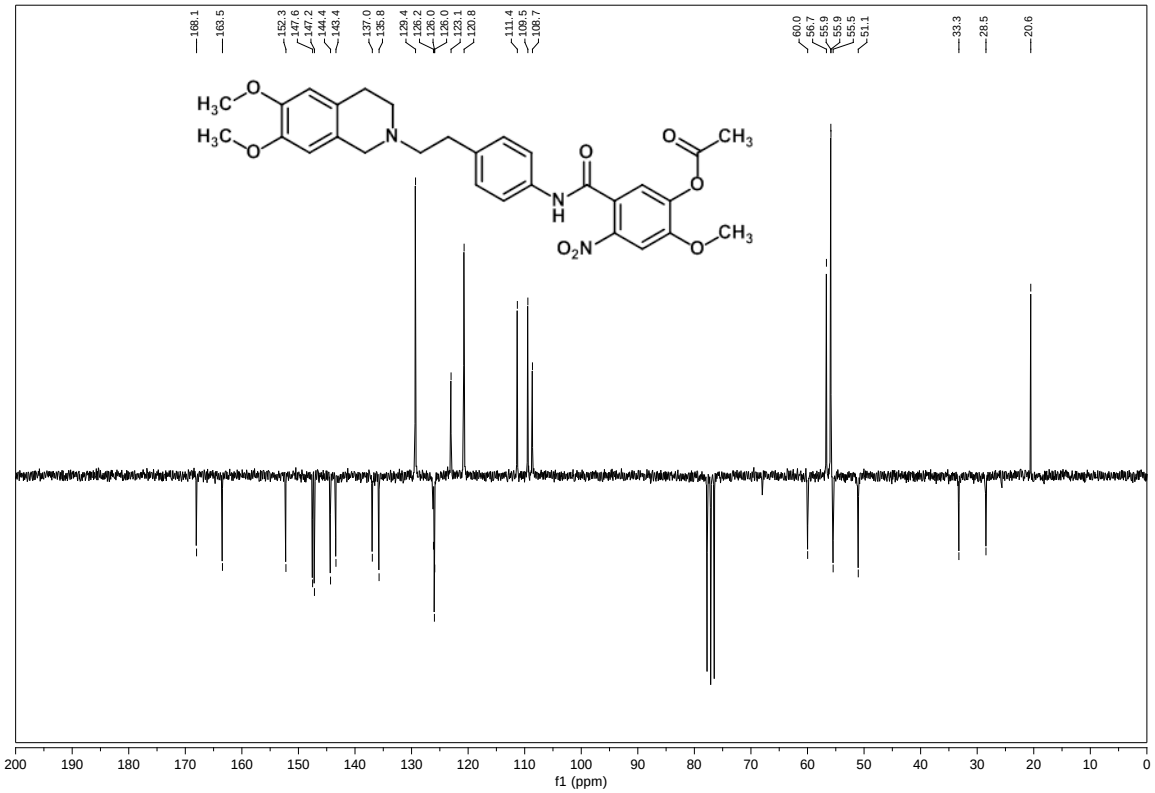

Compound **22**, mass spectrum

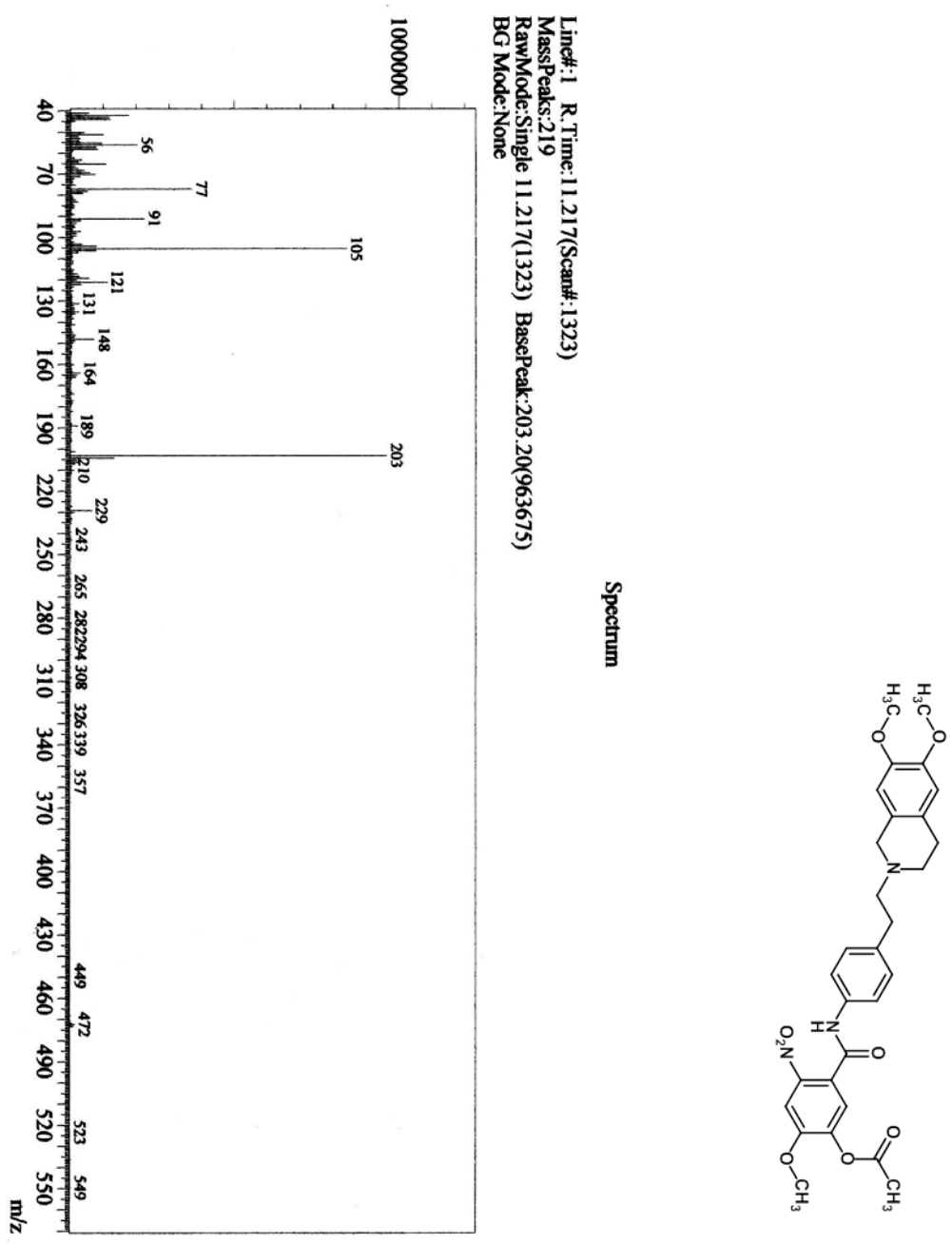

Compound **23**, ^{1}H-NMR (200 MHz, $CDCl_3$)

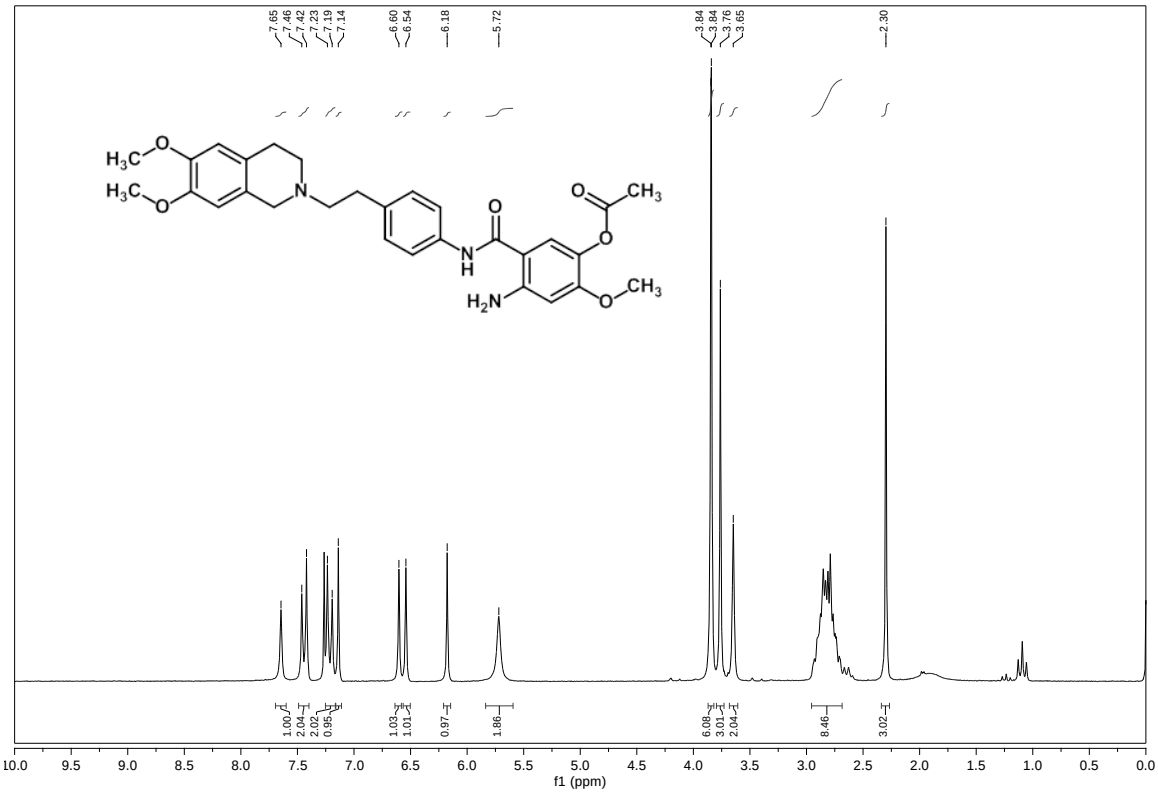

Compound **24**, ^{1}H-NMR (200 MHz, d$_6$-DMSO)

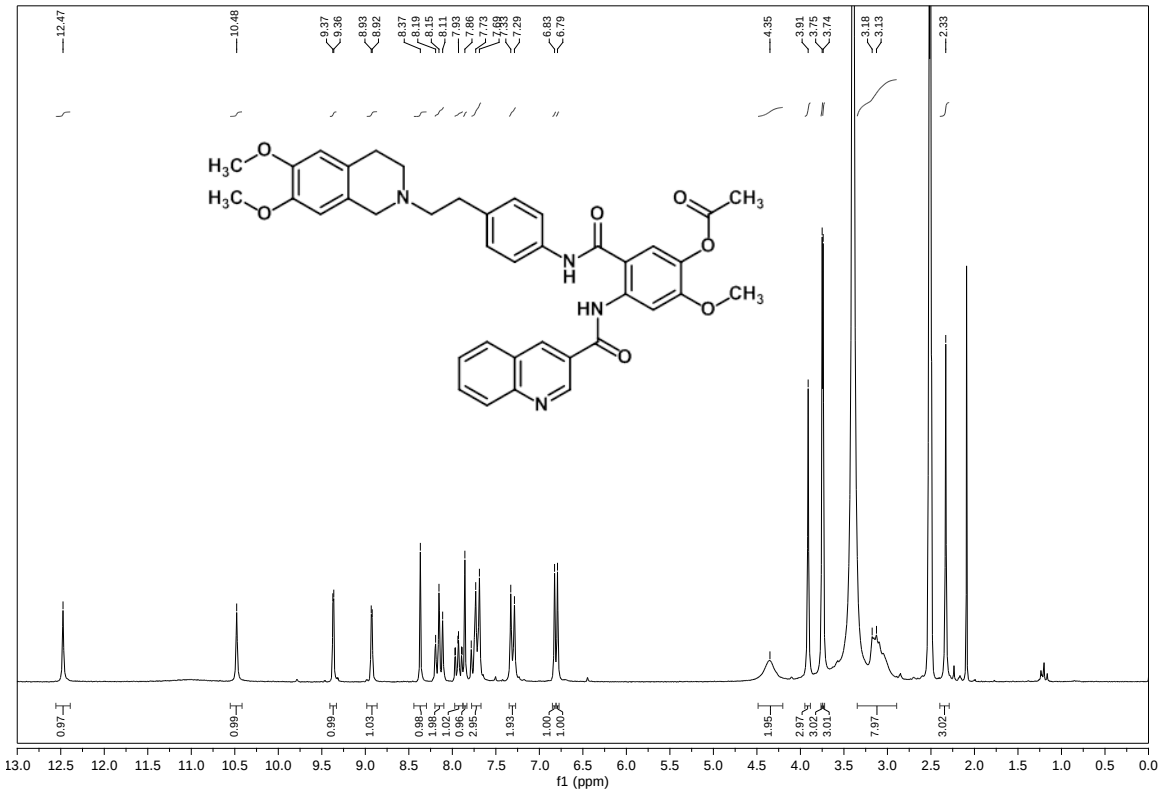

Compound **24**, ^{13}C-NMR (50 MHz, d$_6$-DMSO)

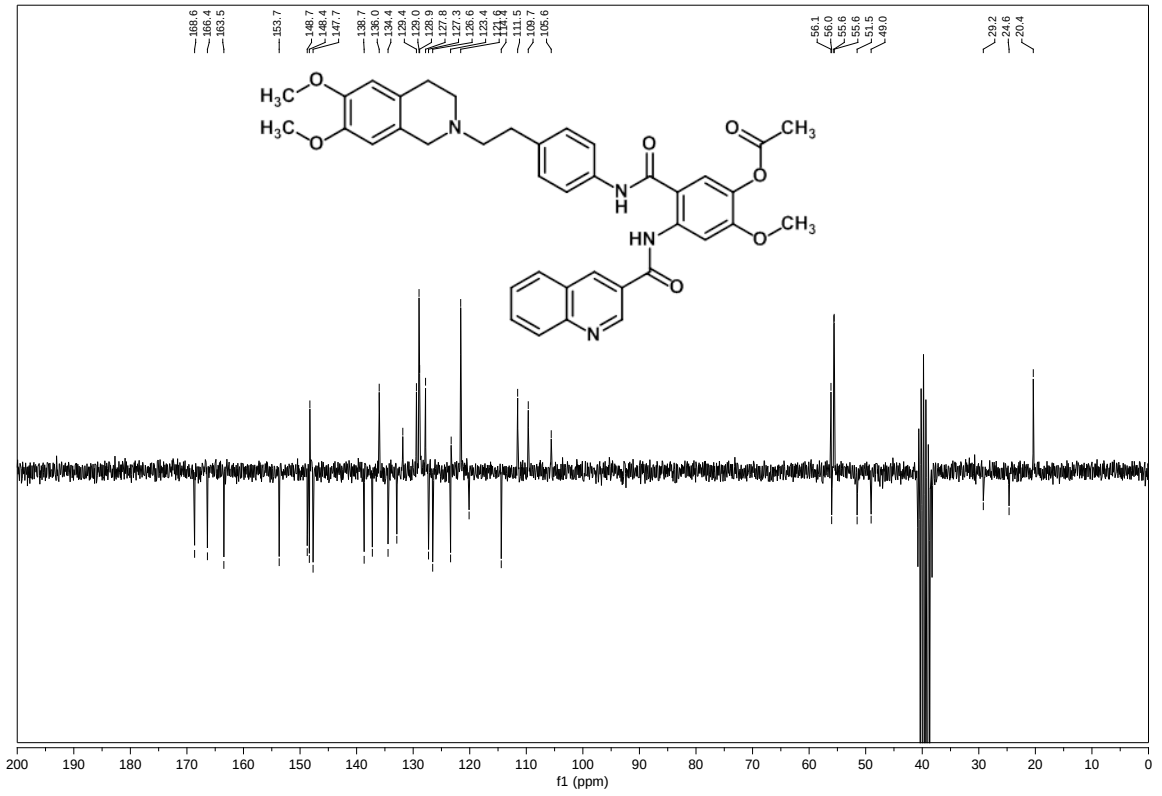

Compound **25**, ^{1}H-NMR (200 MHz, d_6-DMSO)

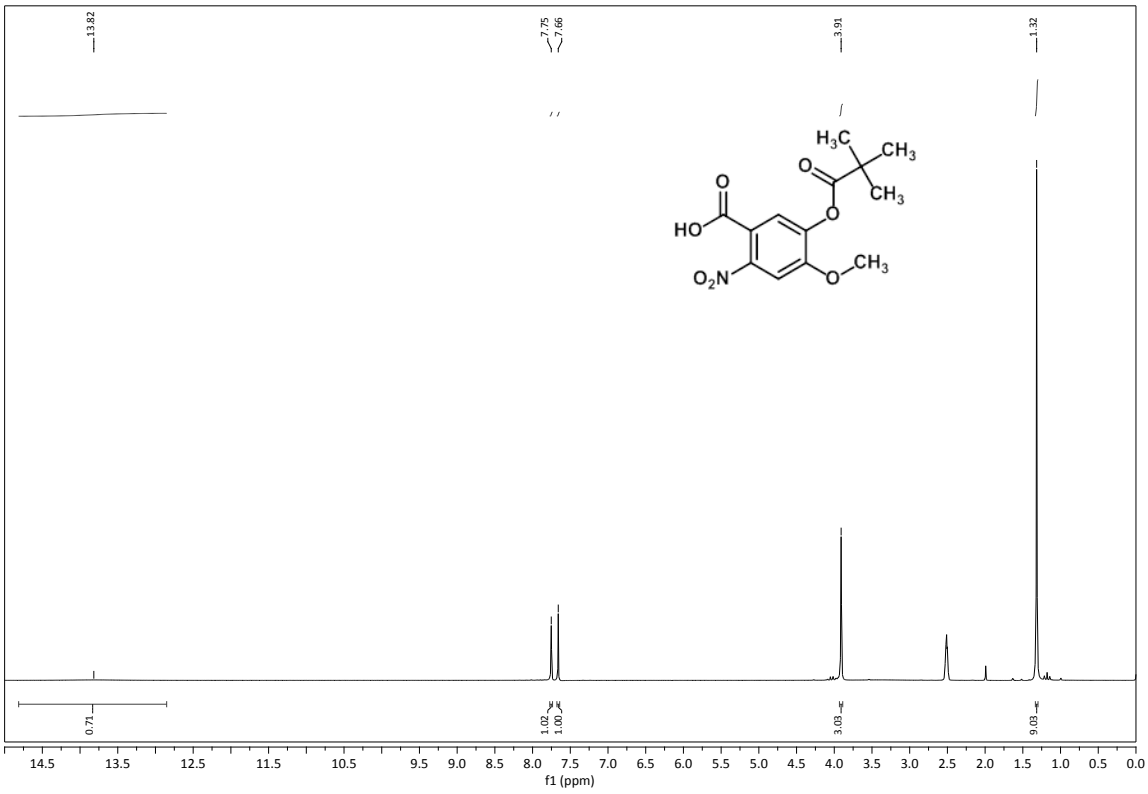

Compound **25**, ^{13}C-NMR (50 MHz, d_6-DMSO)

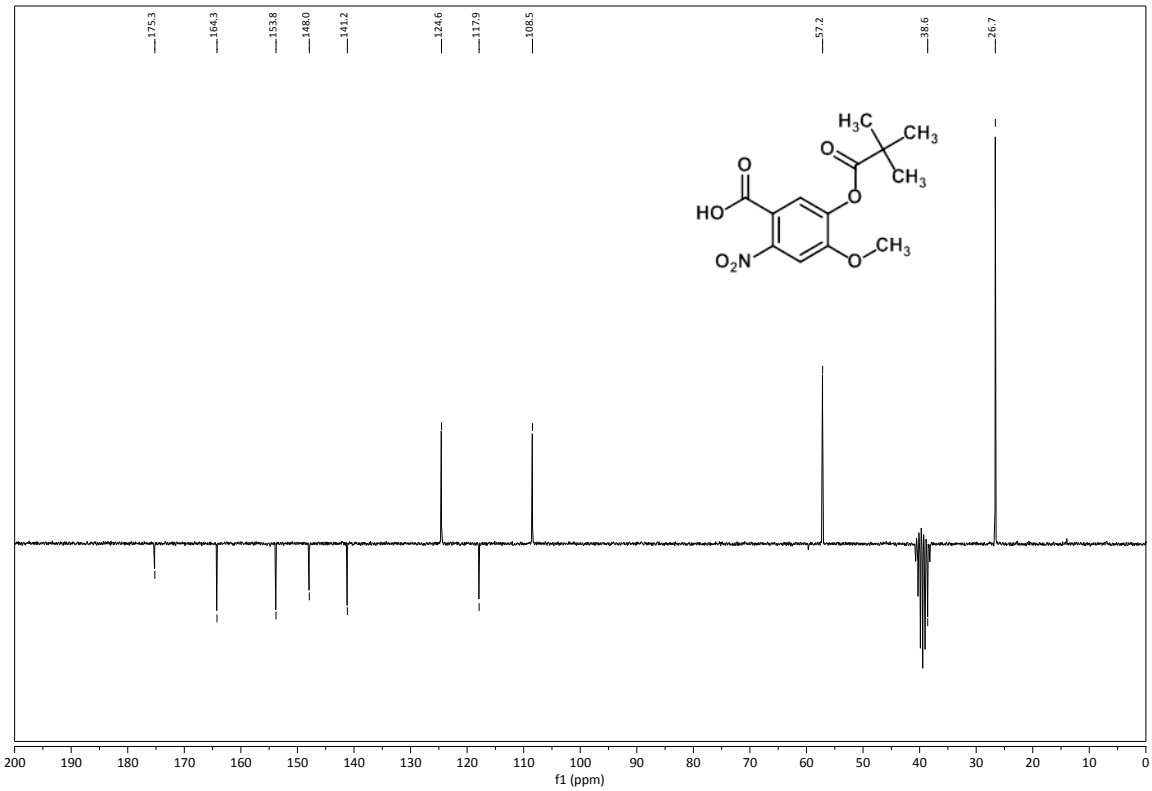

Compound **25**, mass spectrum

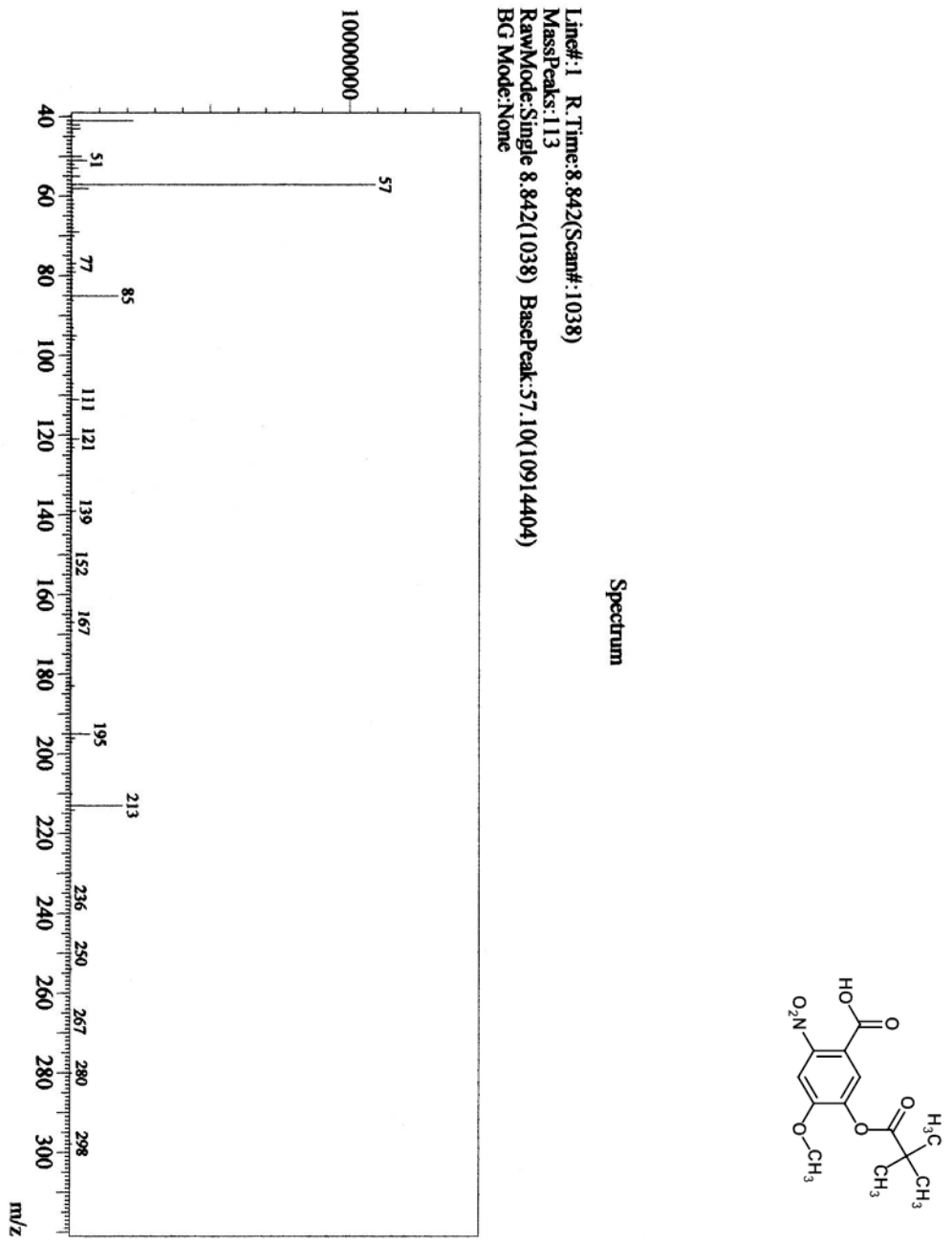

Compound **26**, ^{1}H-NMR (200 MHz, d_6-DMSO)

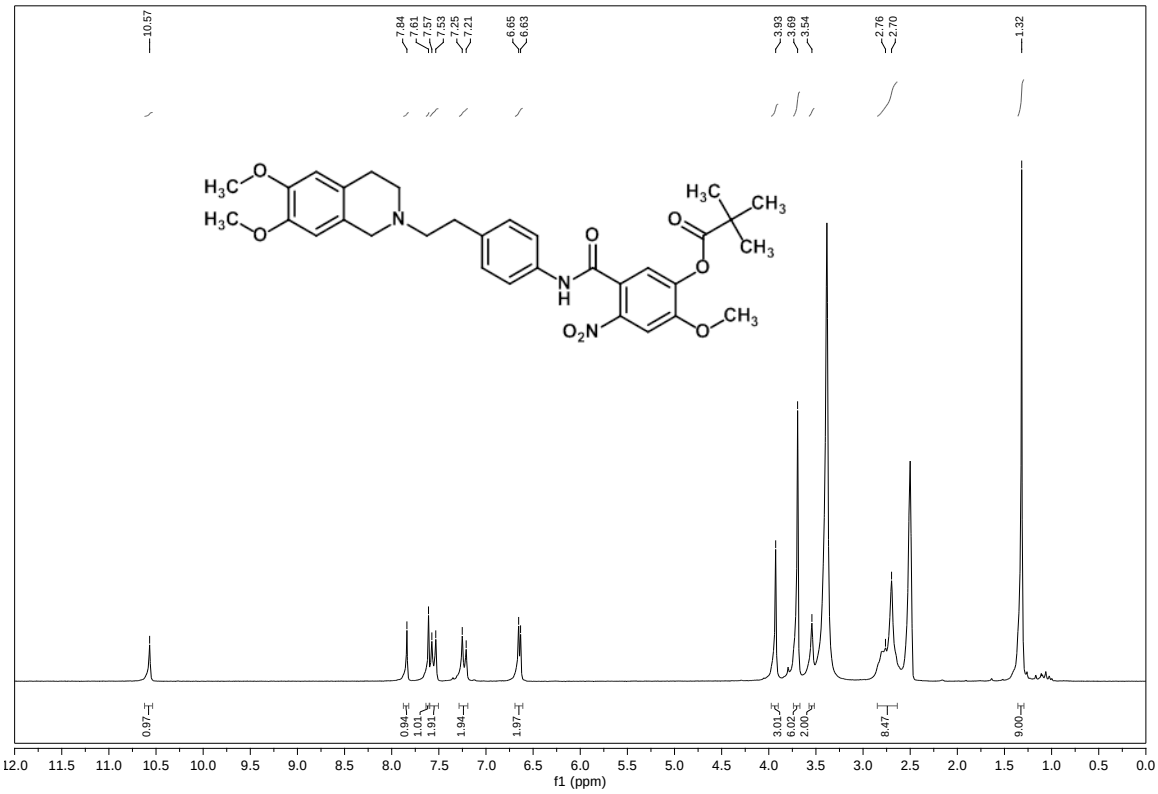

Compound **26**, ^{13}C-NMR (50 MHz, d_6-DMSO)

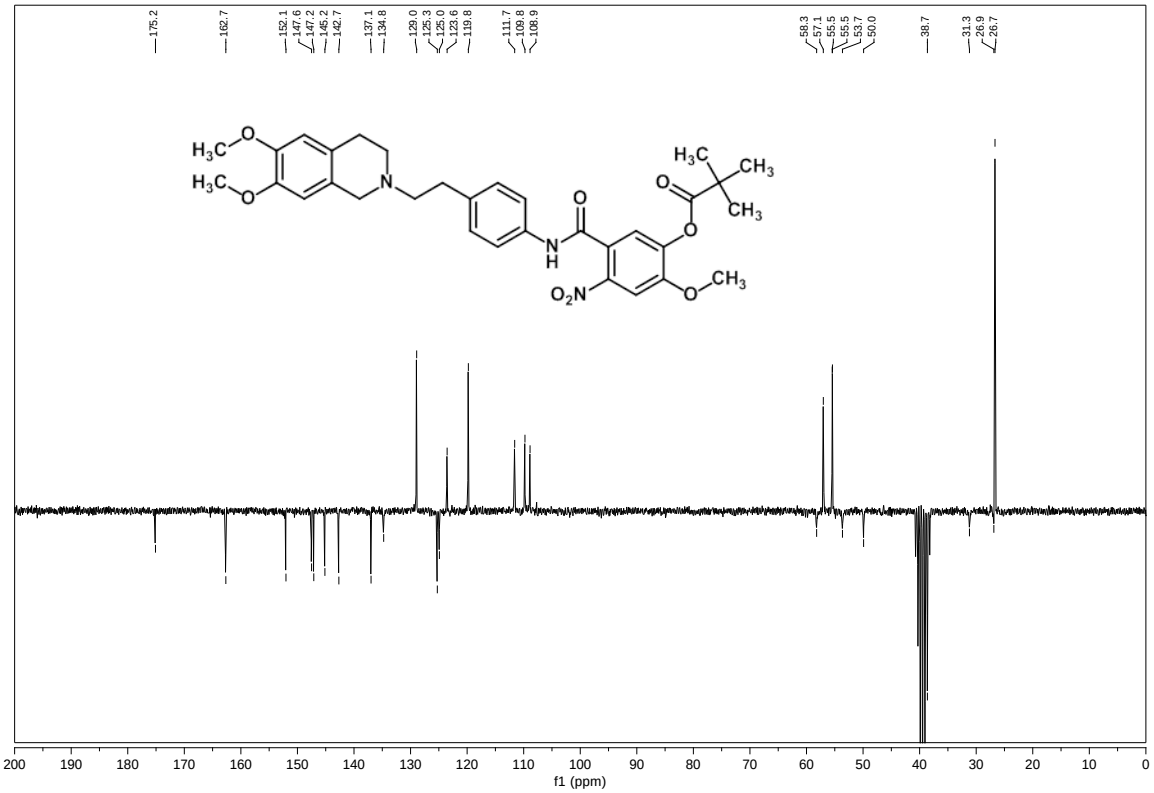

Compound **26**, mass spectrum

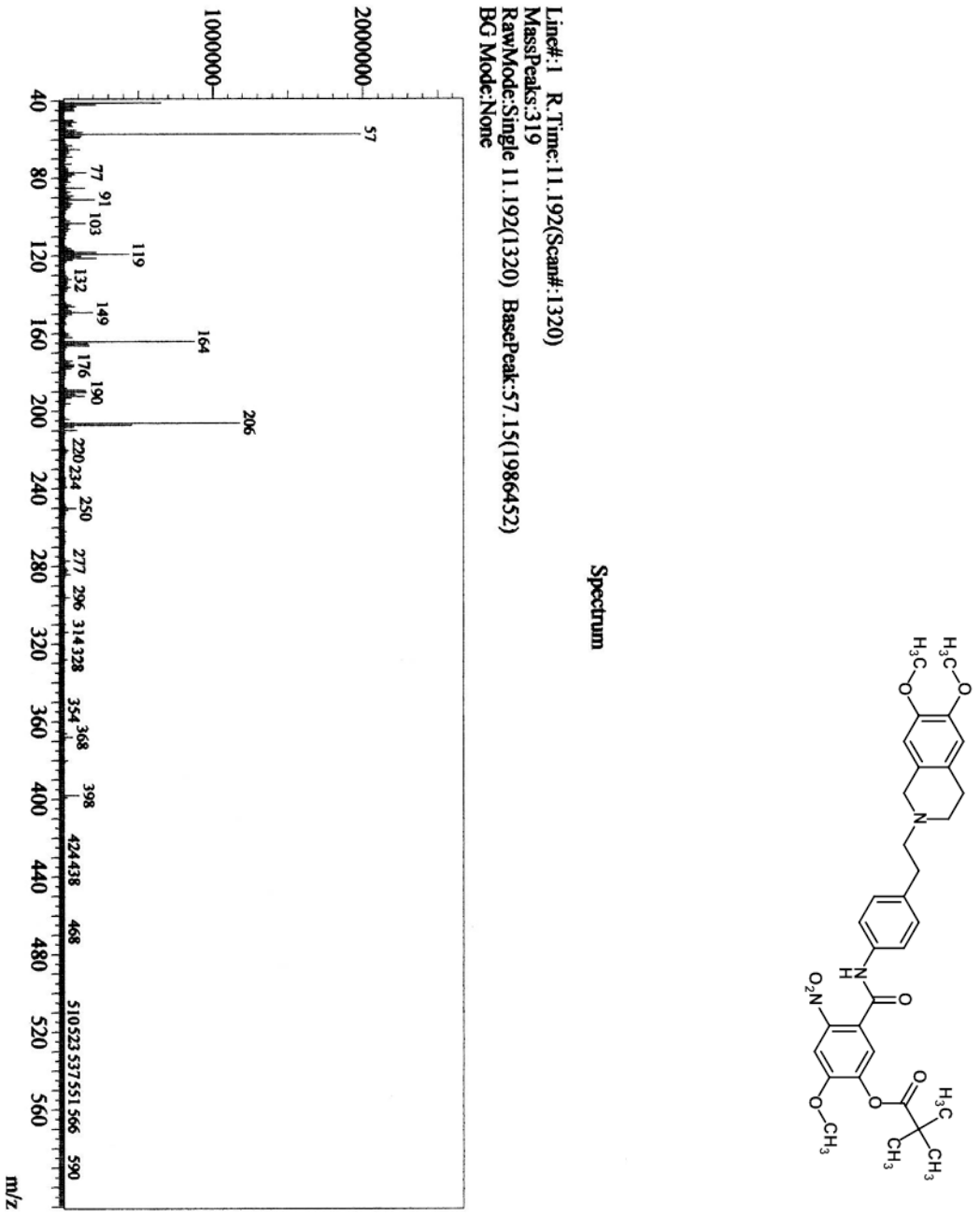

Compound **27**, ^{1}H-NMR (200 MHz, $CDCl_3$)

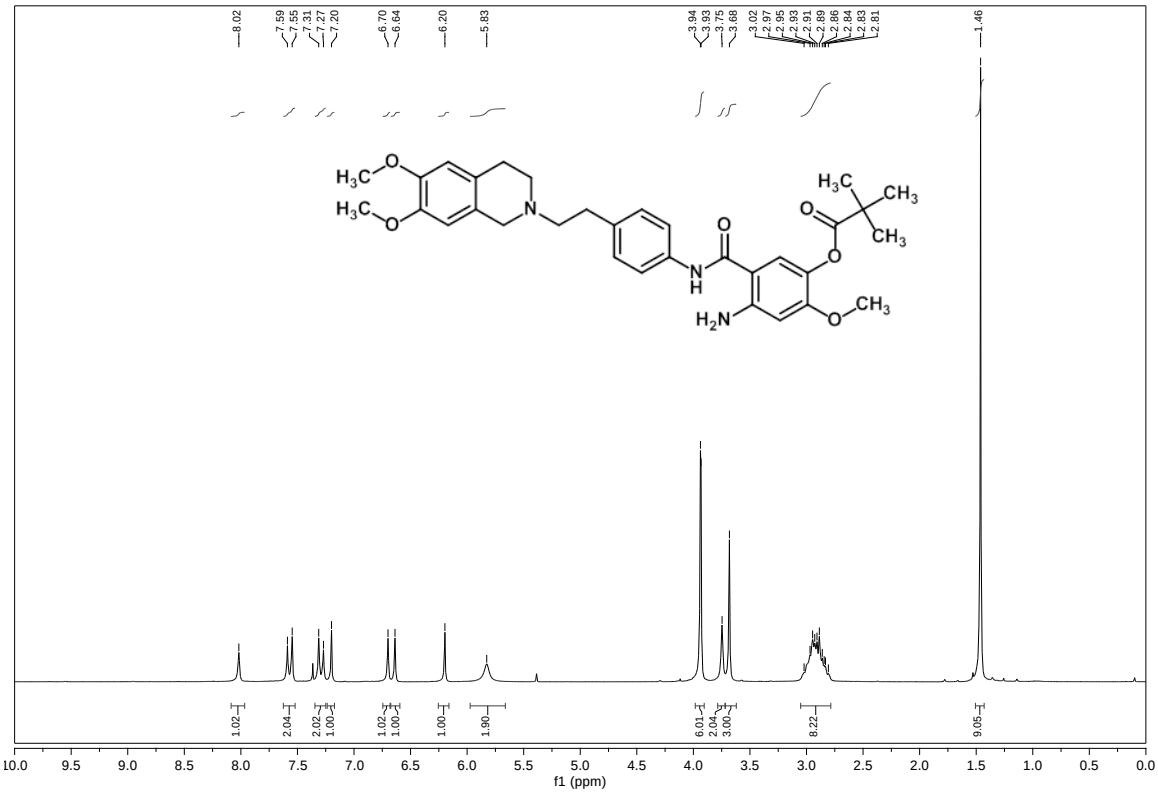

Compound **27**, ^{13}C-NMR (50 MHz, $CDCl_3$)

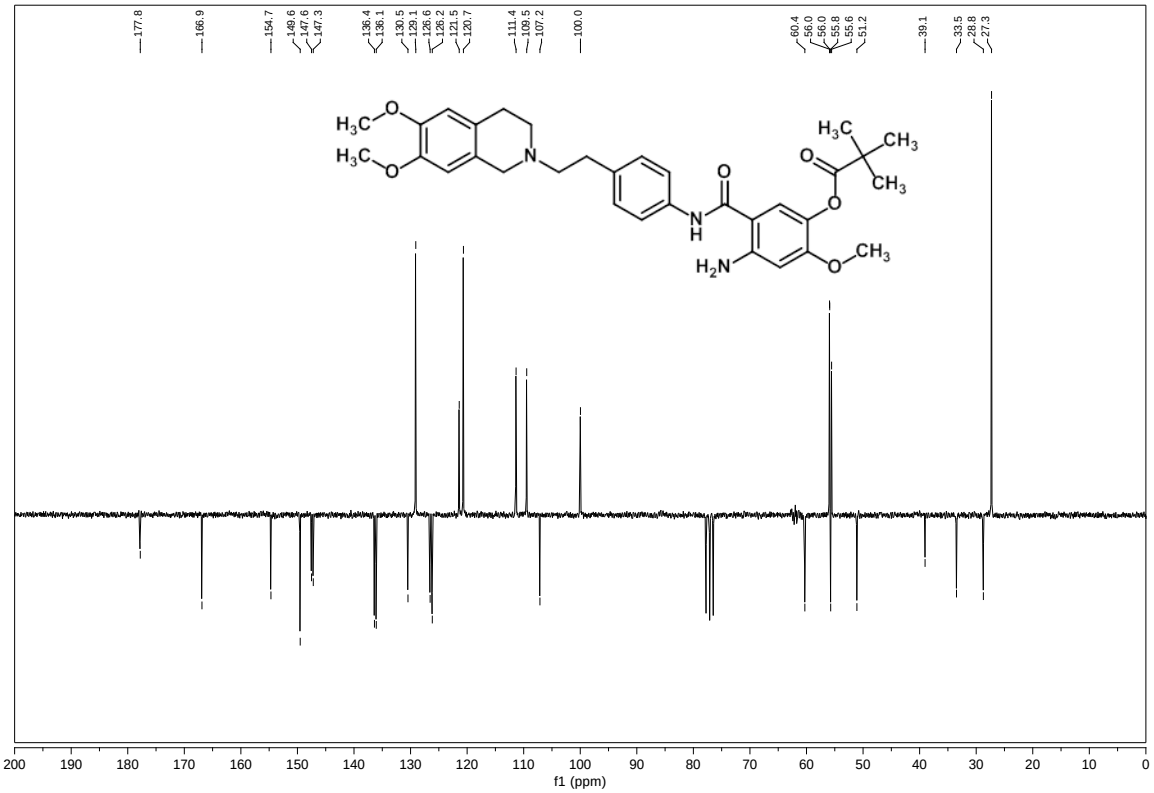

Compound **27**, mass spectrum

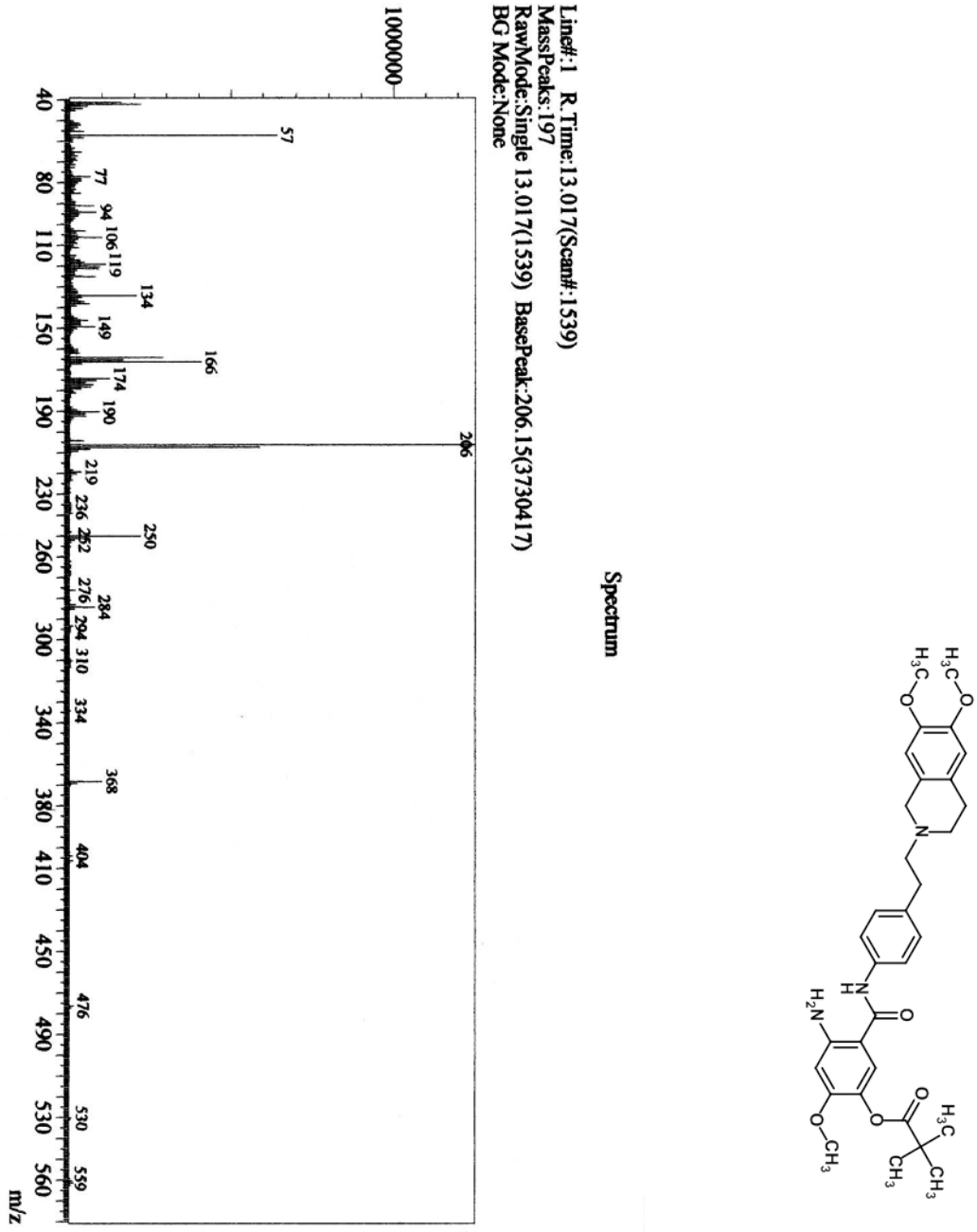

Compound **28**, ^{1}H-NMR (200 MHz, $CDCl_3$)

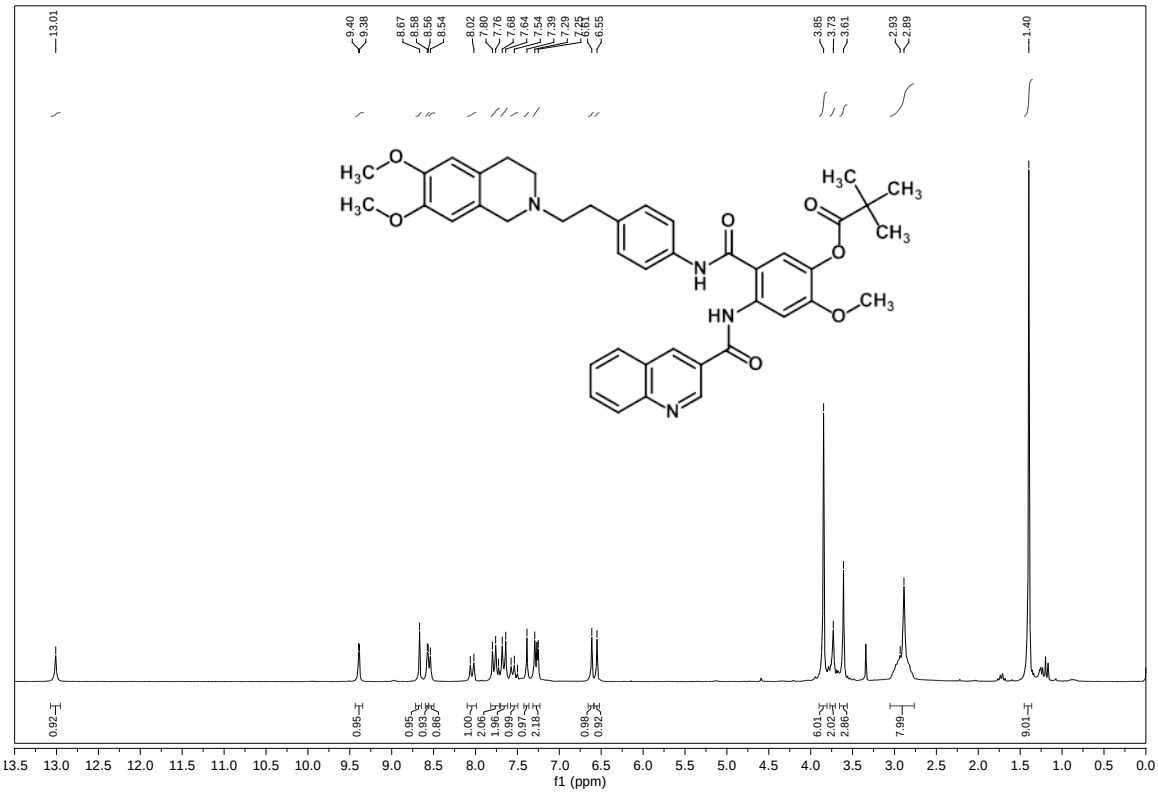

Compound **28**, ^{13}C-NMR (50 MHz, $CDCl_3$)

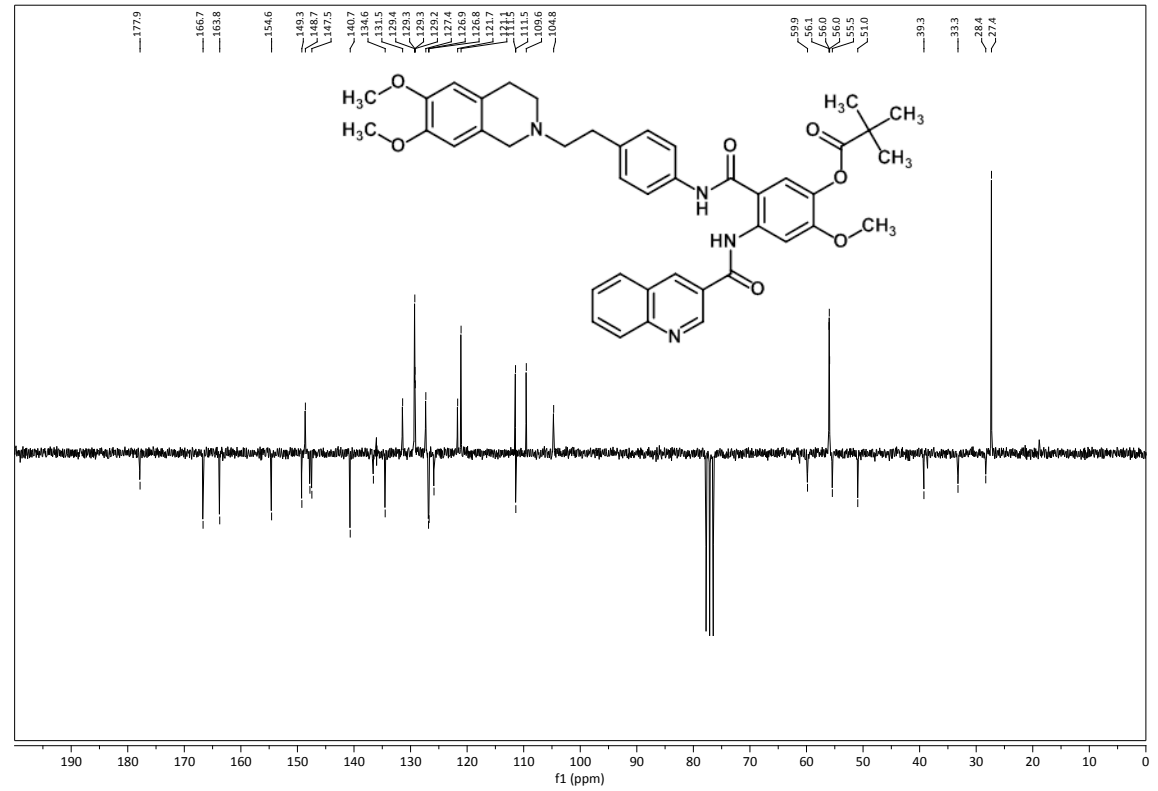

Compound **28**, high resolution mass spectrum

Spektren_Nummer: 35571

Tiegel: / C

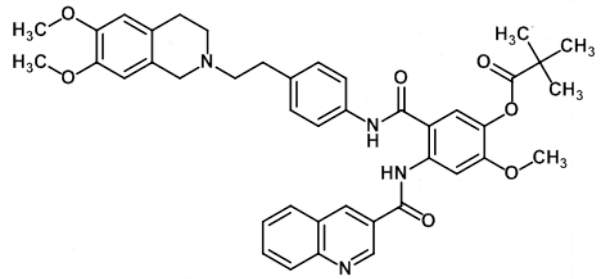

Hochaufloesung:

Berechnet fuer: $C_{42}H_{44}O_7N_4H$ **Exakte Masse:** 717,3288

Gefunden: 717,3285 **+/- 5ppm**

Datum: 27-01-10 **Unterschrift:**

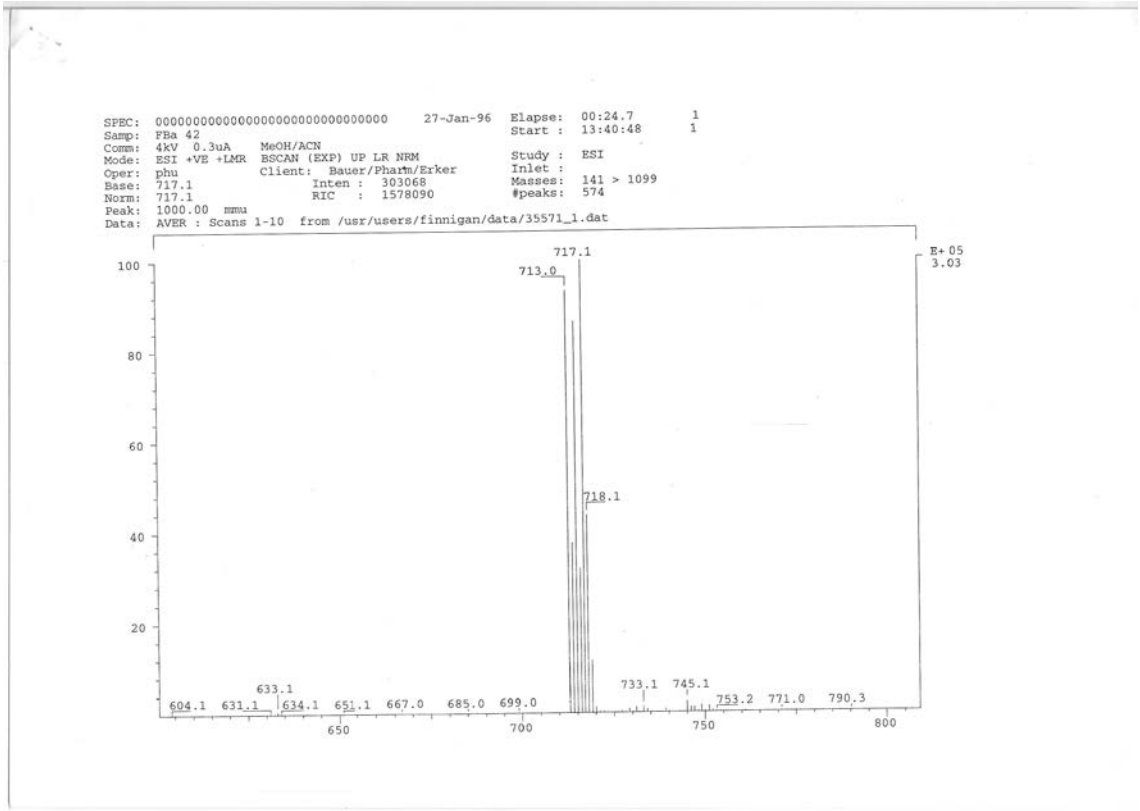

Compound **29**, ^{1}H-NMR (200 MHz, d_6-DMSO)

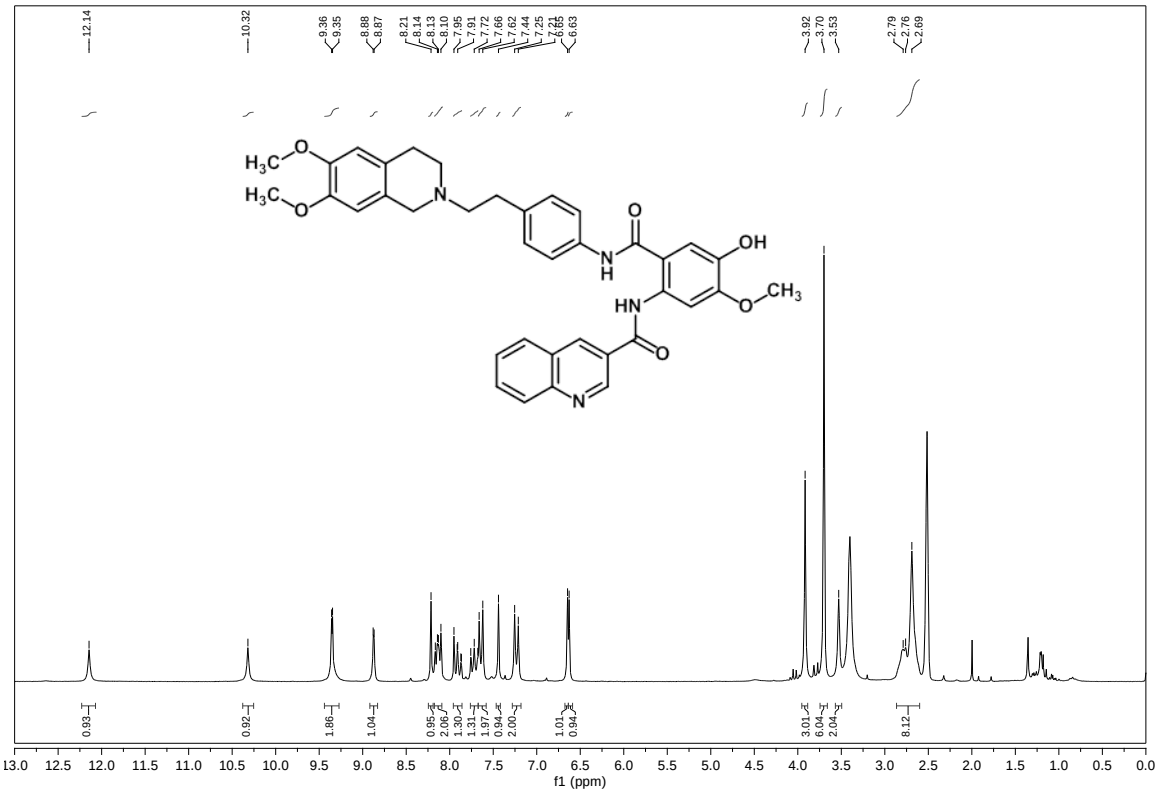

Compound **29**, ^{13}C-NMR (50 MHz, d_6-DMSO)

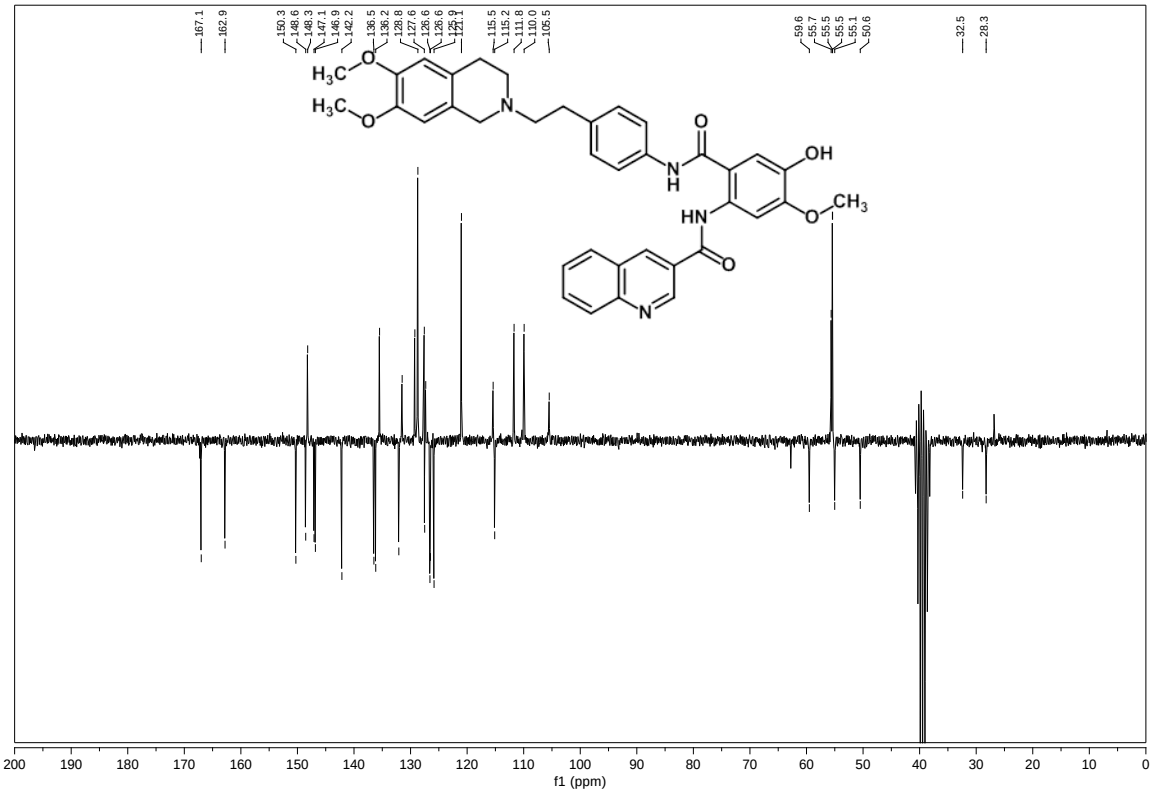

Compound **29**, mass spectrum

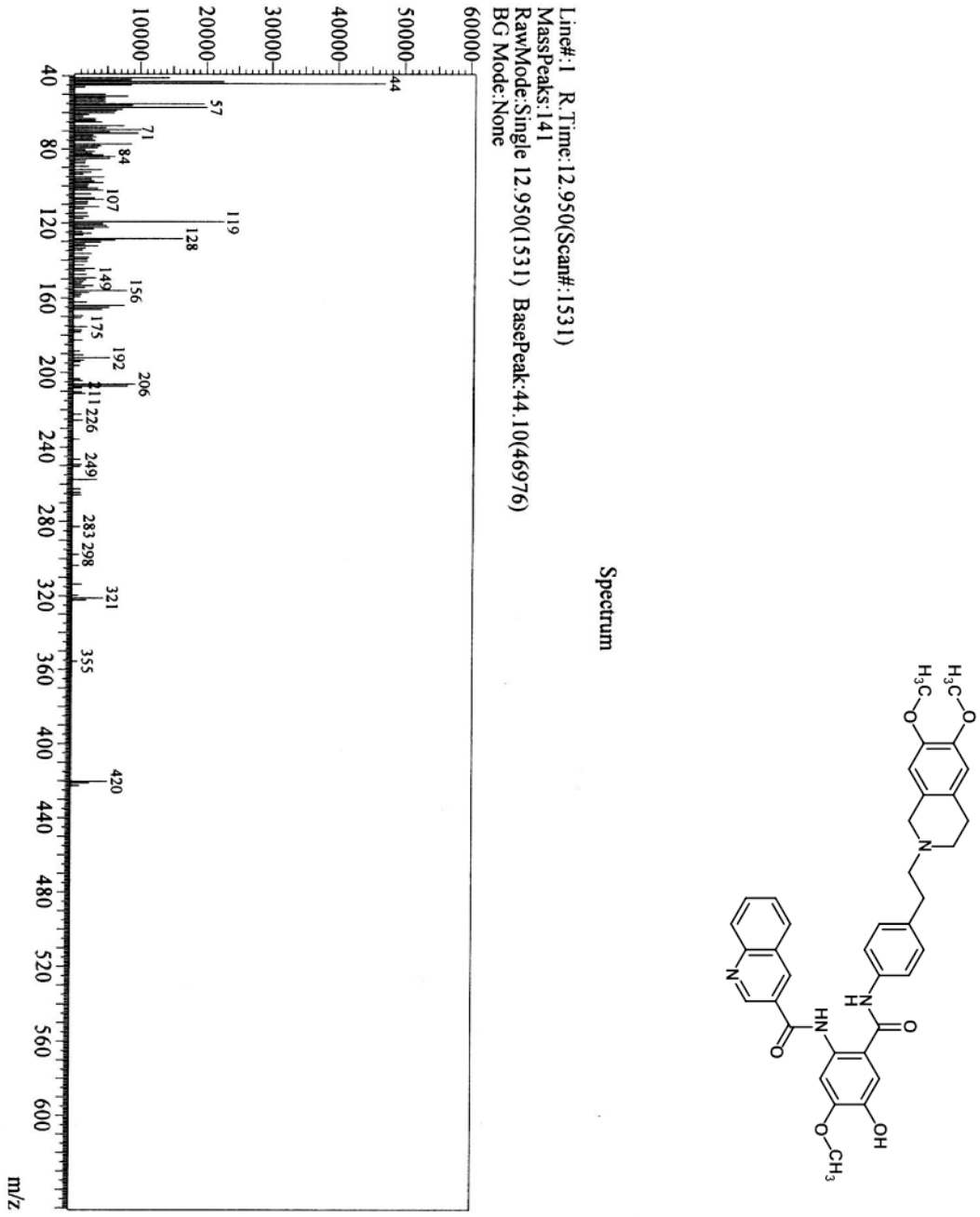

Compound **29**, high resolution mass spectrum

Spektren_Nummer: 35568

Tiegel: / C

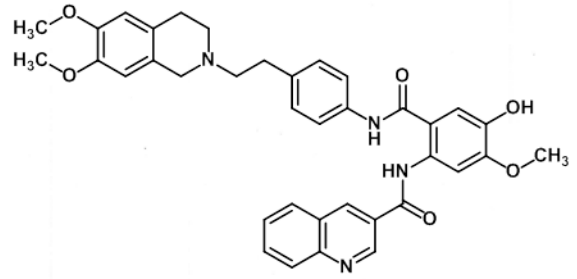

Hochaufloesung:

Berechnet fuer: $C_{37}H_{36}O_6N_4$ **Exakte Masse:** 633,2713

Gefunden: 633,2715 **+/- 5ppm**

Datum: 27-01-10 **Unterschrift:**

SPEC: 00000000000000000000000000000 27-Jan-96 Elapse: 00:24.8 1
Samp: FBa 27 Start : 13:26:39 1
Comm: 4kV 0.3uA MeOH/ACN
Mode: ESI +VE +LMR BSCAN (EXP) UP LR NRM Study : ESI
Oper: phu Client: Bauer/Pharm/Erker Inlet :
Base: 633.1 Inten : 947733 Masses: 141 > 1100
Norm: 633.1 RIC : 1794148 #peaks: 857
Peak: 1000.00 mmu
Data: AVER : Scans 1-10 from /usr/users/finnigan/data/35569_1.dat

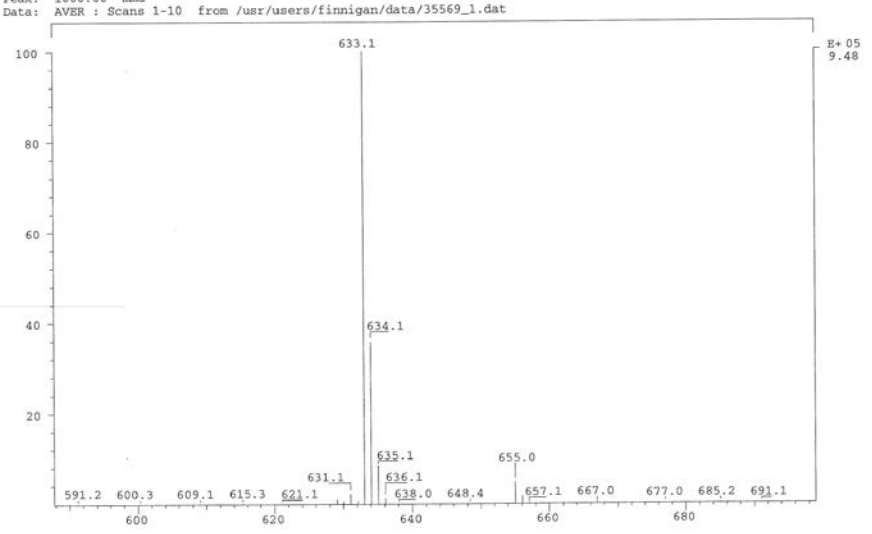

Compound **30**, ^{1}H-NMR (200 MHz, $CDCl_3$)

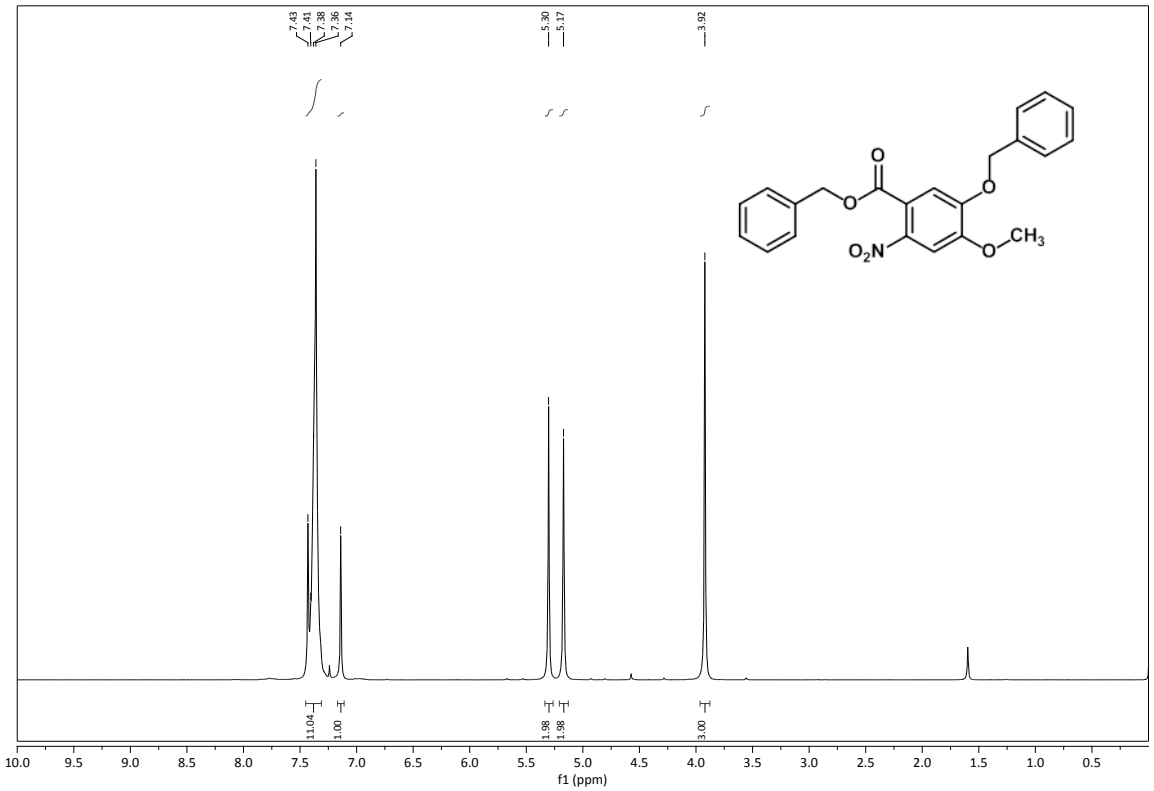

Compound **30**, ^{13}C-NMR (50 MHz, $CDCl_3$)

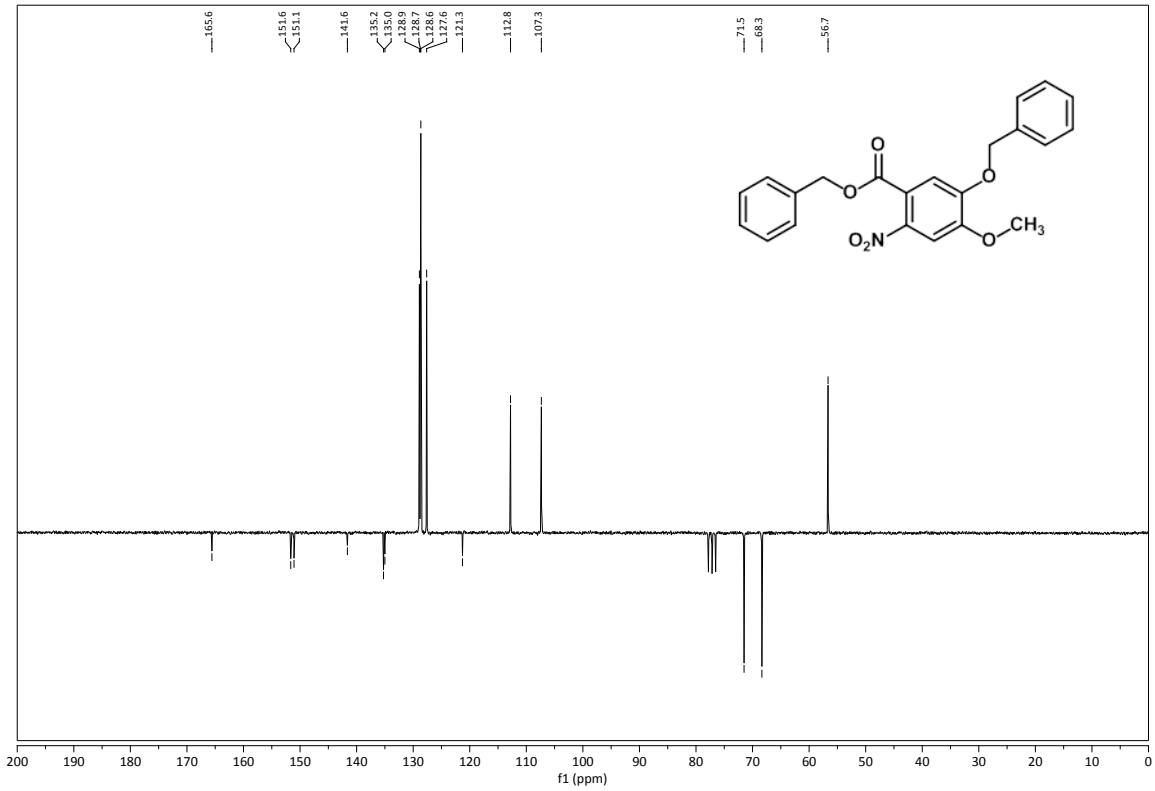

Compound **30**, mass spectrum

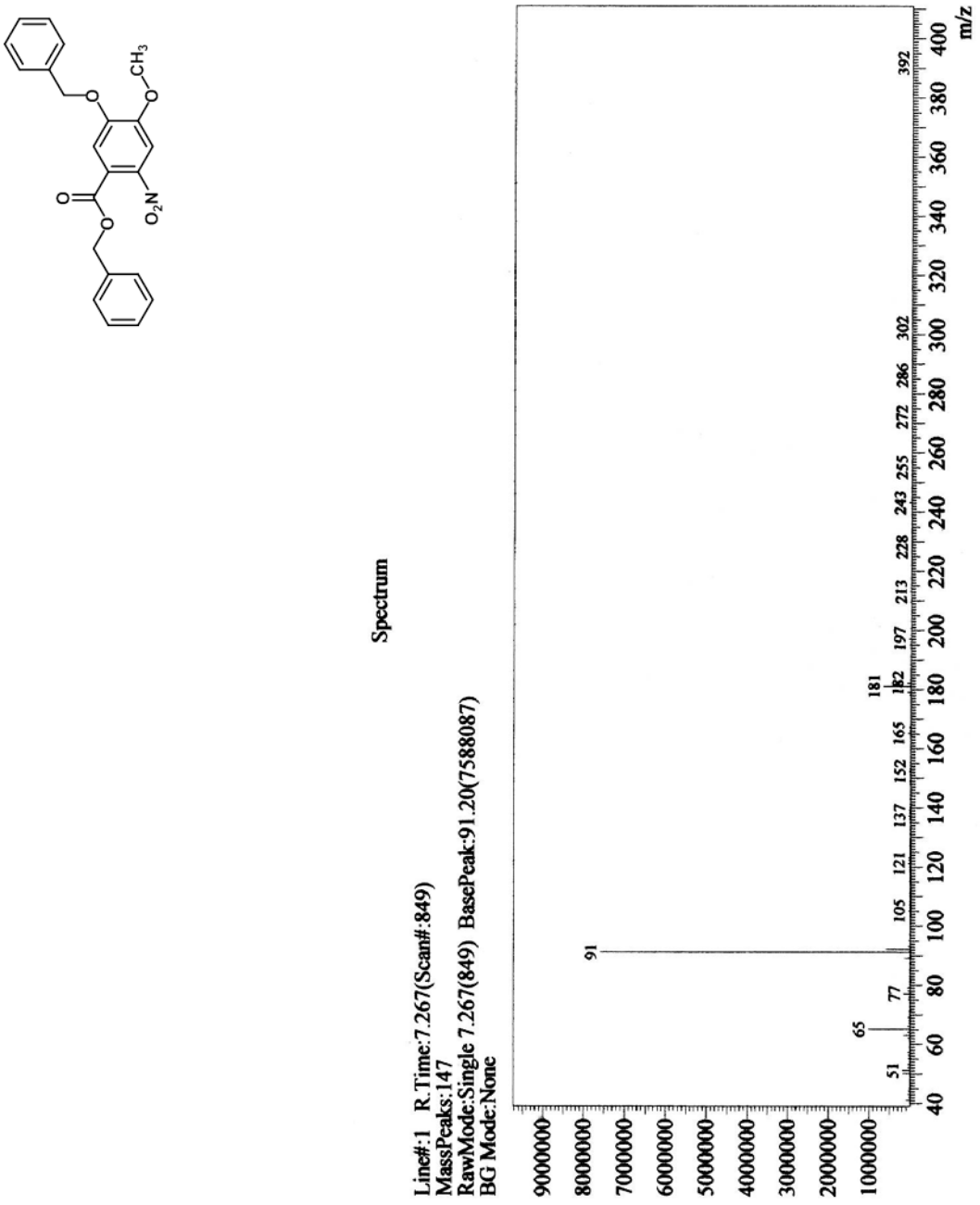

Compound **31**, ^{1}H-NMR (200 MHz, d$_4$-MeOH)

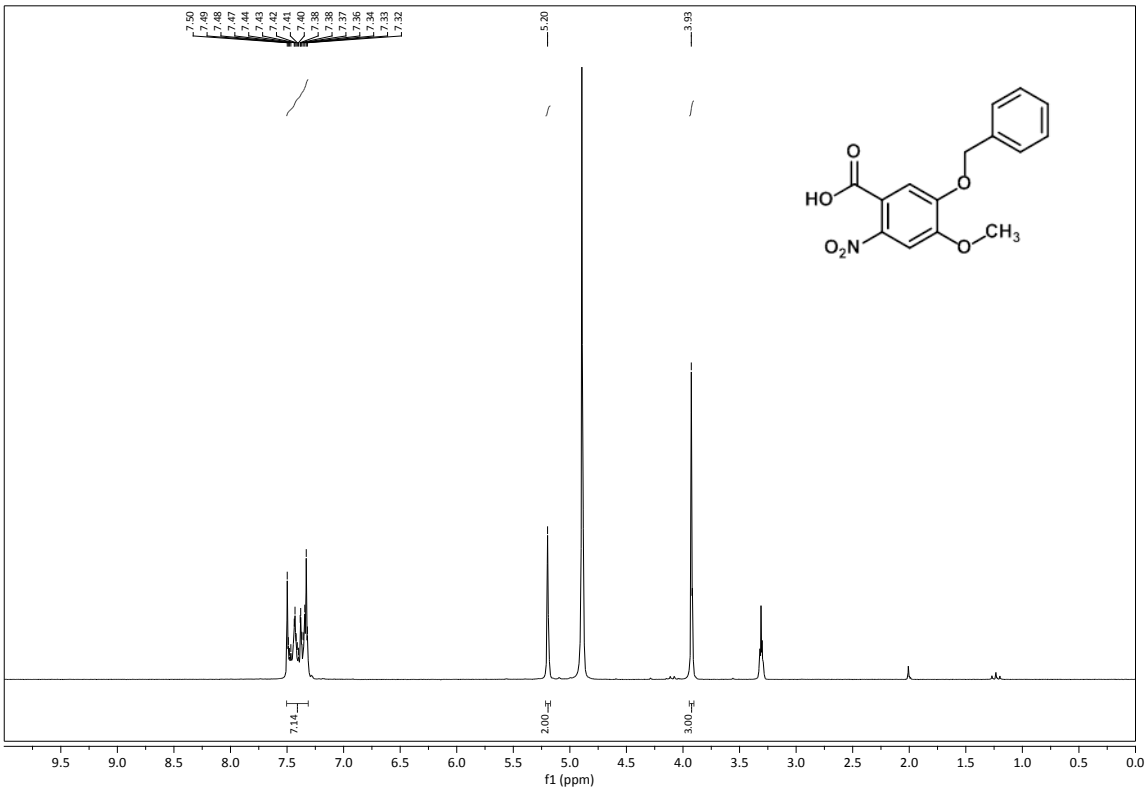

Compound **31**, ^{13}C-NMR (50 MHz, d$_4$-MeOH)

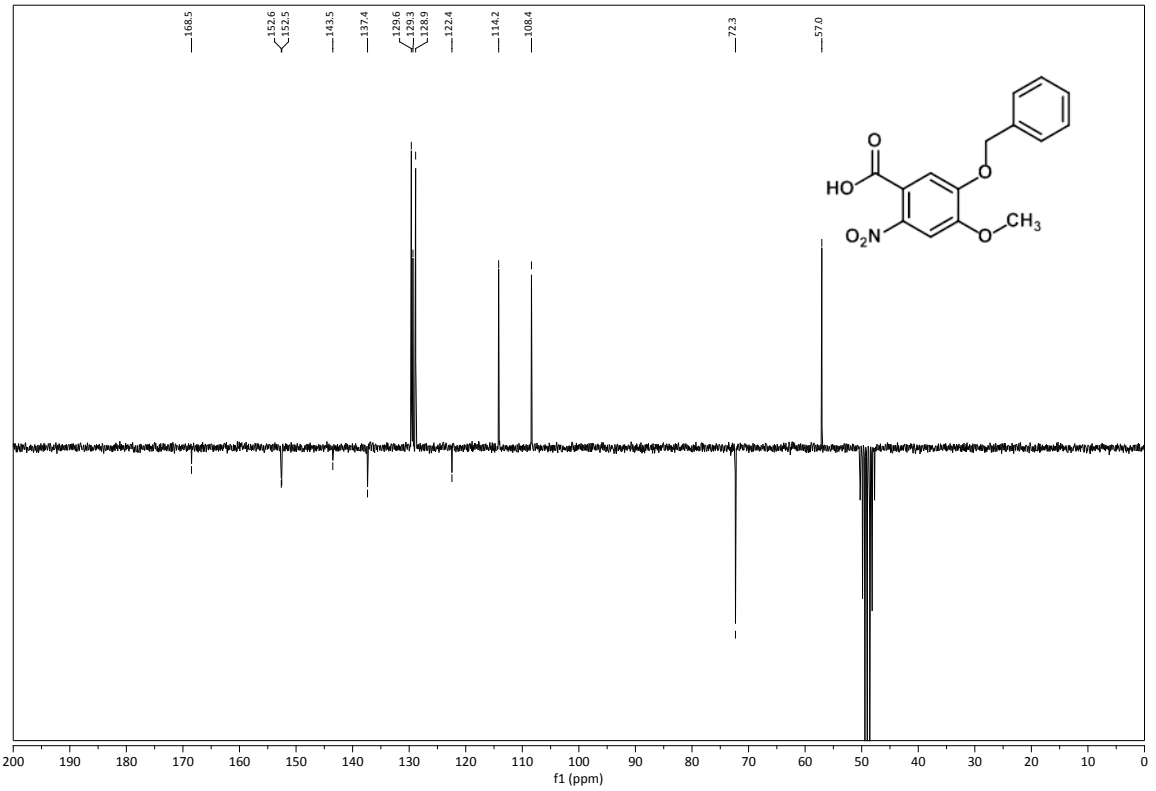

Compound **31**, mass spectrum

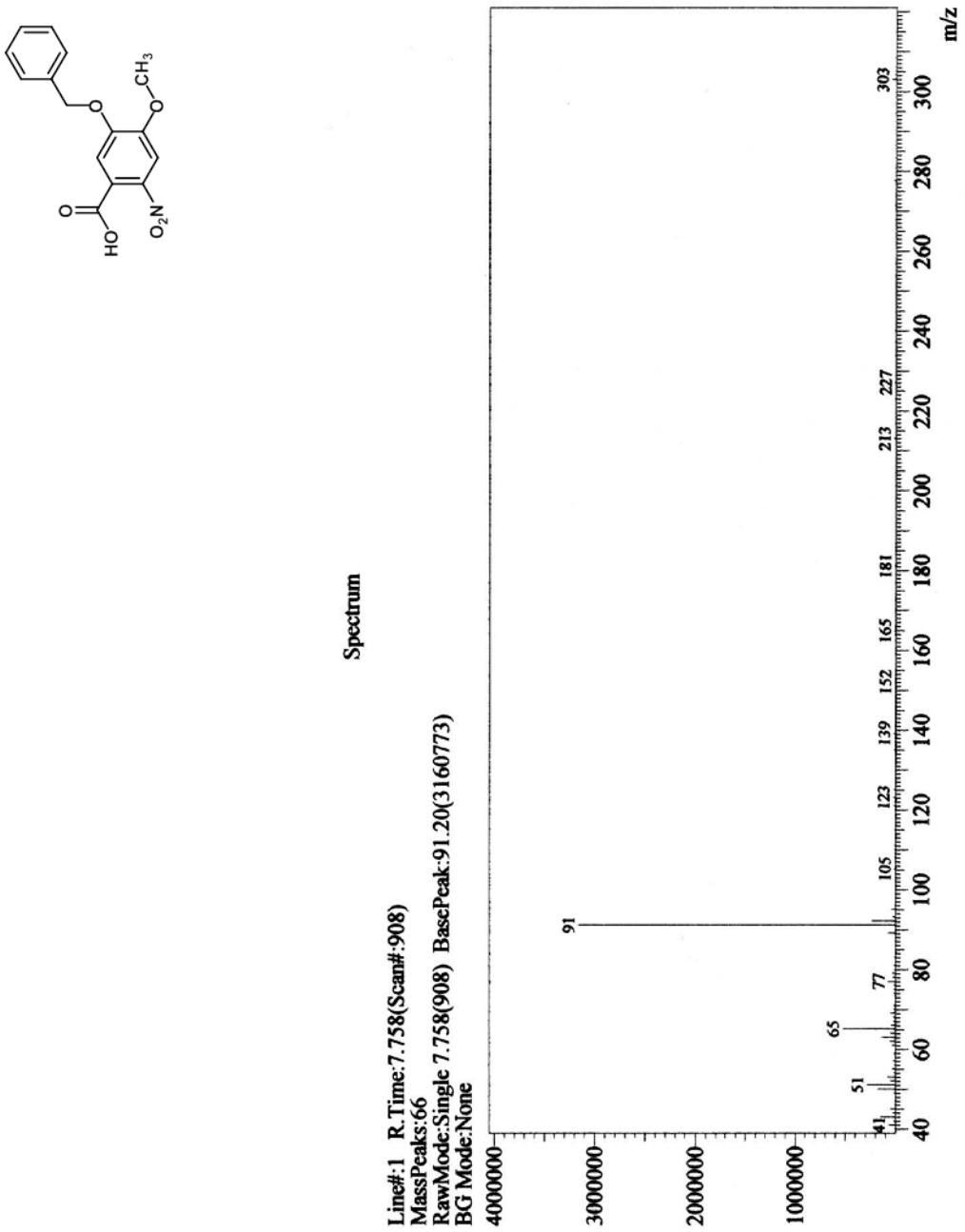

Compound **32**, ^{1}H-NMR (200 MHz, $CDCl_3$)

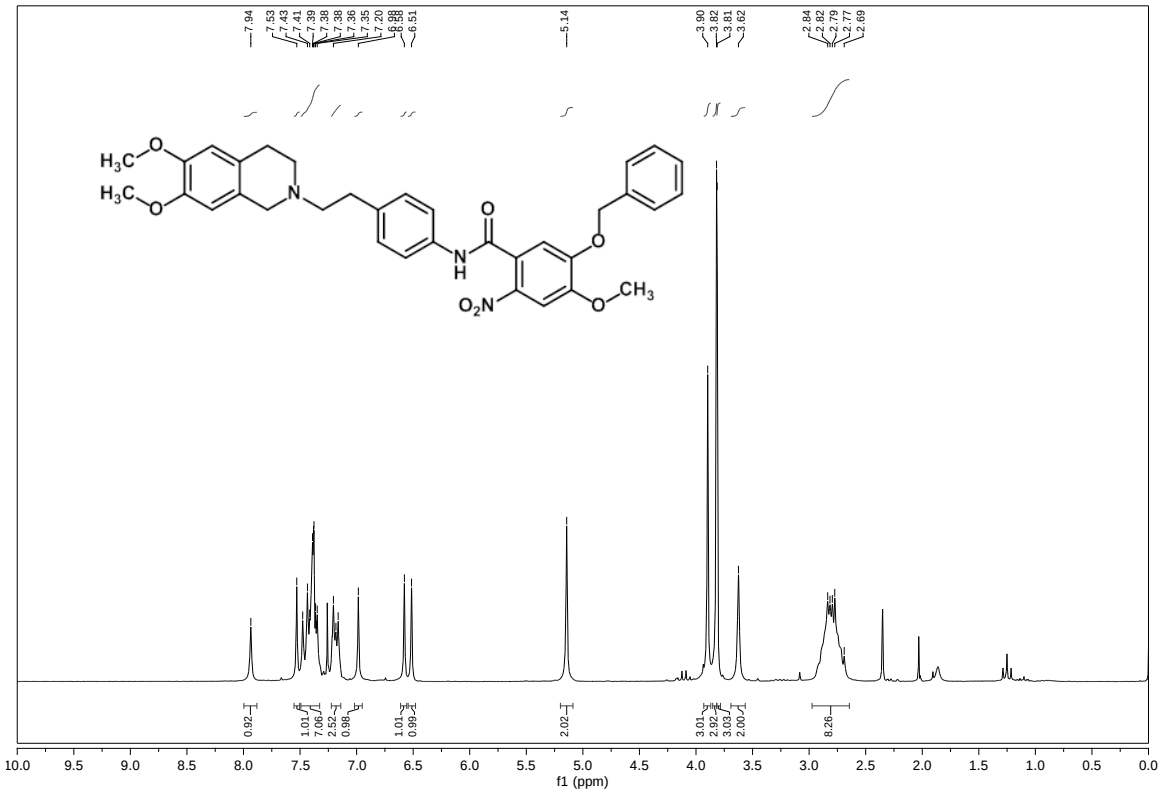

Compound **32**, ^{13}C-NMR (50 MHz, $CDCl_3$)

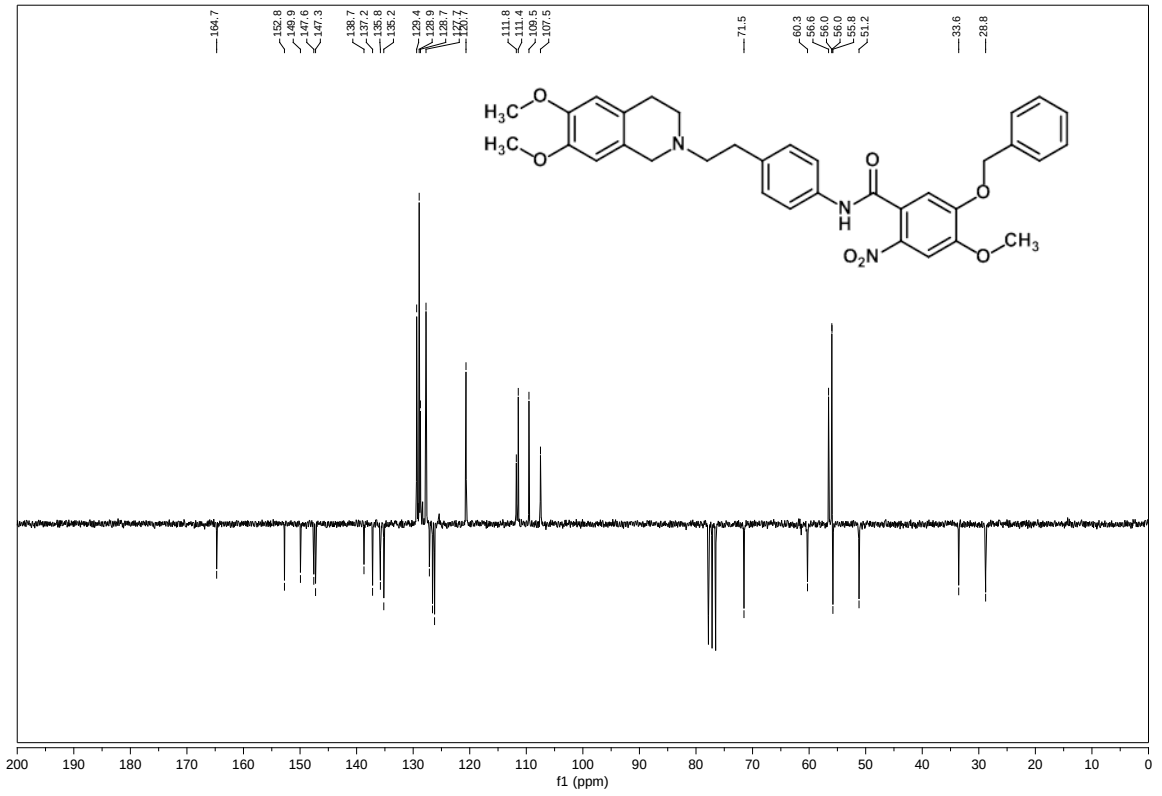

Compound **32**, mass spectrum

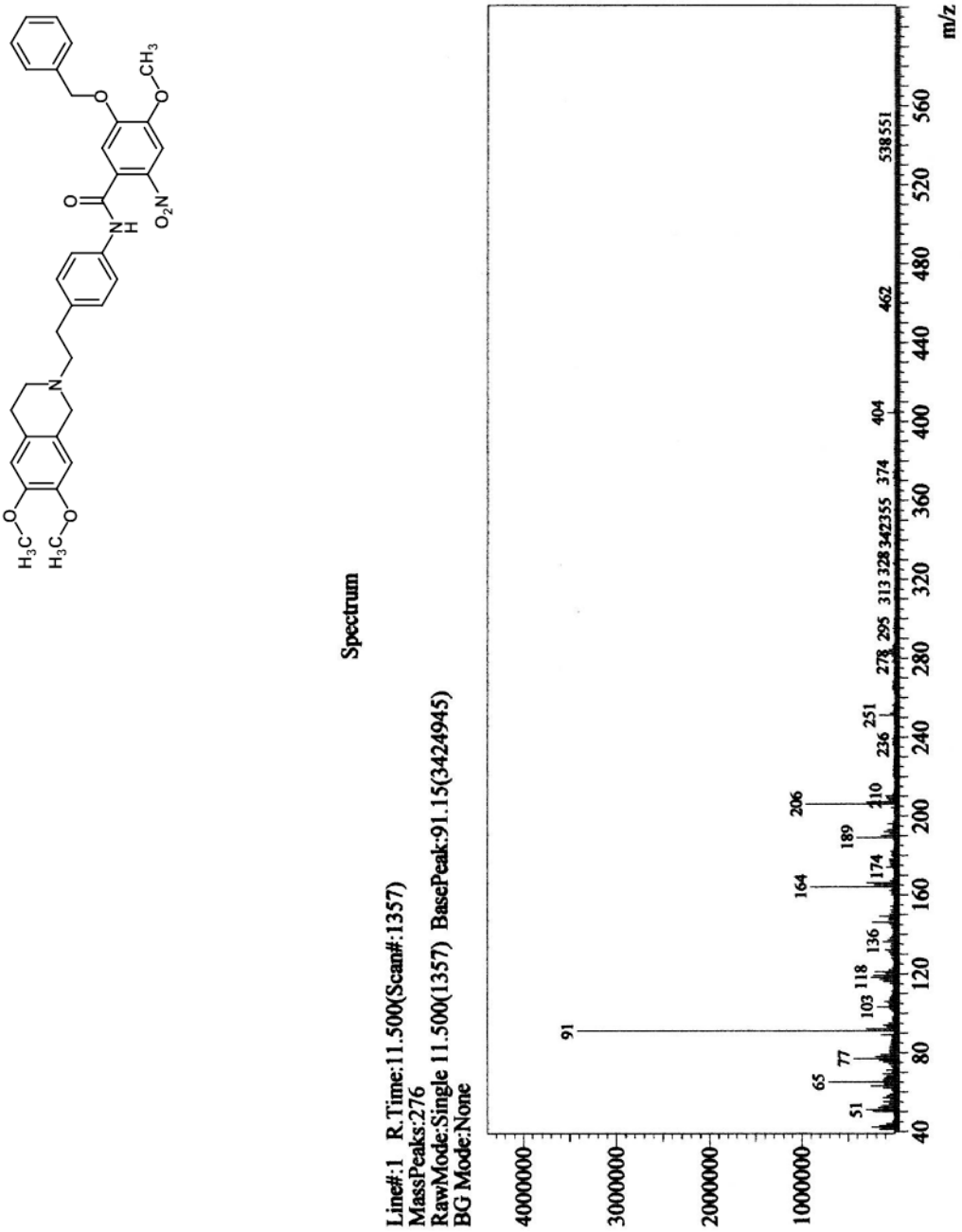

Compound **33**, ^{1}H-NMR (200 MHz, $CDCl_3$)

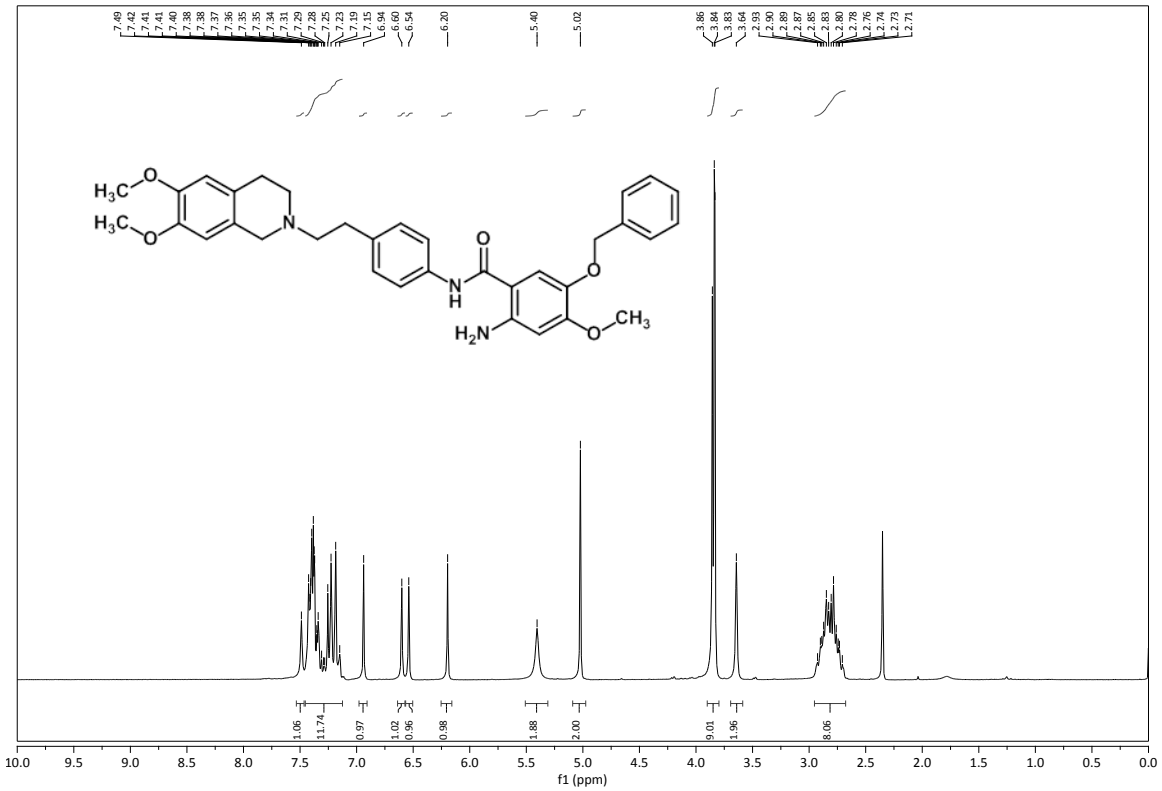

Compound **33**, ^{13}C-NMR (50 MHz, $CDCl_3$)

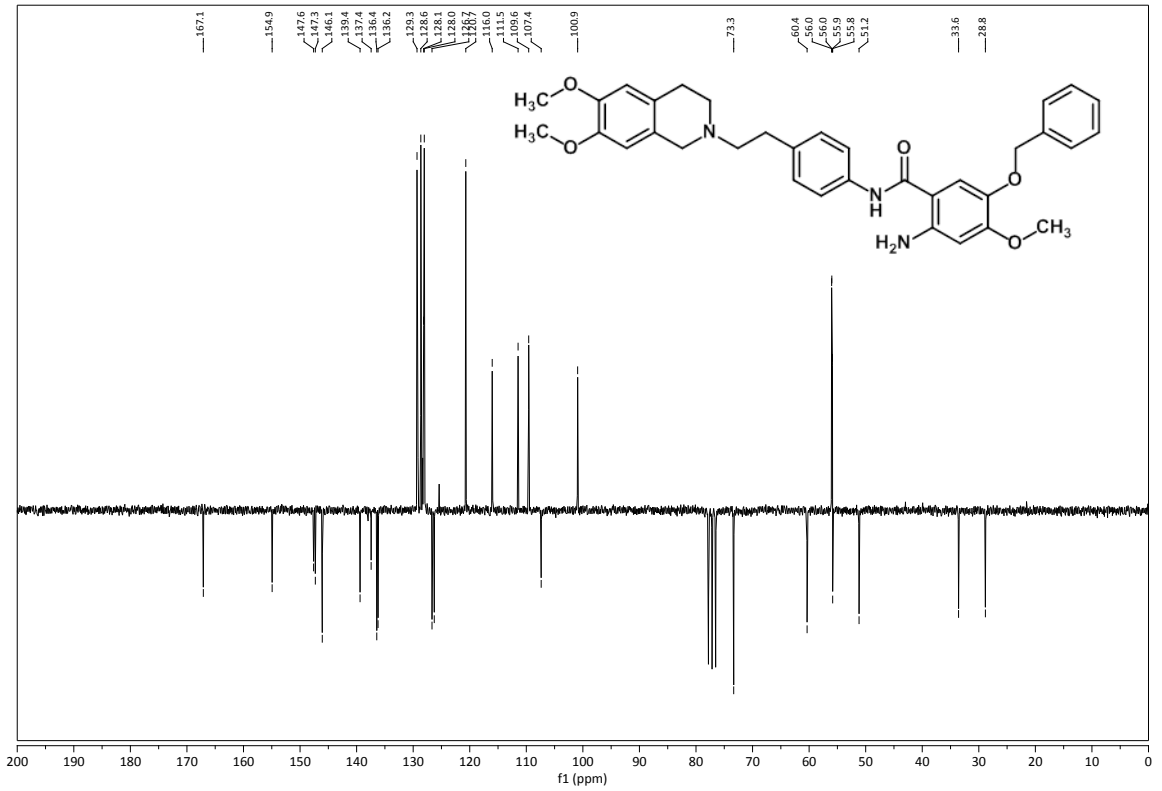

Compound **33**, mass spectrum

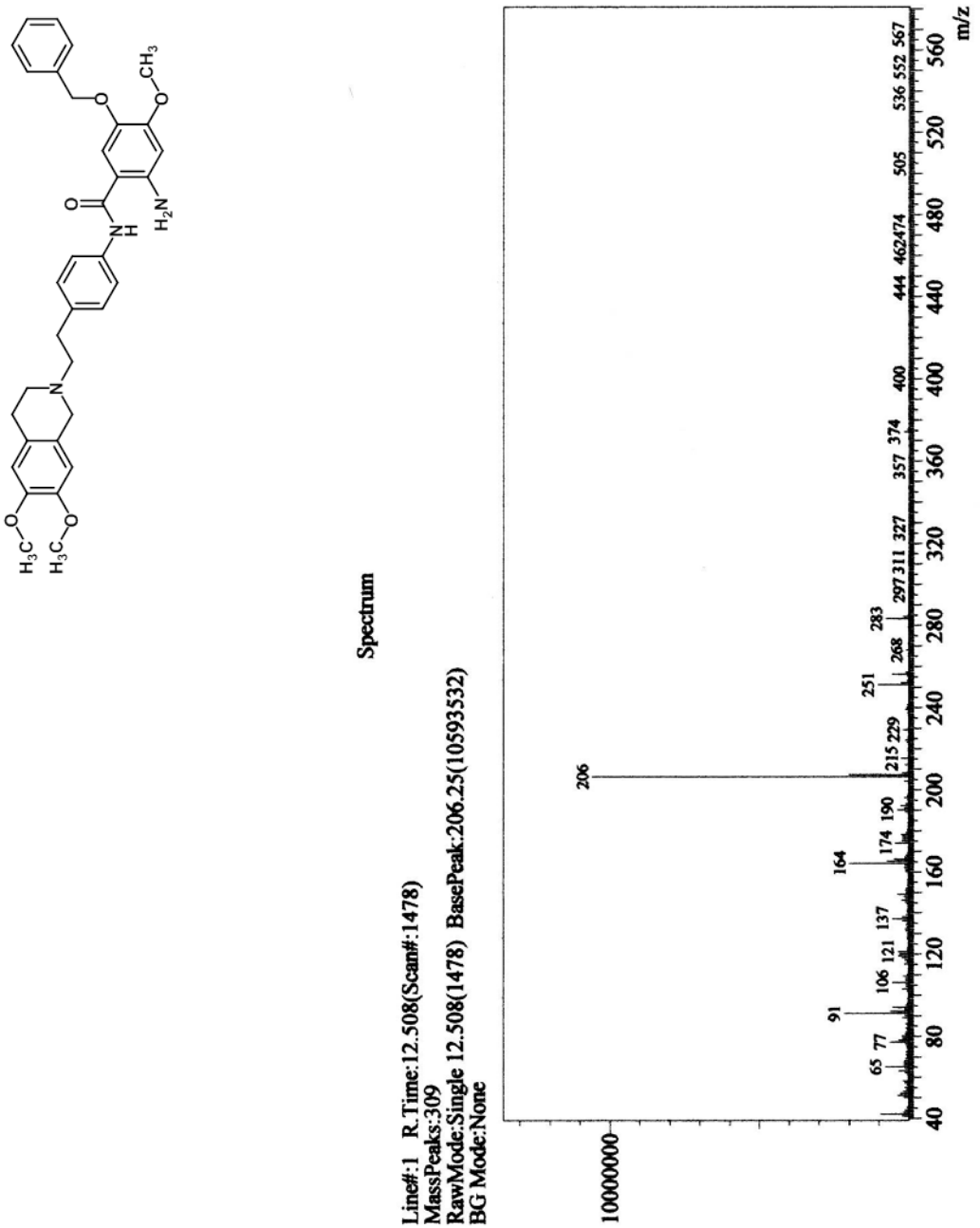

Compound **34**, ^{1}H-NMR (200 MHz, $CDCl_3$)

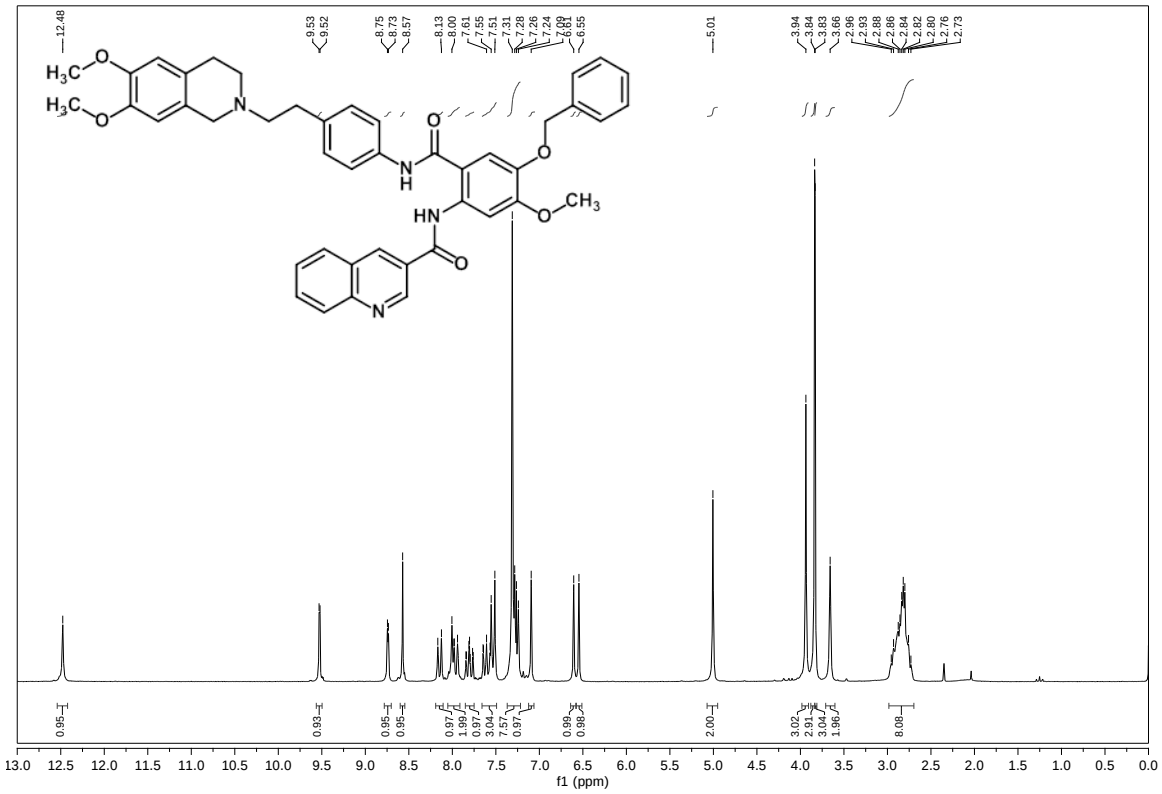

Compound **34**, ^{13}C-NMR (50 MHz, $CDCl_3$)

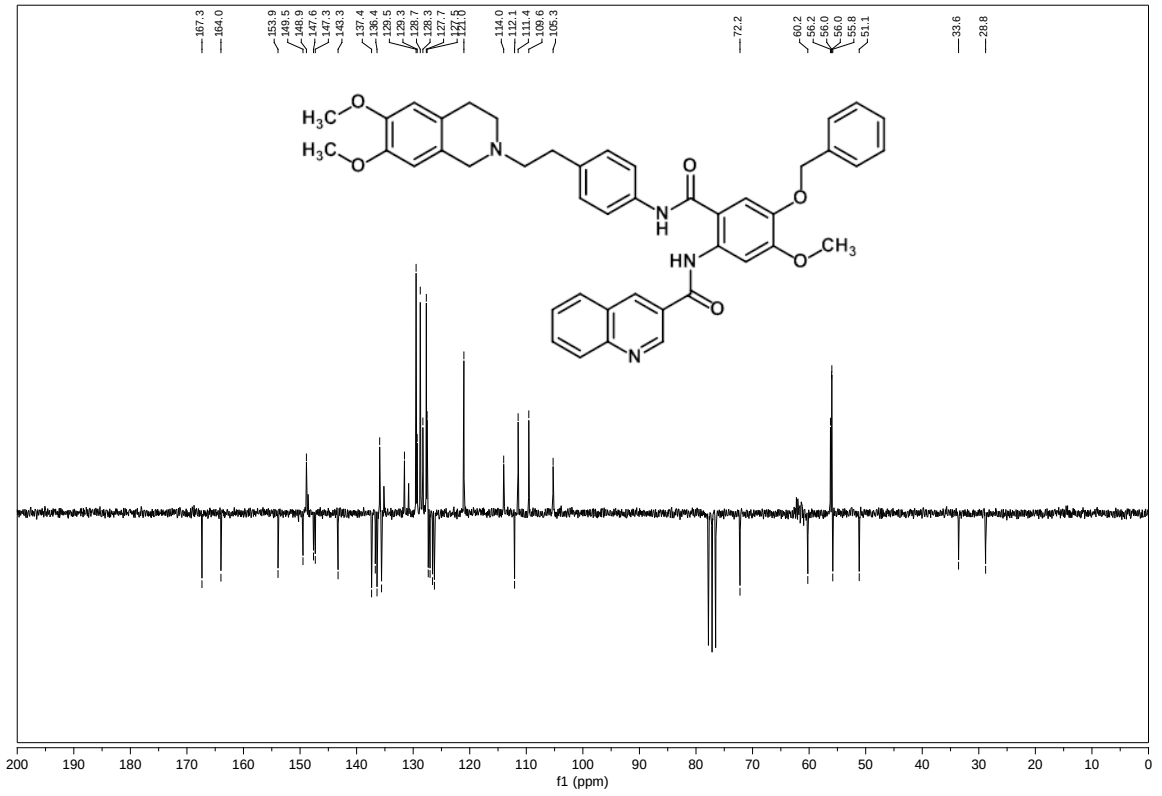

Compound **34**, mass spectrum

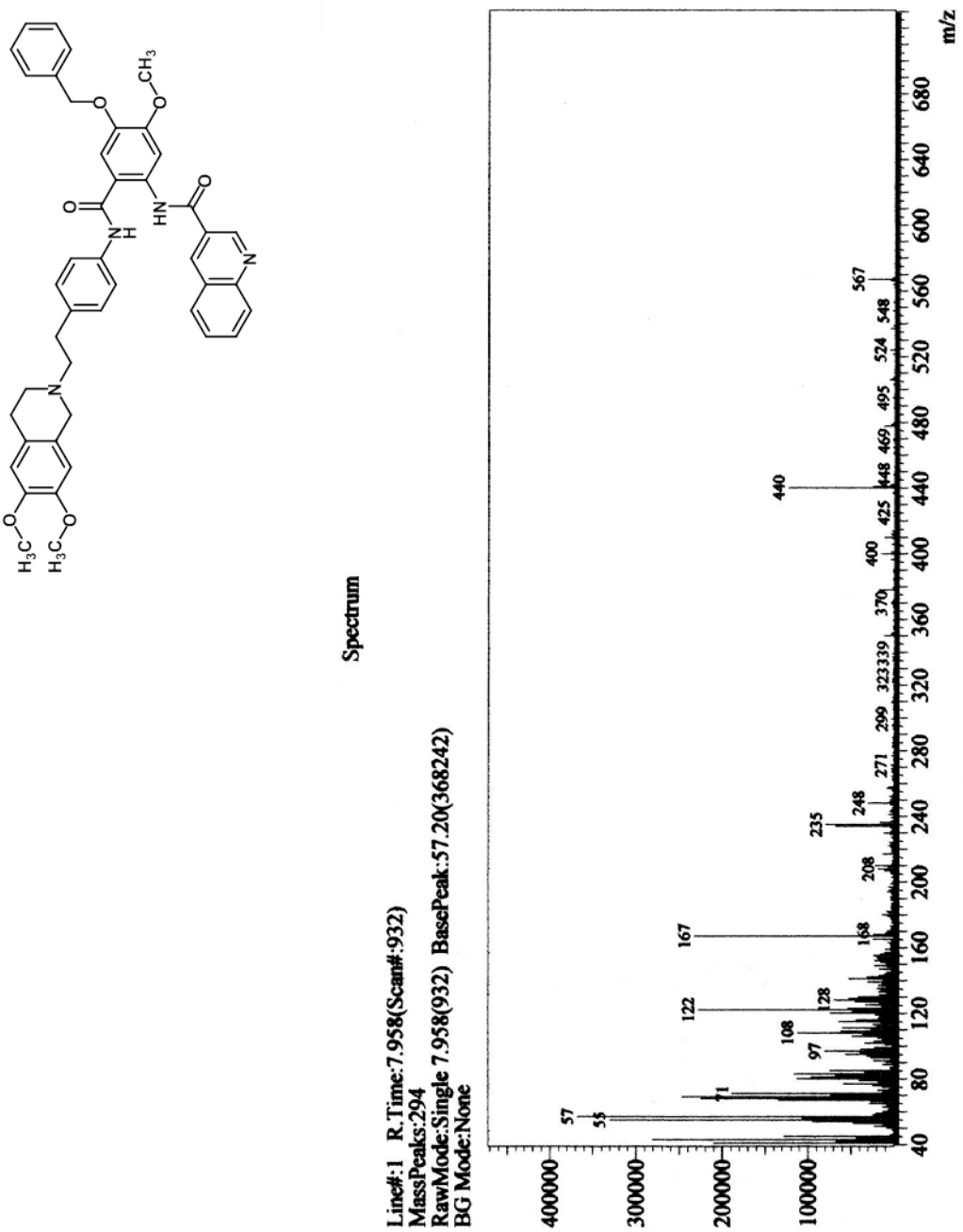

Compound **35•2 HCl**, ^{1}H-NMR (200 MHz, d_6-DMSO)

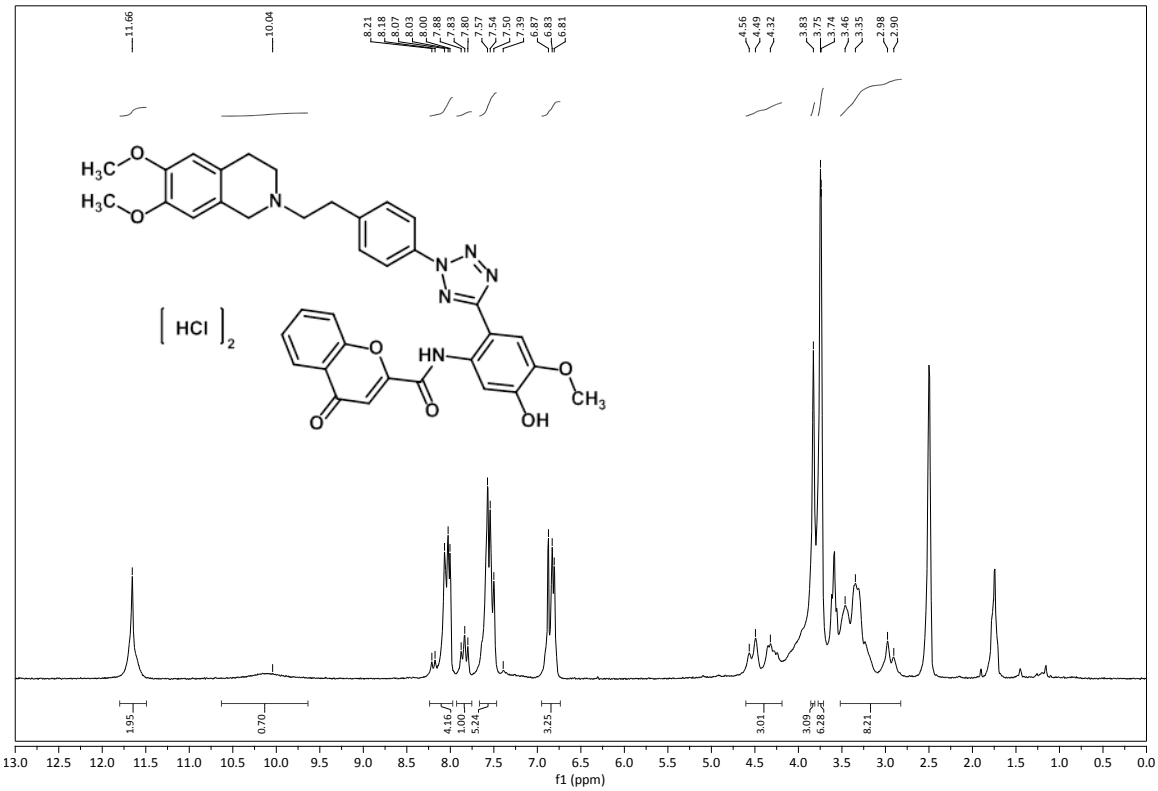

Compound **35•2 HCl**, ^{13}C-NMR (50 MHz, d_6-DMSO)

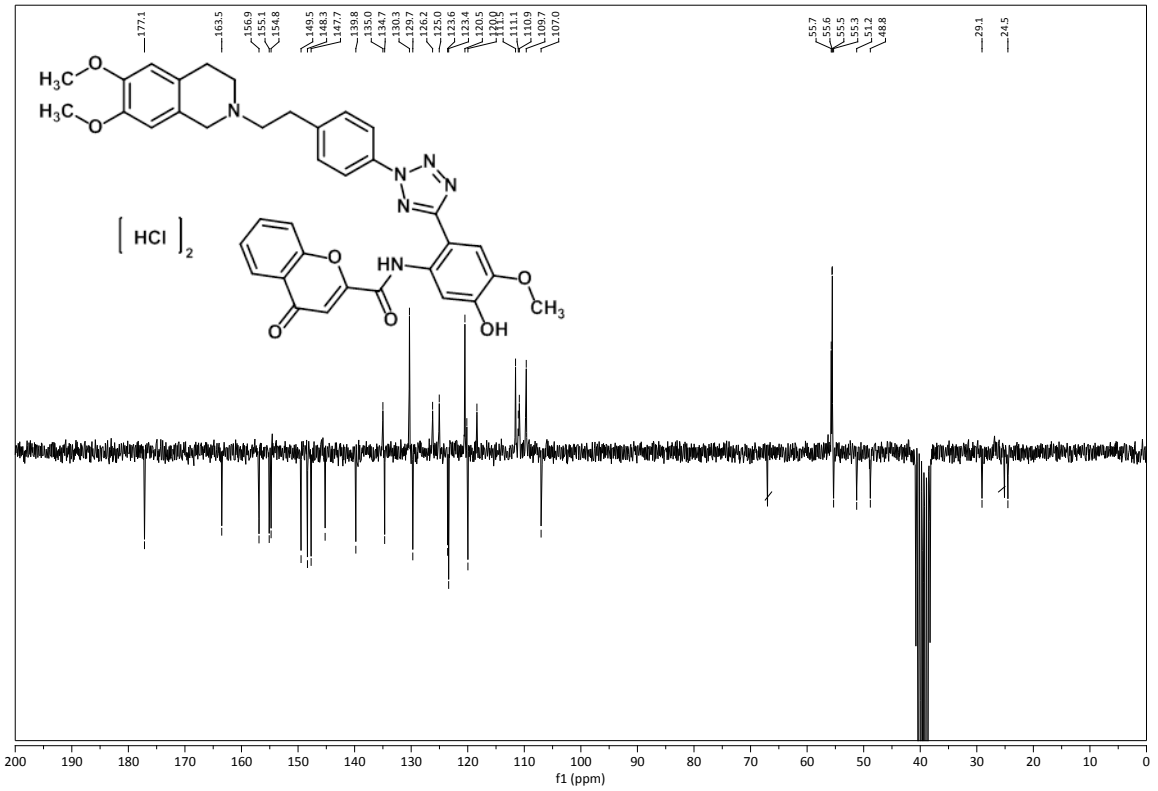

Compound **35**, mass spectrum

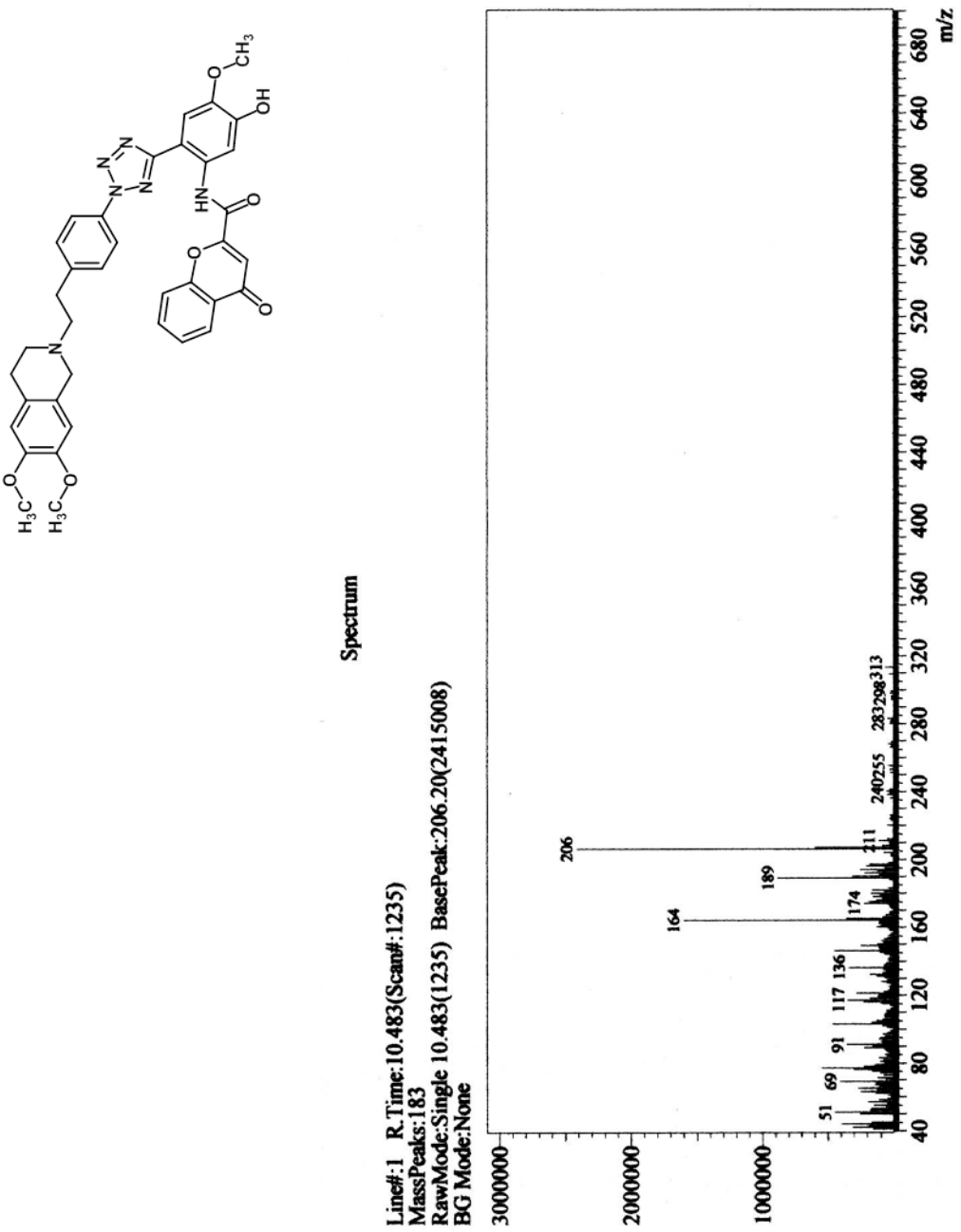

Compound **36**, ^{1}H-NMR (200 MHz, d$_6$-DMSO)

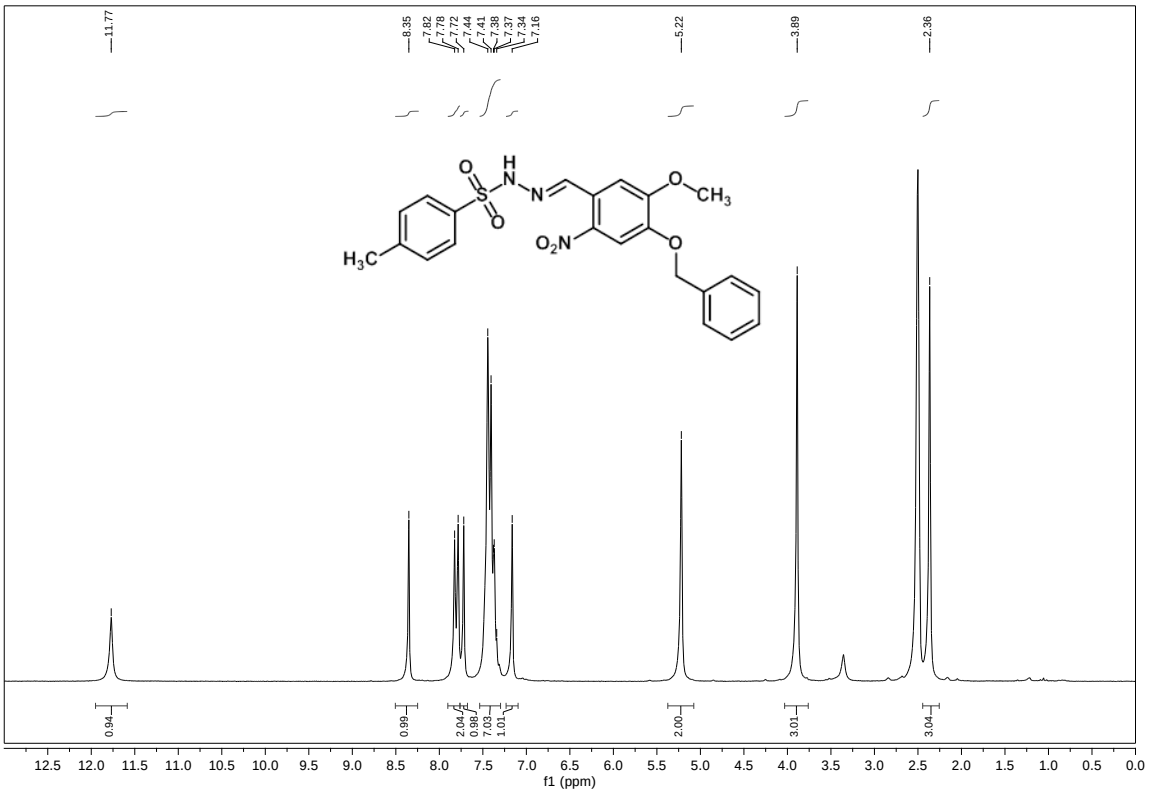

Compound **36**, ^{13}C-NMR (50 MHz, d$_6$-DMSO)

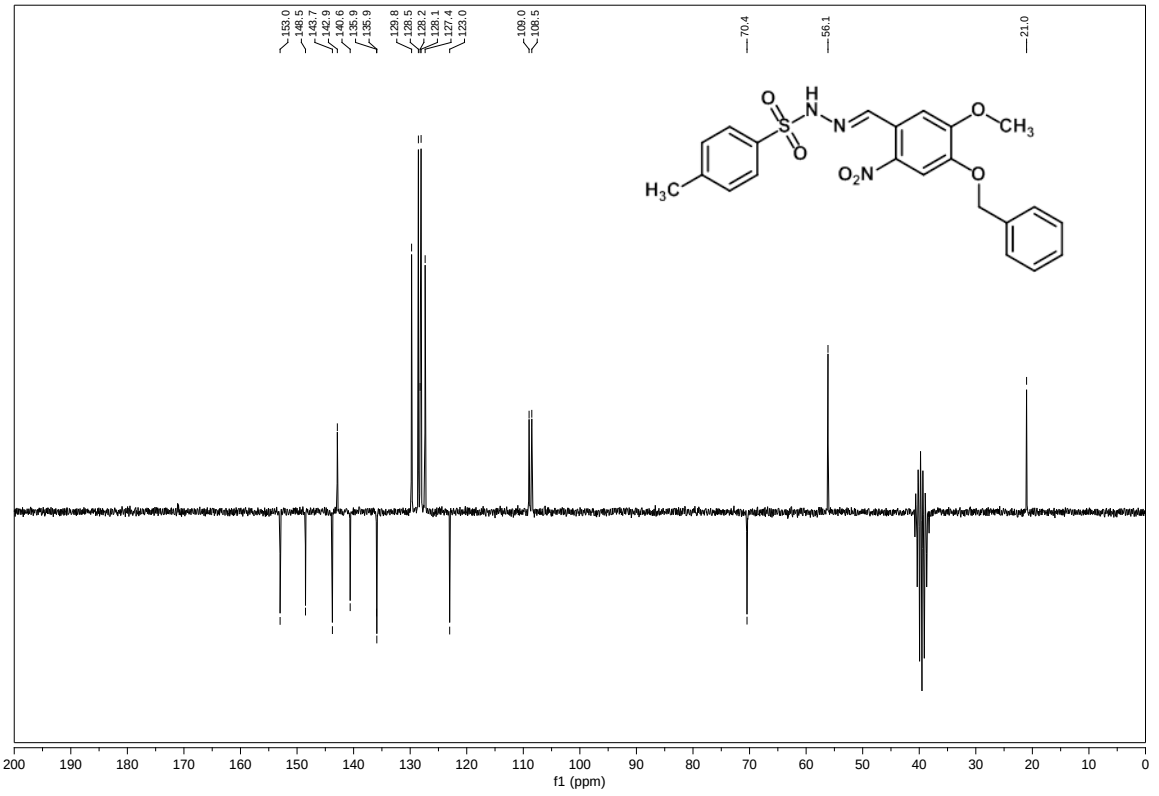

Compound **36**, mass spectrum

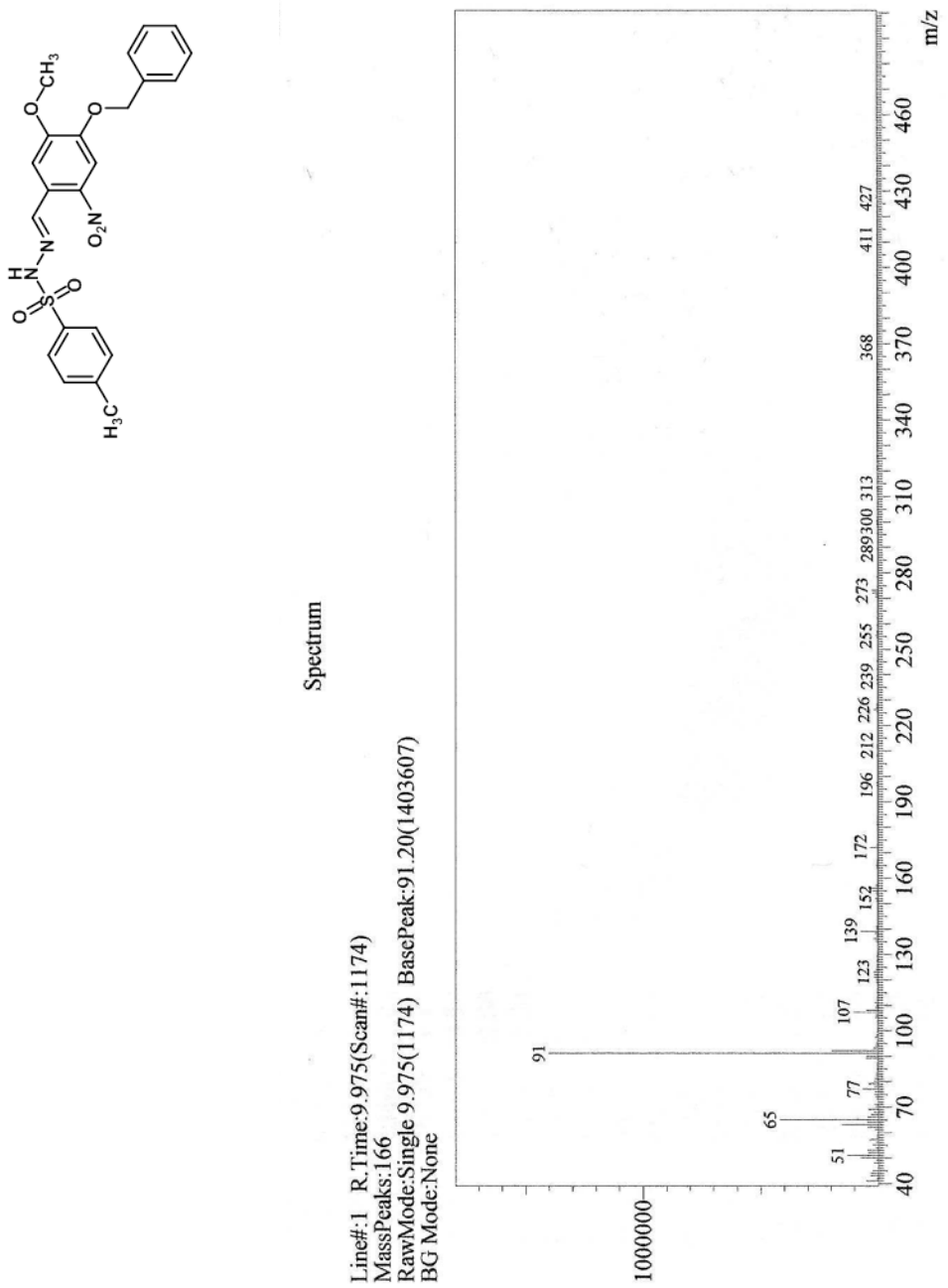

Compound **37**, ^{1}H-NMR (200 MHz, $CDCl_3$)

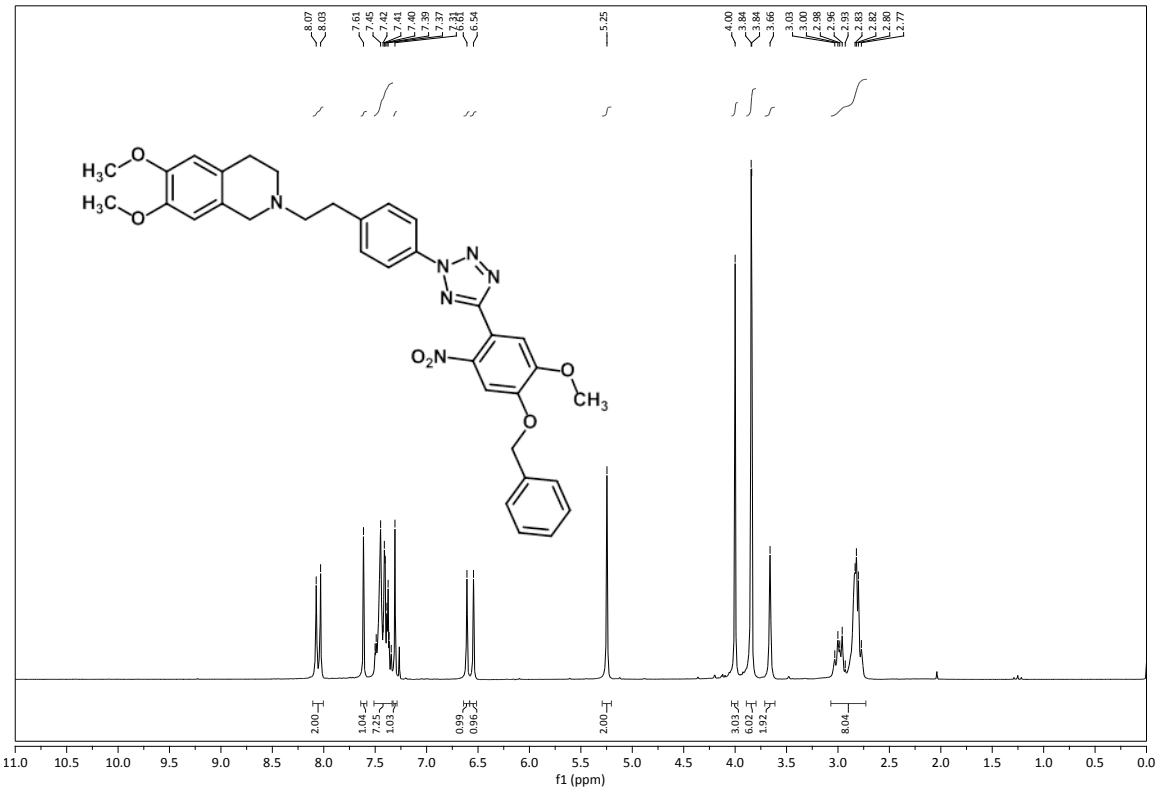

Compound **37**, ^{13}C-NMR (50 MHz, $CDCl_3$)

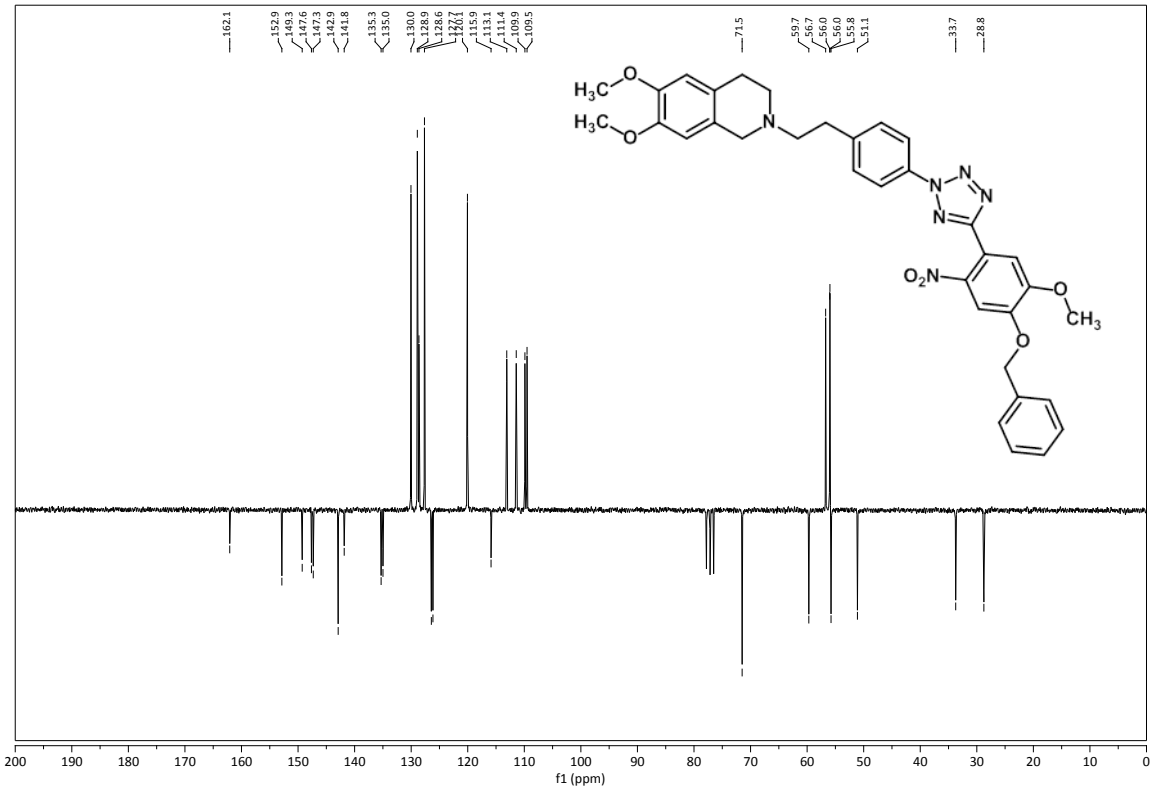

Compound **37**, mass spectrum

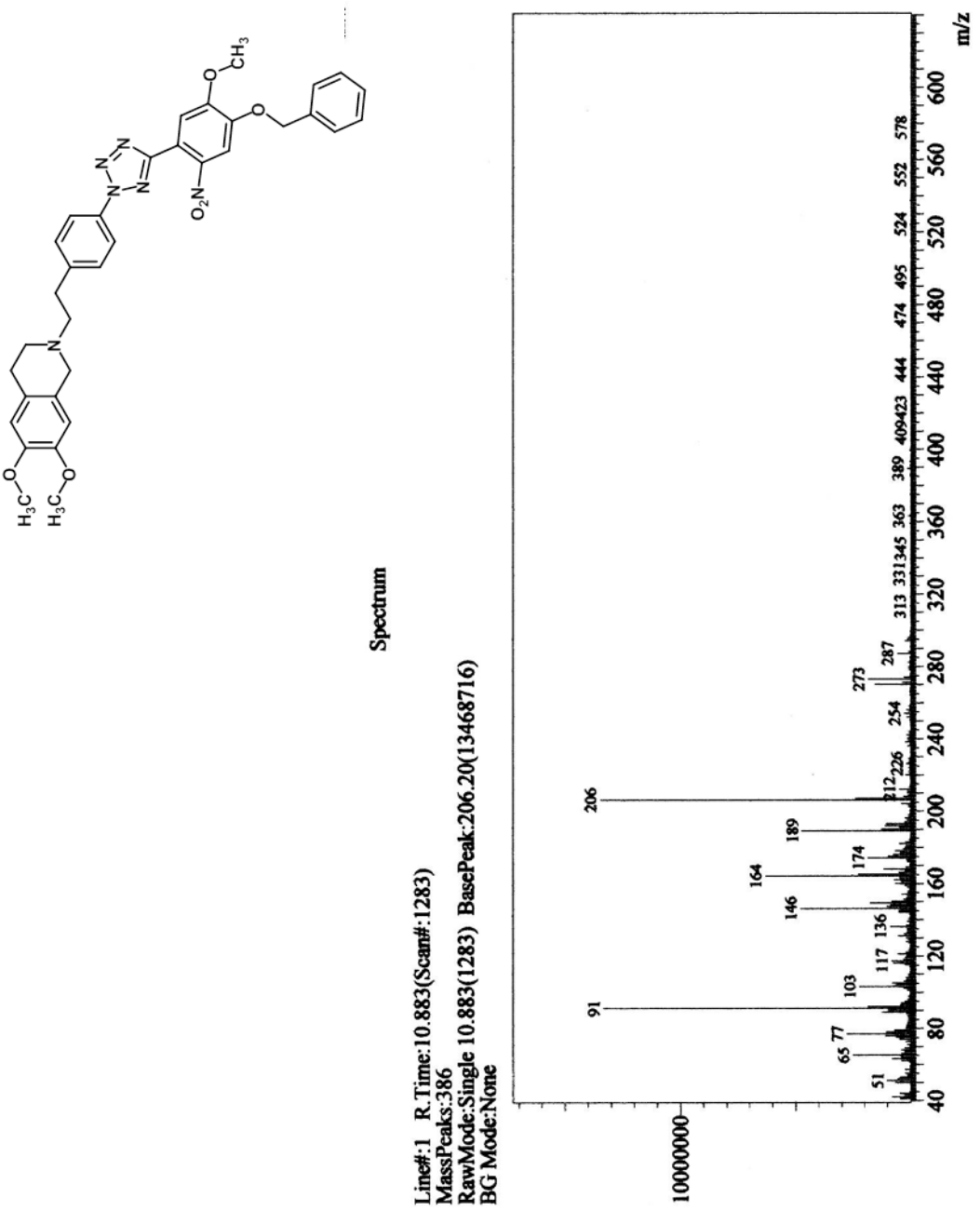

Compound **38**, ^{1}H-NMR (200 MHz, $CDCl_3$)

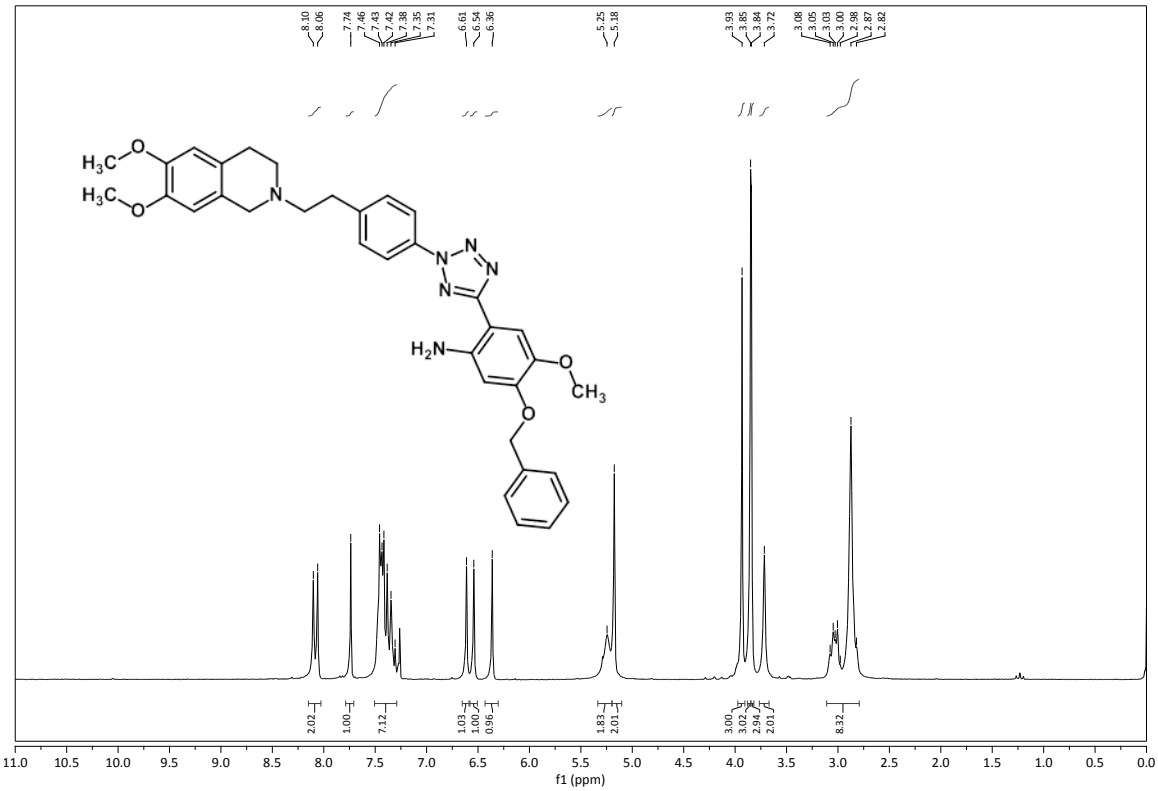

Compound **38**, ^{13}C-NMR (50 MHz, $CDCl_3$)

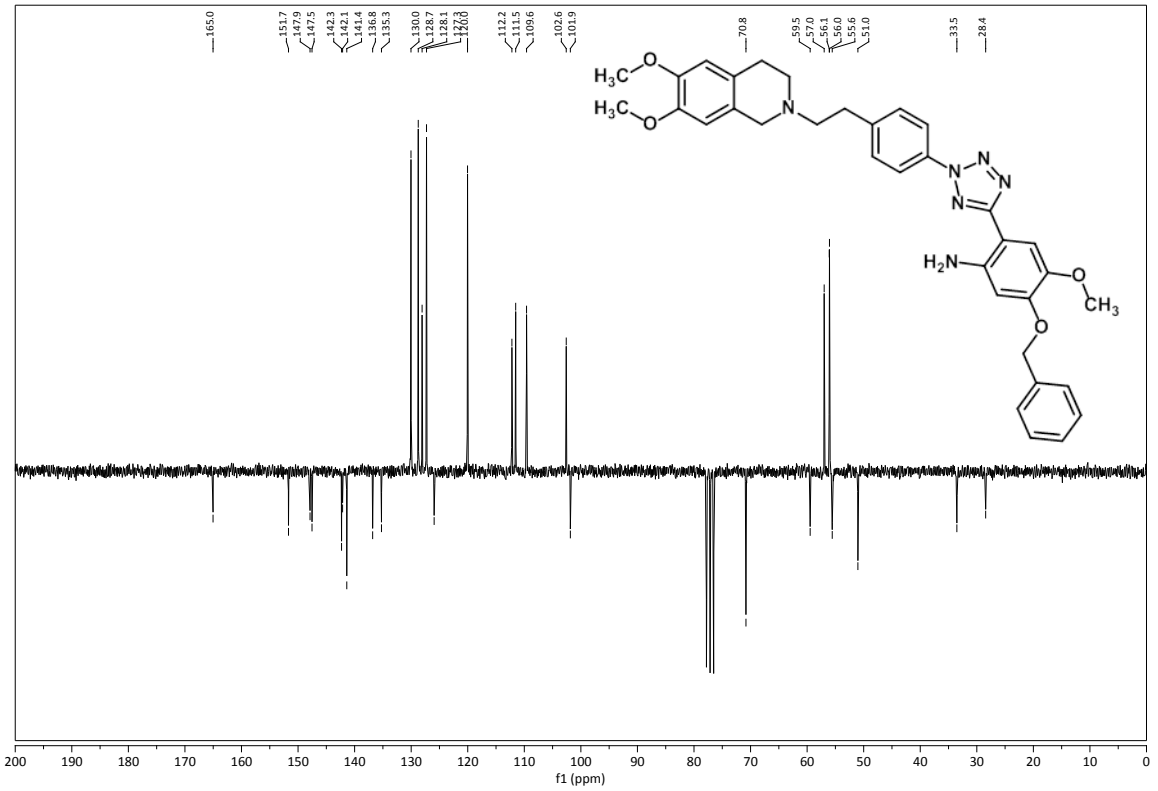

Compound **38**, mass spectrum

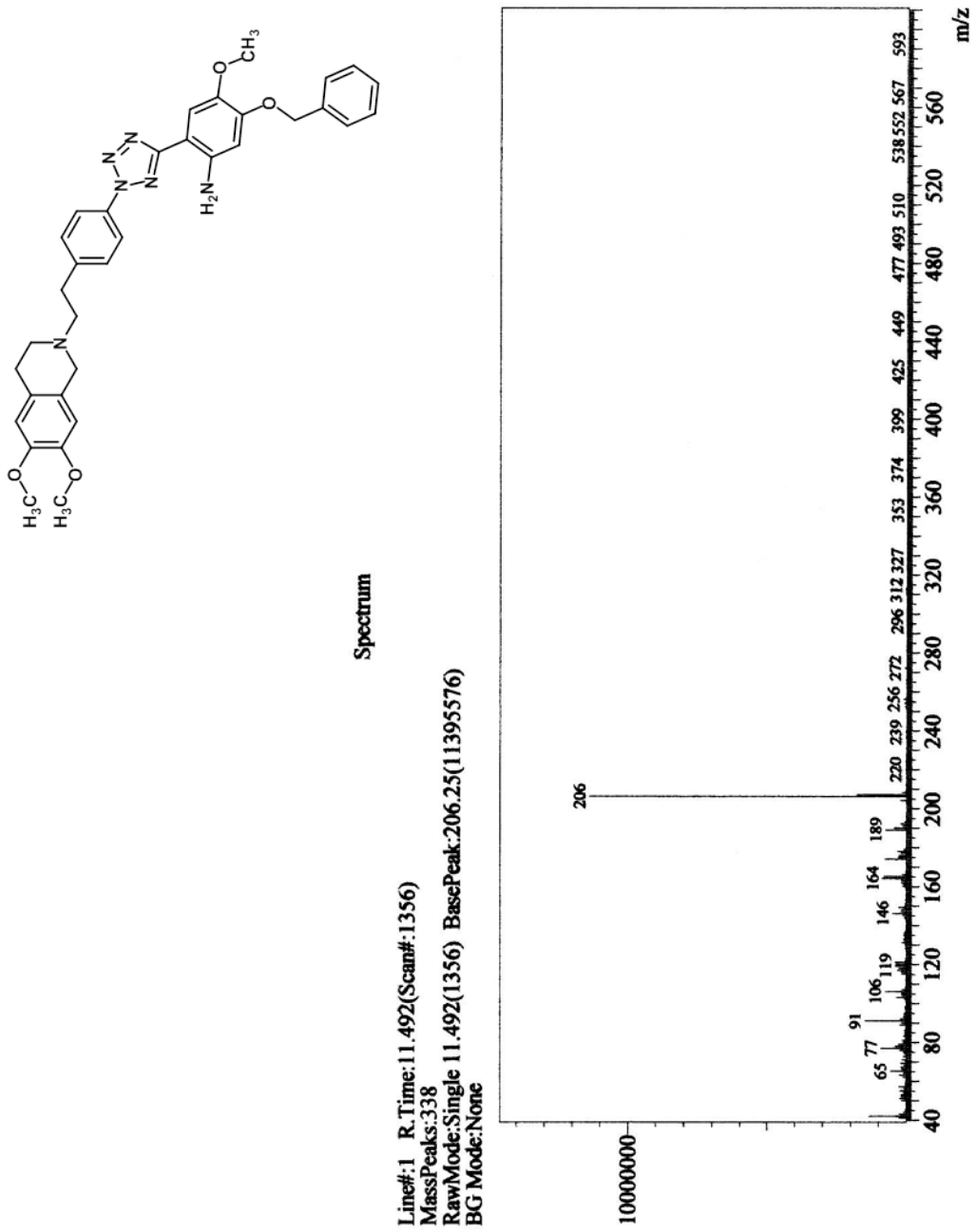

Compound **39**, ^{1}H-NMR (200 MHz, $CDCl_3$)

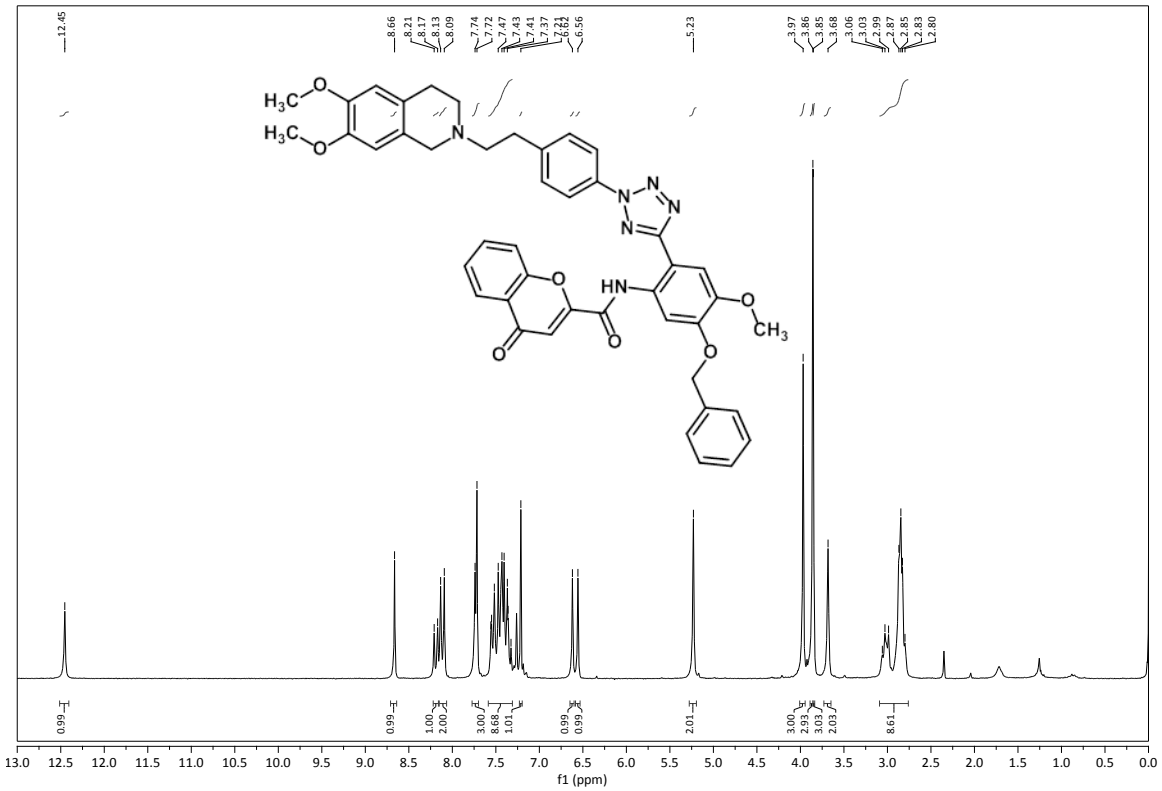

Compound **39**, ^{13}C-NMR (50 MHz, $CDCl_3$)

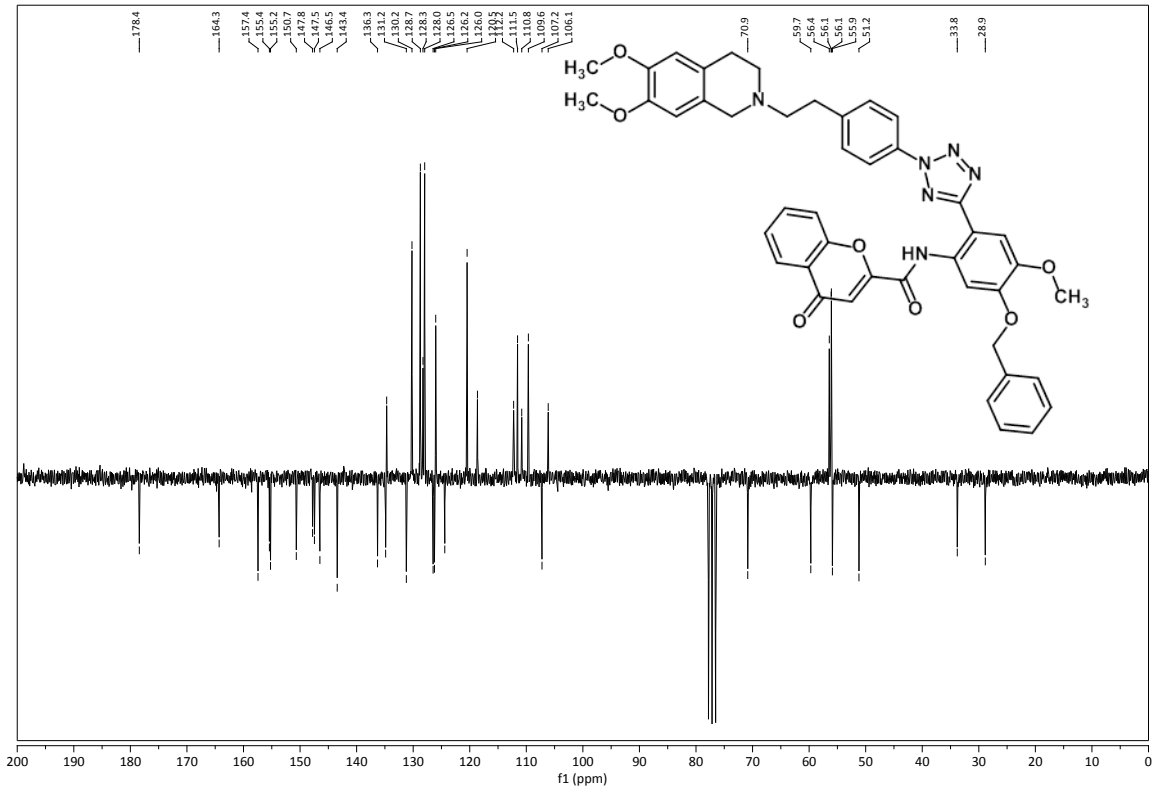

Compound **39**, mass spectrum

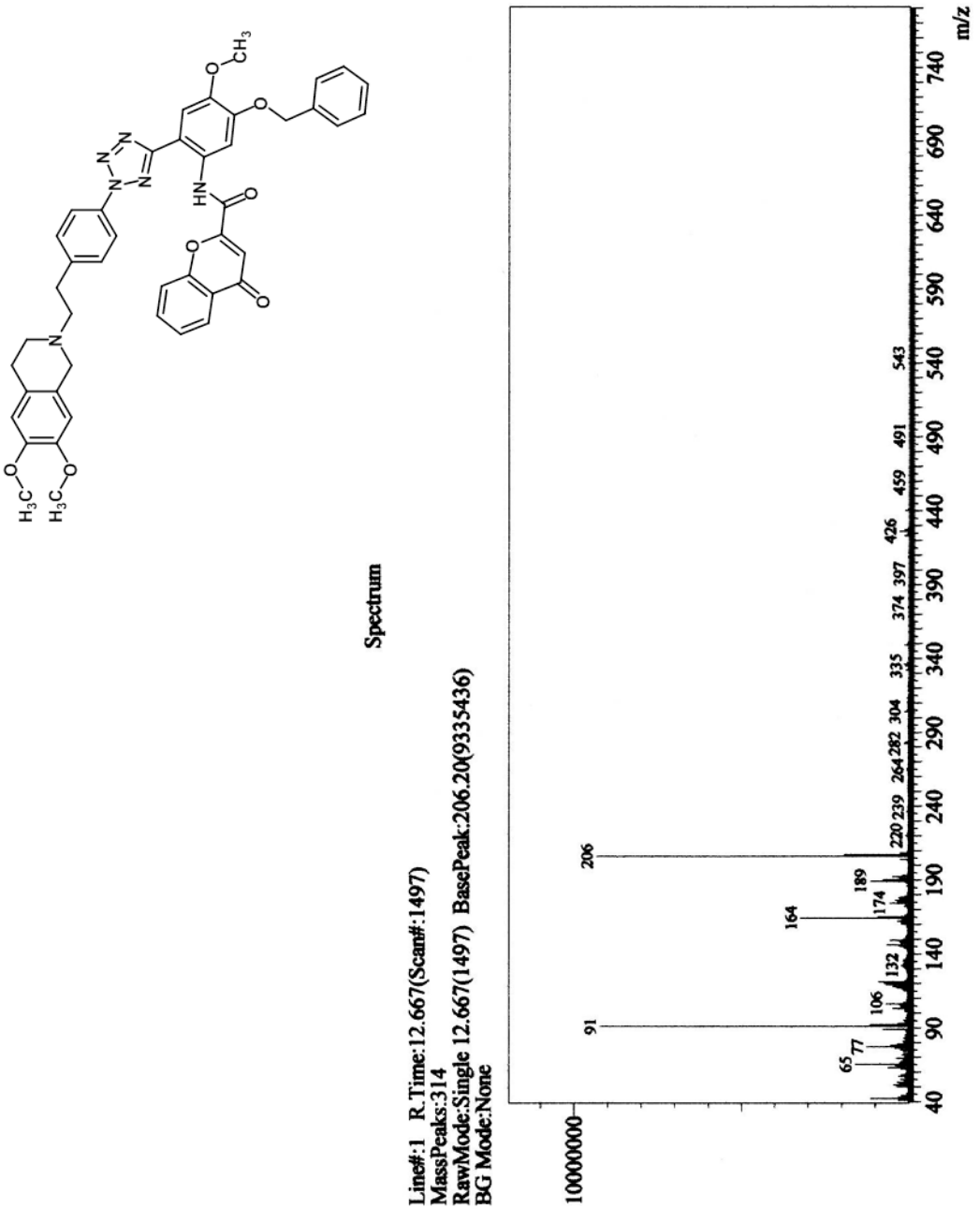

Compound **40**, ^{1}H-NMR (200 MHz, d$_6$-DMSO)

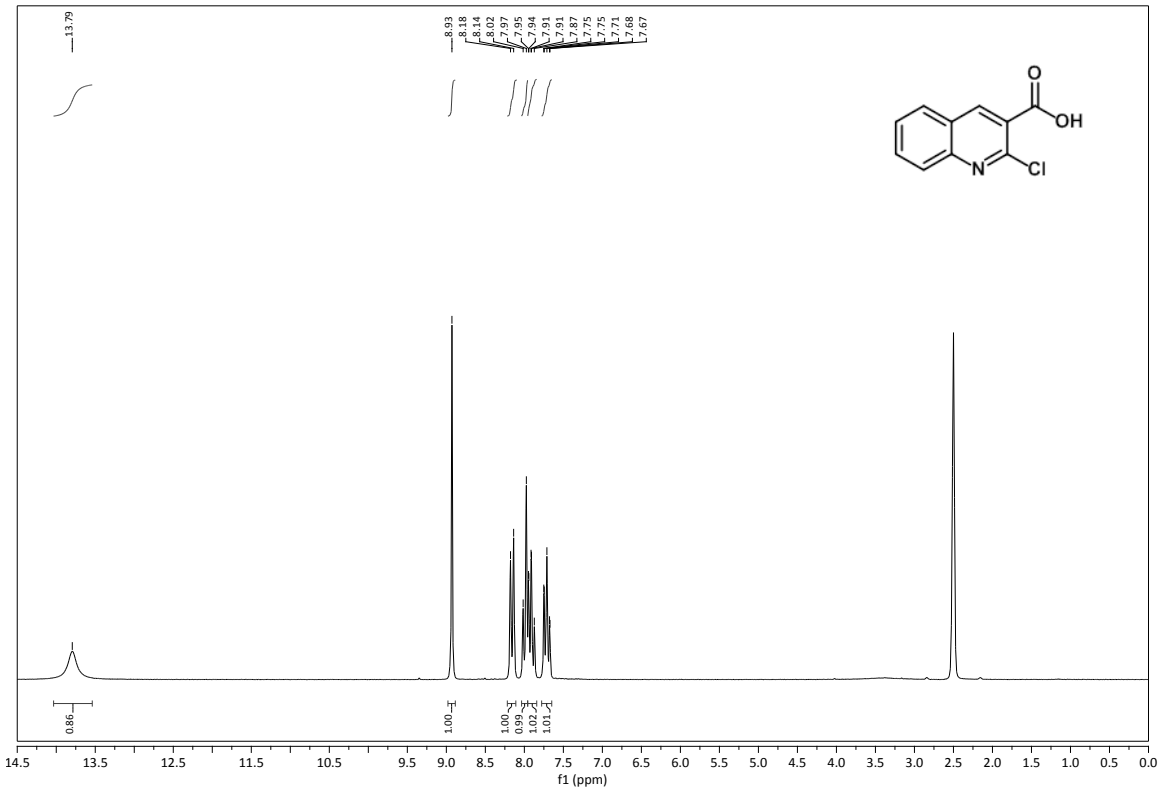

Compound **40**, ^{13}C-NMR (50 MHz, d$_6$-DMSO)

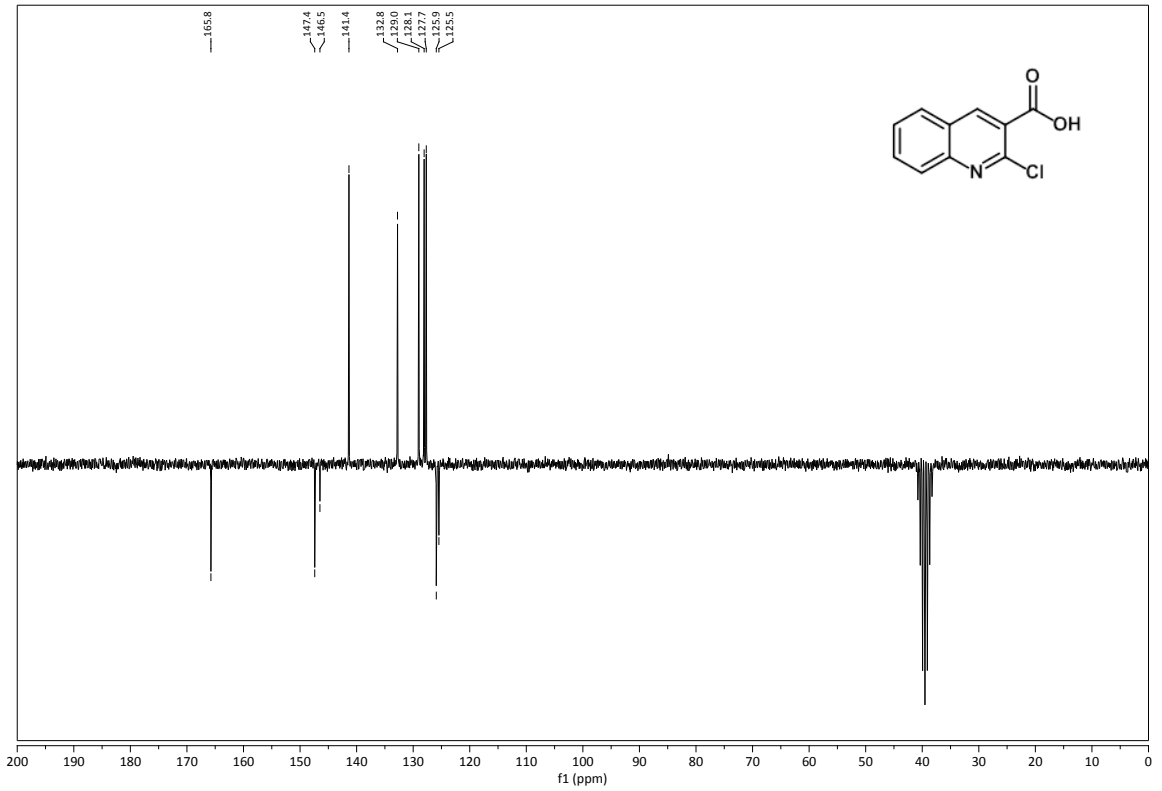

Compound **41**, ^{1}H-NMR (200 MHz, $CDCl_3$)

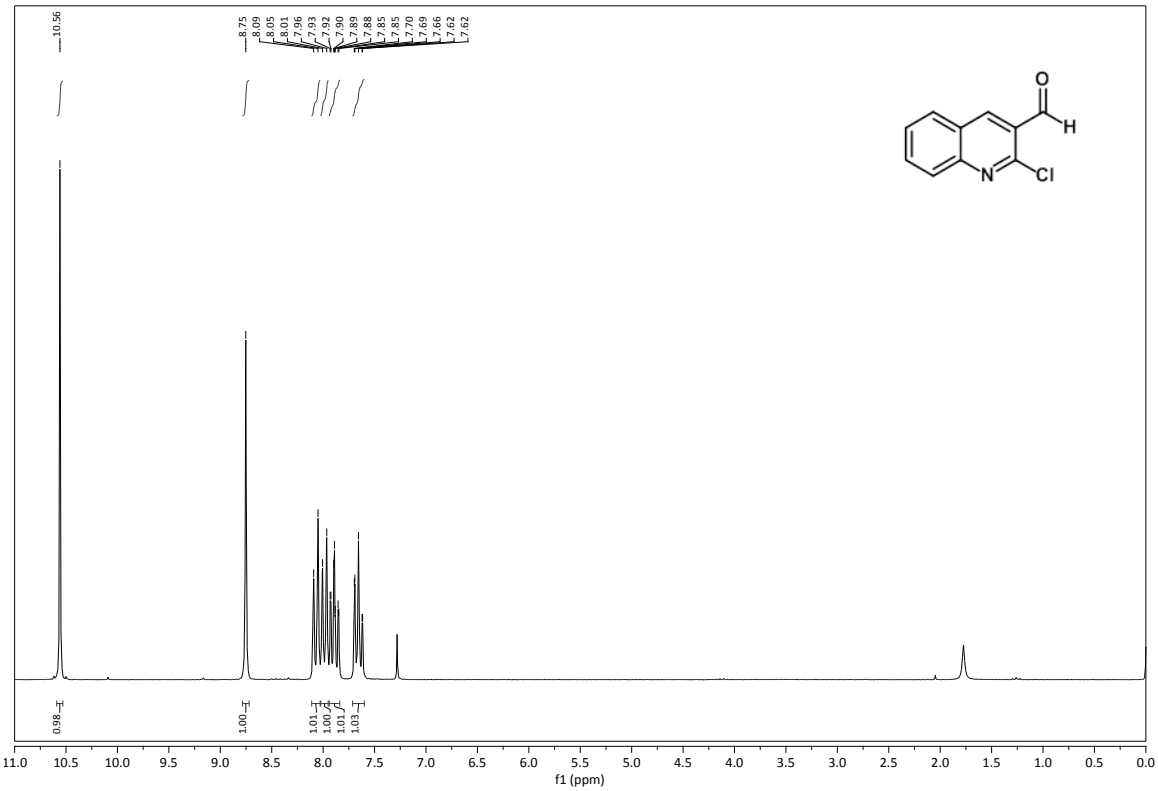

Compound **41**, ^{13}C-NMR (50 MHz, $CDCl_3$)

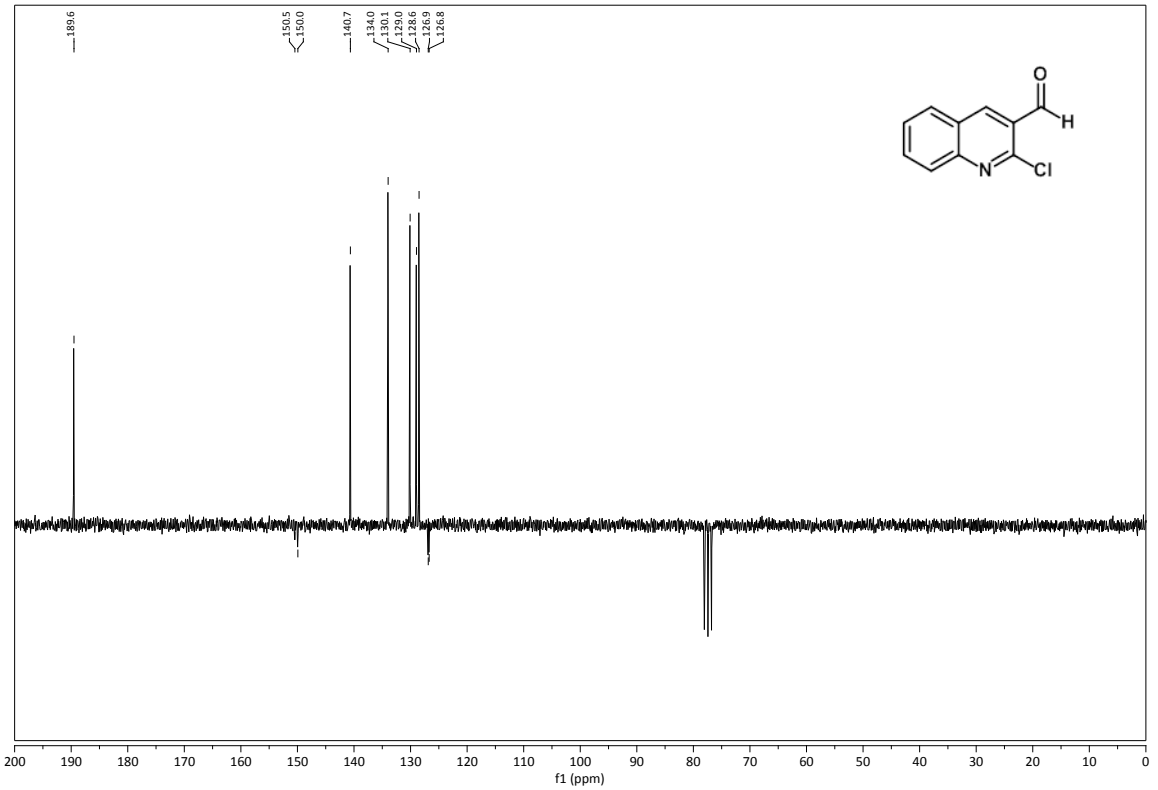

Compound **42**, ^{1}H-NMR (200 MHz, $CDCl_3$)

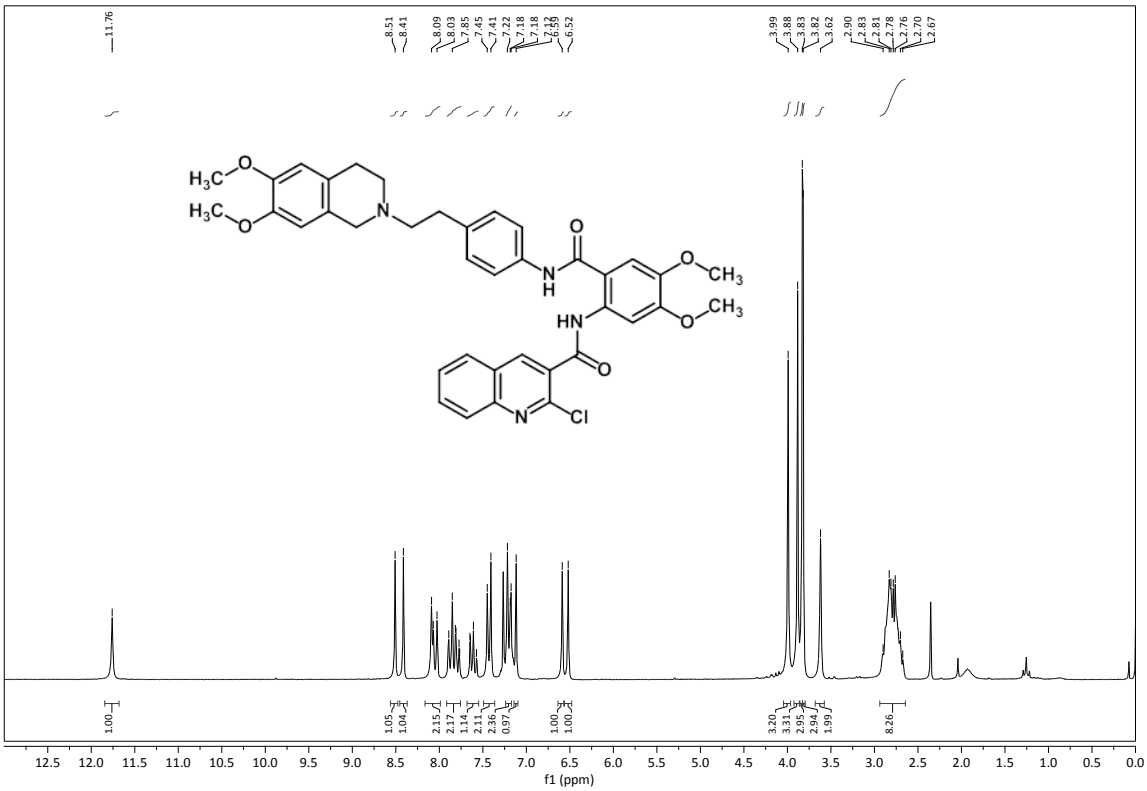

Compound **42**, ^{13}C-NMR (50 MHz, $CDCl_3$)

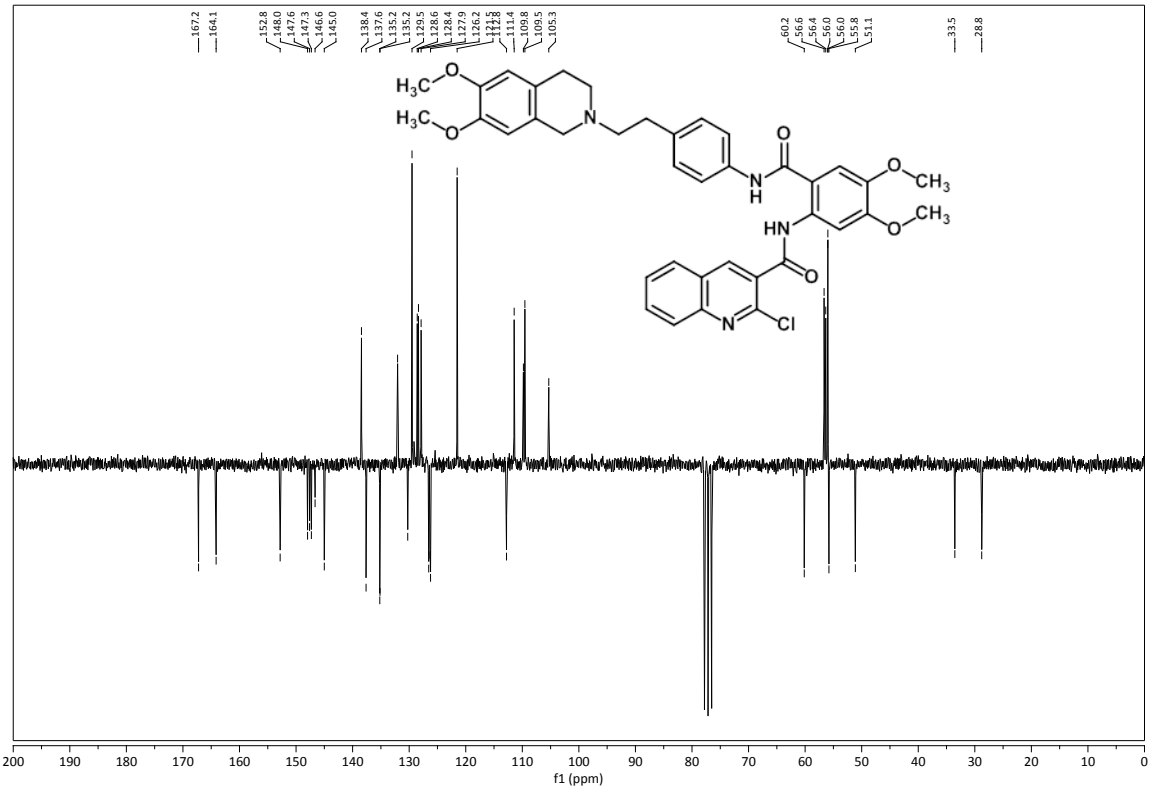

Compound **42**, mass spectrum

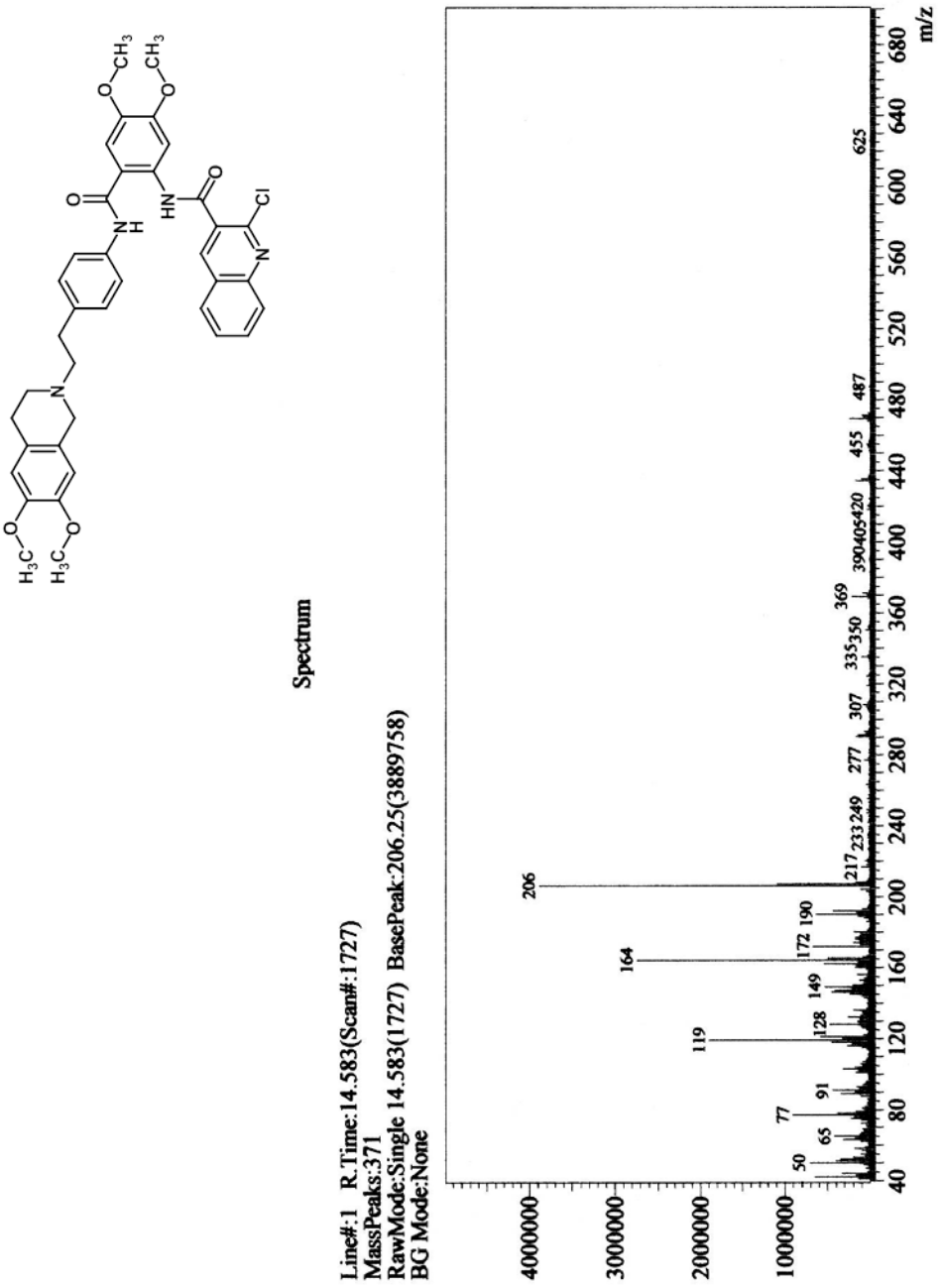

Compound **43**, ^{1}H-NMR (200 MHz, d$_6$-DMSO)

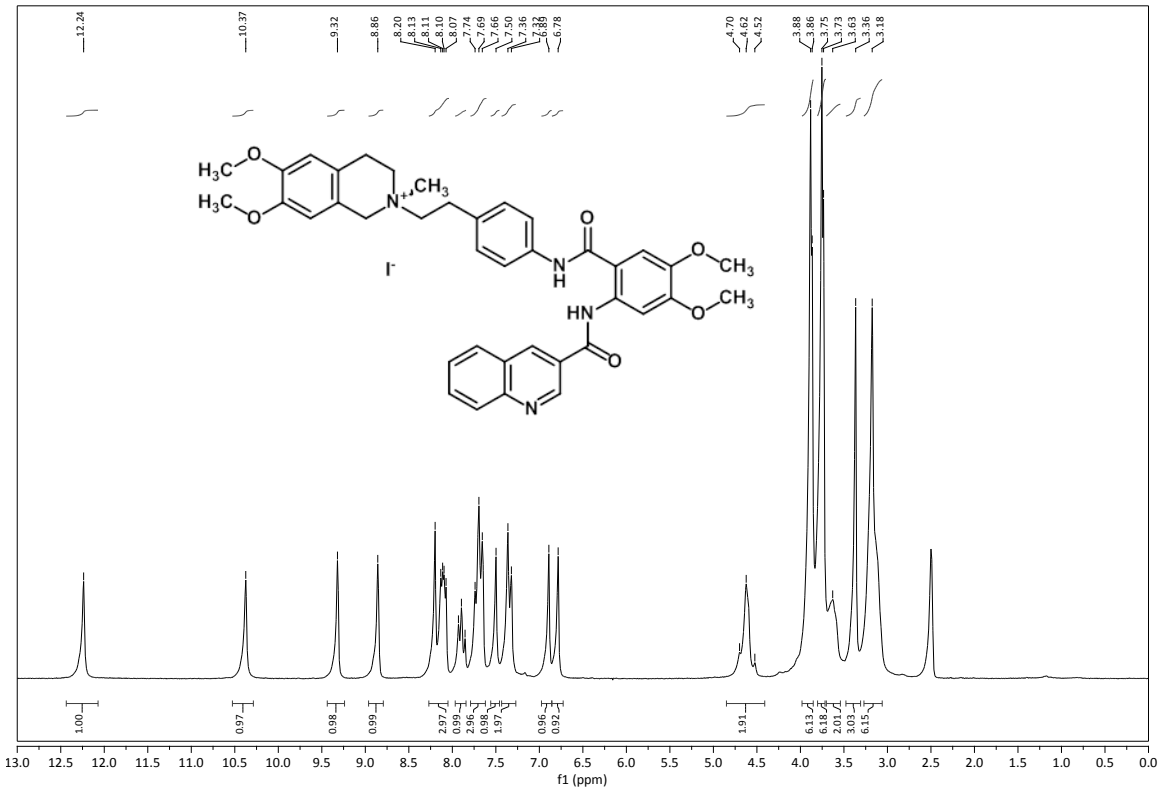

Compound **43**, ^{13}C-NMR (50 MHz, d$_6$-DMSO)

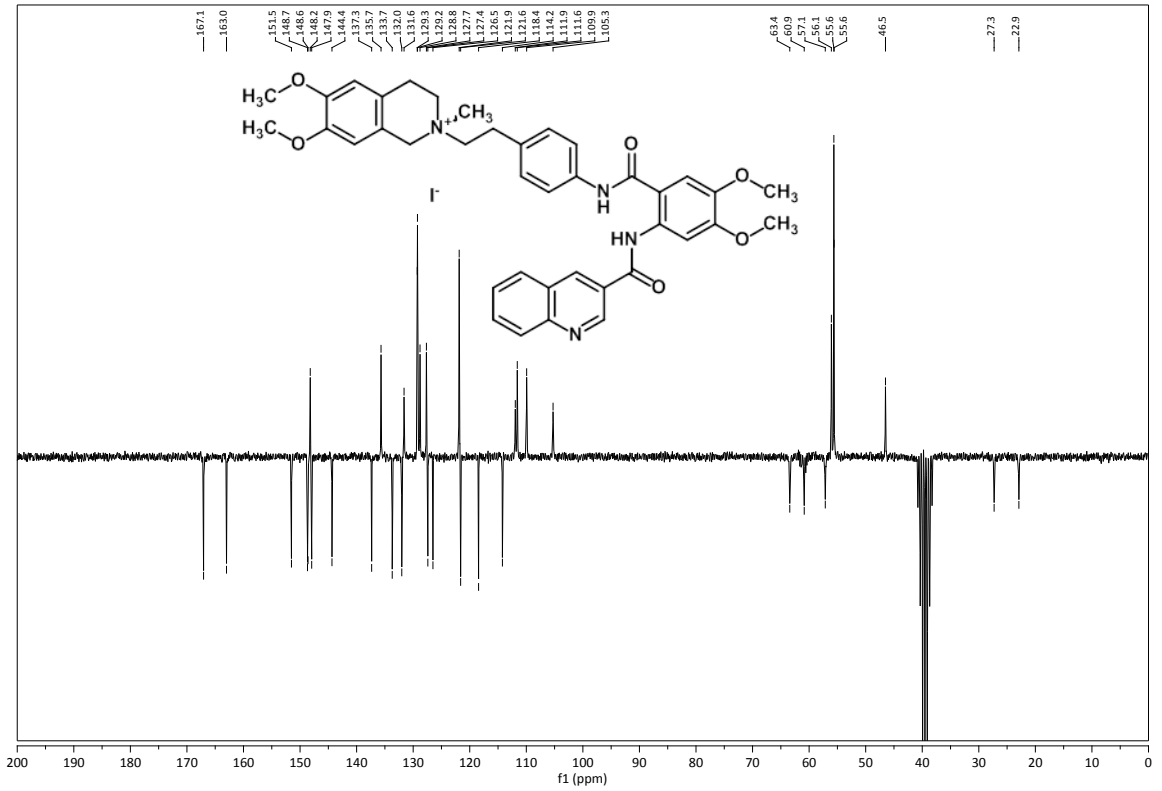

Compound **43**, mass spectrum

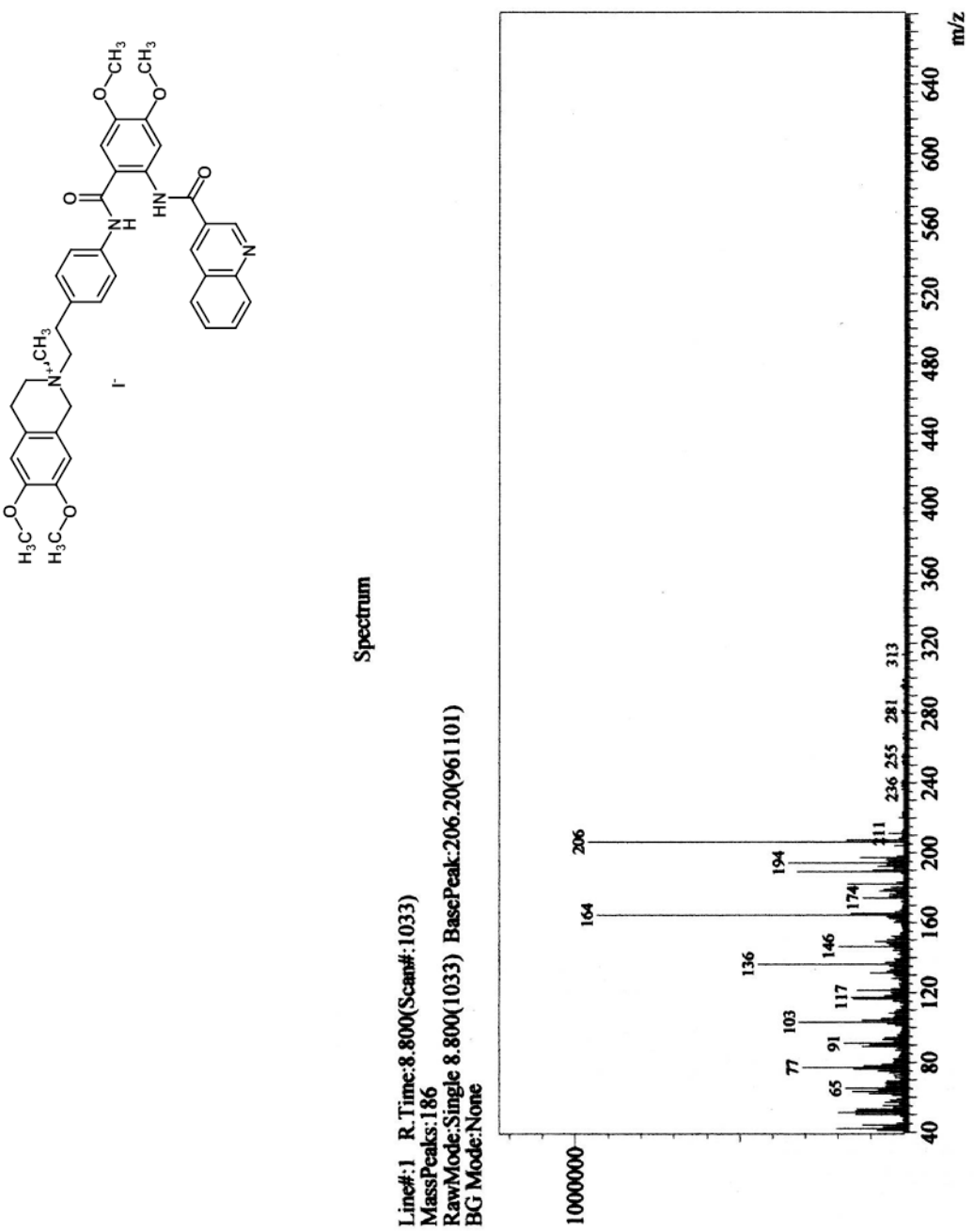

XI Curriculum Vitae

Name: Florian Bauer

Date of Birth: July 28th 1984 in Scheibbs, Austria

Nationality: Austria

Education:

2008 – 2014: Doctoral studies of natural sciences at the University of Vienna, Austria

Thesis: "Synthesis and Bioevaluation of Novel PET Tracers for the Imaging of P-glycoprotein", supervised by Ao. Univ.-Prof. Dr. Thomas Erker and Priv.-Doz. Mag. Dr. Oliver Langer

2003 – 2007: University of Applied Sciences for Biotechnology with specialisation in chemistry of active substances, FH-Campus Wien, Vienna, Austria

Thesis: "Strukturoptimierung von Diarylverbindungen in Bezug auf Wachstums-hemmung und Apoptoseinduktion in Kolonkarzinomzellen", supervised by Ao. Univ.-Prof. Dr. Thomas Erker and Univ.-Prof. Dr. Verena M. Dirsch

1994 – 2002: Stiftsymnasium Melk, Final Examination: June 2002

Experience:

since 2008: External Lecturer, Laboratory course "Arzneistoffanalytik", Department of Medicinal Chemistry, University of Vienna, Austria

2013 (summer term): Lecturer, Laboratory course "Analytical Chemistry II", FH-Campus Wien, Austria

2011 – 2012 (summer term): Tutor, Laboratory course "Analytical Chemistry II", FH-Campus Wien, Austria

2008 – 2012: Research associate, Project: „Imaging the distribution of multidrug transporters in epilepsy patients with PET"

Awards:

2006: Merit grant, FH-Campus Wien, Austria

Miscellaneous:

2002 – 2003: Military Service, Julius Raab Kaserne, Mautern, Austria

XII Record of Publications

Articles in Peer-reviewed journals:

Bauer, F.; Wanek, T.; Mairinger, S.; Stanek, J.; Sauberer, M.; Kuntner, C.; Parveen, Z.; Chiba, P.; Müller, M.; Langer, O.; Erker, T.: Interaction of HM30181 with P-glycoprotein at the murine blood-brain barrier assessed with positron emission tomography. *Eur. J. Pharmacol.* **2012**, *696*, 18-27.

Dörner, B.; Kuntner, C.; Bankstahl, J.P.; Wanek, T.; Bankstahl, M.; Stanek, J.; Müllauer, J.; Bauer, F.; Mairinger, S.; Löscher, W.; Miller, D.W.; Chiba, P.; Müller, M.; Erker, T.; Langer, O.: Radiosynthesis and *in vivo* evaluation of 1-[^{18}F]fluoroelacridar as a positron emission tomography tracer for P-glycoprotein and breast cancer resistance protein. *Bioorg. Med. Chem.* **2011**, *19*, 2190-2198.

Bauer, F.; Kuntner, C; Bankstahl, J.P.; Wanek, T.; Bankstahl, M.; Stanek, J.; Mairinger, S.; Dörner, B.; Löscher, W.; Müller, M.; Erker, T.; Langer, O.: Synthesis and *in vivo* evaluation of [^{11}C]tariquidar, a positron emission tomography radiotracer based on a third-generation P-glycoprotein inhibitor. *Bioorg. Med. Chem.* **2010**, *18*, 5489-5497.

Mairinger, S.; Langer, O.; Kuntner, C.; Wanek, T.; Bankstahl, J.P.; Bankstahl, M.; Stanek, J.; Dörner, B.; Bauer, F.; Baumgartner, C.; Löscher, W.; Erker, T.; Müller, M.: Synthesis and *in vivo* evaluation of the putative breast cancer resistance protein inhibitor [^{11}C]methyl 4-((4-(2-(6,7-dimethoxy-1,2,3,4-tetrahydroisoquinolin-2-yl)ethyl)phenyl)amino-carbonyl)-2-(quinoline-2-carbonylamino)benzoate. *Nucl. Med. Biol.* **2010**, *37*, 637-644.

Presentations and Posters at International Conferences:

Sander, K.; Galante, E.; Yiannaki, E.; Patel, N.; Bauer, F.; Robson, M.; Johnson, S.P.; Badar, A.; Dickens, D.; Langer, O.; Koepp, M.; Årstad, E.: Development of a Pro-drug Tracer for Functional Imaging of Multiple Drug Resistance. 26th Annual Congress of the European Association of Nuclear Medicine (EANM'13), October 19th-23rd, Lyon, France (2013).Abstract in: *European Journal of Nuclear Medicine & Molecular Imaging* **2013**, *40*, Suppl. 2, 114.

Saxena, P.; Erker, T.; Bauer, F.; Stary-Weinzinger, A.; Linder, T.; Hering, S.; Timin, E.: Drug Trapping in hERG Channels does not Require Closure of the Activation Gate. 57th Annual

Meeting of the Biophysical-Society, February 2nd-6th, Philadelphia, USA (2013).Abstract in: *Biophysical Journal* **2013***, 104,* Suppl. 1, 266.

Wanek, T.; Bauer, F.; Mairinger, S.; Kuntner, C.; Parveen, Z.; Chiba, P.; Erker, T.; Müller, M.; Langer, O.: Interaction of HM30181 with P-glycoprotein at the murine blood-brain barrier assessed with positron emission tomography. 5th SFB-Symposium, September 24th-25th, Vienna, Austria 2012.

Wanek, T.; Bauer, F.; Mairinger, S.; Stanek, J.; Kuntner, C.; Müller, M.; Erker, T.; Langer, O.: Small-animal PET evaluation of the putative P-glycoprotein inhibitor HM30181. 2012 World Molecular Imaging Congress, September 5th-8th, Dublin, Ireland (2012).

Bankstahl, J.P.; Bankstahl, M.; Kuntner, C.; Römermann, K.; Wanek, T.; Stanek, J.; Dörner, B.; Bauer, F.; Mairinger, S.; Erker, T.; Müller, M.; Langer, O.; Löscher, W.: Dose dependent transport of 11C-labeled multidrug transporter inhibitors tariquidar and elacridar at the blood-brain barrier measured by small-animal PET and in-vitro-transport assays. 9th International Conference on Cerebral Vascular Biology, June 21-25, Leiden, The Netherlands (2012)_poster

Art, J.; Besche, V.; Bros, M.; Li, H.; Handler, N.; Bauer, F.; Erker, T.; Behnke, F.; Mönch, B.; Förstermann, U.; Dirsch, V.M.; Werz, O.; Kleinert, H.; Pautz, A.: Identification of the KH type splicing regulatory protein (KSRP) as a new important mediator of the anti-inflammatory effects of resveratrol. 78. Jahrestagung der Deutschen Gesellschaft für Experimentelle und Klinische Pharmakologie und Toxikologie (DGPT), March 19th-22nd, Dresden, Germany (2012). Abstract in: *Naunyn Schmiedebergs Arch Pharmacol* **2012***, 385,* Suppl. 1; 6.

Römermann, K.; Bankstahl, M.; Bankstahl, J.P.; Kuntner, C.; Wanek, T.; Dörner, B.; Bauer, F.; Erker, T.; Fedrowitz, M.; Langer, O.; Löscher, W.: Dose-dependent transport of ^{11}C-labeled multidrug transporter inhibitors tariquidar and elacridar at the blood-brain barrier measured by small-animal PET and *in-vitro* transport assays. 41st Annual Meeting of the Society for Neuroscience, November 12th-16th, Washington, DC, USA (2011). Abstract in: *Society for Neuroscience Abstract Viewer and Itinerary Planner* **2011***, 41.*

Dörner, B.; Bankstahl, J.P.; Kuntner, C.; Wanek, T.; Bankstahl, M.; Müllauer, J.; Stanek, J.; Sauberer, M.; Mairinger, S.; Bauer, F.; Erker, T.; Löscher, W.; Müller, M.; Langer, O.: Radiosynthesis and *in vivo* evaluation of [^{18}F]fluoroelacridar as a PET tracer to assess P-glycoprotein and breast cancer resistance protein expression. Gemeinsame Jahrestagung der

Deutschen, Österreichischen und Schweizerischen Gesellschaften für Nuklearmedizin 2011, April 13th-16th, Bregenz, Austria (2011). Abstract in: *Nuklearmedizin* **2011**, *50*, 6, A116.

Mairinger, S.; Bankstahl, J.P.; Kuntner, C.; Wanek, T.; Bankstahl,M.; Römermann, K.; Dörner, B.; Bauer, F.; Erker, T.; Löscher,W.; Müller, M.; Langer, O.: Radiosynthesis and *in vivo* evaluation of [^{11}C]mephobarbital as a PET tracer to assess cerebral P-glycoprotein function. Gemeinsame Jahrestagung der Deutschen, Österreichischen und Schweizerischen Gesellschaften für Nuklearmedizin 2011, April 13th-16th, Bregenz, Austria (2011). Abstract in: *Nuklearmedizin* **2011**, *50*, 6, A115.

Kuntner, C.; Bankstahl, J.P.; Bankstahl, M.; Stanek, J.; Wanek, T.; Dörner, B.; Bauer, F.; Mairinger, S.; Erker, T.; Müller, M.; Löscher, W.; Langer, O.: Evaluation of [^{11}C]elacridar and [^{11}C]tariquidar in transporter knockout mice using small-animal PET. 8th International Symposium on Functional Neuroreceptor Mapping of the Living Brain (NRM2010), July 22nd-24th, Glasgow, UK (2010). Abstract in: *Neuroimage* **2010***, 52, Suppl. 1,* 25.

Kuntner, C.; Bankstahl, J.P.; Bankstahl, M.; Stanek, J.; Wanek, T.; Dörner, B.; Bauer, F.; Mairinger, S.; Erker, T.; Müller, M.; Löscher, W.; Langer, O.:Assessing cerebral P-glycoprotein expression and function with PET by combined [^{11}C]inhibitor [^{11}C]substrate scans. 8th International Symposium on Functional Neuroreceptor Mapping of the Living Brain (NRM2010), July 22nd-24th, Glasgow, UK (2010). Abstract in: *Neuroimage* **2010***, 52, Suppl. 1,* 116.

Bankstahl, J.P.; Bankstahl, M.; Kuntner, C.; Wanek, T.; Stanek, J.; Dörner, B.; Bauer, F.; Mairinger, S.; Erker, T.; Müller, M.; Langer, O.; Löscher, W.: Small-animal positron emission tomography evaluation of ^{11}C-labelled multidrug transporters tariquidar and elacridar in transporter knockout mice. 51. Jahrestagung der Deutschen Gesellschaft für Experimentelle und Klinische Pharmakologie und Toxikologie (DGPT), March 23rd-25th, Mainz, Germany (2010). Abstract in: *Naunyn Schmiedebergs Arch Pharmacol* **2010**, *381*, Suppl. 1, 44-45.

Kuntner, C.; Bankstahl J.P.; Bankstahl, M.; Stanek, J.; Wanek, T.; Dörner, B.; Bauer, F.; Mairinger, S.; Erker, T.; Müller, M.; Löscher, W.; Langer, O.: A new PET study paradiagm to assess cerebral P-glycoprotein expression and function. 29th International Symposium Radioactive Isotopes in Clinical Medicine and Research, January 16th-19th, Bad Hofgastein, Austria (2010), Abstract in: *Nuklearmedizin* **2009**, *48*, 6, A152.

Kuntner, C.; Bankstahl, J.P.; Bankstahl, M.; Stanek, J.; Wanek, T.; Dörner, B.; Bauer, F.; Mairinger, S.; Erker, T.; Müller, M.; Löscher, W.; Langer, O.: Small-animal PET evaluation of [^{11}C]elacridar and [^{11}C]tariquidar in transporter knockout mice. 29th International Symposium Radioactive Isotopes in Clinical Medicine and Research, January 16th-19th, Bad Hofgastein, Austria (2010), Abstract in: *Nuklearmedizin* **2009**, *48*, 6, A143.

Bauer, F.; Mairinger, S.; Dörner, B.; Kuntner, C.; Stundner, G.; Bankstahl, J.P.; Wanek, T.; Stanek, J.; Müller, M.; Langer, O.; Erker, T.: Synthesis and µPET Evaluation of the Radiolabelled P-Glycoprotein Inhibitor [^{11}C]Tariquidar. 22nd Annual Congress of the European Association of Nuclear Medicine (EANM'09), October 10th-14th, Barcelona, Spain (2009). Abstract in: *European Journal of Nuclear Medicine & Molecular Imaging* **2009**, *36*, Suppl. 2, 222.

Dörner, B.; Bauer, F.; Mairinger, S.; Kuntner, C.; Stundner, G.; Bankstahl, J.P.; Müller, M.; Erker, T.; Langer, O.: Synthesis and Micropet Evaluation of the Radiolabelled P-Glycoprotein Inhibitor [^{11}C]Elacridar. 18th International Symposium on Radiopharmaceutical Sciences (ISRS), July 12th-17th, Edmonton, Canada (2009). Abstract in: *Journal of Labelled Compounds and Radiopharmaceuticals* **2009**, *52*, Suppl. 1, 86.